OUR COVER

. . . illustrates the theme of this issue—RCA Superconductive Ribbons and Magnets. The photo shows a superconductive magnet guided by Gerald Storch, EC&D, into a Dewar containing liquid helium at a temperature of 4.2°K. This magnet is used by RCA Superconductive Products to test high-field properties of "Vapodep" ribbon during the manufacturing process, and generates a field intensity of 110 kG in a 2.93-inch clear bore. Recently, RCA announced its new commercial line of high-field, large-bore superconductive magnets having field strengths up to 125 kG. Such magnets will be used in physics research at high magnetic fields for nuclear magnetic resonance (NMR), Mossbauer effect, Zeeman splitting, Faraday rotation, de Haasvan Alphen experiments, magneto-optical, and thermo-magnetic effects. RCA is constructing (for NASA) a superconductive magnet which will generate 150 kG. Its 6-inch bore will make it the largest magnet of that high-field magnetic intensity. (Cover art direction, J. L. Parvin; Photo, J. Semonish).

Tomorrow's Products

Several papers in this issue revolve around the significant progress in technology in the field of superconductivity. The phenomenon itself has been known for many years—practical utilization is only of recent date. Many discoveries in basic physics go through such a period. Other examples could be cited, such as the photoelectric effect and the several thermoelectric effects. Development of a practical product usually results from capitalization on modern technology in one of two or three significant directions.

In many cases, the original discovery was made in terms of materials available to the scientist, usually a university researcher operating on a small budget. He found it necessary, therefore, to turn to materials available on the laboratory shelves. These materials were usually simple chemicals, pure to the normal standards of chemical refinement in existence at the time. Breakthrough in later years consists in many cases either in refining the material to a much more exacting level of purity, or proceeding in the exactly opposite direction—modern developments in the theory of the solid-state may suggest directions for deliberate contamination of the basic material by controlled levels of impurity, a process now given the somewhat slangy description of "doping."

Another basic underlying a marked breakthrough in a field may be the introduction of a new technical process. The rapid development of the transistor art followed the invention of a process known as *zone refining*, and in recent years further development has followed improvements in controlled diffusion and in epitaxial crystal growth.

The third avenue leading to breakthrough may be one of technology in which a somewhat incidental block to progress can exist in the environmental conditions surrounding the device. Improvements in vacuum technology, metal-to-metal joining and bonding technology, protection of the material from external environment by enclosure techniques, such as glassing or the use of plastics, have recently led to significant developments in the solid-state field.

The engineer in a corporation of the complexity of RCA is presented with continual opportunities to draw on his own experience or on information available in the files of laboratory reports and in the technical literature to bring about new products and technologies of major commercial importance. Fundamentally new inventions come along only rarely—the opportunities for capitalizing on older information are multitudinous and constantly at hand. Success comes to the engineer who has the ability to draw on some scrap of information in the back attic of his mind, such as a long-known scientific effect, and then to apply to it the benefit of his thorough knowledge of what can be done with modern materials methods and technologies.

A M Glover

Dr. A. M. Glover
Division Vice President
Technical Programs
RCA Electronic Components and Devices

RCA ENGINEER

VOL. 12, NO. 4
DEC., 1966—JAN., 1967

CONTENTS

PAPERS

NOTES

DEPARTMENTS

A TECHNICAL JOURNAL PUBLISHED BY **RADIO CORPORATION OF AMERICA,** PRODUCT ENGINEERING 2-8, CAMDEN, N. J.

• To disseminate to RCA engineers technical information of professional value. • To publish in an appropriate manner important technical developments at RCA, and the role of the engineer. • To serve as a medium of interchange of technical information between various groups at RCA. • To create a community of engineering interest within the company by stressing the interrelated nature of all technical contributions. • To help publicize engineering achievements in a manner that will promote the interests and reputation of RCA in the engineering field. • To provide a convenient means by which the RCA engineer may review his professional work before associates and engineering management. • To announce outstanding and unusual achievements of RCA engineers in a manner most likely to enhance their prestige and professional status.

RCA ENGINEER articles are indexed annually in the April-May Issue and in the "Index to RCA Technical Papers."

When he was Manager of Engineering Operations, CSD, Mr. Law implemented the management control technique described here. It has been operating in the Engineering Department since February of 1966. A discussion of fundamental factors governing the effectiveness of management control of the efforts on contract projects, is presented along with a case history showing the results obtained as these factors were applied to a number of projects. These results are an unusual record of the relationship between cause and effect in the use of management techniques, and they provide strong evidence to support the effectiveness of these techniques. Of particular significance is an evaluation and reporting system that provides reliable status information in a quantitative form, permitting numerical analysis of performance and performance trends. (*Editor's Note: Mr. Law wrote this paper while Mgr., Engineering Operations, CSD. On Dec. 5, 1966, he was named Chief Engineer, CSD.)

The Engineer and the Corporation

MANAGEMENT CONTROL OF PROGRAM PERFORMANCE

C. K. LAW, Chief Engineer*
Engineering Department
Communications Systems Division DEP, Camden, N.J.

Management in the space age has become as complex as the most advanced weapons system, and it is recognized by the government and by the defense industry that management ability and proper management techniques contribute significantly to satisfactory program performance. In fact, since few programs of substance advance beyond the study stage until solutions to the limiting technical problems can be scheduled with confidence, program success has come to depend fully as much on the competence of its management as it does on the caliber of its engineering effort.

The need for this management direction and control is well recognized by the customers, as well as by industry, and the basic project control techniques necessary for the individual program or project manager to do a satisfactory job have been worked out in detail. Less progress has been made, however, in finding methods to assist higher management to maintain control of multiple programs within their organizations. Typically, the executive management of an operating organization is responsible for meeting the commitments of a large number of programs, ranging in size from the rather large to the very small; in the technical dimension, from the highly advanced to the routine; and in management breadth from the extremely intricate to the relatively straight-forward. To fulfill this obligation, executive management must assure itself that the essential requirements of each individual program are being adequately met and that management is being routinely appraised of the status of all programs through a meaningful and reliable reporting system.

Final manuscript received August 2, 1966.

It is clear that the degree of application of management techniques must be adapted to the nature of each project and that the principles involved must be modulated so that individual project requirements are met in an economical manner. While it is true that the requirements of each project are different, it is also true that a large body of uniform management practices can be quite efficiently employed on all projects, with the unusual or unique requirements accommodated by appropriate tailoring of these practices or by application of specially adapted management organizations and techniques. Common management tools such as PERT, Line of Balance, machine accounting, etc. are available for use, and a few of the most complex projects require the full and systematic program management treatment. As we go down the scale of complexity, the rigorous application of these management tools should be reduced accordingly. In all cases, however, executive management's basic responsibility for program performance and program control does not change—*a point that needs considerable emphasis.*

THE PLAN OF MANAGEMENT

Irrespective of the size or complexity of a given program, or of its assignment within the structure of an organization, the three fundamental phases of management remain: *planning, execution,* and *control* (Fig. 1). While all three of these phases exist on every program, the planning phase is the one most frequently compromised by other pressing needs; because of this fact, the following paragraphs emphasize program planning—with no intent to diminish the equally important phases of execution and control.

The program plan is a definitive blueprint through which executive management can effectively control a program. Without the existence of such plans, soundly developed and carefully reviewed, effective management control of multiple programs certainly cannot be maintained.

The scope of planning will vary with the program, and a relatively small program requires a relatively simple plan. However, it is equally important to realize that all programs, whatever the scope, should have a written program plan at the outset, to explicitly define the objectives of the program, the approach to be used and the commitments of the manager for fulfilling those objectives. The central point here is that the responsible people must think the problems through and record their understandings and intentions. The emphasis should always be on precision and thoroughness, while avoiding the distractions of rigorous formats and elaborate publications.

C. K. LAW joined RCA in 1948 after graduation from Purdue University with BSEE and MSEE degrees. As an engineer and engineering manager he designed aircraft radios and radar altimeters and supervised many of RCA's airborne communications programs for the military services, NASA (then NACA), and the FAA. He was program manager for the Time Division Data Link and, later, the X-20 (Dyna-Soar) Communications and Tracking System Program. He then became Mgr., Programs Management, for the Aerospace Communications and Controls Division. When the Communications Systems Division was formed, he was appointed Mgr., Aerospace Communicatioins Programs. He was then assigned as Mgr., Defense Planning for DEP, until appointed Director, Camden Product Engineering and then in February 1966, Manager, Mgr., Engineering Operations, for CSD. In Dec. 1966 he was named Chief Engineer, CSD. Mr. Law is a Senior Member, IEEE.

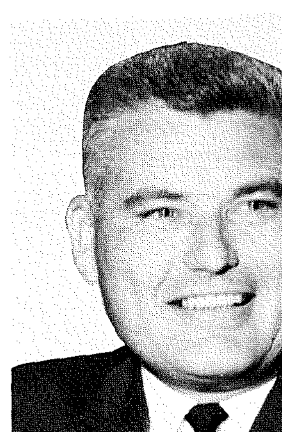

Planning begins in the proposal stage with the interpretation of customer requirements in terms of specific definitive tasks and the determination of how these tasks will be accomplished. Designation of the management responsibilities and preparation of a work breakdown structure, work statements, internal schedules, and budgets should occur during preparation of cost estimates and of the technical proposal. With the proposal work as a starting point, the plan is then updated and extended during the negotiation period and in the initial weeks after award.

In addition to a detailed examination of contractural requirements, the plan should consider such areas as funding limitations, subcontractor default, unexpected technical problems, and other eventualities that may have an impact on the success of the program. The program plan, then, consists of a detailed examination of all aspects of the program and of the manager's explicit plan of action. The elements of delegation of authority and the basis for assessment and measurement of the performance of the program (and its manager) are provided in the program plan. It definitizes standards by which subsequent performance status and appraisal are measured.

As soon as the plan is complete, it is presented to executive management to give them the opportunity to review, understand, and provide guidance and direction at the outset of the program. Management approval of the plan constitutes direction and delegation of authority to the manager to proceed with the implementation of the program in accordance with the plan, subject to the contractual directives of the customer. This approval is the manager's authority to execute and control the program to completion, with provisions for redirection that may be necessary as the program progresses; it is also executive management's tool for measuring the performance of the manager.

The degree to which executive management supports the program plan is a critical factor in its success. Management must not only firmly advocate this method of operation, but in addition, must fully share in its implementation from initial approval to periodic updating and review. The state of mind should be one of firm intent to understand, approve, and periodically review the plan.

Planning is a continuous and dynamic function. Changes in scope, customer redirection, or unexpected problems necessitate an updating of the program plan and for this reason, flexibility must be provided. It is important that executive management make known its intention to periodically review performance against plan to thoroughly analyze this measurement, and to provide appropriate direction and guidance.

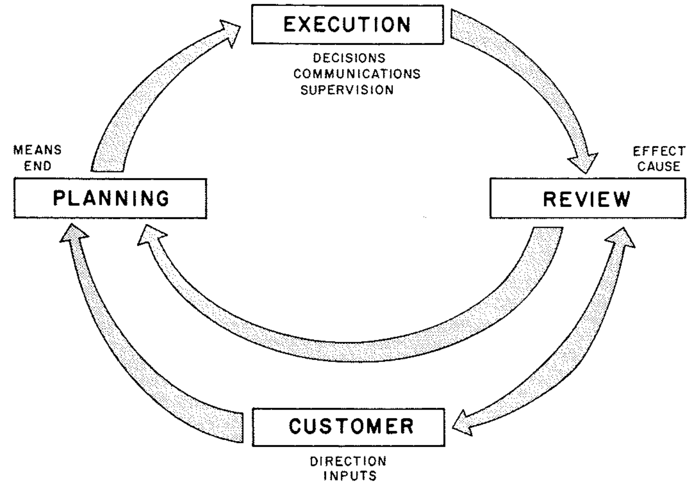

Fig. 2—The management process.

Fig. 1—Program management consists basically of planning, execution and control.

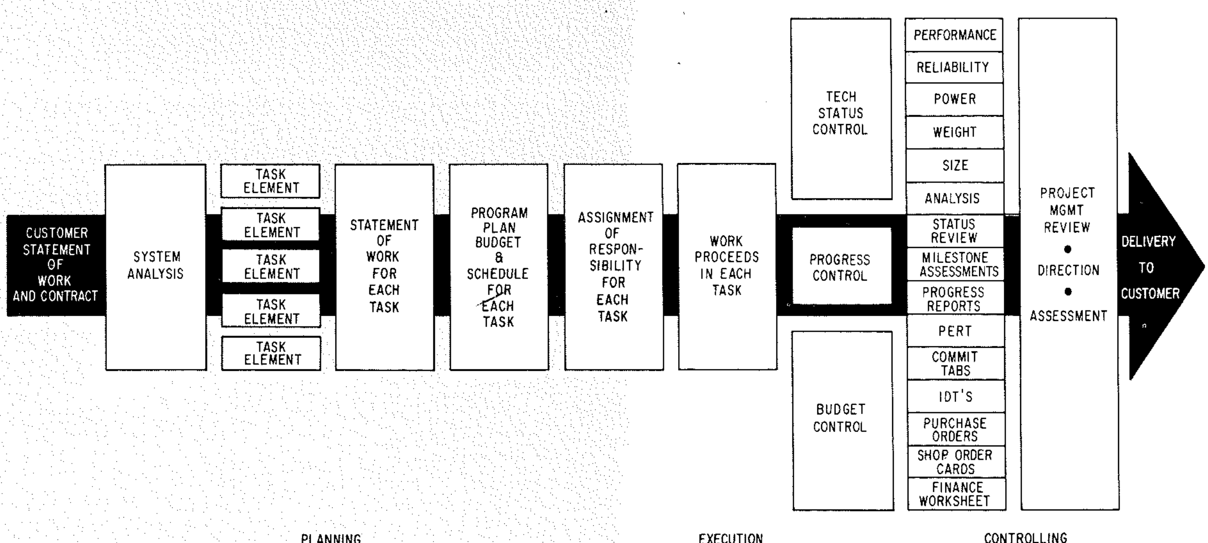

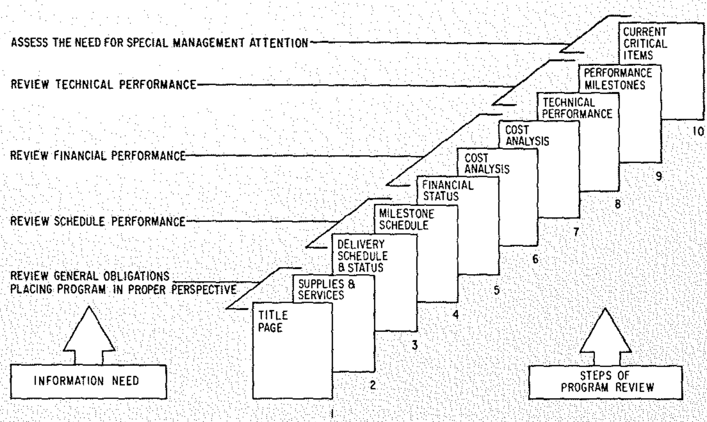

Fig. 3—The program review.

Program control is the comparison and reporting of actual performance against the program plan combined with the determination of significant deviations. With the elements of technical, schedule, financial, and administrative control, and with a detailed understanding and knowledge of the program, the manager has the tools for effective management and successful program performance. The feedback of information generated by measuring performance against plan "closes-the-loop" in the planning, execution, control cycle. This management process is illustrated in Fig. 2.

The preceding fundamentals, with only moderate reservations, are now widely accepted in management circles. But like most theories pertaining to the art of management, their effectiveness is greatly dependent on the circumstances under which they are used; and the measure of any resulting success is influenced by the individual point of view of the person making the assessment.

FROM THEORY TO PRACTICE—A CASE HISTORY

The following case history covers the development and implementation of a management control system designed to overcome these problems. It is unique for several reasons:

1) The above principles were applied to a large number of programs for a significant period of time, while maintaining a reasonably consistent administrative approach (more than 80 programs were involved over a two-year period).
2) Significant procedural changes affecting the key factors of *review* and *planning* (Fig. 2) were independently made, under circumstances that permitted the results of each change to be assessed separately.
3) The status of each of the programs was assessed and recorded each month using a technique that made it possible to indicate status in simple numerical terms.
4) The technique used for status assessment largely eliminated subjective reporting and the inconsistencies associated with it.

Regular program reviews and reports were established in the Aerospace Communications operation in October 1962 for the purpose of providing executive management with general program knowledge and regular assessment of program performance, and to identify critical problems which required action and decision. This information supplemented the existing day-to-day supervision through periodic program reviews and a monthly program status report. Through the program review process shown in Fig. 3, program performance was assessed and critical problems requiring executive management attention were identified. Problem areas usually separated into two categories—those potential problems which were discussed for information purposes only and those where management action or decision was required.

The program status report shown in Fig. 4 was designed to provide executive management with a quick-reference assessment of program performance and a sound basis for determining which programs required special management attention. This monthly program report is a fundamental assessment of contractual status and performance. The format is uniquely factual in nature—the basis for status evaluation being the contract itself. It is based on a forced *yes-no* technique, which demands an objective evaluation and appraisal of contractual status in the technical, schedule, cost, and funding areas. It thereby minimizes subjectivity and editorializing, and further permits a quick-reference assessment of program performance through a color coding system (colors noted by Fig. 4 shades of grey). *Green* coding is used when performance is proceeding in accordance with objectives. *Yellow* indicates a qualified answer with potential serious trouble and suggests that careful attention is warranted. *Red* reflects "out-of-control" situations such as cost overrun, schedule delinquency, or technical problems which are influencing the meeting of contractual obligations. *Red* and *yellow* situations are explained under "remarks". It should be observed that the selection of which of the three colors to use was seldom a problem because the report minimized opinion by forcing factual answers through the *yes-no* technique. The actual color selection was simply the summary of these answers. In retrospect, the information in the status reports was always easy to understand and the accuracy of the color status indicators was rarely questioned or challenged. Throughout the entire two years, there was only one occasion when

Fig. 4—Monthly program status control sheet.

"RED" STATUS
"YELLOW" STATUS
"GREEN" STATUS

PROGRAM C
July 31, 1963

EXAMPLE ONL

CUSTOMER: ECOM, US Navy
CONTRACT #: NOw-63-1234-ab
CONTRACT VALUE: $2,981,557
CONTRACT TYPE: Cost Plus Incentive Fee

INCEPTION: August 1962
COMPLETION: October 1963
PROGRAM MANAGER: W Jones/A Sn
CONTROL ADM: R Brown

PREV	ESSENTIAL ELEMENTS OF INFORMATION	PRES	YES	NO	FORMAL	INFORMAL	REMARKS
	I. MEETING PERFORMANCE REQUIREMENTS		X				
	A. CUSTOMER NOTIFIED						
	B. CUSTOMER APPROVED						
	II. ON CONTRACTUAL SCHEDULE		X				Revised delivery schedules, formally approved by the customer in Jul under Supplemental Agreement #1, are expected to be met.
	A. CUSTOMER NOTIFIED						
	B. CUSTOMER APPROVED						
	III. WITHIN CONTRACTUAL COST			X			Increased costs of $25,000 and added scope in the amount of $93,000 were quoted on May 28, 1963.
	A. OVERRUN $ 25K						
	1. CUSTOMER NOTIFIED		X		X		
	2. CUSTOMER APPROVED		X			X	
	B. SCOPE CHANGE $ 93K						
	1. CUSTOMER NOTIFIED		X		X		
	2. CUSTOMER APPROVED			X			
	3. FUNDS AUTHORIZED			X			
	4. WORK STARTED		X				
	IV. CUSTOMER FUNDING ADEQUATE		X				
	A. CUSTOMER NOTIFIED						

V. GENERAL COMMENTS

Management Alert Item (MAI) submitted to DEP Management 10/5/62, 11/23/62, 12/13/62, 12/26/62, 1/9/63, 1/23/63, 2/25/63, 3/8/63, 3/22/63, 4/8/63, 5/3/63.

there was reason to doubt the integrity of a report—this was a special situation that was quickly remedied; on the other hand a separate attempt to apply the *green-yellow-red* status coding without first fully answering the *yes-no* questions gave much less reliable results.

Fig. 5 is a graphical illustration of program performance based entirely on program status reports over a two-year period. Beginning with the month of November 1962, an individual status report (Fig. 4) for each program and a status summary report (Fig. 6) were submitted monthly to executive management. To provide an indicator that was independent of the number of programs reported, percentages rather than absolute numbers were used in plotting the program performance curve.

In November 1962, the first month of 100% reporting, 33% of all programs was *red*, 37% *yellow*, and 30% *green*. (The October 1962 figures represent only 72% coverage, and are charted only for purposes of completeness.) With such a large number of programs in difficulty, the executive management attention during the first eight or nine months was directed toward immediate corrective action, with minimum emphasis on long-term planning. In this situation a great number of problem programs were frequently reviewed at executive management request in order to understand, evaluate, and correct critical problems. The need for long-term planning was recognized, but during this period emphasis was necessarily placed on correction instead of prevention. The results of this intensive management attention to critical problems are clearly shown. From November 1962 to May 1963 *red* status programs were reduced from 33% to 11%. Equally clear was the fact that during this period there was no favorable trend in *green* status and that in May *yellow* status had in fact increased to a new high of 54%. A further analysis of this eight-month period indicates that executive management's approach in understanding, evaluating, and correcting critical problems through the program review process changed a substantial number of programs from *red* to *yellow* status, and in June 1963 executive management attention shifted from correction to prevention with the initiation of a detailed programming and planning procedure.

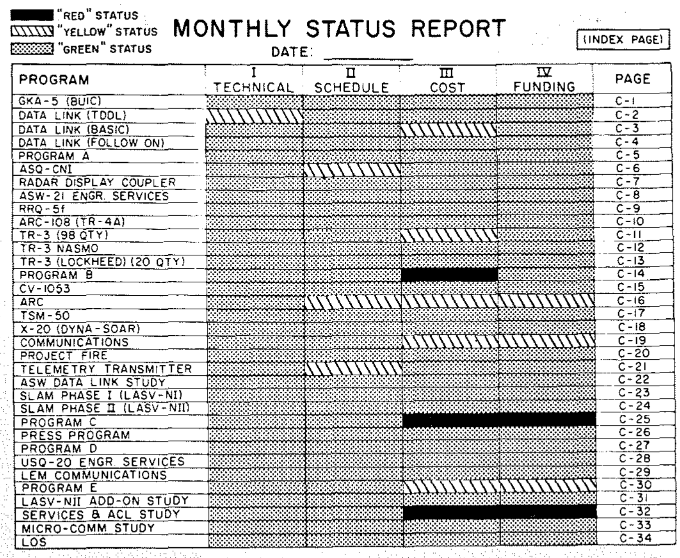

Fig. 6—Monthly status includes technical, schedule, cost and funding.

During the initial eight-to-nine month period the one conclusion which became increasingly obvious was that most difficulties encountered in the management of a program can be traced to unrealistic, incomplete, or erroneous planning. There were few programs where a sound and definitive blueprint had been established for future measurement and effective program control. In June 1963 detailed program planning practices were established under the full authority, support, and participation of executive management. The details of this practice are outlined in Fig. 7. In an attempt to establish a correlation between the program performance curve and the implementation of program

Fig. 5—Graphical analysis of program status and performance.

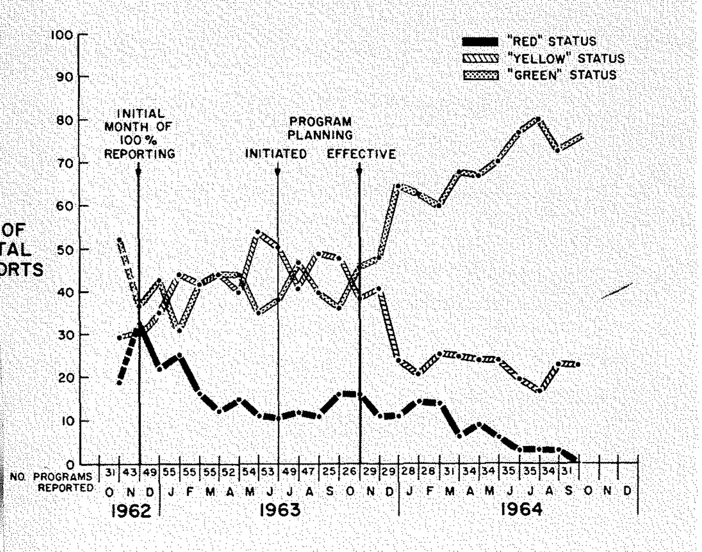

Fig. 7—Steps included in executive management of program plan.

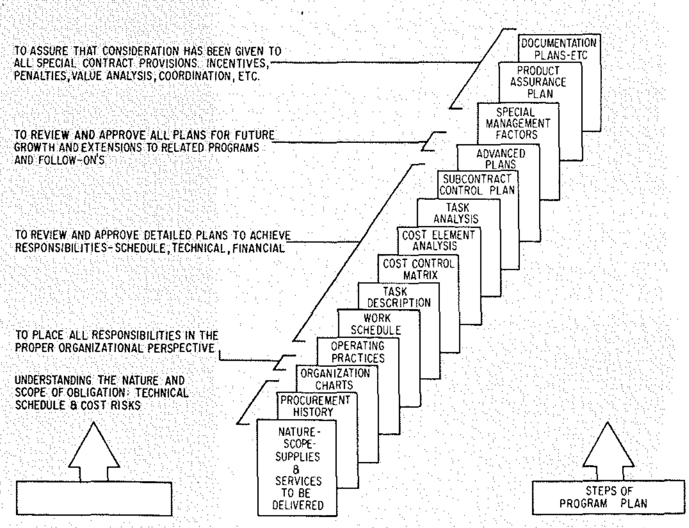

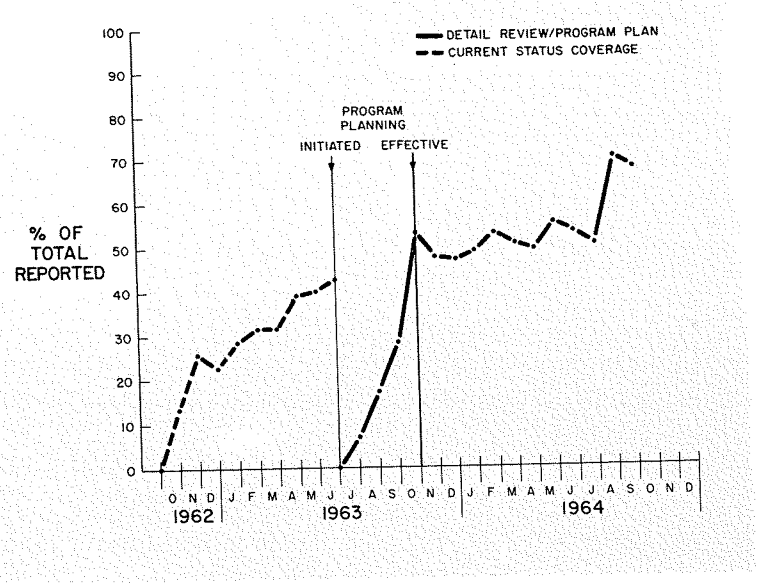

Fig. 8—Coverage of program plan.

planning, programs to which these practices were applied are plotted in Fig. 8. As the application of program planning techniques increased, *red* status was arrested and ultimately reduced significantly, and perhaps of even greater importance, a sharp decrease in *yellow* status and corresponding increase in *green* status was realized. Through the understanding, approval, and periodic review of the program plan by executive management, emphasis had shifted to problem prevention with favorable effects. To further substantiate these results we have charted incidence of loss variances over the two year period. Fig. 9 reflects the significance of program planning in the critical area of cost.

Although established to supplement existing day-to-day supervision, the Program Planning, Program Review, and Program Reporting techniques had a significant impact on this supervision. Managers became sensitive to the *green-yellow-red* status indicators and exerted extraordinary effort to avoid or correct a *"red* situation." It became a real point of pride to keep a program "in the *green*". Promotions and increases seemed to be related to these indicators of performance, and this point was missed by few. In the first months several managers expressed hostility to the approach. These feelings subsided when it became apparent that executive management support and assistance had become more effective, and that there was generally a better appreciation of the problems that were being faced.

The cost of administering the reporting system amounted to only a few hours each month, probably less than the narrative reporting methods that it replaced. We are convinced that the Management Control System not only did not increase operating costs, but that it contributed to substantial savings on individual programs as well.

The most valuable benefits were those that executive management derived from these methods:

1) By scheduling their participation in all programs through the program plan reviews they were better able to keep in touch with the business they were running, and they were able to more effectively help their people avoid trouble.
2) The program plans provided a means of delegating authority and assigning responsibility on a clear-cut basis, giving individual managers the backing they needed to efficiently run their programs. The review and approval provisions retained for executive management the necessary means of controlling and measuring the performance of their individual managers.
3) The status reports highlighted trouble areas on a continuing basis, indicating where particular attention was needed. Coupled with this the status indicators also showed whether a particular situation was worsening or improving.
4) The program reviews and the status reports provided a degree of assurance that the essential requirements of each program were being routinely met, and that most problems were being solved before they grew to expensive proportions.

SUMMARY

Most of the growth of program management has occurred within the last decade, and has resulted from the need to get increasingly complex jobs done on time and within budget. The techniques of project or program management have been applied in many ways to meet these needs. The technical problems have varied widely and specifically with each project; however, the basic rules of management, organized in the format of the Program Plan, and applied through the medium of the Program Plan Review, have proved highly effective in practice—irrespective of the nature of the technology involved, the size of the project, or the manner in which it is organized.

Several very important points must be remembered:

1) *Fundamentally sound management is as important as ever*—these techniques do not reduce the need for competence.
2) *Timely and factual reporting is still vitally important*—these techniques do not reduce the need for objectivity.
3) *Unqualified executive support is indispensable*—these techniques do not reduce the need for high level attention.
4) *The program planning-program review cycle requires attention to detail on a daily basis*—these techniques do not reduce the need for hard work.

An approach to program control using these management principles was tested over a two-year period without any net increase in operating cost, and quantitative results were obtained. These results show striking improvements as the techniques of program reporting and the program plan—program review cycle became effective.

Perhaps the most important benefit of such an approach is the assurance it can give executive management (and the customer) that scheduling and forecasting is realistic, and that there will be fewer costly surprises.

Fig. 9—Major program loss variance.

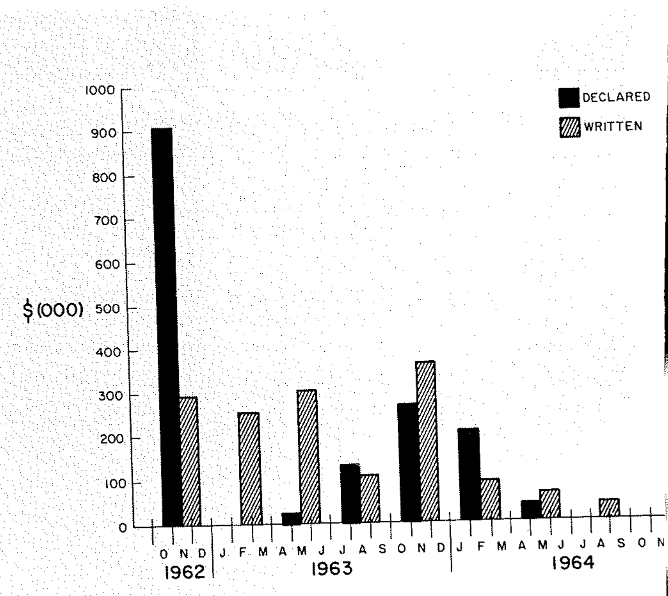

SUPERCONDUCTIVE MATERIALS AND MAGNETS
A Review of Progress at RCA

The successful performance of very-high-field superconductive magnets is evidence of the recent large strides made in the technology and manufacture of practical high-field superconductive materials and of the application of these unique materials to magnets. The recent availability of medium-bore, very-high-field magnets made possible with RCA superconductive ribbons signifies an important technological breakthrough which will result in wide availability of very-high magnetic fields in laboratories throughout the world.

N. S. FREEDMAN, Mgr.
Superconductive Products Operations Dept.
Special Electronic Components Division
Electronic Components and Devices, Harrison, N.J.

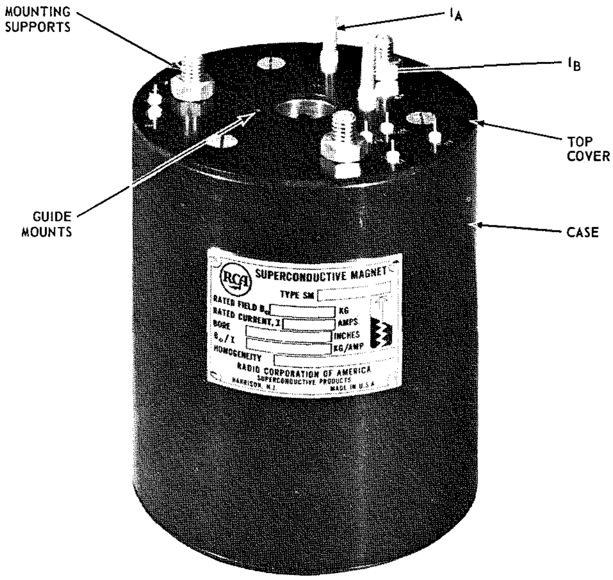

Fig. 1—Photograph of first commercial superconductive magnet having a field above 100 kilogauss and a bore size of one inch. The maximum central field value for this magnet was 108 kilogauss.

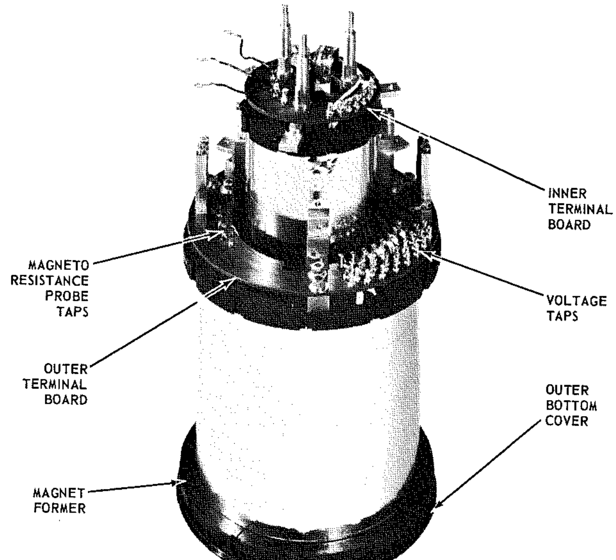

Fig. 2—Photograph with cover removed of first compound commercial superconductive magnet having a field above 100 kilogauss and a bore size of 1.28 inches and a field of 55 kilogauss in a bore size of 3.375 inches. The maximum central field value for this magnet is 112 kilogauss in the 1.28-inch bore.

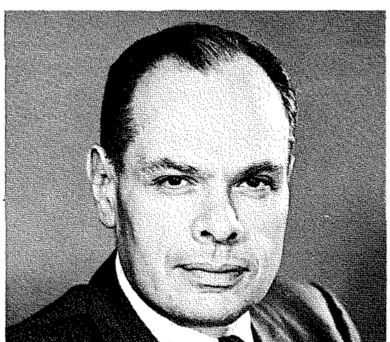

NORMAN S. FREEDMAN received the BS in Chemical Engineering from New York University in 1943, and has since done graduate work at Columbia University. He joined RCA in 1943, and has since specialized in electrochemical work and the process development of materials and electron devices. Mr. Freedman received an RCA Laboratory Award in 1950 for outstanding work in the research and development of "The Method Employed in the Fabrication of Phosphor Screens in Tri-Color Kinescope Tubes." In 1953, he became Manager, Methods and Process Laboratory, in Receiving Tube Product Engineering. In 1954, he was on special assignment to the Color Kinescope Operations in Lancaster, Pa., where he was responsible for developing precision aperture masks for color tubes. In 1955, he became Manager, Process and Test Engineering, and in 1958 Manager, Chemical and Physical Laboratory, in the Harrison plant. From 1961 to 1962 his responsibilities included the direction and management of work on thermoelectric and superconducting materials and devices. In July 1962, he was made Manager of the Superconductor Materials and Devices Laboratory of the Electron Tube Division at Princeton, N.J. In 1963, he received the David Sarnoff Team Achievement Award in Engineering for heading up a team which developed practical structures and production methods for thermoelectric power generators. In 1963, he was promoted to Manager, Special Project Development, in the newly formed Special Electronic Components Division. In 1965, he was advanced to his present position as Manager, Superconductor Products Operation. Mr. Freedman is a registered P.E., is a Member of the APS, and a Senior Member of the IEEE.

In a previous RCA article[15] early developments in high-field superconductors were discussed, and it was concluded that "the RCA process for depositing Nb_3Sn continuously on ribbon does produce a unique and practical superconductor and that the RCA modular design for constructing a superconductive solenoid using this ribbon has excellent chance for providing the needed breakthrough in the technology of large-size superconductive very-high field magnets".

On May 19, 1964, at an RCA Laboratories seminar on superconductivity held for the press at Princeton, RCA announced the successful attainment of 107 kG in an experimental magnet with a practical bore size of 1 inch. Previous to this announcement, the largest bore of an experimental superconductive magnet developing 100 kG was only ¼ of an inch.

The first commercial superconductive magnets above 100 kG had bore sizes of 1 inch and 1.28 inches (Figs. 1 and 2) and were delivered by RCA early in 1966. The only other known commercially delivered 100-kG magnets which were not made and marketed by RCA were constructed by other magnet manufacturers who used RCA "Vapodep" Nb_3Sn superconductive ribbons in the magnet windings. Thus, in three years, the earlier promise for success in the development of large-size superconductive high field magnets has been fulfilled.

Some of the more significant material and magnet developments in low fields as well as in high fields are reviewed in this article. Other articles in this issue discuss in more detail the performance of superconductive materials as well as the unique problems of magnet calculations, design, and fabrication techniques.

SUPERCONDUCTIVITY AND SUPERCONDUCTIVE MAGNETS

Over the last few years, much information has been published on the phenomenon of superconductivity and on the need, advantages, and the potential use of superconductors for the windings of very large-bore (10 to 20 feet) magnets with field strengths in the order of 20 to 40 kG and of medium-to-large-bore (6 to 12 inches) magnets with field strengths as high as high as 150 kG.[1,2,3] Background information on superconductive magnets need not be repeated here. A 1963 review of the EC&D program on superconductivity using vapor-deposited Nb_3Sn and a discussion on superconductive magnets vs. conventional water-cooled copper magnets are given in an earlier article by the author.[15] An excellent 1965 review by Dr. F. D. Rosi on research work at the RCA Laboratories is in Ref. 16.

Final manuscript received October 17, 1966

However, the following two examples provide illustrations of magnet-field requirements that can only be attained practically and economically with superconductive magnets.

In June 1966, the Argonne National Laboratory announced their decision to make the low-field 25-kG, 15.5-foot bore magnet for their new 12-foot hydrogen bubble chamber as a superconductive magnet instead of a conventional water-cooled magnet. This magnet[4] (superconductive or normal) will require approximately 6×10^6 ampere-turns at an average diameter of 16.5 feet for a total of 135,000 feet of 3,000-ampere conductor. Because copper is not a "perfect" conductor, a nonsuperconductive water-cooled copper magnet would require a prohibitive 10 MW of continuous power to overcome the finite electrical resistance in the conductor windings. Because an electromagnet is a device with zero percent efficiency, all the I^2R heat loss from these 10 MW of power must be conducted out of the magnet by cooling water and then dissipated.

At the high-field end, a record 225 kG were obtained in a 1¼-inch-bore water-cooled copper magnet at the National Magnet Laboratories at MIT.[5] To develop this field, the magnet required 10.5 MW of power but could be operated only for short intervals because of the serious heat-dissipation problems. Due to the cooling problems as well as peak power requirements, it is not expected that this magnet will be operated for significantly-long duty cycles.

Superconductivity (electrical conductivity with theoretically zero resistance, i.e., as small a value as has been measured, $R << 10^{-15}$ ohm-cm), where I^2R losses in the conductor are essentially negligible, is thus proving to be the only reasonable answer to obtaining, in a practical manner, magnets of extreme size and/or very high fields. Because some superconductive materials can support exceptionally high current densities ($>1 \times 10^5$ A/cm^2), large-volume high-field magnets may be designed with surprisingly thin winding cross sections resulting in compact overall magnet structures.

Not too many years ago, device operation in a 4.2°K environment presented severe problems of technology, economics, and equipment and refrigerant logistics even to the knowledgeable low-temperature laboratory worker. However, recent engineering developments in cryogenics have resulted in substantially lower operational costs, convenient closed-cycle 4.2°K refrigerators, and new cryogenic materials and structures with proven good reliability. Additional progress in cryogenic technology and lower costs are still necessary but it is expected that these advances will be made as required. It is concluded that cryogenic engineering is sufficiently advanced today so that problems of operation in a 4.2°K environment are not retarding present-day development of large-scale superconductive magnet systems.

Nb_3Sn "VAPODEP" RIBBON

Prior to January, 1966, the RCA Superconductive Products Department sold small quantities of Nb_3Sn superconductive ribbon, RCA Dev. No. R60214, on a testing and sampling basis to research laboratories, government agencies and other magnet manufacturers. Having established material production and device feasibility as well as customer acceptance of developmental-type Nb_3Sn ribbons, RCA introduced two commercial ribbons in January 1966. These new commercial superconductive ribbons, in addition to sampling quantities of other developmental conductors, are now being sold in the United States and, through RCA International, to customers in Canada, Europe, and Japan.

The gas-phase reduction reaction developed by RCA Labs[6,7] for continuous deposition of single-phase stoichiometric Nb_3Sn on a moving substrate has been modified and further improved. (RCA Labs personnel have continued to consult and work with EC&D personnel to provide several important process improvements.) It remains, today, the basic process for the manufacture of RCA's superconductive ribbons. The production facility of the Superconductive Products Operations Dept. at Harrison, N.J. is capable of producing more than 50,000 meters per month total of RCA SR2100, SR2101, and several other developmental ribbons. Fig. 3 shows a general view of the Nb_3Sn-deposition equipment and Fig. 4 shows two lines for electroplating a silver coating having a high conductivity ratio ($R_{300°K}/R_{4.2°K}$) on the surface of the Nb_3Sn deposit. In contrast to a competitive diffusion-type process in which a ductile low-strength niobium ribbon or wire is coated with tin and subsequently heat treated, the RCA vapor-deposition process produces a layer of stoichiometric, single-phase pure Nb_3Sn on a high-strength substrate. The RCA deposition process and its versatility is discussed in another paper in this issue.[8]

Inasmuch as all the "supercurrent" is carried in the Nb_3Sn, the RCA process is particularly useful and unique in that the thickness of the Nb_3Sn is varied to provide superconductive ribbons with different current-carrying properties. The ribbons are designed to carry either different currents at identical fields or the same current at different field ranges. The unique characteristics of the RCA Nb_3Sn ribbons were previously described[9] but have been updated and are more fully covered by Schindler in another paper[10] in this issue. The flexibility of the RCA process is reflected in the various performance curves shown in Fig. 5 for RCA SR2100, SR2101 and Developmental type, Dev. No. R60291.

As the rapid progress in superconductive magnets continues, a need for higher-current conductors has been developing. This requirement can, and is being met in the 65-to-220-ampere range at 100 kG by the introduction of thicker layers of Nb_3Sn on the presently marketed 0.090-inch-wide ribbons. However, for still higher currents, ribbon widths as well as Nb_3Sn thickness is being increased. By the time this article is published, various developmental ribbons 0.5 inch wide × 0.0042 inch thick capable of carrying from 350 to more than 1,200 amperes at 100 kG (1,150 to 4,000 amperes at 25 kG) will be available.

SUPERCONDUCTIVE MAGNETS

The first superconductive magnet which developed a 100-kG field in a *practical* working volume was the RCA superconductive magnet announced on May 19, 1964 which generated 107 kG in a 1-inch bore. (Previously, another laboratory reported a ¼-inch-bore magnet which had attained 101 kG.) The RCA magnet had the highest field obtained anywhere with a superconductive magnet having so large a bore. Late in 1964 a 112-kG magnet having a 1¼-inch bore was produced at the Brookhaven National Laboratory. This magnet was designed and constructed by Dr. W. B. Sampson using all RCA Nb_3Sn ribbons.[11] RCA subsequently announced a 2.93-inch-bore, 111-kG magnet[12], and the attainment of 140-kG in a 1-inch bore was announced in June 1966 by Brookhaven National Laboratory. The reason for providing these statistics is to emphasize that magnets having very high fields and practical working bore sizes *were first attained and commercially marketed by RCA*. Moreover, at this writing, still higher field and/or bore magnets have been made *only* by RCA or by others using RCA ribbons.

In addition to manufacturing the commercial magnets previously mentioned, the Superconductive Products Activity at Harrison is currently working on two research and development contracts for NASA, Lewis Research Center, Cleveland, Ohio. Under contract NAS 3-7101, RCA is constructing a 150-kG 6-inch-bore magnet. This superconductive magnet will have a stored magnetic energy of nearly 2 megajoules and, when de-

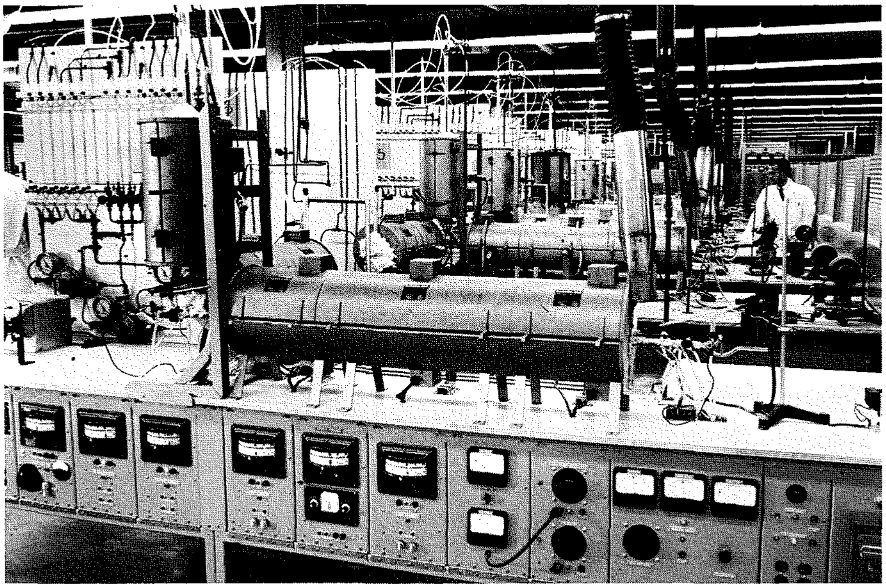

Fig. 3—View of production facilities at Harrison for vapor deposition of niobium stannide superconductive material. Cylindrical furnaces produce stoichiometric, single-phase pure Nb_3Sn.

Fig. 4—View of production equipment used for electroplating a silver coating on the surface of the deposited Nb_3Sn.

Fig. 5—Range of application of RCA Vapodep Superconductive ribbons.

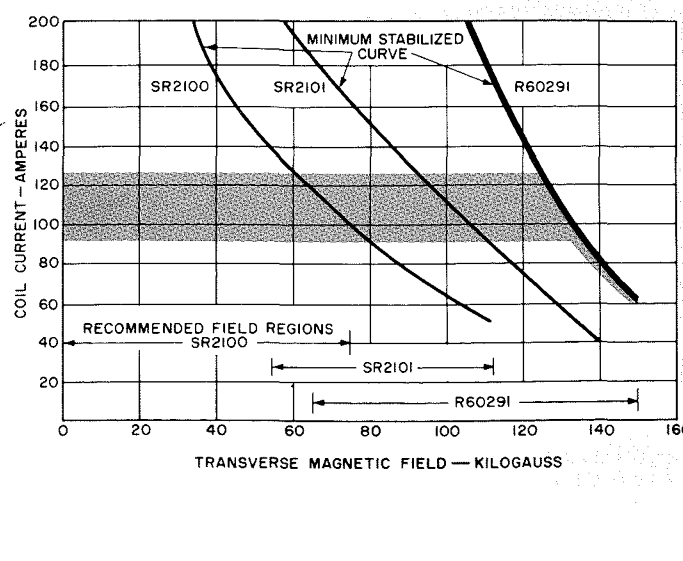

livered late in 1966, will be the highest-field, largest-bore magnet in existence. Capable of operating at a duty cycle of 100%, this magnet will be part of a magnet mirror system to be used for plasma physics experiments. Compared to the very-high-field 110-to-140-kG magnets in the 1-to-3-inch bore sizes, this advanced work at RCA further extends superconductive magnet technology by a substantial degree. The present contract to construct the 150-kG, 6-inch-bore magnet and power supply was a logical follow-on to two previous research and development contracts with NASA which started in March 1963. At that time, RCA had undertaken an evaluation study to determine the feasibility of designing and constructing large-size, high-field superconductive magnets. Affirmative conclusions by RCA on both study contracts resulted in the NASA decision to go ahead with the design and construction of the large high-field magnet system.

Under a second contract with NASA, Lewis Research Center, (NAS 3-7928), RCA has completed the design of and is now constructing four magnets with 20-inch inside diameter windings. Designed to be operated in a magnet system, these four magnets will be spaced with 6 inches between windings; the central field in the 20-inch-winding bore will exceed 72-kG. Operated individually, each magnet will develop 40-kG in the bore. Magnets of this large size at medium-high magnetic fields present unique problems. These problems are due to the forces exerted by the magnetic fields and by the potential heat and stress concentrations resulting when the calculated stored magnetic energy of 7 megajoules (in the 4-magnet system) must be quickly and safely dissipated when the magnet reverts to the normal state and the magnetic field suddenly collapses.

The design of these unique, large-size, high-field magnets requires the development of new concepts in energy control and dissipation, cryogenic heat transfer techniques, and mechanical structures that provide maximum support with minimum structural volume. These concepts are discussed by Schrader in an acompanying paper[13] in this issue.

The calculation of spatial force vectors within the magnets and of magnetic field vectors both internal and external to the magnets is rather tedious but relatively straightforward. However, complex iterative calculations are required to minimize the total length of superconductive materials used. The optimum lengths are obtained by varying the amounts of different superconductive materials used consistent with both the magnetic field and forces distribution throughout the magnets and magnet system. Special computer programs for the RCA 601 were developed to generate the necessary data. This work[14] is discussed by Thompson elsewhere in this issue.

CONCLUSION

At RCA, efforts have been concentrated primarily on the development of a manufacturing process for producing Nb_3Sn-coated superconductive ribbons and on the application of these superconductors to high-field magnets having practical working bores. A chronological listing of significant developments given in Table I provides an over-all view of both industry progress and technological developments in the rapidly changing field of very high-field superconductive magnets.

Although this paper and the accompanying papers in this issue primarily describe work at RCA, rapid progress is also being made in the development of low-field superconductive magnets. Recent major developments in large-bore, low-field superconductive magnets are shown in Table II.

TABLE I—Chronological listing of significant developments in high-field superconductive magnets.

Field, kG*	*Bore, Inches*	*Type of Conductor*	*Date Announced or Tested*	*Source*	*Delivered Commercially*
70[1]	0.25	Sintered Nb-Sn[2]	1961	BTL	No
101	0.25	Diffusion Nb-Sn[3]	Sept. 1963	G.E.	No
100	0.19	NbZr, Nb-Ti	April 1964	West.	No
107	1.0	RCA Vapodep Nb_3Sn	May 1964	RCA	No
112	1.25	RCA Vapodep Nb_3Sn	1964	BNL	No
132[4]	0.25	Diffusion Nb-Sn[3]	Feb. 1965	G.E.	No
80	3.3	RCA Vapodep Nb_3Sn	Aug. 1965	RCA[5]	No
112	1.5-2.6[6]	RCA Vapodep Nb_3Sn	Sept. 1965	BNL	No
100	1.0	Nb-Sn Diffusion[7]	Jan. 1966	G.E.	No
108[8]	1.0	RCA Vapodep Nb_3Sn	March 1966	RCA	Yes
112[8]	1.28	RCA Vapodep Nb_3Sn	March 1966	RCA	Yes
103	2.0	RCA Vapodep Nb_3Sn	June 1966	Magnion	Yes
111	2.93	RCA Vapodep Nb_3Sn	June 1966	RCA	No
140	1.0	RCA Vapodep Nb_3Sn	July 1966	BNL	No
101	1.0	RCA Vapodep Nb_3Sn	Aug. 1966	Oxford	Yes
100	0.87	RCA Vapodep Nb_3Sn	Sept. 1966	Oxford	Yes
137	1.93	RCA Vapodep Nb_3Sn	Sept. 1966	RCA	No
104[8]	1.01	RCA Vapodep Nb_3Sn	Oct. 1966	RCA	Yes

NOTES: *Magnet operated at 4.2°K unless otherwise noted.

1. Magnet operated at 1.5°K.
2. Sn and Nb powder in Nb tube, swaged and drawn into wire; reacted *after* winding.
3. Sn coated on Nb; diffusion reacted *after* winding.
4. Magnet failed at maximum field.
5. NASA Contract No. NAS 3-5240.
6. Conical bore, field recently increased to 115 kilogauss.
7. Sn coated on Nb, diffusion reacted *before* winding.
8. Maximum central field. This value is consistent with all other reported data in this table. However, a commercial magnet is rated nominally at 100 kilogauss.

Abbreviations: BTL — Bell Telephone Labs.
G.E. — General Electric Company
West. — Westinghouse
BNL — Brookhaven National Labs.
Magnion — Magnion, Inc., Burlington, Mass.
Oxford — Oxford Instrument Company, England

TABLE II—Recent major developments in large-bore low-field superconductive magnets.

Central Field, kG	*Bore, Inches*	*Type Conductor*	*Source*
34	6¾	NbTi Cable	Argonne National Laboratory
17	18	NbZr Cable	Argonne National Laboratory
67	6¾	NbZr and NbTi Cable	Argonne National Laboratory
43	11	NbZr Cable	Argonne National Laboratory
10	8	NbZr Wire	The Culham Laboratory, U.K.
21	8	NbZr Wire	Centre d'Etudes Nucleaires de Saclay, France
1	72	NbZr Wire	Lockheed Missile & Space Research Laboratory
42	5⅛	NbZr Wire Imbedded in Copper Strip	Avco Everett Research Laboratory
39	12	NbZr Wire Imbedded in Copper Strip	Avco Everett Research Laboratory

BIBLIOGRAPHY

1. J. E. Kunzler "Superconductivity in High Magnetic Fields at High Current Densities," *High Magnetic Fields*, MIT Press, 1962, p. 574.
2. J. K. Hulm et al, "High-Field Superconducting Magnets," *Advances in Cryogenic Engineering*, Vol. 8, 1963, p. 17.
3. D. Bruce Montgomery, "Superconducting Magnets," *IEEE Spectrum*, Feb. 1964, p. 103.
4. "Superconducting Magnet Developments," by C. A. Laverick to be published in Jan., April and July 1967 issues of *Argonne Reviews*.
5. D. Bruce Montgomery, "High Strength Conductors for Supermagnets," *IEEE Spectrum*, 3, No. 8, Aug. 1966, pp. 111-114.
6. J. J. Hanak, "Vapor Deposition of Nb_3Sn," *Metallurgy of Advanced Electronic Materials*, AIME, Vol. 19.
7. Hanak, Strater, and Cullen, "Preparation and Properties of Vapor Deposited Niobium Stannide," *RCA Review, XXV* No. 3, p. 342.
8. F. R. Nyman, "Vapor Deposition of Nb_3Sn, A Versatile Process," *RCA* ENGINEER, this issue.
9. Schindler and Nyman, "Electromagnetic Performance of Niobium-Stannide Ribbon," *RCA Review, XXV* No. 3, p. 570.
10. H. C. Schindler, "Electromagnetic Performance of Nb_3Sn Vapor Deposited Ribbon Up to 200 Kilogauss," *RCA* ENGINEER, this issue.
11. W. B. Sampson, "112 kG Superconducting Magnets," *Rev. of Sci. Inst. 36*, No. 4, April 1965, p. 565.
12. H. C. Schindler, *to be published*.
13. E. R. Schrader, "Design and Construction of Nb_3Sn Superconductive Magnets," *RCA* ENGINEER, this issue.
14. P. A. Thompson, "Computer Calculations for the Design of Large, High-Field Superconductive Magnets," *RCA* ENGINEER, this issue.
15. N. S. Freedman, "Superconducting Magnets," RCA ENGINEER, Vol. 9, No. 3, Nov. 1963, p. 44.
16. Dr. F. D. Rosi, "Research in Superconductivity at RCA Laboratories," RCA ENGINEER, Vol. 11, No. 1, June-July 1965, p. 18.

VAPOR DEPOSITION OF NIOBIUM STANNIDE—A VERSATILE PROCESS

This paper describes the process chemistry, the equipment, and the substrate materials as they relate to the RCA niobium stannide deposition process and to the product geometries which have been fabricated.

F. R. NYMAN

Ribbon Development and Pilot Production
Electronic Components and Devices, Harrison, N. J.

THE intermetallic compound Nb_3Sn was first synthesized from the elements in 1954 by Mathias et al[1] by metallurgical sintering techniques. Metallurgical preparation of this superconducting compound yielded a mixture of non-stoichiometric, multiphase Nb-Sn compounds.

Research at RCA Laboratories was highlighted in 1960 by Hanak's development[2] of a vapor-phase transport technique for the preparation of single-phase Nb_3Sn having a controlled chemical composition and grain structure. This technique has several distinct advantages over metallurgical procedures for the preparation of Nb_3Sn:

First, it permits examination of the effect of lattice defects and of purity on the critical current, critical field, and critical temperature of the material.

Second, the application of this technique, whereby Nb_3Sn is deposited on metallic and ceramic substrates in varied geometries, permits the study of flux shielding and trapping, tunneling, and tube magnetization.[3]

Third, the technique can be adapted to the continuous deposition of Nb_3Sn on high-strength stainless-steel ribbon or wire substrate for use in high-field superconductive magnets. Thus, the layer thickness of Nb_3Sn can be tailored to meet the current and field requirements of specific magnet designs without loss of tensile strength and flexibility imparted to the composite ribbon by the substrate.

Production of long lengths of ribbon for diversified magnet applications at RCA for over two years has proven this vapor-deposition process to be a practical technique.

PROCESS CHEMISTRY

In essence, the vapor-deposition process is the simultaneous hydrogen reduction of the mixed chlorides of niobium and of tin at the substrate material surface to form the intermetallic compound Nb_3Sn without the intermediate formation of the free metals. Although the hydrogen-reduction process has been successfully conducted at substrate temperatures as low as 730°C and as high as 1600°C, the deposition of Nb_3Sn is generally performed between 900°C and 1200°C. The over-all chemical reaction for the production of Nb_3Sn deposits is given as:

$$3NbCl_4 + SnCl_2 + 7H_2 \rightleftharpoons Nb_3Sn + 14HCl \quad (1)$$

The ratio of the niobium chloride to tin chloride gases which are fed into the deposition zone strongly influences the composition of the resultant deposit.[3] Consequently, it is necessary to use chloride ratios richer in $SnCl_2$ than is indicated by Eq. 1. Atomic ratios from 1:1 to 3:1 Sn:Nb in the chloride vapors are used to obtain Nb_3Sn deposits composed of 75%-atomic niobium. Separate chlorination of the metals actually permits direct control of deposit composition by regulating the relative amounts of $NbCl_4$ and $SnCl_2$ generated in the individual chlorinators. The reactions for $NbCl_4$ formation are given as:

$$2Nb + 5Cl_2 \rightleftharpoons 2NbCl_5 \quad (2)$$

and:

$$4NbCl_5 + Nb \rightleftharpoons 5NbCl_4 \quad (3)$$

Fig. 1—Schematic diagram of quartz apparatus used in vapor deposited process.

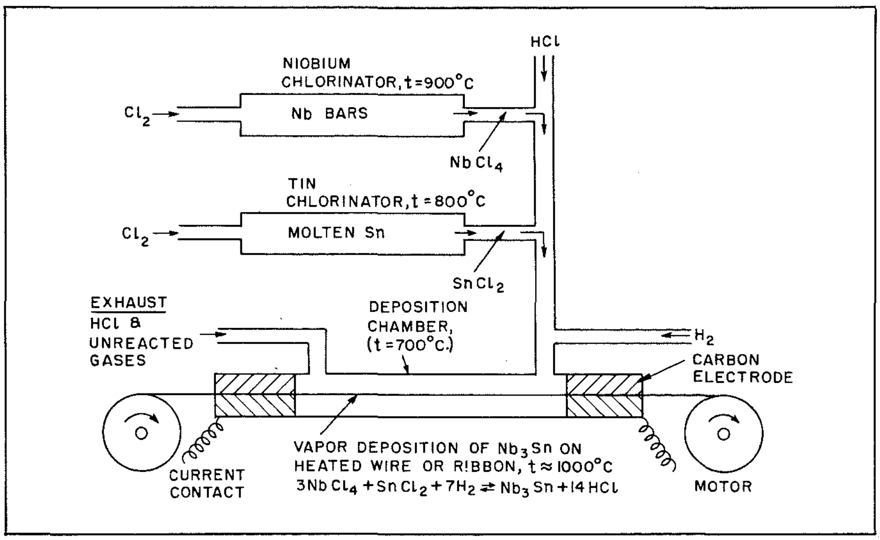

Fig. 2—Equipment used for production of Nb_3Sn superconductive ribbon by vapor deposition process.

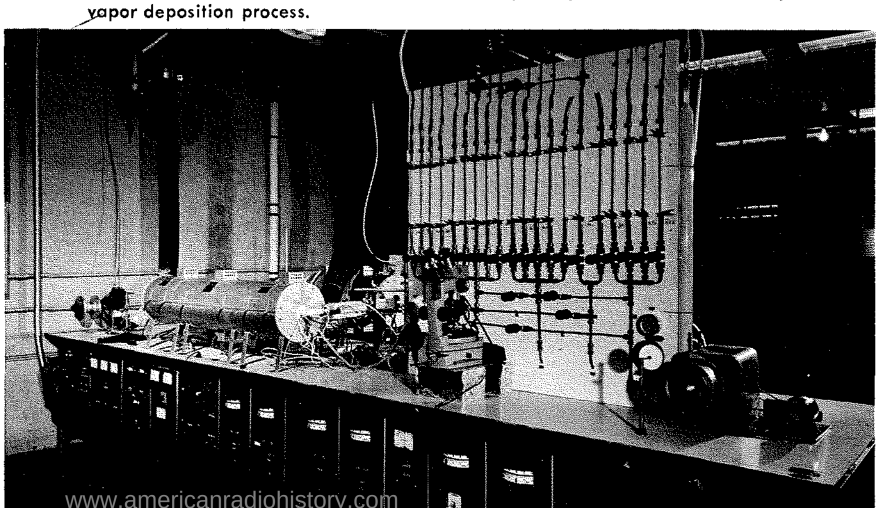

Final manuscript received October 12, 1966.

The reaction for the formation of $SnCl_2$ is given as:

$$Sn + Cl_2 \rightleftharpoons SnCl_2 \qquad (4)$$

Long beds of niobium and tin metal are used to provide sufficient reaction time to prevent free chlorine from passing into the deposition zone from the chlorinators.

PROCESS EQUIPMENT APPLICATION

The chemical vapor-deposition process has been used to deposit Nb_3Sn on a variety of ribbon-substrate sizes by means of continuous-process deposition equipment made of quartz. The continuous-deposition process was developed to deposit a thin layer of adherent Nb_3Sn on a flexible metal wire or ribbon substrate to obtain long lengths of conductor suitable for use in magnet windings. Short lengths of ribbon up to 2 inches wide and long lengths with widths up to ½ inch have been successfully coated by this process.

During the process, the gaseous chlorides produced by individual chlorination of Nb and Sn metals or by volatilization of the $NbCl_5$ and $SnCl_2$ mixtures

F. RUSSEL NYMAN received his B.S. degree in chemistry from Wagner College in 1954. From 1954 to 1956 he performed research on high-temperature selective chlorination of titanium-bearing ores and zirconium ores as a research chemist at the research laboratories of the National Lead Company. While in the U.S. Army between 1956 and 1959, he was attached to the U.S. Army Ballistic Missile Agency, Huntsville, Alabama, where he performed research on thermal properties of materials for use in missile and satellite programs. Mr. Nyman joined the RCA Semiconductor and Materials Division in March, 1959 and performed research and development on vacuum sintering of tantalum, anodization of tantalum, and high temperature pyrolysis of inorganic salts for the development and pilot manufacture of miniature-size tantalum solid electrolytic capacitors. In November, 1962, Mr. Nyman first became associated with the Superconductor Materials and Devices Laboratory at Princeton where he was responsible for the process development of Nb_3Sn films on ceramic and metal substrates of all geometries other than wire and ribbon. In connection with this work, he received the RCA Laboratory Outstanding Achievement Award. Since June, 1964, he has been responsible for ribbon development and pilot production facilities at EC&D, Harrison, New Jersey.

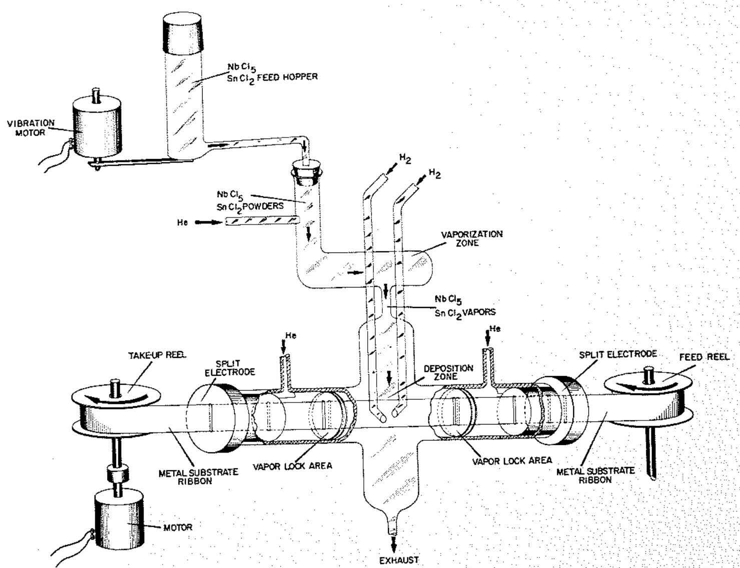

Fig. 3—Diagram of equipment used for production of wide superconductive ribbon.

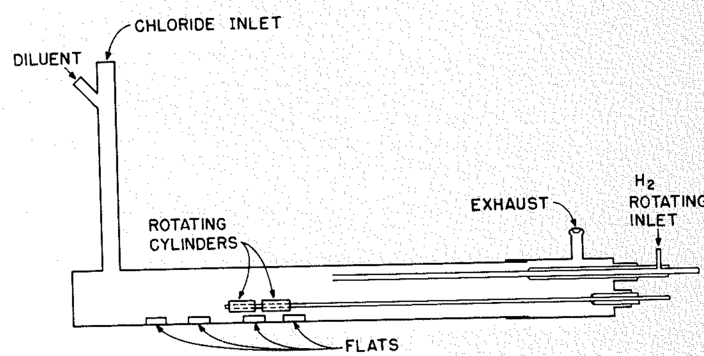

Fig. 4—Schematic diagram of apparatus used for a static deposition of Nb_3Sn on ceramic substrates.

Fig. 5—Processing of concentric ring pattern by means of photoresist and etching techniques.

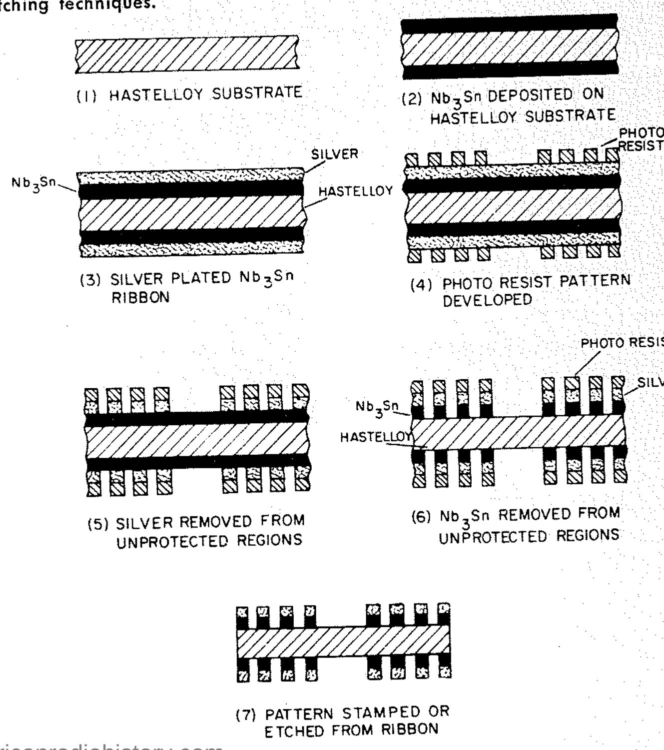

are transported into the deposition zone by an inert carrier-gas. The reducing hydrogen gas is introduced into the deposition zone under critical control to promote good mixing of the reacting gases at the substrate surface. The quantities used exceed the amount required to satisfy the equilibrium conditions of Eq. 1.

The metal substrate is drawn through the deposition zone at a pre-determined rate to continually deposit Nb_3Sn on the moving ribbon or wire. The thickness of the resultant Nb_3Sn coating is a function of the deposition rate (which is maintained at a fixed rate to control the kind of Nb_3Sn deposited) and the interval in the deposition zone. The thickness can be varied, as desired, by changing furnace lengths or by adjusting the speed of the substrate through the deposition zone. A schematic diagram of the quartz apparatus is shown in Fig. 1. The ends of the deposition chamber are fitted with carbon electrodes or integral mercury contact cups which seal the chamber from the atmosphere. Electrical contact is made to the electrodes so that the substrate ribbon can be resistance-heated to the deposition temperature required for the desired deposition rate. The quartz apparatus is heated by electric furnaces to the temperatures shown in Fig. 1. The equipment used for production of superconductive ribbon at the Harrison plant is shown in Fig. 2.

The application of the vapor-phase reduction process to substrate geometries having relatively large surface areas, such as 2-inch-wide ribbon, requires that a uniform mixture of reacting gases be evenly distributed over the substrate surface and that the entire surface be heated to the deposition temperature. A low rate of metal-chlorides utilization is also desirable to prevent the deposition rate from becoming diffusion-limited. This technique is utilized in the deposition of Nb_3Sn on 2-inch-wide ribbon described by Strater[4]. Careful orientation of the plane of the ribbon to the reacting gas streams is necessary for obtaining uniform deposits. Careful positioning of the hydrogen inlets in the deposition zone is necessary to provide sufficient turbulence to prevent gravity separation of the gases in the deposition zone. The equipment used in this work is shown in Fig. 3.

The vapor-deposition process has also been used to deposit Nb_3Sn on ceramic substrates[3], notably the magnesium silicates, in a variety of shapes such as one-inch square flats and cylinders ranging in size from ¼-inch diameter to 1.0-inch diameter. A diagram of the apparatus used for static deposition is shown in Fig. 4.

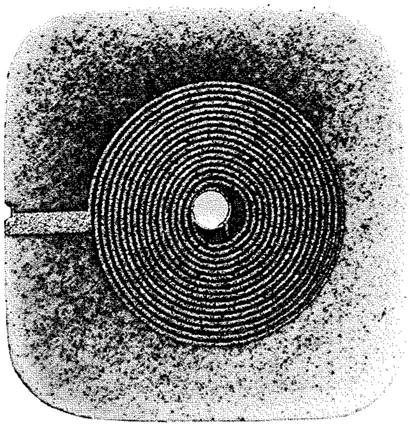

Fig. 6—Continuous spiral of Nb_3Sn deposited on ceramic.

SUBSTRATE MATERIALS

Materials selected for use as a substrate must meet three basic requirements. The material must have a suitable coefficient of thermal expansion, a melting point high enough to withstand process temperatures, and chemical inertness to the chloride's atmosphere during deposition. In the case of metal substrates, it is additionally desirable that the material have a beta-tungsten structure or that it react with niobium to form such a structure to aid in the nucleation of Nb_3Sn. Matching of the thermal coefficients of expansion is required to prevent stress-induced fracture of the Nb_3Sn deposit on cooling from deposition to ambient temperatures as would be the case when substrates having a lower coefficient of thermal expansion than Nb_3Sn are used. In fact it is desirable to use substrates which have an expansion coefficient slightly greater than that of Nb_3Sn so that the deposited coating is under slight compression.

Several commercially available alloys, particularly the stainless-steel-type materials, have been used to manufacture superconductive ribbon and wire for the fabrication of superconductive magnets. Very adherent coatings of single-phase niobium stannide are being continuously deposited on these alloys at the Harrison Plant. These high-strength alloys offer not only the obvious commercial advantage of comparatively low cost but also increase the flexibility and strength of the composite ribbon. The results are easier handling during magnet-winding and the use of considerably less magnet-support structure to contain the stresses of high fields. For example, the ultimate tensile strength of a composite ribbon composed of Nb_3Sn, 0.00025-inch thick deposited on stainless steel 0.002-inch thick is 95,000 psi at room temperature.

Unique geometries, such as "printed" patterns, have been obtained by the application of conventional photoresist and etching techniques[4] (Fig. 5). Another method is the preformation of the substrate prior to deposition. The unwanted Nb_3Sn is subsequently removed by grinding. Examples are shown in Figs. 6 and 7 (courtesy of Dr. C. Cullen, RCA Laboratories, Princeton, N.J.). Unsupported Nb_3Sn has been obtained by the use of suitable substrate material and then selectively dissolving the substrate in hydrofluoric acid.

CONCLUSIONS

1. Nb_3Sn obtained by the vapor-phase hydrogen reduction of the metal chlorides is characteristically single-phase, high-purity material which has excellent properties for use in high-field superconductive magnets.

2. A variety of ribbon substrate widths and thicknesses has been successfully coated with adherent Nb_3Sn deposits to controlled thicknesses which have been tailored to specific magnet applications.

3. The vapor-deposition process has been demonstrated as a practical production process in line operations at Harrison where commercial quantities of superconductive Nb_3Sn coated ribbon are made.

4. Process chemistry and technology have been developed to the point where equipment could be designed to coat with Nb_3Sn suitable substrate materials of virtually any geometry.

BIBLIOGRAPHY

1. B. T. Mathias, T. H. Leballe, S. Geller and E. Corenzwit, "Superconductivity of Nb_3Sn", *Phys. Rev.*, Vol. 95, p. 1435, Sept. 15, 1954.
2. J. J. Hanak, *Metallurgy of Electronic Materials*, G. E. Brock, ed., Interscience Publishers, New York, 1963, p. 161.
3. J. J. Hanak, K. Strater, and G. W. Cullen, "Preparation and Properties of Vapor-Deposited Niobium-Stannide", *RCA Review*, Vol. XXV, p. 342, Sept. 1964.
4. H. C. Schindler, F. R. Nyman, K. Strater, *High Magnetic Field Superconducting Properties of Nb_3Sn Films*, Final Report, Contract NAS 3-4113, National Aeronautics and Space Administration, August, 1965.

Fig. 7—Rings of Nb_3Sn deposited on a ceramic cylinder.

COMPUTER CALCULATIONS FOR THE DESIGN OF LARGE HIGH-FIELD SUPERCONDUCTIVE MAGNETS

For the past two years, design calculations for superconductive magnets have been carried out on the RCA 601 computer located at the RCA Laboratories, Princeton, N. J. This paper briefly outlines these calculations and discusses the general topic of magnetic calculations and the mathematical bases for the specific calculations employed. Special emphasis is placed on complex problems involved in designing large, high-field superconductive magnets.

P. A. THOMPSON
Magnet Design and Systems Development
Electronic Components and Devices, Harrison, N. J.

ELECTROMAGNETS have a wide range of uses. In the home, these uses range from the intermittent solenoid of a buzzer to the electron-beam focusing coil of the TV picture tube; in industry, from the crane magnet in scrap lifters to the armature windings of large motors and generators; in research, from the small, iron-pole-face general-purpose laboratory magnet to the large magnetic components of a cyclotron. In the design of all but the simplest of these magnets, the prime consideration is the nature of the magnetic field produced by current flow through conductors, i.e., the field magnitude as a function of current flow and the direction of the field.

GENERAL GEOMETRIES

For the general case, information about the magnetic field is obtained for each point in the magnet volume by summation of the fields contributed by the currents flowing through the individual segments of wire in the entire device. In differential form, using MKS units, this magnetic field information is expressed as follows:

$$d\mathbf{H} = \frac{I}{4\pi R^3}(\mathbf{R} \times d\mathbf{l}) \qquad (1a)$$

where the pertinent vectors (bold-face type) are defined in Fig. 1. The magnitude of the induction field $|\mathbf{H}|$ for the closed circuit is then expressed as follows:

$$|\mathbf{H}| = \frac{I}{4\pi}\oint\frac{\mathbf{R} \times d\mathbf{l}}{R^3} \qquad (1b)$$

The type of current path most commonly used to produce a magnetic field is a loop or series of loops. Such a path may be approximated by a series of circular filaments, as shown in Fig. 2. Provided no ferromagnetic material is used in the magnet, the magnetic flux density B has the same vectorial direction as the magnetic induction and is numerically proportional to it, as follows:

$$B = \mu_o H \qquad (2)$$

In the classical case (i.e., for nonsuperconductors), therefore, the magnitude of the flux density is a direct, linear function of the current in the coil windings. In this relationship, the diamagnetism of superconductors produces a small perturbation which, fortunately, is usually insignificant because it is difficult to treat analytically.

When ferromagnetic material is used in a magnet, the total magnetic field is determined by both the induction of the coil windings and of the effects of fictional magnetic dipoles in each volume element of the ferrous material. The direction and strength of these dipoles depend, in turn, on both the induction of the windings and the fields of all the other dipoles. The proportionality factor is no longer a constant, but rather a nonlinear function of the induction field.

It is apparent that the general case can produce formidable calculational difficulties which are amenable only to computer solution, particularly when ferromagnetic material is used. Complex programs on the largest computers are necessary for the field calculations of cyclotron accelerating magnets of general geometry and the like.[1] For cases of more regular or symmetrical geometry, many approximations and simplifications can be used to aid the calculation.

AIR-CORE SOLENOID MAGNETS

The most interesting type of device for RCA Superconductive Products is the research magnet which contains no iron and has the highly symmetrical geometry of a solenoid with rectangular cross section. This unit, shown in Fig. 2, is basically a composite structure of many circular loops, electrically in series. The field of each such loop, anywhere on its axis of rotation, is given by the familiar relationship:

$$B = \frac{\mu_o I a^2}{2\,(a^2 + z^2)^{3/2}} \qquad (3)$$

Final manuscript received Oct. 28, 1966.

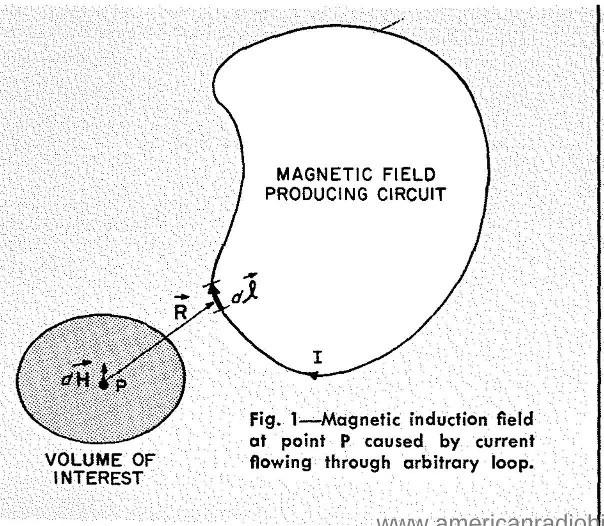

Fig. 1—Magnetic induction field at point P caused by current flowing through arbitrary loop.

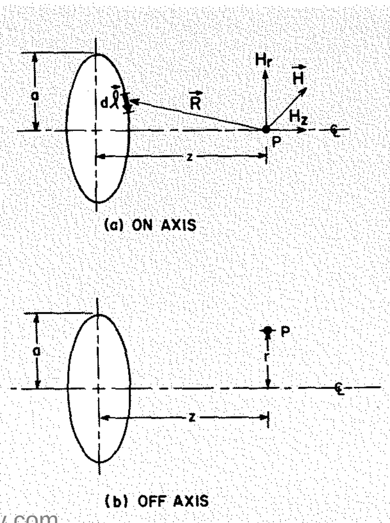

Fig. 2—Magnetic field at point P of a circular filament, (a) on geometric axis and (b) off axis.

PHILIP A. THOMPSON received his A.B. degree in music from the University of Tennessee in 1951, being elected to membership in Phi Kappa Phi the same year. After doing graduate work in German literature, he joined the U.S. Army serving from 1952 to 1955 in the Army Security Agency. From 1955 to 1960 he was Manager of Radio Station WUOT at the University of Tennessee and holds a Federal Communications Commission First Class Radio Telephone License. In 1959, he was awarded an Atomic Energy Commission grant for his experimental thesis study in plasma physics, and in 1960 received an M.S. degree in physics from the University of Tennessee. In August, 1960, he joined the Thermonuclear Division of the Oak Ridge National Laboratory as an Associate Physicist. While at ORNL, he engaged in magnetic studies and experimental research on soft superconductors and he co-authored papers on both plasma physics (electron beam instabilities) and superconductivity (proximity effects). Mr. Thompson also pursued further graduate studies in physics at the Oak Ridge Branch of the Graduate School of the University of Tennessee. In July of 1964, he joined RCA as a Member of the technical staff of the Superconductor Materials and Devices Laboratory, Princeton, New Jersey, later transferred to Harrison, N.J. to work primarily in magnet design and systems development. Mr. Thompson is a member of Sigma Xi, the Institute of Electrical and Electronics Engineers, and the American Physical Society.

By symmetry considerations, the field is parallel to the axis and the radial and azimuthal components are identically zero. Usually the helical pitch of the solenoid windings is small enough to permit the assumption of only an axial field component for the actual device. For cases of large pitch, the exact equations are obtainable in the thorough treatment by Smythe.[2]

(For the remainder of this paper, *magnetic flux density* will be referred to by the imprecise, but almost universally used term (magnetic) *field.* Because the direction of the field is either obvious or of no importance, only the magnitude will be indicated. However, the μ_o will be retained to assure the proper units of teslas, or gauss, as the case may be.)

The field vector off the axis of a loop is a much more complicated expression than Eq. 3, and, for convenience, is usually given in vector potential notation. This expression can be reduced in complexity by replacing the geometric considerations with elliptical integrals. When this replacement is made, the field components (there still is no azimuthal field) are expressed by:

$$B_z = \frac{\mu_o I}{2\pi}\left(\frac{1}{[(a+r)^2+z^2]^{1/2}}\right)\left(K + \left[\frac{a^2-r^2-z^2}{(a-r)^2+z^2}\right]E\right) \quad (4a)$$

$$B_r = \frac{\mu_o I}{2\pi}\left(\frac{z}{r[(a+r)^2+z^2]^{1/2}}\right)\left(-K + \left[\frac{a^2+r^2+z^2}{(a-r)^2+z^2}\right]E\right) \quad (4b)$$

where K and E are elliptical integrals.

In principle, then, the solenoid field can be calculated as a summation of many closed-loop fields. For example, these loops would be: 1) representative of the actual winding turns, 2) arranged in a regular fine network throughout the entire winding cross section, or 3) located so that one or two will approximate the entire windings. In any case, the product NI of the number of turns and the current through each must be kept constant. The first two of these approaches are highly inefficient, even with modern, high-speed computers; the third, exemplified by the Lyle Approximation,[3] has accuracy only in the immediate vicinity of the solenoid centroid. A greater shortcoming of these field-calculation methods is that the infinite discontinuity at any loop (or filament) can cause great inaccuracies for points within the actual magnet windings. This deficiency is significant, as will be shown presently, because knowledge of the fields within the windings is of prime importance for superconductive magnets.

To increase the efficiency of calculation while maintaining accuracy, a formula (containing elliptical integrals) which employs infinitely thin, cylindrical current sheets can be used to represent the magnet windings. Each sheet is equivalent to a uniformly distributed layer of turns, and a number of these sheets can be used to replace the radial extent of the coil cross section. For hand calculations, there exists an excellent tabulation of fields of semi-infinite sheets.[4] An interesting variation of this calculational method is the set of tables and graphs by Brown et al.[5] of semi-infinite conducting solids in the form of cylinders with zero inside diameter. The difference of four of these solids represents the complete solenoid without any numerical integration being necessary. For hand calculations with either the semi-infinite sheet or the semi-infinite solid method, there remain problems of double interpolation and the inherent lack of reliability of small numbers obtained by subtracting large numbers. Even with computerized forms of these methods, the possibility of infinite discontinuities for points within the windings is still present. However, the Garrett Code, which will be discussed later, avoids this pitfall.

Fig. 3—Cross-section diagram of simple air-core solenoid indicating dimensionless parameters.

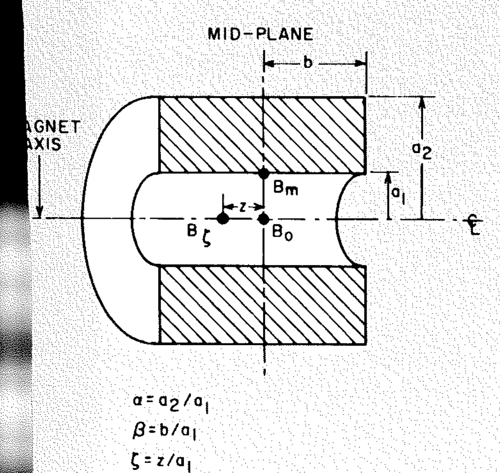

Fabry Method

Before discussing the Garrett Code, it is appropriate to digress briefly to mention an alternate, extremely simple expression for the field along the axis of a solenoid with rectangular winding cross section and uniform current density.

An adaptation,[6] by Gauster, of one of Fabry's basic formulations for so-called "thick solenoids" of various shapes and current distributions, has been used widely in our programming when applicable. The basic geometry is shown in Fig. 3, expressed (in MKS units) as:

$$B_\zeta = \frac{10\mu_o}{4\pi}[F\ (\alpha, \beta, \zeta)\ a_1 i] \quad (5a)$$

or in the more familiar form (in CGS units):

$$H_\zeta = F\ (\alpha, \beta, \zeta)\ a_1 i \quad (5b)$$

where i is the current density and the Fabry factor F is given by:

$$F_\zeta = \frac{\pi}{5}\left\{(\zeta+\beta)\ ln\left[\frac{\alpha+\sqrt{\alpha^2+\zeta+\beta)^2}}{1+\sqrt{1+\zeta+\beta)^2}}\right] - (\zeta-\beta)\ ln\left[\frac{\alpha+\sqrt{\alpha^2+(\zeta-\beta)^2}}{1+\sqrt{1+(\zeta-\beta)^2}}\right]\right\} \quad (6)$$

which simplifies at the centroid to:

$$F_o = \frac{2\pi\beta}{5}\left\{ln\left[\frac{\alpha+\sqrt{\alpha^2+\beta^2}}{1+\sqrt{1+\beta^2}}\right]\right\} \quad (7)$$

The availability of $F_o\ (\alpha, \beta)$ graphs[7] makes this method a very convenient one for the calculation of the centroid field by hand. By the superposition of rectangular cross-section solenoids, with both positive and negative current densities, it is possible to represent more complicated magnets and systems of magnets,[8] e.g., simple magnets with two different current densities, split or window magnets, and any number of similar

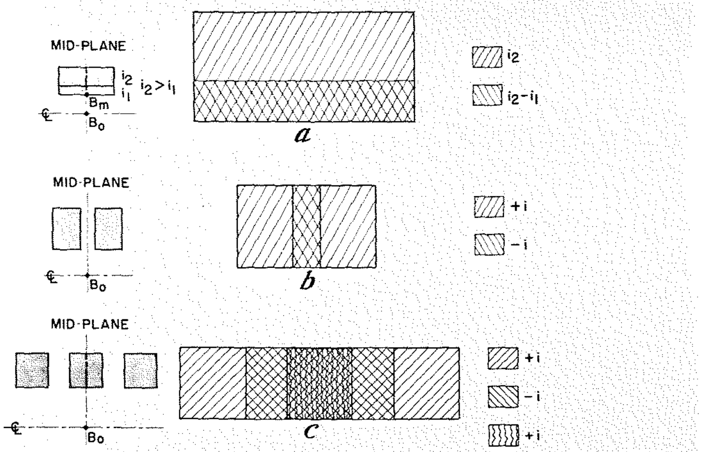

Fig. 4—Superposition of simple solenoids to simulate more complex magnets—(a) magnet with two different current densities, (b) window magnet ("split pair"), (c) system composed of three regularly space, identical, co-axial magnets.

magnets spaced at regular intervals (see Fig. 4).

For both hand and computer calculations of fields on the axis of a rectangular cross-section magnet, this Fabry method can be extremely fast and is exact for the consideration of uniform current density throughout the magnet winding volume. (A subroutine called Fabry has been written for Equation 5 with proper checks and safeguards.)

Garrett Computer Codes

For off-axis fields and for irregular systems of coils, a more general calculational approach is required. M. W. Garrett has written a versatile and rather general computer code based on a Gaussian quadrature numerical integration of current sheets, with automatic features to prevent discontinuities in field values even within the magnet windings.[9] It is this carefully-tested code that forms the basis for almost all the programs used on the RCA 601 computer (located at the RCA Labs, Princeton) for work which requires knowledge of the fields within the magnet. Another more widely known code[10] by Garrett uses a zonal harmonic algorithm which, although quite efficient in many cases, is not valid within the windings.

The Garrett Elliptical Integral Code, which calculates inductances and forces as well as fields, has been adapted for use on the RCA 601 as an eight-subroutine program called Ellie. Garrett's original subroutines written in FAP, the IBM 7090 assembly language, were translated by the author into the RCA 601 version of Fortran II. The Fortran sections of Garrett's code had to be slightly modified to meet the RCA 601 specifications, and new subroutines were added to provide time, date, and identification outputting. In its present form, Ellie can calculate fields, inductances, and forces for any system of up to 40 separate coaxial coils, each with rectangular cross sections and uniform current density.

Other Computer Codes

A code called Modder has been written to calculate the field at the design point (usually the centroid of the system) and the fields at the corners of each section or module comprising the magnet system. (It can be demonstrated that for almost all cases, the maximum field occurs at the corners of a module.) This code can handle up to 40 separate modules and uses both Fabry and Ellie as subroutines.

A variation of Modder contains a relaxation process within the framework of a fixed geometry and it is called Modrlx. It provides current changes in each section to obtain the design requirement in the centroid field while limiting the current to that value permissible for the local fields in the module, as defined by any arbitrary critical density vs local field characteristic.

For a given magnet bore, field, and homogeneity requirement, another code called Simple computes the minimum volume, simple magnet design, i.e., one section with uniform current density, assuming a given set of superconductor parameters. This method is semi-analytical in that the absolute minimum volume and, therefore, minimum conductor length magnet is computed. Then, if the homogeneity proves to be unsatisfactory, the code does a search, keeping the centroid field at the design requirement, but increasing the magnet length until the desired homogeneity is achieved. (Cf, an infinitely long solenoid which has a perfectly homogeneous field everywhere in its bore.)

MAGNET DESIGN LIMITATIONS

For magnets and systems of magnets wound from nonsuperconductors, the main consideration usually is to limit the current density to that for which adequate cooling can be provided (about 50 kA/cm^2). By increasing the size of a magnet, it is generally possible to reduce the current density necessary to produce the required field. In fact, the Fabry formulation takes this maximum current-density specification directly into account. However, arriving at the geometry and current distributions for systems of special field shape or, especially, of high field-homogeneity in a given region, can provide formidable difficulties. These situations have received consideration by Gauster[11] in his analytic approaches to the general problem of designing a magnet configuration which will produce a specific field shape. Furthermore, considerations of field homogeneity about a magnet system centroid have been given a unified treatment by Garrett.[12] His procedure includes Helmholz pairs of finite dimensions as a "coil" design in which all terms to the 4th order in the zonal harmonic expansion of the central field have been made to vanish. The treatment is most familiar from the "Garrett 6th Order Coil," which is a simple solenoid with extra compensating windings on the end.

For magnetic systems wound with superconductors, there is more than just a current-density restriction. As explained in a previous paper,[13] there is a unique combination of maximum current density and local field at the conductor for any operating temperature (usually 4.2°K, the boiling temperature of liquid helium at atmospheric pressure). This situation underscores the importance of having a computer code which can reliably calculate the field values within the actual winding volume. For any proposed design, the highest field in the windings must be checked against the critical current density vs the local field value to see if the necessary working current is possible. If more than one uniform current density section is to be used in the proposed magnet design, the maximum field point of each section must be so checked.

DESIGN PROCEDURES FOR LARGE HIGH-FIELD MAGNETS

A multiplicity of superconductive materials, each with different critical-current characteristics is necessary for the most economical design of large high-field magnets.[14] A modular design is indicated for winding convenience of these different materials as well as for providing mechanical strength. With the critical-current characteristics established for the specific conductor in each module, a modified relaxation procedure is applied to obtain the necessary geometry and current. The method is illustrated by the discussion of the steps involved in the design of a 6-inch-bore, 150-kG magnet for the Lewis Research Center, NASA.[15]

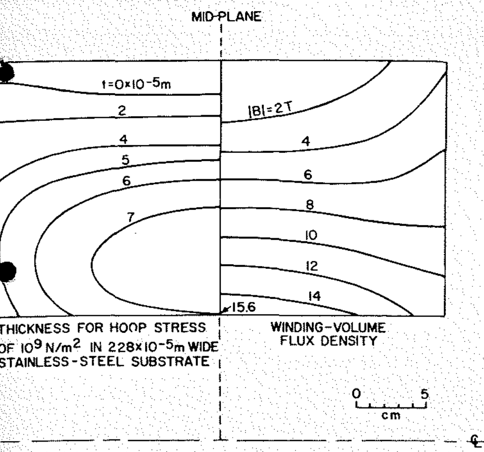

Fig. 6—NASA 150-kilogauss magnet initial equivalent solenoid for relaxation process, showing contours of constant substrate thickness and of constant field magnitude. (N.B. 10^9 N/m^2 $\approx$ 150 kps, 1T = 10^4 kG.)

Equivalent Simple Magnet

As the starting point for the relaxation method, a simple (single-module) equivalent magnet with an average current density is used. (The average current density is an average current divided by an average over-all effective area per turn.) The magnet current is obtained from the approximate average of "working currents" curves of the actual critical-current characteristics. As a safety factor, the working current is usually taken to be about 10% less than the critical current. The pertinent curves for the NASA magnet under discussion are plotted in Fig. 5. The average over-all effective area per turn is obtained from the sum of the areas of the assumed conductor and of the pro-rated interleaving. An additional allowance (20% for the first assumption) is made for the mechanical structure of the modules.

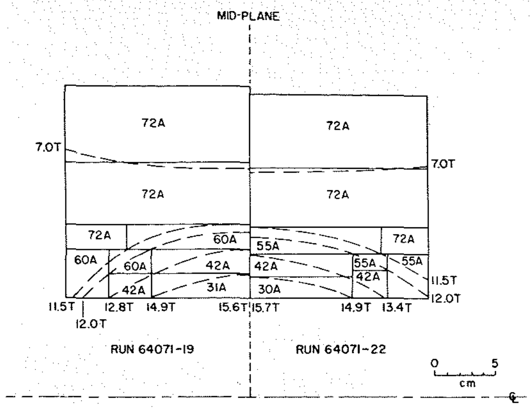

Fig. 7—Module parameters and resulting module geometries for NASA 150-kilogauss magnet at two stages of relaxation process.

With these data the SIMPLE code can be used to find the required dimensions for the equivalent, uniform-current-density magnet. For the present case, field homogeneity is not specified; therefore, the geometric shape requiring the minimum amount of conductor is used for the initial equivalent magnet, as shown by the outline of Fig. 6.

After the dimensions of the starting magnet are established, contours of equal flux density within the cross section are generated by ELLIE. From the conductor winding radius, the local axial component of the field, and the assumed average current, a plot of constant substrate thickness for the limiting hoop stress can be expressed by:

$$t = \frac{IB_z r}{\sigma_{max} W} \qquad (8)$$

where t is the (variable) structural thickness; I the current through the conductor; B_z the axial component of the field vector at the conductor; r the radius of the conductor; σ_{max} the maximum allowable hoop or tensile stress; and w the (fixed) structural width of the conductor. These fields and conductor substrate thickness lines are indicated in the cross section of the equivalent magnet in Fig. 6.

Initial Modular Magnet

Three separate conductor supercurrent characteristics were considered sufficient to provide the necessary flexibility in keeping to a minimum the total length of the conductor for the 6-inch bore, 150-kG magnet. Rectangles of various shapes and sizes (representing modules containing a single type of conductor) are fitted within the pertinent field contours so that the field range for the type conductor in each module falls within the limits specified in Fig. 5. For each module, the current limit is established by the maximum field occurring anywhere in the module cross section.

The effective winding area per turn for the modules is the sum of the cross section of the superconductive and stabilizing coatings of the conductor (determined by the chosen critical characteristics), and the conductor mechanical cross-section (substrate), and the interleaving cross section. From the available contour plots (Fig. 6), a compromise of two substrate sizes was established. The resultant combination of the two substrate sizes and critical characteristics of the three different conductors leads to a total of four discrete conductor types.

Computational time in the iteration loop which follows is greatly reduced by adding an over-all factor for the mechanical structure to the effective areas per turn in the winding cross section. As mentioned previously, for modules which do not cross the midplane, the extremes of field magnitude almost always occur in the module corners, i.e., at points shared by contiguous modules. Thus, by considering the winding without specific intervening mechanical structure, the total necessary number of discrete fields can be limited to reduce the computer effort.

Iteration Loop

At this point, the actual iteration loop for the relaxation process begins. By use of the code MODRLX, new magnetic-field values and hoop stresses at the module corners are calculated, and ELLIE gives the axial component of the resultant electromagnetic force on each module. New working currents are obtained from the

Fig. 5—Measured and assumed field-current characteristics for superconductors used in NASA 150-kilogauss magnet.

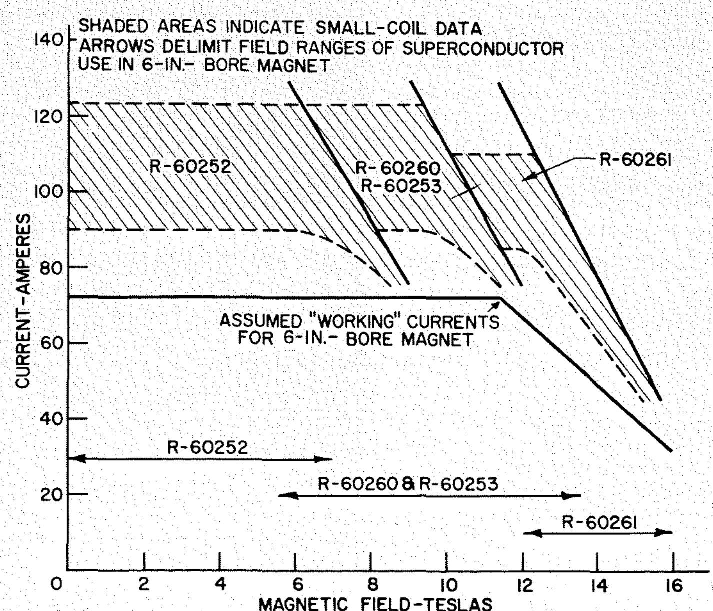

TABLE I—Summary of Computer Codes (All RCA 601 Fortran II)

Code Name	Fields	Inductance	Axial Forces	Hoop Forces	Mechanical Design	Notes
ELLIE	X	X	X	—	—	Up to 40 coils or modules (adapted from Garrett's Elliptical Integral Code).
MODDER	X	—	—	—	—	Up to 40 modules; direct geometry input, output is Fabry parameters and module corner fields.
KOPARC	X	—	—	—	—	Grid of input parameters for simple magnet; output is Fabry parameters and maximum winding fields.
TUPART	X	—	—	—	—	Grid of input parameters for two-part magnets and split pairs; output is Fabry parameters, maximum winding fields, and bore fields.
MODRLX	X	—	—	X	—	MODDER modified to current relaxation and to give hoop stresses.
FFC	—	—	—	—	X	Stresses and deflections for filleted flanges of modules.
FCC	—	—	—	—	X	Stresses and deflections for filleted cylinders of modules.
SSB	—	—	—	—	X	Flange thickness necessary for maximum stress requirements.
FAPP	—	—	—	—	X	Stresses and deflection of flange with radially varying load.
SIMPLE	X	—	—	—	—	Geometry and cost breakdown for simple magnets from bore, field, and homogeneity requirements.
WINDY	X	—	—	—	—	Geometry for split pairs from field, bore, and separation requirements.

composite curve in Fig. 5. The factor added to the areas per turn for the mechanical structure is re-estimated, based on the resultant axial forces. The maximum hoop stress in a given module array may indicate the need for a change in substrate thickness. Depending upon the calculated values, a change in the size and shape of the module may speed relaxation. Thus the data for the next iteration are generated. Module parameters at two stages of this relaxation process for the NASA 6-inch bore, 150-kG magnet are illustrated in Fig. 7.

Iteration is performed through the relaxation loop until the results are self-consistent, i.e., the assumed currents do not exceed those dictated by the current characteristics for the highest field in each module; the maximum hoop stress criterion is not violated, and the factor for structure is deemed sufficient for containment of the calculated axial forces. In addition, the self-consistent design must produce the required central field and, if required, the field homogeneity; if it does not, the over-all dimensions of the magnet must be changed and the process repeated.

Introduction of Explicit Mechanical Structure

At this point in the relaxation method, the saving in computer time effected by combining the space required for module structure with the effective area per turn of the conductor must be sacrificed to the necessity of obtaining the exact mechanical design of the flanges and cylinders of the modules. For the specific geometry of the subject magnet, computer codes (based on the work done by J. File, Forrestal Research Center of Princeton University, consultant to RCA on mechanical design) were written to use the axial electromagnetic forces generated by ELLIE for determining the dimensions of the flanges, the cylinders, and the resulting deflections for a given, maximum design stress. (In the present case, the design stress is 75,000 psi for 304 stainless steel at liquid helium.) One code, SSB, approximates the flanges as *s*imply *s*upported *b*eams. Another, FFC (*f*illeted *f*lange *c*ode), calculates the necessary reinforcing fillets at the point between the flange and cylinder of each module, using the approximation of a beam clamped at the filleted end and simply supported at the other. Among the other codes written for mechanical design assistance was FAPP (*F*ile *a*nnular *p*late *p*rogram), which considers the exact case of a plate in the form of an annulus, simply supported at both edges with a radially variable load.

CONCLUSIONS

Although the approximate design of simple solenoids can be done with graphs, tables, and hand calculations, the detailed information required for the design of superconductive magnets and magnet systems, especially those of large size and producing high fields, can only be acquired with the aid of specialized computer codes. Such programs for the RCA 601 computer located at the RCA Laboratories, Princeton, have been written and used by RCA Superconductive Products over the past two years. The basic codes, adapted from the work of others and programmed from original sources, have concentrated on the calculation of the electromagnetic fields, the forces, and the inductance of the magnet system once the design had been made. Later coding has been directed toward automatic design from specified geometry, field, and homogeneity requirements, all within the empirically derived characteristics of the superconductor to be used. Also, special purpose and one-time codes have been written as the occasion demanded.

More work is now being done on automatic design codes, with an immediate goal being the Garrett 6th Order Coil configurations. Another high priority project currently under way is the analysis of RCA Superconductive Productive programs for feasibility of their subsequent adaptation to the RCA Spectra 70/45 remote consoles, which should be available in early 1967.

ACKNOWLEDGEMENTS

The author wishes to express his appreciation to T. M. Stiller and his staff at the RCA 601 computer facility, RCA Laboratories, Princeton, N. J. Also, special recognition should be given to J. R. Golden and J. C. Durkin for mathematical and computer assistance.

BIBLIOGRAPHY

1. H. Brechna and H. S. Gordon, eds., *Proceedings of the International Symposium on Magnet Technology*, "Section I—Magnet Technology and Field Analysis." Stanford Linear Accelerator Center, Stanford University, Stanford, Calif., CONF-650922, UC-28 Particle Accelerators and High-Voltage Machines (TID-4500, 44th Ed.), Clearinghouse for Federal Scientific and Technical Information, National Bureau of Standards, U.S. Dept. of Commerce, Springfield, Va.
2. W. R. Smythe, *Static and Dynamic Electricity*, McGraw-Hill Book Co., Inc., New York, 1950, p. 276 ff.
3. T. R. Lyle, "On Circular Filaments or Circular Magnetic Shells, Equivalent to Circular Coils, and on the Equivalent Radius of a Coil," *Philosophical Magazine*, Series B, Vol. 3, pp. 310-329 (1902).
4. N. B. Alexander and A. C. Downing, *Tables for a Semi-Infinite Current Sheet*, Oak Ridge Technical Report, ORNL-2828 (1959).
5. G. V. Brown, L. Flax, E. C. Itean, and J. C. Laurence, *Axial and Radial Magnetic Fields of Thick, Finite-Length Solenoids*, NASA TR R-170 (1963).
6. R. W. Boom and R. S. Livingston, "Superconducting Solenoids," *Proceedings of the IRE*, Vol. 50, No. 3, pp. 274-285, 1962.
7. "Procedure for Electromagnetic Design of Superconductive Magnets," *RCA Application Note SPAN-5085*, RCA, Harrison, N.J.
8. P. A. Thompson, "Magnet Design Aid," *ST-3100*, 1-66, Superconductive Products, RCA Electronic Components and Devices, Harrison, N.J.
9. M. W. Garrett, "Calculation of Fields, Forces, and Mutual Inductances of Current Systems by Elliptical Integrals," *Jour. Applied Physics*, Vol. 34, No. 9, pp. 2567-2573, (1963).
10. M. W. Garrett, *Computer Programs Using Zonal Harmonics for Magnetic Properties of Current Systems*, Oak Ridge National Laboratory Report, ORNL-3318, (1962).
11. W. F. Gauster, "Fitting of Magnetic Fields Over Specified Volumes"—*Thermonuclear Project Semiannual Report for Period Ending January 31, 1960*, Oak Ridge National Laboratory, ORNL-2926, pp. 84-91, (1960).
12. M. W. Garrett, "Axially Symmetric Systems for Generating and Measuring Magnetic Fields, Part I," Jour. Applied Physics Vol. 22, No. 9, pp. 1091-1107, (1951).
13. E. R. Schrader, "Design and Construction of Nb_3Sn Superconductive Magnets," RCA ENGINEER, *this issue*.
14. E. R. Schrader and P. A. Thompson, "Use of Superconductors with Varied Characteristics for Optimized Design of Large-Bore, High-Field Magnets," *IEEE Transactions on Magnetics*, MAG-2, No. 3, pp. 311-314, (1966).
15. Lewis Research Center, NASA, Cleveland, Ohio, Contract NAS 3-7101.

DESIGN AND CONSTRUCTION OF Nb_3Sn SUPERCONDUCTIVE MAGNETS

Superconductive magnets, like conventional copper magnets, develop magnetic fields by current flow in a conductor. However, the use of liquid helium to achieve zero resistance at a temperature of 4.2°K makes the technology of superconductive-magnets design different from that of conventional magnets in which power is dissipated. This technology is discussed in this paper along with an example of the construction of a superconductive magnet system designed to achieve 150 kG in a 6-inch bore.

E. R. SCHRADER, Ldr.
Magnet Design and Development
Electronic Components and Devices
Harrison, N. J.

A MAGNETIC field exists around any conductor which carries current. By changing the orientation of the conductor in space, the geometry of the magnetic field can be varied. For example, if the wire is wound into a solenoid having contiguous, close-packed loops, the axial magnetic-field components concentrate in the center of the loops and create a relatively higher field than for most other winding configurations. Variations of such solenoids are used in a wide range of magnetic devices from doorbell buzzers to highly precise electromagnets for scientific research.

If the current density in the windings cross section is equal, the central magnetic field of a solenoid is the same whether there are a thousand turns which carry one ampere or one turn which carries a thousand amperes. When field strength is considered as a function of amperes - per - square - centimeter of winding cross-section area, anything which reduces the actual conductor area or current level is detrimental to the development of maximum field. A serious, practical limitation to the current density of conventional copper-wound solenoids is the space required within the windings for a coolant to remove the Joulean heat.

For the development of magnetic fields up to 20 kG, the use of high-permeability iron cores intensifies and shapes the field developed by the current in the copper windings. Existing, large-dimension magnets for cyclotrons and bubble-chambers require tremendous quantities of iron. However, 20 kG is no longer considered a high field. Applications are developing for the highest possible fields attainable, e.g., magnetic fields of over 200 kG have been developed at MIT, and fields which exceed a megagauss are attainable with the aid of pulsed techniques. In the development of these high fields, iron is only of minor use because it saturates at low fields. Therefore only air-core-type solenoids are usable for high fields and unless superconductors are used, the problems associated with high power losses are a significant part of magnet design.

Final manuscript received October 27, 1966.
This paper was prepared in conjunction with the work done under Contract NAS 3 -7101, NAS 3-7928.

The decreasing cost of cryogens has encouraged attempts to reduce power losses by lowering conductor temperatures. Although this technique has been successful through the use of liquid neon (27.2°K) or by liquid hydrogen (20.4°K), copper magnets utilizing such coolants are only specialized extensions of the water-cooled magnets, and have approximately the same limitations.

During the last five years, magnet technology has been revolutionized by the use of superconductors. With a superconductor, the formation of the magnetic field by current in a wound conductor is essentially the same as with a copper magnet. However, because of the zero-resistance characteristic of the superconductor, engineering problems associated with power dissipation are virtually eliminated. Zero resistance is achieved when the temperature of the superconductor windings is reduced to a value below the transition temperature of the superconductor. The transition temperature is the temperature at which a superconductive material changes from a conventional conductor having a finite resistance to a superconductor having virtually zero resistance. For niobium stannide, the transition temperature is above the boiling point of liquid helium (4.2°K at atmospheric pressure). Thus, the problems related to the handling and to the cost of megawatts of power for a conventionally wound copper magnet are traded for those of liquid helium and its associated dewars. The decline in the cost of liquid helium ($3.50 or less per liter) and the relatively high efficiency of the dewars (approximately 1% per day loss of liquid helium) make the superconductive magnet attractive for today's applications.

This paper specifically discusses the technology associated with the use of niobium-tin (Nb_3Sn) in magnets. Niobium tin is one of three "hard" superconductors suitable for high-field magnet fabrication. The other two, niobium-zirconium and niobium-titanium, are alloys which are superconductive for more than one ratio of their constituent elements. Niobium tin, an intermetallic compound, derives the desired superconductive properties with a relatively rigid stoichiometry. Niobium tin carries useful currents in developing fields in the 200-kG range compared with niobium zirconium which is useful in magnets developing fields up to 60 kG, and niobium titanium used in magnets developing fields up to 90 kG.

Niobium-zirconium wire was the first superconductor extensively used to make commercial solenoids. Recently, niobium-tin and niobium-titanium have also

EDWARD R. SCHRADER received his B.A. degree in Physics from Columbia University in 1950 and his M.S. degree in Physics from the Polytechnic Institute of Brooklyn in 1953. Mr. Schrader was associated with the American Museum of Natural History in oceanographic exploration in 1950 and was subsequently employed as a project engineer in aircraft instrument research by the Sperry Gyroscope Company. In 1954 he joined the RCA Tube Division in Harrison, New Jersey, where he studied the effects of tube materials upon tube performance. This included a two-year period during which he served as Senior Project Engineer on a Bureau of Ships contract on the kinetics of tube deterioration. On July 1, 1962, Mr. Schrader was appointed to head the Magnet and Measurements Group of the newly established RCA Superconductor Materials and Devices Laboratory located in Princeton, New Jersey. He has been the Senior Project Engineer on four contracts with the Lewis Research Center, NASA, in which studies were made of the feasibility of designing and constructing large-bore, high-field superconductive magnets. Mr. Schrader was responsible for the design and development of the RCA 107-kilogauss, 1-inch bore superconductive magnet. During the past three years he has made significant contributions to the scientific literature in high-field superconductive magnets. Mr. Schrader is a member of Sigma Xi, the American Physical Society, and a Senior Member of the Institute of Electrical and Electronic Engineers. He is now an Engineering Leader and has overall responsibility for all magnet design and development activities in the RCA Superconductive Devices Development Department at Harrison, New Jersey.

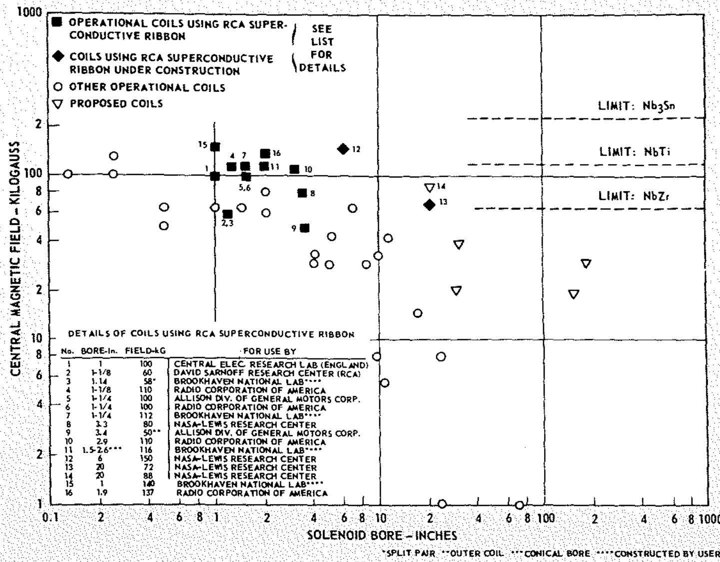

No.	BORE-In.	FIELD-kG	FOR USE BY
1	1	100	CENTRAL ELEC. RESEARCH LAB (ENGLAND)
2	1-1/8	60	DAVID SARNOFF RESEARCH CENTER (RCA)
3	1.14	58*	BROOKHAVEN NATIONAL LAB****
4	1-1/8	110	RADIO CORPORATION OF AMERICA
5	1-1/4	100	ALLISON DIV. OF GENERAL MOTORS CORP.
6	1-1/4	100	RADIO CORPORATION OF AMERICA
7	1-1/4	112	BROOKHAVEN NATIONAL LAB****
8	3.3	80	NASA-LEWIS RESEARCH CENTER
9	3.4	50**	ALLISON DIV. OF GENERAL MOTORS CORP.
10	2.9	110	RADIO CORPORATION OF AMERICA
11	1.5-2.6***	116	BROOKHAVEN NATIONAL LAB****
12	6	150	NASA-LEWIS RESEARCH CENTER
13	20	72	NASA-LEWIS RESEARCH CENTER
14	20	88	NASA-LEWIS RESEARCH CENTER
15	1	140	BROOKHAVEN NATIONAL LAB****
16	1.9	137	RADIO CORPORATION OF AMERICA

*SPLIT PAIR **OUTER COIL ***CONICAL BORE ****CONSTRUCTED BY USER

Fig. 1—Central magnetic field vs. superconductive solenoid bore for some existing and proposed magnets.

gained commercial importance. Fig. 1 shows the bore-field relationships and ranges for some present and some proposed magnets.

REQUIREMENTS FOR MAGNET DESIGN

The requirements for the design of a practical magnet are as follows:

1) A mathematical method of accurately calculating the magnet fields and forces in space as a function of the current density and the geometry of the windings
2) Data on the current-carrying capacity of the conductors in magnetic fields and under stress
3) Means of rigidly holding the conductors to the desired geometry and of providing access for electrical leads and cooling media.

These requirements are essentially the same for any air-core electromagnet whether superconductive or conventional copper. The first requirement is discussed in a paper by P. A. Thompson.[1] Although the mathematical methods make no distinction between superconductive and conventional magnets, a measurable diamagnetic property in superconductors "shields" and partially distorts the magnetic field in the solenoid bore. However, except for magnets which are to be designed for very homogeneous fields, this effect is minor and is usually neglected.

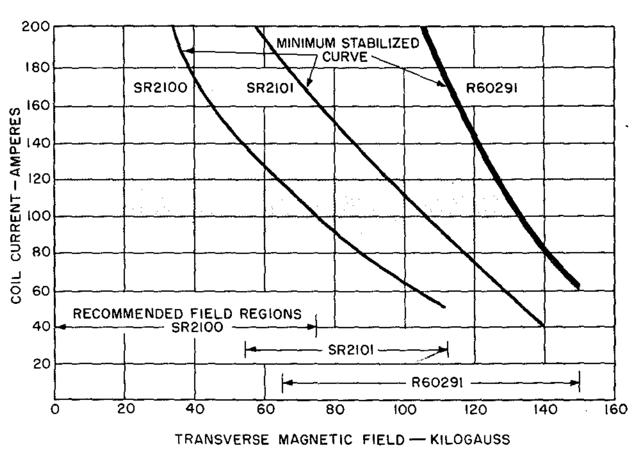

Fig. 2—Transverse magnetic field — critical current characteristics of three commercial Nb_3Sn vapor—deposited ribbons with shaded area illustrating typical coil performance.

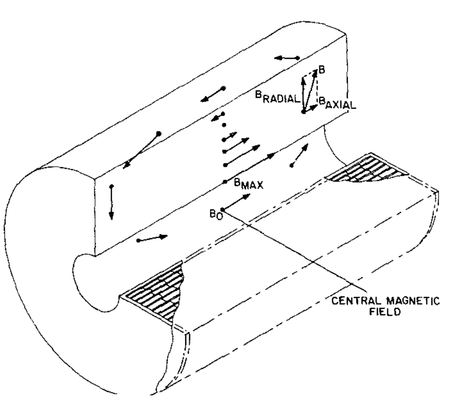

Fig. 3—Cutaway view of a solenoid illustrating typical magnetic field directions.

The second requirement has two parts: the first part concerns the reliable data of the current-carrying capacity of the conductor. However, except for a special class of superconductors which is characterized by the intimate presence of a large amount of high-conductivity normal metal and is termed *stabilized*, the maximum current-carrying capacity is not always easily predictable. Instability in superconductors of this type is the product of the same mechanism which produces the high current-carrying capability of the device. This mechanism consists of various types of lattice-defects which "pin" the magnetic flux in place until externally added energy causes the flux to avalanche. The probability of uncontrolled flux movements which prematurely cause a superconductive magnet to go normal, causes an effective reduction of the current-carrying capacity of the superconductor. This current reduction is dependent in an as yet unknown way on the thermal and electromagnetic environment of the magnet. These effects are generally most severe in the low-field region of the magnet volume and in magnets which are physically large.

To date, the practice has been to set the design-current of the superconductor at least as low as experience has shown it to be reproducible. Fig. 2 is a composite plot of the critical characteristics of the commercial, RCA, vapor-deposited Nb_3Sn ribbons. The expected critical current in supermagnets in low fields is shown by the shaded regions. Because all solenoids built until now have exhibited critical currents within these shaded regions, the design-current is generally assumed no higher than the lowest (90 amperes) in the shaded region. The critical current-drop in the high-field regions is a natural and predictable property of superconductors. To permit the use of a single value of current (and therefore one power supply) in a series-wound magnet, each of the three conductors described in Fig. 2 is wound into a specific portion of the solenoid which will have a field range matching the specific design limitations of the conductor. A discussion of the conductor-design details is given in other papers of this issue.[3,4]

This part of the second requirement concerns the effect of mechanical stress on the current-carrying capacity of the superconductor. The force F on any conductor-carrying current I in a magnetic field B is expressed vectorially:

$$\mathbf{F} = \mathbf{I} \times \mathbf{B} \qquad (1)$$

where $\mathbf{F}$ is in newtons, $\mathbf{I}$ is in amperes, and $\mathbf{B}$ is in teslas (i.e., webers/cm^2).

In a simple, solenoid cross section, Fig. 3, the direction of the magnetic-flux density creates a compressive force which squeezes the windings toward the zero-magnetic field point of the solenoid. The force on each turn can be divided into two components, expressed by:

$$dF_z = IdB_r$$
$$dF_r = IdB_z \qquad (2)$$

where B_r is the radial field component, B_z is the axial field component, F_r is the radial force component, and F_z is the axial force component.

In this simple solenoid, the axial components add inwardly from winding to winding on each end of the magnet, and are neutralized at the central plane. The resultant radial force is directed outward and must be retained by some sort of outer ring, or else each winding must be self-supporting. Inasmuch as Nb_3Sn is inherently brittle and weak in tension, it cannot be allowed to stretch. Therefore, the over-all Nb_3Sn conductor must be structurally strong enough to withstand these radial, or "hoop", forces.

The third magnet-design requirement is the practical one of providing a structure to define the windings geometry, and to furnish any necessary structural support, an access to the electrical leads, and an entry for a coolant. For a simple, low-field coil, the structure is a winding bobbin with slots in one flange for the power leads. As magnets become larger and develop higher fields, more provisions must be made for liquid helium and lead-access as well as for an internal structure to relieve severe axial forces. As the volume of the internal strength-bearing structure becomes a significant fraction of the windings volume, it reduces effective magnet current density. This condition, added to problems associated with differential thermal contraction, materials embrittlement at 4.2°K, and unwanted ferromagnetic effects of many materials, makes the structural design of large magnets far from trivial.

MAGNET DESIGN AND CONSTRUCTION WITH Nb_3Sn VAPOR-DEPOSITED RIBBON

Magnet design is usually determined by the need for a magnetic-field magnitude and geometry within a given working volume which, in most cases, is the solenoid bore. When radial access to the working volume is important, such as for radial entry of accelerated nuclear particles into a bubble chamber, it is necessary to divide the solenoid into two parts to form a "split pair". However, for the purposes of this paper, the design procedures can be illustrated by the simple solenoid.

The mathematical procedure is described in another paper in this issue.[1] In essence, approximate values for the current density expected in the windings cross section are assumed for the calculation of a solenoid geometry which will create the required field. Radial and axial forces are then calculated to determine the requirements for conductor and magnet-structure strength and geometry. The deviations between the resulting calculated current density and that originally assumed, determine the degree of further iteration necessary to make the conductor and the magnet-structure design consistent with the field and bore requirements.[5]

SMALL MAGNETS

As an example of known parameters, an enlarged typical winding cross section of a small (i.e., 100-kG, 1-inch-bore) solenoid is shown in Fig. 4. It illustrates layers of ribbon 0.093 inch wide with 0.007 inch spacing to give a winding pitch of 0.100 inch.

Insulating interleaving composed of laminated Mylar*-copper-Mylar sheets is wound between each of the layers. (The copper stabilizes magnet operation.) The shaded portion in the illustration is the effective area of one turn, equal to the total winding cross-section area divided by the number of turns. This area-per-turn can be approximated by addition of the individual contributions as follows:

Ribbon typical of SR2100:	
Substrate	1.8 mils
Nb_3Sn, 2 sides	0.5 mil
Silver, 2 sides	1.9 mils
TOTAL	4.2 mils
Interleaving:	
Mylar, 2 pieces	0.5 mil
Copper	0.8 mil
TOTAL	1.3 mils
Other factors (by experience):	
Interleaving wrinkles, encapsulating grease, shorting strips, etc. (averaged) *TOTAL*	0.4 mil
TOTAL LAYER THICKNESS $(4.2 + 1.3 + 0.4) = 5.9$ *mils*	

Effective area-per-turn:

$$A_e = 5.9 \times 100 = 590 \text{ mils}^2$$
$$= 3.8 \times 10^{-3} \text{ cm}^2$$

If a current of 90 amperes per turn is assumed from Fig. 2, the current density J_w in the windings is expressed as:

$$J_w = \frac{I}{A_e} = \frac{90}{3.8 \times 10^{-3}} = 23{,}700 \text{ A/cm}^2 \qquad (3)$$

* *Registered trademark of E. I. DuPont de Nemours.*

This current-density can be considered as typical of the small-bore, high-field magnets fabricated with RCA vapor-deposited Nb_3Sn ribbon. Because the current and area-per-turn in this case are known from experience, the current-density value can be used with assurance to calculate magnet dimensions.

The hoop stress is found by integrating the radial force IdB_z and calculating the stresses in the ribbon substrate which result from this force. Stainless steel-type substrates have a tensile strength of over 150,000 psi at 4.2°K. When the device is a typical small magnet, the hoop stress σ_H on the inner turns of a 100-kG (10-tesla) solenoid with a 1-inch inner-winding diameter is given by:

$$\sigma_H = \frac{IB_z r}{A_s} = \frac{(90)(10)(0.0127)}{(1.04)(10^{-7})}$$
$$= 1.1 \times 10^8 \text{ N/m}^2$$
$$= 15{,}900 \text{ psi}$$

where I = current through the conductor, (assumed as 90 amperes), B_z = axial field at the conductor in teslas (1T = 10,000 G), r = radius of the conductor in meters, and A_s = cross-section area of the strength-bearing members in square meters. (For 0.0018×0.090-inch substrate, this area is 1.04×10^{-7} square meters.)

This value is considerably lower than the 150,000-psi minimum tensile strength of a stainless-steel type substrate and shows that the substrate thickness for the ribbons used in the 100-kG, 1-inch bore type of magnet is more than adequate to contain hoop (radial) stresses. For simplified stress calculations, Fig. 5 shows a plot of hoop force for a 100-ampere conductor as a parameter in a graph of the field at a turn vs. the turn diameter.

Axial stresses, on the other hand, are not so easily analyzed, and experience must be relied on to determine fabrication limits. Equation 2 is a differential expression which is used to calculate the axial force on a length of current-carrying conductor by integration of the radial component of the field over the conductor length. For example, for a single, 90-ampere turn in a radial-field component of approximately 70 kG (near the ends of the solenoid where the field lines

Fig. 4—Typical winding cross section—simple solenoid.

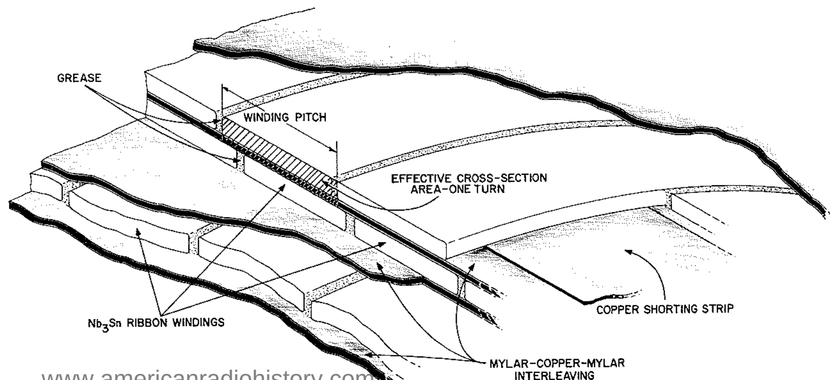

bend around) at a 1-inch diameter, the axial force F_z is given by:

$$F_z = (90\text{A})(7\text{T})(0.08\text{m}) = 51 \text{ newtons} = 11.4 \text{ lbs}$$

Although an axial force of 11.4 pounds is not large, this force is exerted by the edge of one turn on the adjacent turn. This adjacent turn also has some axial force which adds to the one just calculated, and the result is a progressive addition of the forces of many turns. These axial forces are eventually neutralized by equal forces from the opposite end of the solenoid. However, the internal buildup of these forces can be considerable, as will be shown in a later example.

Axial forces are controlled by avoidance of any large, local stress buildup. The coils are wound with 1.3 to 1.5 kilograms of tension on the ribbon to form a tightly packed mass. In addition, a completed layer is partially impregnated with high-thermal-conductivity grease which hardens at liquid helium temperatures. The net effect is that the windings partially act as a homogeneous mass.

The total axial force at the midplane of the solenoid can be estimated by numerical integration of IdB_r at each radius of interest. For magnets which have large enough size and developed field to make the axial forces a serious problem, computer methods are used.[1]

LARGE MAGNETS

At some range of magnet-field and bore-diameter, and depending upon the characteristics of the superconductive ribbon or wire, magnet design is relatively complex because of the strong interrelation of parameters. An example of a simple magnet is the 110-kG, 2.9-inch-bore solenoid where axial and hoop forces are minor and need not be considered. However, an example of a complex magnet is the 6-inch-bore, 150-kG magnet now under construction for the Lewis Research Center, NASA, Cleveland, Ohio.[2] In magnets of this magnitude, the mechanical design requires much more engineering effort than do the simple magnets.

Fig. 6—Relief of axial-stress buildup by force-bearing flanges in a complex solenoid.

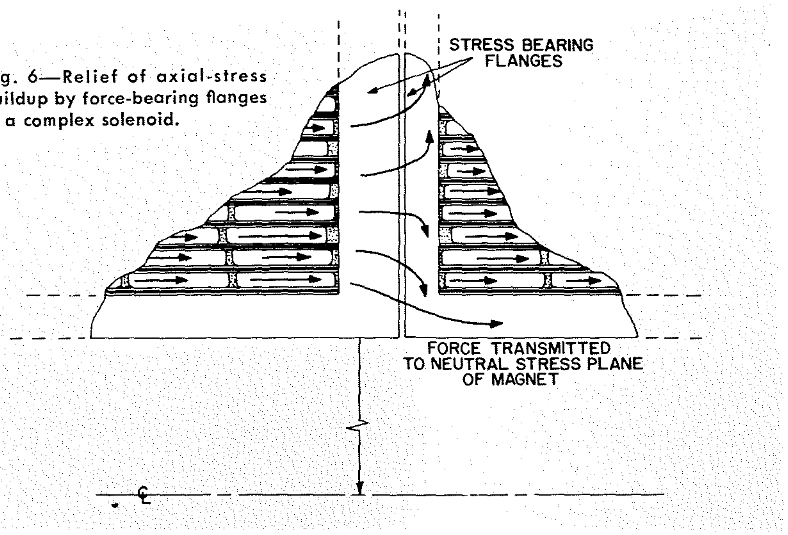

The initial calculations of the ampere-turns necessary to develop 150 kG in a 6-inch bore indicate that reasonably high current-density in the windings is necessary. This requirement practically eliminates the use of the more stable superconductive ribbon which has a low ($\approx$5,000 A/cm^2) current-density. However, with large volumes of high current density windings, current instability occurs, and magnets go normal at lower currents than are expected for the smaller magnets discussed above. A reproducible operating current is based upon extrapolations from the best available experience. Thus for the 6-inch-bore, 150-kG magnet, four different current levels were chosen between 72 amperes in the lower field regions (as against 90 for smaller magnets) and 30 amperes in the highest field region of the magnet.

Fig. 5—Hoop force (lbs. and kgs) on a magnet turn carrying 100 amperes as a function of the turn diameter and the axial magnetic field component at the turn.

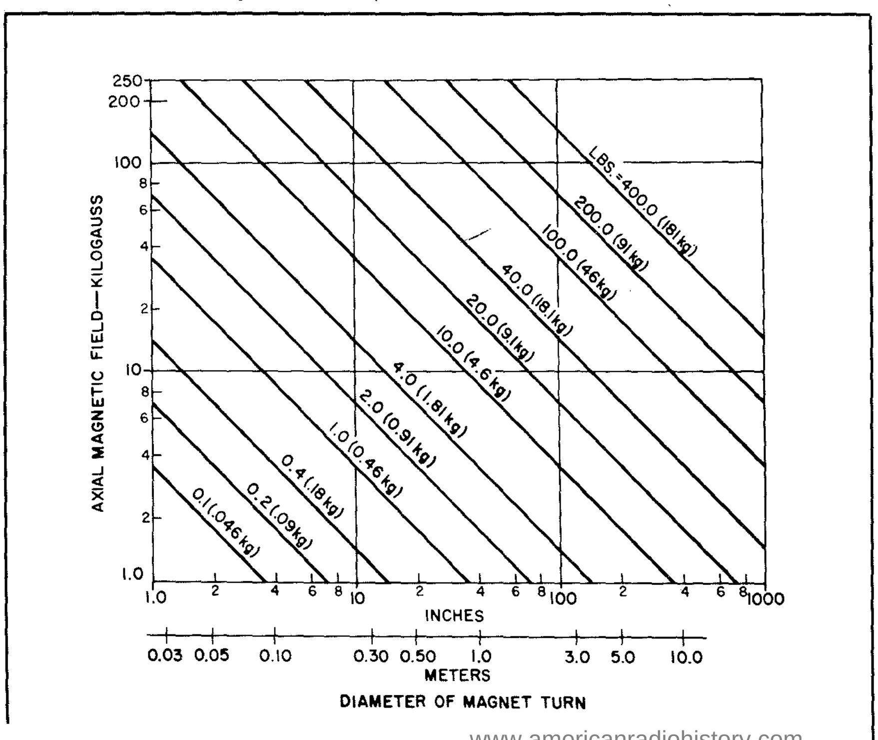

The solution of Eq. 4 yields a substrate thickness of 0.0025 inch to support a hoop stress in a conductor carrying 30 amperes in an axial field of 150 kG (15 teslas), at a radius of 3 inches (0.076 meter). Thus, the current density of the inner windings is lowered because of the extra cross-sectional substrate area necessary.

A similar loss of current-density occurs because of the axial forces. Somewhere within the windings off the central plane, there are high radial-field components which in some cases cover significant portions of the cross section. As an example, suppose the average radial-field component over a square inch of the windings cross section is 80 kG and that the conductor in that region carries 72 amperes around a turn 1 meter in circumference. For conventional fabrication techniques, these values correspond to a current density of 19,000 A/cm^2. The total current in the 1-inch cross section is then 19,000 A/cm^2 $\times$ 6.45 cm^2 = 122,000 A. The product of $\int \mathbf{I} \times \mathbf{B}_r$ is then (122,000A)(8T)(1m) = 980,000 newtons, or 218,000 pounds of axial force. Thus, a windings annulus of one square inch of cross section and 1-meter circumference at a section of the magnet with an 80-kG radial-field component will press toward the central plane with a total force of over 100 tons.

This pressure build-up can be relieved

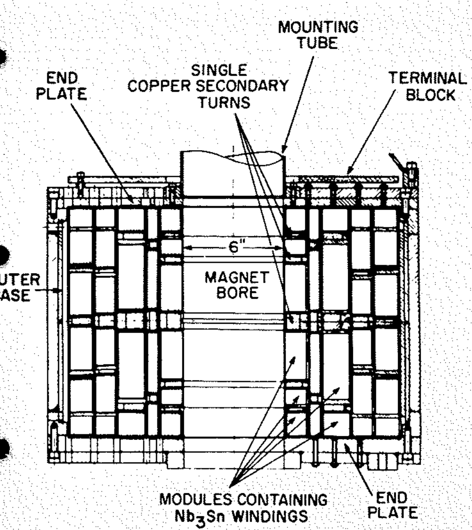

Fig. 7—Cross section view showing mechanical design of a 150-kilogauss magnet with a 6-inch bore.

by inserting stress-bearing flanges in the windings in such a way as to transmit the forces from one group of windings around adjacent windings to the neutral stress plane. Fig. 6 illustrates a cross section of windings which bear against a flange, something not required in the simple solenoid shown in Fig. 4. But the presence of these stress-bearing flanges reduces the space which would have been used for windings in a simple solenoid, and consequently results in a reduction in effective current density.

Other factors, unique to large magnets, account for a further loss in current density. One of the most important is that of magnet protection when the device "goes normal." The creation of a magnetic field requires an energy input W (exclusive of any dissipative losses) expressed as:

$$W = \frac{1}{\mu_o} \int_v B^2 dv \qquad (5)$$

where μ_o is the permeability of a vacuum $= 4\pi \times 10^{-7}$, and v is the volume.

Large, high-field magnets store considerable energy in the magnetic field. If this energy is uncontrollably released as the field suddenly collapses when the magnet goes normal, it is possible that local heating and arcing will occur and damage the magnet. Various methods are used to minimize this problem. For example, the energy is either partially removed from the magnet by dumping it into external secondary windings or resistors, or else local concentrations of the energy are avoided by provision of distributed dissipation within the magnet. Generally, if the energy can be distributed equally, the heat capacity of the magnet structure is sufficient to absorb the energy of the magnetic field with only mild temperature increases.

In the 6-inch-bore, 150-kG magnet under construction, the protection is provided by the combined contribution of:

1) silver plate on the ribbon,
2) shorting strips of copper foil across each layer or ribbon,
3) interleaves of Mylar-copper-Mylar sheets with the copper shorted upon itself to form shorted secondaries highly coupled with the superconductive primary and,
4) secondaries made of massive copper shorted turns, placed between the modules and surrounding the magnet; the shorted turns between modules occupy volume within the windings and a loss of over-all magnet current density results.

Fabrication techniques, which are only briefly mentioned here, also contribute to a decrease in current density. In large, complex magnets, it is necessary to provide access to the interior of the windings for leads, probes, and liquid helium. In the 150-kG NASA magnet, there are about 200 current and signal leads which exit from the top flange. The presence of so many leads and the magnetic forces on those which carry large currents, require volume for insulation and the cooling of resistive portions.

These factors which make large-bore, high-field superconductive magnets different from simple solenoids reduce the effective average magnet current density by approximately a factor of two. However, this resultant 10 kA/cm^2 of current density is considerably more (2 to 3 times) than that achieved in the simpler, large, low-field magnets wound with stable superconductors.

Fig. 7 shows a cross section diagram of the 6-inch bore, 150-kG magnet which contains the features previously discussed; the modules and the copper secondaries are labeled.

MAGNET DESIGN VARIATIONS

From the viewpoint of general mathematical design, the current density is assumed to be uniform throughout the actual magnet volume containing the windings of superconductive ribbon. In the case of the 6-inch-bore, 150-kG NASA magnet, the current density is assumed to be finite and uniform within the windings of each module and to be zero within the support structure. The actual current distribution, which is non-uniform, causes perturbations in the magnetic-field distribution in the bore. The degree of these perturbations determines the homogeneity of the magnetic field. Some scientific experiments which use magnetic fields, require a specified degree of homogeneity, usually given as a maximum variation in magnetic field within some specific volume of interest in the magnet bore. When the homogeneity requirements become severe, the magnet must be designed to minimize the discrete character of the windings current density. For magnets requiring very high homogeneity such as those used in Nuclear Magnetic Resonance (NMR) work, even the discrete geometry of the superconductive ribbon is a problem which must be considered in design and fabrication.

Magnet-fabrication techniques other than the layer-winding method shown in Fig. 4 can be used. The reversal of the winding pitch at the end of each layer can set up stresses in wide ribbon that is layer-wound. For instance, it would not be practical to layer-wind ½-inch-wide ribbon on a small-diameter bobbin. Therefore, wide-ribbon conductors are usually wound in the form of "pancakes" and stacked to form a magnet. The mechanical design of the support structure then changes to permit access for the electrical leads and liquid helium and to provide axial stress-bearing members where necessary. The radial dimensions of each pancake compared to the axial length (ribbon width) also determine whether special precautions are necessary in winding each pancake under tension to avoid slippage of the turns.

This paper has described the conventional solenoid geometry where a magnetic field is developed within the center of the windings. Other types of field geometries require modified types of windings. For instance, magnetohydrodynamics (MHD) apparatus requires a magnetic field directed at right angles to ionized gas flowing in a pipe. This requirement is usually met by distortion of the windings into "saddle"-shapes around the pipe. Other windings modifications are designed to yield very high magnetic-field gradients to enable high-energy-charged accelerator beams to be focussed. The design techniques needed for these applications vary, but essentially they are based upon the need for current density, adequate cooling, stability, safety, and strength. Each magnet application stresses these features differently, e.g., a magnet which is to be used around a potentially explosive liquid-hydrogen bubble chamber must be exceptionally stable and safe; a magnet needed for the highest possible field in the smallest volume will stress current-density.

BIBLIOGRAPHY

1. P. A. Thompson, "Computer Calculations for the Design of Large, High-Field Superconductive Magnets", RCA ENGINEER, *this issue.*
2. Contracts NAS3—7101 and 3—7928, with NASA, Lewis Research Center, Cleveland, Ohio.
3. H. C. Schindler, "Electromagnetic Performance of Nb_3Sn Vapor-Deposited Ribbon up to 200 Kilogauss", RCA ENGINEER, *this issue.*
4. F. R. Nyman, "Vapor Deposition of Nb_3Sn—A Versatile Process", RCA ENGINEER, this issue.
5. E. R. Schrader and P. A. Thompson, "Use of Superconductors With Varied Characteristics for Optimized Design of Large Bore, High Field Magnets", *IEEE Transaction on Magnetics,* MAG-2, No. 3, pp. 311-315, April, 1966.

IMPROVED STABILITY OF Nb_3Sn RIBBON BY PLATING OR CLADDING WITH A HIGH-CONDUCTIVITY METAL

Early superconductors, now known commercially as "soft superconductors," had very low critical fields. Even though they were able to carry hundreds of amperes in zero fields, these superconductors were unable to transmit superconductive current when wound into any configuration that concentrated a field which exceeded a few kilogauss. In the late 1950's and early 1960's, the development of high critical-field superconductors such as NbZr, NbTi, Nb_3Sn, and V_3GA led to renewed efforts for evolving high-field magnets. This paper discusses techniques for improving the stability of vapor-deposited Nb_3Sn ribbon by utilizing different substrates, and silverplating and copper cladding techniques.

H. C. SCHINDLER and R. J. GREEN
Electronic Components and Devices
Harrison, N.J.

RCA's outstanding contribution to high-field superconductivity is vapor-deposition of Nb_3Sn on a continuously moving platinum wire and ribbon substrate.[1]

The significance of this unique vapor-deposition process is that higher current-density values were obtained from the Nb_3Sn layers than those yielded by measurements on earlier materials. Fig. 1 illustrates a typical, critical-current I_c, critical-field H_c curve for the Nb_3Sn layer on the platinum substrate and, by vertical, horizontal, and oblique lines, indicates the order of current and field application on the short sample. The alphabetical listing indicates the successive tests. The envelope of this curve is expressed as:

$$J_c = \frac{\alpha}{B_o + H_o \sin\theta} \qquad (1)$$

as developed by Kim et al.[2] and modified by Cody et al.,[3] where J_c is the current density; α is the material constant proportional to the density of pinning centers; B_o is a measure of current density when the field- and the sample-current directions are parallel; θ is the angle between the field directions and the sample current; and H_o is the magnetic field (independent variable).

PROBLEMS WITH SUBSTRATES

Because of the high cost and the relatively low tensile strength of the platinum substrate, the deposition process was slightly altered to permit deposition of Nb_3Sn on other metallic substrates such as stainless-steel. But when short-sample, critical-current, critical-field measurements were made of these Nb_3Sn layers, it was difficult to obtain well defined envelope curves. Moreover, with the same test conditions, the tests listed below yielded different critical currents although they were spaced only a few minutes apart. Fig. 2 shows typical critical currents as a function of transverse field for vapor-deposited Nb_3Sn on a stainless steel substrate; the dots denote the critical currents.

1) *Tests a and b:* A background current was applied, and the background transverse field was varied.
2) *Tests c, d, and e:* A background transverse magnetic field was applied, and the current was increased.
3) *Test f:* The background transverse field and the current were varied simultaneously.

The lowest critical currents were obtained in Test f, followed in ascending order by Tests a, b, c, e, and d. The relative critical currents were interpreted as a measure of the instability of the Nb_3Sn layers to various testing techniques.

The failure of the critical currents to repeat consistently can be explained by P. W. Anderson's[4] theory which assumes

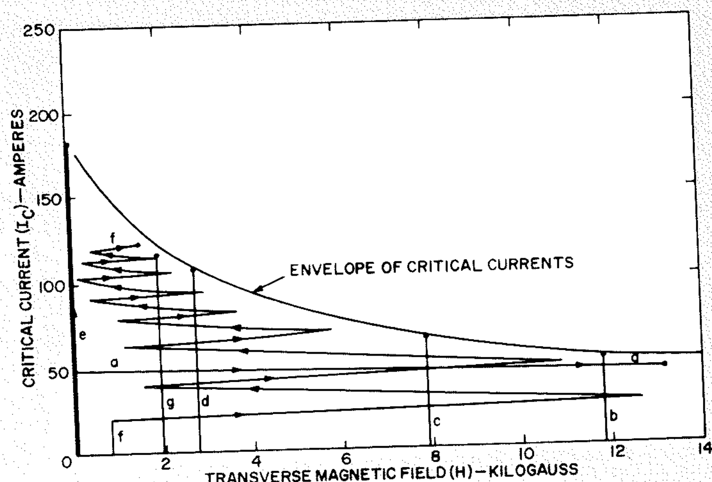

Fig. 1—Critical current vs. transverse magnetic field of Nb_3Sn deposited on a platinum substrate.

Final manuscript received October 26, 1966

HENRY C. SCHINDLER received his BChE degree from Cooper Union in 1955, and an M.S. degree in Physics from the Stevens Institute of Technology in 1959. He is currently working toward a Doctorate in Physics. Mr. Schindler was employed for four years at Picatinny Arsenal where he formulated and tested rockets and jet devices. Subsequently, he joined General Instrument Corporation as a senior engineer in developing semiconductor devices. In June 1962, Mr. Schindler was engaged by the RCA Superconductor Materials and Devices Laboratory of the Special Electronic Components Division at Princeton, N.J. He participated in the development of the niobium-tin vapor deposition process and studies the effect of the physical, chemical, and electrical properties of Nb_3Sn films with particular reference to superconductor device application. As a result of this work, he received the RCA Laboratory Outstanding Achievement Award. In April 1966, Mr. Schindler transferred to the RCA Superconductive Products Operation, EC&D, in Harrison, N.J. Since that time, he has been involved with the Development and electromagnetic evaluation of superconductive ribbons for magnet applications. Mr. Schindler is a member of the American Physical Society.

RALPH J. GREEN received his B.S. degree in Chemical Engineering from the Newark College of Engineering in 1946 and has done graduate work in chemistry, transistory physics, radio, and television. From 1946 to 1955, he did analytical and development work at Bart Laboratories and Westinghouse Electric Corp., where he specialized in the application of electroplating and electroforming processes to the fabrication of electronic components and devices. From 1955 to 1965, Mr. Green developed processes for fabricating solid state devices at Tung-Sol Electric Corp. and I.B.M., including glass passevating of silicon planar structures. In 1965, Mr. Green joined the RCA Electronic Components and Devices Division and is presently responsible for developing electrotype processes to stabilize superconductors by electrodeposition. He is a member of the Electrochemical Society and Elliott Camera Club, and holds three patents on electron-tube and solid-state devices.

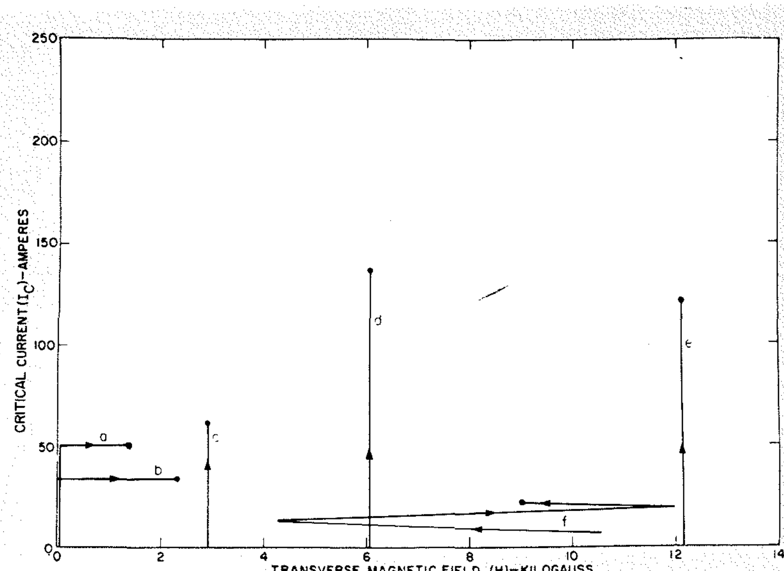

Fig. 2—Critical current vs. transverse magnetic field of Nb_3Sn deposited on a stainless steel substrate.

that the flux lines are pinned to the crystal structure by lattice defects and stressed by the Lorentz force, $J \times B$. When this force exceeds the flux-pinning forces of the crystal, the flux lines begin to creep and, subsequently, become a turbulent flow, generating heat which drives a local portion of the superconductor normal. Consequently, the stainless steel in parallel with the Nb_3Sn layer both of which are characterized by low thermal and electrical conductivity, creates more Joulean heat to support the transport current. Because the substrate is a poor thermal conductor, this heat cannot be readily dissipated internally, and so a normal front (the region separating the normal and the superconducting portions) propagates and drives the superconductor normal below the inherent critical current.

However, the use of the platinum substrate which has high electrical and thermal conductivity, permits local heat created by flux motion to be readily dissipated internally. Thus, the short sample is not driven normal by the heat generated by the flux motion, and the anticipated critical-current, critical-field envelope is obtained.

In terms of magnet performance, when this unstable Nb_3Sn-coated stainless steel ribbon is wound into a coil, the critical currents are as much as one or two orders of magnitude below that of the short-sample performance of the same ribbon. For example, at comparable fields, critical currents of 20 to 40 amperes are common in large coils, whereas, in short-sample tests, the ribbon supports currents which range from 200 to 300 amperes. Similar results have previously been reported with NbZr and NbTi superconductors.[5,6]

TECHNIQUES FOR QJASI-STABILIZATION OF SUPERCONDUCTIVE RIBBON

To reduce the tendency of the superconductor to revert to the normal state, the vapor-deposited Nb_3Sn is electroplated with such normal metals as copper or silver to provide a thermal sink and electrical conductor parallel to the superconductor. This plating improves the stability of the Nb_3Sn such that the critical currents obtained in magnets approach the short-sample performance more closely. The readily measurable factor which most significantly influences the stability of the ribbon is the electrical conductivity of the metal at liquid helium temperatures. For a particular thickness of normal-metal coating, this electrical conductivity is frequently expressed in terms of its resistance-ratio at room-to-helium temperatures. The resistivity ρ

of a normal metal which contains impurities and lattice defects is given as:

$$\rho = \rho_i + \rho_l \qquad (2)$$

where ρ_l is the resistivity caused by the thermal motion of the lattice and ρ_i is the resistivity caused by scattering waves. At low temperatures, ρ_i approaches zero, and $\rho = \rho_i$. At room temperatures, ρ_l is the dominant term. An indication of the impurity and imperfections of the plated metal can be expressed from the following ratio:

$$\frac{\rho \text{ (room temp)}}{\rho \text{ (liquid He temp)}} = \frac{\rho_{l(273°K)}}{\rho_{i(4°K)}}$$

The resistivity ρ and the resistance ratio $\rho_{l(273°K)}/\rho_{i(4°K)}$ of the metal plate are strongly dependent upon the type of plating and the plating rate. The lowest resistivity and largest resistivity ratio are obtained from very pure plating solutions applied at very low plating current densities. The use of low current density produces a purer plating and a more regular crystal growth. Fig. 3 illustrates the effect of plating current density on the metal-plate-resistance ratio, viz., that a two-fold increase in electrical conductance is obtained with the lower current densities. Other plating parameters such as metal concentration and plating temperatures are equally significant.

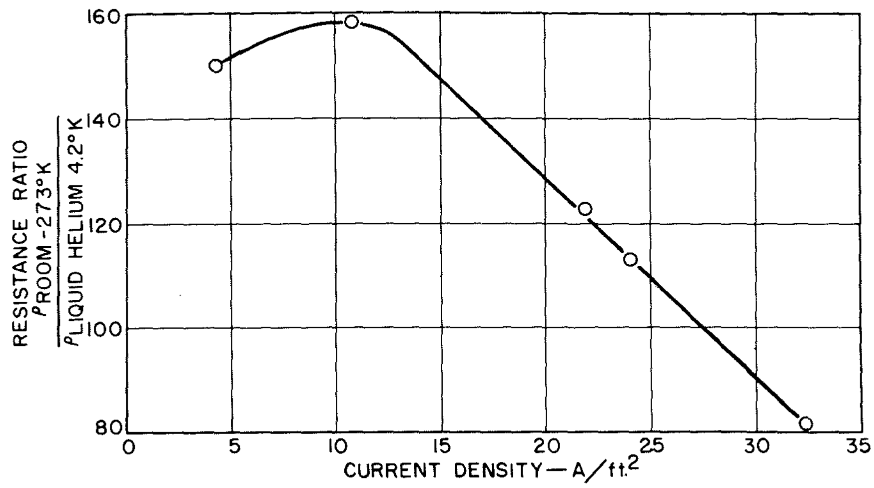

Fig. 3—Effect of plating current density on resistance ratio of silver.

The following particulars briefly describe the technique used to obtain high-resistance-ratio silver plating. The plating line is shown in Fig. 4.

Niobium-stannide-coated ribbon is silver plated in a continuous, high speed operation by automatic electroplating equipment. This equipment, which is similar to a conventional wire-plating machine, was designed by RCA engineers, and comprises a ventilated enclosure which contains two series of tanks and associated devices. The first series of tanks is used for surface cleaning, activating, and preplating the ribbon. In the second series of tanks, the ribbon is silver-plated to the desired layer thickness. Ribbon-lengths from a few hundred to several thousand meters are run through the equipment at relatively high speeds, with a plating current density uniformly distributed throughout the entire length of ribbon. The resultant silver deposit has a high resistance ratio. Plating yields ranging from 95% to 100% have been obtained consistently because of the carefully planned program of solution-control analysis, speed and current-density monitoring, continuous surveillance, testing, and mechanical maintenance.

Effect of normal metal plate resistance on short-sample stability is shown in Fig. 5. Curve A represents a plating of very high purity (high resistance ratio) having a sufficient thickness to produce the full H_c-I_c curve repeatedly. Regions B, C, and D represent platings of progressively lower resistance ratios having the same plating thickness.

TECHNIQUES FOR COMPLETE STABILIZATION OF SUPERCONDUCTOR RIBBON

The achievement of the upper current-field curve in Fig. 5, commonly referred to as the completely stabilized current-field characteristic, can be theoretically analyzed.[7] To prevent premature, normal zone propagation so that the full, short-sample, superconductor current can be achieved reliably under test conditions independent of current rate or field application, it is necessary that some of the Joulean heat produced by the temporary reversion to normal state be transferred to cryogenic baths. This transfer permits the superconductor to be cooled again below its critical temperature and to sub-

Fig. 4—Equipment for silver plating Nb_3Sn ribbon.

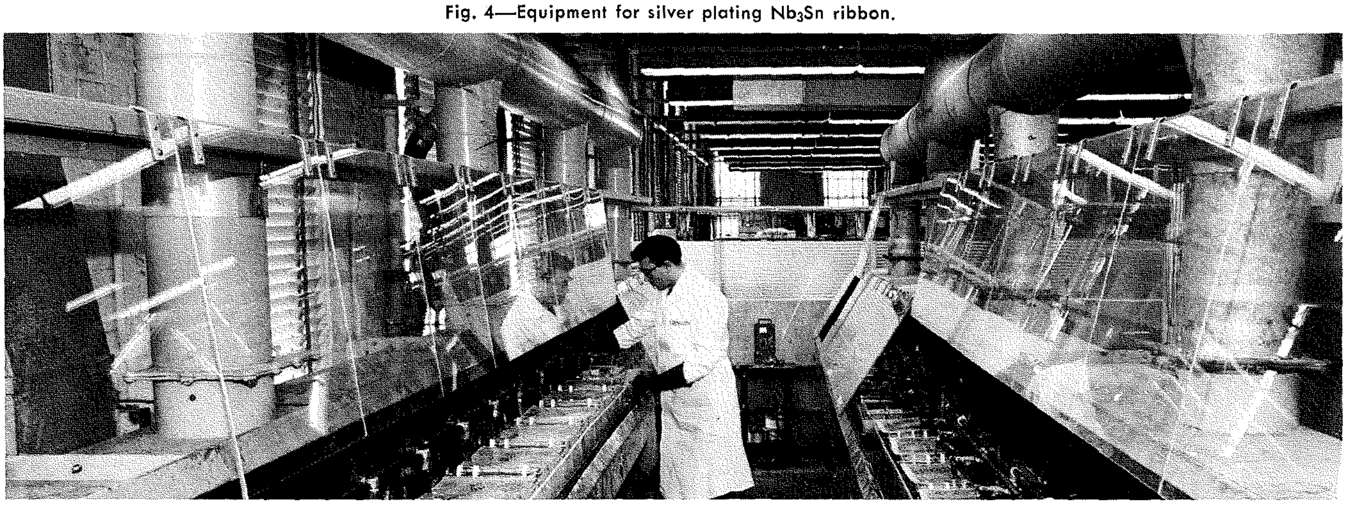

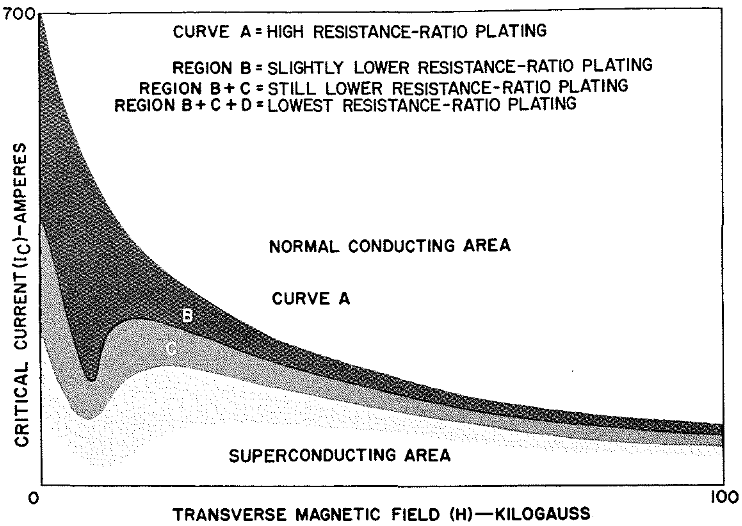

Fig. 5—Effect of plated-metal resistivity ratio on short-sample stability.

sequently revert to the superconductive state. Thus, ideally the generated Joulean heat must equal the heat dissipated through the bath, and is expressed by:

$$I^2R = hS\Delta T$$

where I = transport current in amperes, R = resistance of normal region in ohms, h = film heat transfer coefficient in W/cm^2 °K, S = surface area in cm^2, and ΔT = temperature rise in °K. For complete stabilization, the stabilized, short-sample critical current is substituted in Eq. 3.

In practical cases for fully stabilized conductors, only a short length of superconductor is generally quenched at any one time. Because only surface cooling of the conductor is considered, Eq. 3 can be converted to a heat balance per unit length, given as:

$$I^2\rho/A = hS\Delta T \qquad (4)$$

where ρ = resistivity of normal conductor in ohm-cm, and A = cross-sectional area of normal conductor in cm^2.

Layer-wound coils with ribbon-type conductors are cooled across the width of the conductor which has an active heat-transfer area that consists of the two larger surfaces and the edges. However, these edges can be ignored in relation to the conductor width, and consequently, Eq. 4 may be expressed as:

$$\frac{I^2\rho}{wt_n} = h\ (2w)\,\Delta T \qquad (5)$$

where w = width of the conductor in cm, and t_n = total thickness of the normal conductor in cm.

Heat is transferred from the conductor to the liquid helium by one of two mechanisms, nucleate or film boiling. Nucleate boiling occurs when the heat flux ranges from 0.0 to 0.7 W/cm^2 and produces an associated temperature difference of from 0.1°K to 0.8°K between the conductor and the liquid. If greater heat fluxes occur, the heat-transfer mechanism shifts to less efficient film boiling, and the associated temperature difference then rises of the order of 10°K. With a temperature rise of this magnitude, the major portion of the current in the superconductor shifts to the copper and produces additional Joulean heat, thereby creating normal regions. Consequently, it is impossible for the normal portion of the conductor to return to the superconductive state. Therefore, to assure that heat transfer will occur by nucleate boiling, heat flux from the conductor to the surrounding liquid helium bath is limited to something less than 0.5 W/cm^2. Experience with small, completely stabilized coils built with an experimental Nb_3Sn conductor has shown that a heat-transfer coefficient ($h\Delta T$) of 0.250 W/cm^2 is readily achievable.

Eq. 5 can now be further rearranged by substituting the heat-transfer coefficient of 0.250 W/cm^2 and a resistivity of $(0.73 \times 10^{-8})\ (1 + 0.03\,B)$ for the copper conductor, where B is the magnetic field in kilogauss. This resistivity is based on a resistance ratio (at room-to-liquid helium temperature of 200 for OFHC copper in the absence of a magnetic field and on a four-fold increase in magnetoresistance from 0 to 100 kG. The yield is expressed as:

$$w^2 = \frac{KI^2}{t_n} \qquad (6)$$

where:

$$K = \frac{\rho}{2h\Delta T} = \frac{(0.15 \times 10^{-8})\ (1 + 0.03\,B)}{\Delta T}$$

Fig. 6—Equipment for coppercladding Nb_3Sn ribbon.

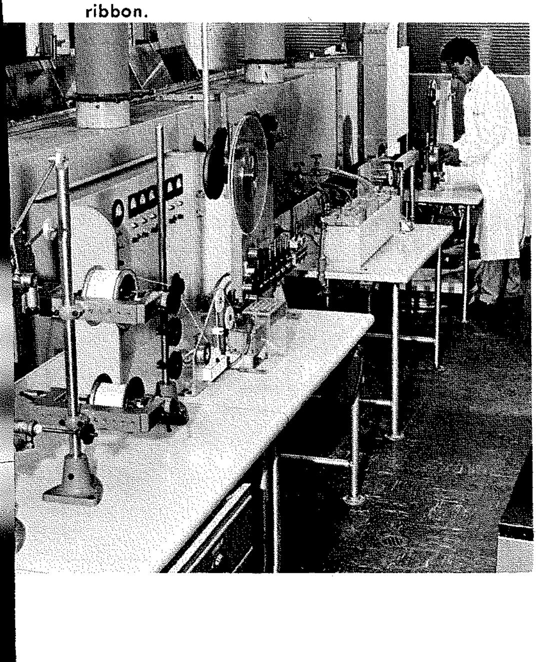

Fig. 7—Typical copperclad conductors.

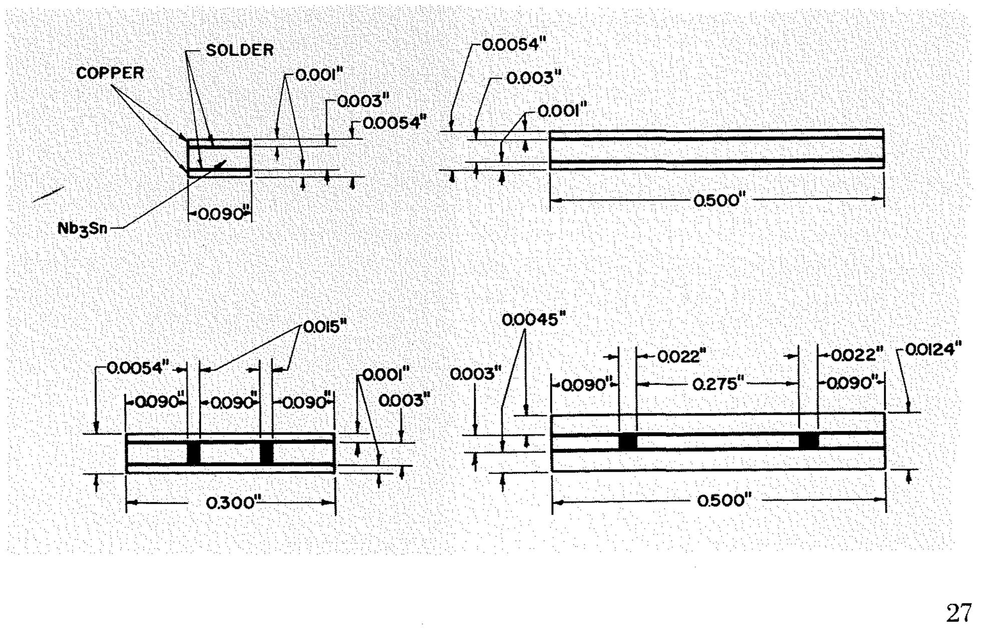

In terms of magnet design, discussed in another article in this issue by P. A. Thompson,[8] the magnetic field produced by a particular magnet geometry is inversely proportional to the effective conductor cross-sectional area.

To minimize the effect of decreased current density caused by the additional thickness of copper for stabilization of a magnet, the shape of the stabilized conductor should be optimized. The effective conductor current density per turn (i) in a magnet is calculated by knowing the effective area of a single turn which is the product of the conductor width (w) plus the spacing between turns (S_1), times the total thickness of the normal conductor (t_n) plus the sum of the superconductive ribbon thickness and liquid helium cooling channels (S_2). Thus:

$$i = \frac{I}{(w + S_1)(t_n + S_2)} \tag{7}$$

where i = effective conductor current density per turn in A/cm^2, I = maximum operating current in amperes, S_1 = distance between adjacent turns in cm, and S_2 = total thickness of superconductive ribbon and liquid helium channels in cm.

The current density may be maximized by substituting copper thickness t_n from Eq. 6 into Eq. 7, and then setting the derivative of Eq. 7 with respect to the thickness equal to zero. With this procedure, a maximum current density is obtained for each current level. This optimum occurs when the normal metal thickness is equal to the sum of the superconductive conductor and helium cooling channels, given as:

$$t_n \approx S_2 \tag{8}$$

A review of Eqs. 3 through 8 indicates that stabilization causes two opposing changes in the effective coil current density. Although stabilization permits the use of higher conductor currents, it adversely affects conductor area per turn. Thus, the advantage of improved operating characteristics which results from complete stabilization is necessarily offset by decreased current density in the magnet. If the I^2R losses in Eq. 5 are maintained lower than the effective thermal dissipation in the liquid helium bath, the conductor becomes *overstabilized.* An overstabilized magnet can be successfully operated at currents even higher than superconductive critical current without quenching the superconductor, but the resultant I^2R loss will cause proportionate liquid-helium boil-off. Therefore, magnet design must be carefully evaluated, because overstabilization does not provide an increased operating current, but, rather serves to further decrease magnet current density.

METHOD OF CLADDING NORMAL METAL TO SUPERCONDUCTORS

The concept of complete stabilization requires a normal metal layer ranging from approximately 5 to 40 mils per Nb_3Sn layer. These heavy layers cannot be practically built up by plating, and consequently, a cladding process has been evolved whereby the normal metal is bonded to the Nb_3Sn layer by a solder such as indium or lead-tin. The normal metal cladding permits the unique opportunity of selecting and optimizing both the quality and quantity of normal metal in intimate, bonded contact with the Nb_3Sn. A typical cladding line is shown in Fig. 6. The copper and superconductive ribbons are unreeled from spools A; bonding is performed in bonding shoes B; the hot water washing and the drying are then performed in area C; and the final product is spooled at D. Differently clad configurations produced to date by the process are shown in Fig. 7. A typical stabilized magnet wound with 60 meters of a stabilized conductor over a 1⅛-inch bore had a critical superconductive current of 290 amperes but was capable of operating with 370 amperes at 600 millivolts without propagating a normal front. To permit the escape of vaporized helium, channels were provided by a stainless steel mesh network of 0.016-inch-diameter wire in one direction and 0.005-inch-diameter wire in the other (Fig. 8). If these channels were not provided, the helium gas would be vapor locked within the magnet, and the previously discussed heat-transfer coefficient of 0.250 W/cm^2 could not be achieved.

Fig. 8—Helium channeling for completely stabilized magnets.

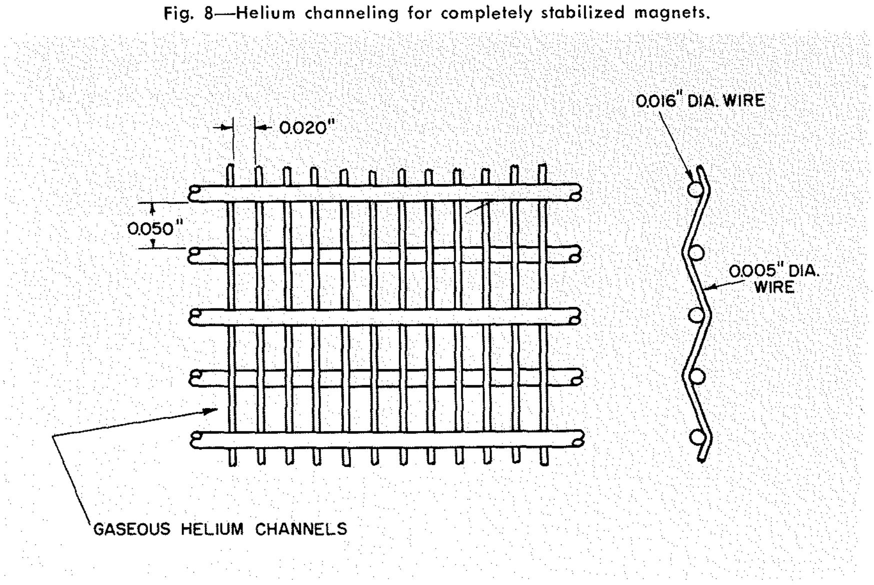

CONCLUSION

The choice of materials used in the fabrication of quasi- or fully-stabilized magnets depends on the specific application. Frequently, for small-bore laboratory magnets, the quasi-stable magnets are more desirable. They are wound with a 0.001-inch silver-plated ribbon having an over-all conductor current density of 2.5×10^4 A/cm^2. For the larger diameter, low-field bubble-chamber magnet, a completely stabilized magnet is frequently preferred. These magnets have a lower over-all conductor current density of only 9×10^3 A/cm^2. The design considerations and discussions attendant on the applications of both the quasi- and the fully-stabilized ribbons in magnets are contained in another article[9] in this issue.

BIBLIOGRAPHY

1. Sponsored under Contract No. AF33(616)-6405 or Physics Laboratory, ASD Wright-Patterson AF Base Report ASD-TRD-62-269, 1962.
2. Y. P. Kim, C. F. Hempstead, A. R. Strad, "Critical Resistant Current in Hard Superconductors", *Phys. Rev.*, Vol. 9, p. 306, Oct. 1962.
3. G. D. Cody, G. W. Cullen, J. P. McEvoy, "Field and Angular Dependence of Critical Currents in Nb_3Sn II, *Revs. Mod. Phys.*, Vol. 36, p. 65, Jan. 1964.
4. P. W. Anderson, "Theory of Flux Creep in Hard Superconductors", *Phys. Rev. Letters*, Vol. 9, p. 309, Oct. 1, 1962.
5. D. Bruce Montgomery, "Superconducting Magnets", *IEEE Spectrum*, p. 103, Feb. 1964.
6. Chas. Laverick, "Superconducting Magnets", *Nucleonics*, p. 46, Jan. 1966.
7. Z. J. J. Steckly, J. L. Zar, *Stable Superconducting Coils*, Avco-Everett Research Report 210, March 1965.
8. P. A. Thompson, "Computer Calculations for the Design of Large, High-Field Superconductive Magnets", RCA ENGINEER, *this issue.*
9. E. R. Schrader, "Design and Construction of Nb_3Sn Superconductive Magnets", RCA ENGINEER, *this issue.*

ELECTROMAGNETIC PERFORMANCE OF Nb_3Sn VAPOR-DEPOSITED RIBBON UP TO 200 KILOGAUSS

The relative stability and overall electromagnetic performance of niobium-stannide ribbon in high-field magnets is described in this paper. Knowing the relationship between the volume of Nb_3Sn layers and stability, ribbons can be designed and selected for use in magnetic fields up to 200 kilogauss.

H. C. SCHINDLER
Electronic Components and Devices
Harrison, N. J.

The electromagnetic performance of high-field superconductors is significantly affected by structural changes such as crystal size, crystal orientation, or crystal strain. The versatile, vapor-deposition (Vapodep) process (described elsewhere in this issue[1]), which superposes single-phase Nb_3Sn on a moving substrate, can easily control these structural changes and is used, consequently, for the deposition of continuously monitored layers of Nb_3Sn on long lengths of ribbon substrate. These long lengths of superconductive ribbon are used in magnet-winding applications.

The critical current of a superconductor, i.e., a current at which superconductivity disappears and normal resistance appears, is a function of its magnetic field and temperature. Experiments in superconductivity have been performed in liquid helium because its boiling point at 4.2°K is lower than the critical temperature of the Nb_3Sn superconductor. Fig. 1 illustrates the variation of critical current as a function of transverse background field at 4.2°K for a typical 2.5 x 10^{-4} inch layer of Nb_3Sn on metallic substrate approximately 0.090 x 0.0018 inch.

THEORETICAL CONSIDERATIONS

Based on Anderson-Kim flux-flow models, the present theories on Type II superconductors describe the current-field relationships as those in which the magnetic field enters between the lower (H_{c1}) and the upper, (H_{c2}) critical fields in quantized flux bundles. The lower critical field (H_{c1}) is where the magnetic field first penetrates the superconductor. This field is approximately 200 G for Nb_3Sn at 4.2°K. In the field region from approximately 0 to 200 G, the magnetic field does not penetrate the superconductor. This phenomenon is commonly referred to as the *Meissner effect.*

The upper critical field (H_{c2}) is the magnetic field at which bulk superconductivity in the layer ceases; for Nb_3Sn, this field has been determined at the National Magnet Laboratory, M.I.T.,[2] and ranges to 220 kG at 4.2°K. With a transport current applied transversely to the magnetic field, a classic magnet pressure, which is proportional to the Lorentz force F, acts on the flux bundles across the superconductor. This force F is expressed as:

$$F = \frac{(j \times H)V}{c} \qquad (1)$$

where j is the local transport current density, H is the transverse magnetic field, c is the velocity of light, and V is the volume of the flux element (core of the flux vortex). If the flux moves freely, a voltage appears across the superconductor. However, if no voltage appears, it must be assumed that absence of flux motion is caused by the impeditive potential of the crystal imperfections. Consequently, when the first measurable voltage level does appear, it must be inferred that the action of the Lorentz force on the flux bundles has exceeded the flux-pinning forces of the crystal and has initiated flux motion. Supported by these concepts, Anderson[3] presented a qualitative expression for the critical current density J_c in a transverse field between H_{c1} and H_{c2}, expressed by:

$$J_c = \frac{\alpha}{H + B_o} \qquad (2)$$

where α is a material constant, and B_o was originally a curve-fitting constant. This expression has been extended by Cody and Cullen[4] for other than transverse fields to yield the angular dependence expressed as:

$$J_c = \frac{\alpha}{H \sin\theta + B_o} \qquad (3)$$

where θ is the angle between current and magnetic field. This expression has been applied to Type II superconductors, and for the most part has yielded a good correlation for low-α material. Furthermore, neutron damage and annealing tests of Type II superconductors have further supported the Anderson model.[5]

ELECTROMAGNETIC PERFORMANCE OF VAPOR-DEPOSITED Nb_3Sn ON METALLIC SUBSTRATES AT HIGH FIELDS

If Equation 3 is now applied to the critical-current, transverse-field relation shown in Fig. 1, serious discrepancies result. In Fig. 2, $1/I_c$, where I_c is current in amperes, is plotted as a function of background field. The quantity $1/I_c$ is proportional to $1/J_c$. If Equation 3 is correct, the curve should yield a straight line with the slope equal to α, and the abscissa-intercept equal to B_o. As indi-

Final manuscript received Nov. 1, 1966.

HENRY C. SCHINDLER received his BChE degree from Cooper Union in 1955, and an M.S. degree in Physics from the Stevens Institute of Technology in 1959. He is currently working toward a Doctorate in Physics. Mr. Schindler was employed for four years at Picatinny Arsenal where he formulated and tested rockets and jet devices. Subsequently, he joined General Instrument Corporation as a senior engineer in developing semiconductor devices. In June 1962, Mr. Schindler was engaged by the RCA Superconductor Materials and Devices Laboratory of the Special Electronic Components Division at Princeton, N.J. He participated in the development of the niobium-tin vapor deposition process and studies the effect of the physical, chemical, and electrical properties of Nb_3Sn films with particular reference to superconductor device application. As a result of this work, he received the RCA Laboratory Outstanding Achievement Award. In April 1966, Mr. Schindler transferred to the RCA Superconductive Products Operation, EC&D, in Harrison, N.J. Since that time, he has been involved with the Development and electromagnetic evaluation of superconductive ribbons for magnet applications. Mr. Schindler is a member of the American Physical Society.

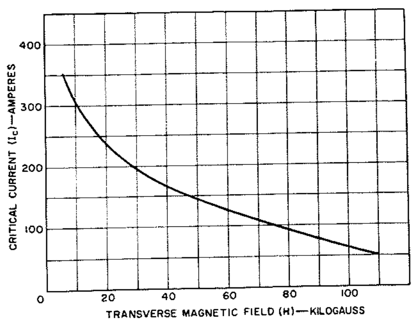

Fig. 1—Critical current as a function of transverse magnetic field for a nominal 2.5×10^{-4} inch vapor-deposited Nb_3Sn layer.

cated in Fig. 2, there is correlation with Equation 3 up to 60 kG; however, above 60 kG, the correlation is violated. This result is somewhat surprising, because Nb_3Sn deposits on ceramic substrates have previously yielded excellent correlations[6] up to 105 kG. A plausible explanation for this deviation is that with ceramic substrates there are practically no diffusion regions between the substrate and the Nb_3Sn layers and, consequently, a pure Nb_3Sn having a critical temperature of 18.3°K is obtained.

However, when niobium stannide is vapor-deposited on a metallic substrate, a significant diffusion zone in both the substrate and the single-phase deposit appears. Furthermore, critical temperature measurement of this deposit indicates a range of transition temperatures from 13°K to 18°K. Thus, it is reasonable to assume that the initially deposited Nb_3Sn layer has a lower critical temperature as the result of diffusion zones and stresses within the Nb_3Sn layer. It is this initially deposited layer that gradually begins to lose its superconductive properties above 60 kG. Consequently, a progressively smaller portion of niobium-stannide cross-sectional areas is available at the higher fields where the deviations occur. In the lower magnetic-field regions, the lower critical-temperature deposits have excellent superconductive properties, and the impurities in the diffusion zone significantly aid in flux-pinning, and consequently are helpful in the attainment of high current densities. The diffusion-zone thicknesses depend on the processing parameters, but generally are 5% to 20% of the total niobium-stannide deposits. The lower percentages are obtained with thicker Nb_3Sn layers.

The thickness of the Nb_3Sn layer can readily be varied by altering the vapor-deposition-process parameters. Even with heavier deposits, the grain structure and orientation can be maintained the same as with the thinner deposits. Variations of the Nb_3Sn layer thicknesses ranging from 1.5×10^{-4} to 1.3×10^{-3} inch have been obtained in this fashion. In Fig. 3, the critical current, as a function of transverse magnetic field, is plotted for niobium-stannide-layer thicknesses from 0.15 to 1.00×10^{-3} inch. This family of curves can be unified by normalizing each curve with its respective current at 100 kG; the results are plotted in Fig. 4. The significance of this relation is that it permits the critical current to be expressed analytically as a function of transverse magnetic field, independent of Nb_3Sn thickness. For instance, from 20 kG to 100 kG, the normalized current I_n is expressed as:

$$I_n = \frac{I_c}{I_{100kG}} = \exp\,(-0.00639H + 0.672) \qquad (4)$$

From 100 kG to 150 kG, the following approximate expression can be used:

$$I_n = \frac{I_c}{I_{100kG}} = \exp\,(-0.011H + 1.1) \qquad (5)$$

The use of an average current density at 100 kG of the various Nb_3Sn layer thicknesses, and the incorporation of the Nb_3Sn thickness and the ribbon width in equations 4 and 5, is expressed for from 20 kG to 100 kG as:

$$I_c = \frac{W}{0.090}[\exp\,(-0.00639H + 0.672)]\,[37.4 \times 10^4\,(t - 7.5 \times 10^{-5})] \qquad (6)$$

And for from 100 kG to 150 kG as:

$$I_c = \frac{W}{0.090}[\exp\,(-0.011H + 1.1)]\,[37.4 \times 10^4\,(t - 7.5 \times 10^{-5})] \qquad (7)$$

where W is the ribbon width in inches and t is the Nb_3Sn layer thickness in inches.

As previously discussed, the initial layer has a slightly lower critical temperature. In the above expressions, it is assumed that the decrease in current capacity which results from the lower critical temperature T_c is neglected. This effect is discussed in the following paragraphs.

If other geometric substrates such as wire are considered, the Nb_3Sn cross-sectional area can be readily substituted to obtain the current-field relationships. These interrelations now permit the selection of an entire family of ribbons for magnet design considerations in terms of Nb_3Sn layer thickness and ribbon width, or of Nb_3Sn layer thickness and wire diameter. In the previous discussion, the primary assumption, which has recently been fairly well substantiated, is that by variation of the process parameters for the different Nb_3Sn thicknesses, the current density can be maintained essentially constant. The only slight modification is that for the heavier niobium-stannide deposits, there is a decrease in the proportion of the thickness of the Nb_3Sn layer which is diffused in the substrate. Consequently, a slight increase in current density is obtained at the higher fields. This condition is evident in Fig. 4 in the field region from 120 to 200 kG. In Equation 5, only the upper curve was used.

Critical current measurements made in transverse magnetic fields up to 200 kG have established that the upper critical fields for thin Nb_3Sn deposits are lower than those for the heavier deposits.

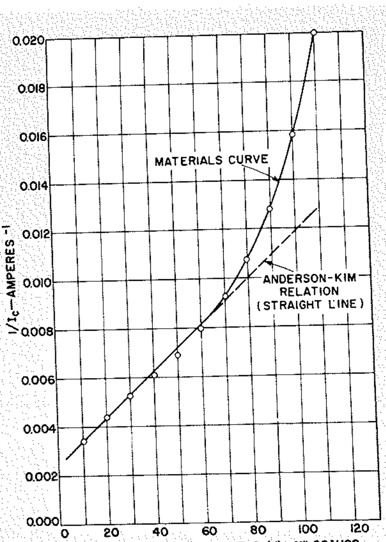

Fig. 2—Deviation of material curve from Anderson-Kim relation.

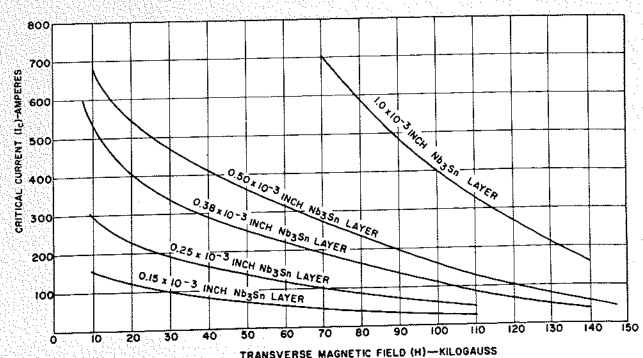

Fig. 3—Critical current as a function of transverse magnetic field for various thicknesses of Nb_3Sn.

Thus, for deposits with a Nb_3Sn layer thickness of 1.5 x 10^{-4} inch, the upper critical field is 174 kG; for deposits with a Nb_3Sn layer thickness of 2.5 x 10^{-4} inch, the upper critical field is 190 kG; and for deposits with a Nb_3Sn layer thickness upward of 3.8 x 10^{-4} inch, the upper critical field is 220 kG. This increase of upper critical field with increasing thicknesses of Nb_3Sn deposits may possibly be explained by: 1) a decreased stress within the Nb_3Sn deposit due to the mismatch in the coefficient of contraction between the substrate and the Nb_3Sn layer as thickness increases and, 2) a lessening of the diffusion effect from the substrate as deposits become thicker.

The upper critical field of 220 kG for Nb_3Sn deposited on a metallic substrate correlates with the upper critical-field measurements made on an Nb_3Sn vapor-deposit on ceramic substrate, and on Nb_3Sn obtained by diffusion processes.[2,4]

STABILITY OF DIFFERENT Nb_3Sn DEPOSITS

The critical currents discussed up to now were based upon maximum critical currents obtained under optimum conditions. As indicated previously, in the presence of a transport and a transverse magnetic field, the flux lines are restrained by the pinning forces of the crystal. When the flux force exceeds the flux-pinning force at the local crystal site, flux motion results and generates heat which can prematurely drive the superconductor to the normal state. To minimize this premature normalcy, a metallic layer having optimum high electrical and thermal conductivity plus high specific heat is placed parallel to the superconductor. Thus, if a local portion of the superconductor becomes normal, the current passes from the superconductor to the parallel conductor, and the heat generated by the normal portion can readily be dissipated by the metallic layer. This action prevents the local normal front from propagating. The thermal conductivity of the Nb_3Sn is four to five orders of magnitude less than that of the copper.[7,8] Consequently, the heat generated within the superconductor becomes more difficult to remove as the thickness of the niobium-stannide layer is increased. This phenomenon is the basis for the curves plotted in Fig. 5 which indicate the stability characteristic for various thicknesses of Nb_3Sn, based on magnets constructed with ribbon upwards of 50 meters long. The long dashed lines and solid extensions represent the inherently stable H_c, I_c performance of the Nb_3Sn layers; the short dashed lines and solid extensions represent actual coil data. The difference in current between the long dashed and the short dashed lines for each thickness is a measure of its stability.

The above-defined stability regions are strongly influenced by:

1) the length of superconductive ribbon used,
2) the quality (resistance ratio from room-to-helium temperature) and quantity (thickness) of the metallic layer in contact with the superconductor,
3) the interleaving employed (i.e., Mylar,* anodized aluminum, on Mylar-copper-Mylar), and
4) the degree of cooling within the magnet.

The stability regions for the various Nb_3Sn layer thicknesses indicate only the relative stability of the different layers. In very large magnets which utilize several thousand meters of ribbon, the instability region becomes broader and sometimes reaches the upper critical field. However, the relative stability of the materials discussed remains the same.

CONCLUSION

In the design of high-field magnets, the stability regions and upper critical field for the various materials must be carefully considered. Furthermore, because it is usually desirable to operate a magnet from a single power source, it is possible to select progressively heavier Nb_3Sn layers for the higher field regions. The heavier deposits compensate for the decrease in critical current with increased magnetic fields. Some of these considerations are discussed in a separate article[9] in this issue.

From our present knowledge of the relationship between the volume of niobium stannide and its stability, it is possible to design ribbon for use in magnets up to 160 kG with a single current level. For higher field magnets, up to the 180-kG or the 190-kG range, multipowered magnet systems are required. At the present stage of development, magnets of the 150-to-180-kG class are about the highest fields that can be practically achieved with niobium stannide at helium temperatures. The reduction of the vapor pressure of helium by mechanical evacuation lowers its temperature. If the temperature is below the lambda point[10], the field region can be raised another 20 to 30 kG thus permitting the design of 200-kG magnets.

* Registered Trademark of E. I. Dupont de Nemours

BIBLIOGRAPHY

1. F. R. Nyman, "Vapor Deposition of Nb_3Sn A Versatile Process" RCA ENGINEER, *this issue.*
2. D. Bruce Montgomery, *Applied Physics Letters,* Vol. 6, No. 6, Mar. 15, 1965.
3. P. W. Anderson, "Theory of Flux Creep in Hard Superconductors", *Phys. Rev. Letters,* Vol. 9, p. 309, Oct. 1, 1962.
4. G. D. Cody, G. W. Cullen, J. P. McEvoy, "Field and Angular Dependence of Critical Currents in Nb_3Sn II", *Revs. Mod. Phys.,* Vol. 36, p. 65, Jan. 1964.
5. G. D. Cody, *et al., Phenomenon of Superconductivity,* Technical Report AFML-TR-169, pp. 71-85, June, 1965, Wright-Patterson AF Base, Dayton, Ohio.
6. *Ibid,* p. 33.
7. *Compendium of the Properties of Materials at Low Temperatures,* National Bureau of Standards, Cryogenic Engineering Laboratories, Boulder, Colo., Dec. 1961, p. 46.
8. G. D. Cody, *et al., Phenomenon of Superconductivity,* Technical Report AFML-TR-169, pp. 162-169, June 1965, Wright-Patterson AF Base, Dayton, Ohio.
9. E. R. Schrader, "Design and Construction of Nb_3Sn Superconductor Magnets", RCA ENGINEER, *this issue.*
10. W. Sampson and R. Britton, *personal communication.*

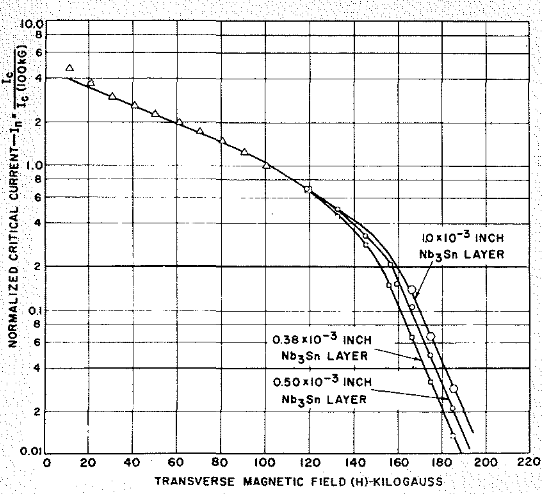

Fig. 4—Normalized critical current as a function of transverse magnetic field. (Based on results obtained by the author at M.I.T., June 1966.)

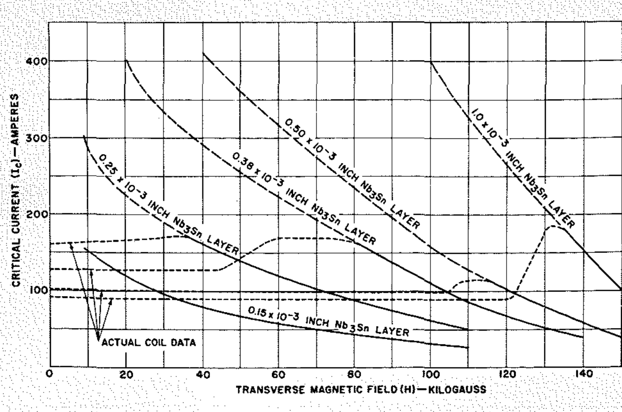

Fig. 5—Stability as a function of Nb_3Sn layer thickness.

SUPERCONDUCTING MICROWAVE DEVICES

Superconductors have contributed to the field of microwave (and millimeter-wave) devices in two distinct ways. First, they have led to a number of new devices which use phenomena peculiar to superconductors. Secondly, their superior characteristics, particularly low loss, permit orders-of-magnitude improvement in conventional devices. The former category includes devices useful for the generation, amplification, and detection of radiation. The improved conventional devices include filters and delay lines. In this paper we review first the properties of superconductors pertinent to microwave frequencies and then consider their application to the above mentioned devices. Switching devices, which generally operate at submicrowave frequencies, are not discussed here.

DR. A. S. CLORFEINE and DR. B. N. TAYLOR

RCA Laboratories, Princeton, N.J.

For a review article on the microwave properties of superconductors which covers, in more detail, some of the material discussed here, the reader is referred to an article by Gittleman and Rosenblum.[1] (For a concise review of superconductors in general, we suggest the book by Lynton[2]).

BULK AND THIN-FILM PROPERTIES OF SUPERCONDUCTORS

It is a familiar fact that superconductors are characterized by the complete vanishing of DC resistance as the temperature is lowered below a critical value T_c. The impedance of a superconductor at microwave frequencies, however, is finite and may be described, qualitatively, by means of the so-called *two-fluid* concept. In a two-fluid model, the electron gas is assumed to be composed of two interpenetrating groups—superconducting electrons and normal electrons. The latter behave as they would in a normal metal; i.e., under the influence of an electric field they lose energy to the lattice via scattering. The superconducting electrons, however, exhibit no resistance; the only impedance they manifest is inductive in nature and is due to their finite mass.

Final manuscript received, September 22, 1966

Since the currents contributed by the individual electrons are additive, a parallel equivalent circuit is called for. Such a circuit (representing, say, a very small unit cube of superconductor) is given in Fig. 1a. Each superconducting electron is represented by an inductance L and each normal electron, by a resistance R. (The inductive impedance of a normal electron may be neglected in comparison to its resistance except for pure samples at exceedingly high frequencies). The final equivalent circuit appears in Fig. 1b where n_s and n_n represent the density of superconducting and normal electrons respectively. It should be understood that Fig. 1 represents only the internal impedance of a superconductor. In general, energy stored in fields outside the sample will add a "geometric" inductance to the complete equivalent circuit. Clearly, when $T = T_c$ (or, in the usual notation, when $t \equiv T/T_c = 1$), $n_s = 0$ and $n_n = n$, the total density of electrons. The sample at subcritical temperatures was assumed by Gorter and Casimer[3] to be described by $n_s/n = 1 - t^4$. If the total number of electrons is to be conserved, then $n_n/n = t^4$. The Q of the sample in Fig. 1 is, therefore, given by:

$$Q = \frac{\dfrac{R}{n_n}}{\dfrac{\omega L}{n_s}} = \frac{R}{\omega L}\,\frac{1 - t^4}{t^4} \qquad (1)$$

It should be emphasized that Equation 1 and the discussion leading to it have many limitations; however, the qualitative behavior indicated is correct; i.e., a superconductor at microwave frequencies undergoes a continuous transition from a resistive material at $T = T_c$ to one of enormous Q at $T << T_c$. It is this property which permits one to fabricate passive devices with Q's many orders of magnitude higher than attainable with normal metals.

A population redistribution between superconducting and normal electrons can be effected not only by a change in temperature but also by a change in current. This conclusion follows from a microscopic theory of Parmenter[4] as well as the phenomenological Ginzbùrg-Landa (G-L) theory[5] and has been demonstrated in the laboratory.[6] Calculations by Clorfeine and Young[7] of the percent change in inductance vs. dc bias current for thin films and certain bulk samples were based on the G-L theory and are plotted in Fig. 2. These results, which show strongly nonlinear behavior, assume conditions are such that the sample is in a pure superconducting state rather than a "mixed" state. A mixed state, which is characterized by "vortices" or normal-like regions within a superconductor, can be initiated in samples—depending on geometry and surface condition—at fields well below the usual critical field. The microwave behavior of a sample in the mixed state is quite complex and also very nonlinear. It is the nonlinear inductance of superconductors, in either the pure or the mixed state, which makes possible active parametric devices.

TUNNEL JUNCTIONS

The superconducting tunnel junction in its most common form consists of two superimposed films separated by a very thin ($\lesssim$ 20 angstroms) insulating oxide layer (see Fig. 3). The mechanism for current flow from one superconductor to another is, as in the Esaki diode, electron tunneling. To date, superconduct-

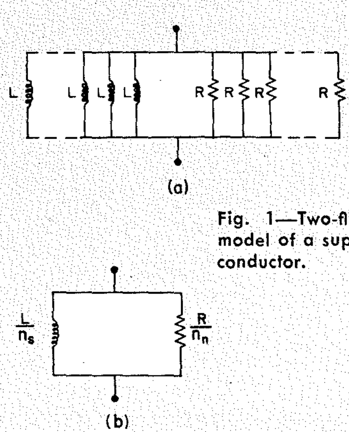

Fig. 1—Two-fluid model of a superconductor.

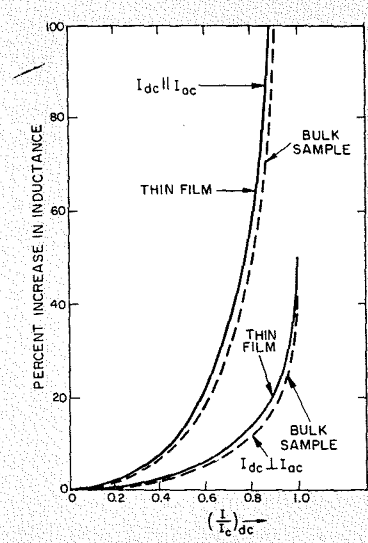

Fig. 2—Inductance change vs. current.

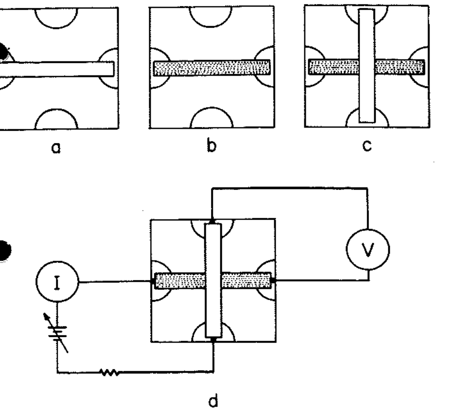

Fig. 3—Step by step procedure for fabricating superconducting tunnel junctions: (a) deposition of the bottom film in strip form (about 0.25 mm wide by 2000Å thick) onto a substrate (1″ square) with pre-evaporated electrodes; (b) oxidation of the surface of this film in air or oxygen to a thickness of about 10-20 Å; (c) deposition of a top strip similar to the bottom strip, forming a junction; (d) measurement of the current-voltage (I-V) curve of the junction.

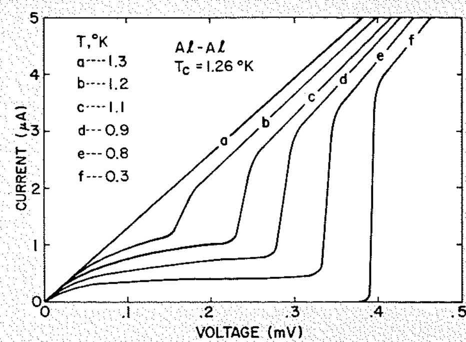

Fig. 4—Typical normal-electron I-V curves for a superconducting tunnel junction composed of bottom and top films of the same superconductor. The onset of the sharp break in the curves for $T < T_c$ occurs when $eV = 2\Delta(T)$.

ing tunnel junctions have been used primarily as a tool for research on the more fundamental aspects of superconductivity since the highly nonlinear current-voltage (I-V) curves of such junctions are directly related to the normal electron energy spectrum of the superconductors. These same I-V curves, however, also presage a number of microwave device applications. Additionally, a quantum phenomenon known as the AC Josephson effect (after B. D. Josephson who first predicted it), which occurs in tunnel junctions with oxide layers $\lesssim 10$ angstroms, can also be used for microwave device applications. Such applications shall be considered below. First, however, we discuss superconducting tunneling in general, the type of I-V curves experimentally observed, and the nature of the AC Josephson effect.

Normal-electron Tunneling[8]

As mentioned previously, a superconductor can be viewed as being composed of two interpenetrating electron fluids, one normal and the other a superfluid. The latter consists of strongly correlated or paired electrons (Cooper pairs) of equal but opposite spin and momentum. The binding energy of an electron pair corresponds to an energy gap in the single particle excitation spectrum of a superconductor. The energy gap is temperature dependent and is usually denoted by $2\Delta(T)$. Thus, at temperature T, if energy equal to $2\Delta(T)$ is absorbed by an electron pair, the electrons become unbound and part of the normal fluid. For most superconductors, the energy gap at $T = 0°K$, $2\Delta(0)$, is related to the transition temperature of the superconductor by $2\Delta(0)/kT_c \approx 3.5$ (k is Boltzmann's constant).

For a range of oxide layer thicknesses of order of 15 to 20 angstroms, the two superconductors comprising the junction are only slightly coupled and the strong correlations between Cooper pairs do not extend through the oxide barrier so that only normal unpaired electrons tunnel. For applied bias voltages V such that $eV<\Delta(T)$ (e is the electron charge), the tunnel current will decrease with decreasing temperature since the number of normal electrons decreases. For applied voltages such that $eV>2\Delta(T)$, the tunnel current will remain essentially constant with temperature since energy sufficient to break up pairs into normal electrons is always available via the bias voltage. Thus, at $eV=2\Delta(T)$, a sharp increase in the tunnel current is expected which should become quite marked for $T<<T_c$. This behavior is found experimentally as in Fig. 4 for an Al/Al-oxide/Al junction.

If the superconductors comprising the junction are not the same, then the I-V curve is somewhat more complex because of the different energy gaps of the two superconductors. For this case, a negative resistance region will be present as shown by the I-V curves of Fig. 5 for a Sn/Sn-oxide/Pb sample. In some respects, such a junction is similar to an Esaki diode and indeed, the equivalent circuits for the two devices are the same. However, the magnitudes of the elements comprising the equivalent circuits differ significantly.

Pair Tunneling and the Josephson Effects

For extremely thin insulating layers ($\lesssim 10$ angstroms), the two superconductors comprising a junction will be more strongly coupled and correlations between Cooper pairs will extend through the insulating barrier layer. For this case, the entire junction behaves in many respects as a single block of superconductor (so called weak superconductivity). For example, the I-V curve of such a junction displays a zero-voltage current for currents less than a certain critical value. When this critical value is exceeded, a voltage appears across the junction and it switches along the measuring-circuit load line to the normal electron tunneling I-V curve. This zero-voltage current, which is shown in Fig. 6 for a Pb/Pb-oxide/Pb junction at 1.2°K, is called the DC Josephson current. It arises from the nondissipative tunneling of electron pairs from one superconductor to the other through the oxide layer.

In addition to this DC supercurrent, Josephson also predicted[9] that an AC supercurrent should be present when the junction is biased at a finite voltage V. The frequency, υ, of this supercurrent—which consists of Cooper pairs tunneling back and forth from one superconductor to the other through the insulating layer—is related to V by the equation:

$$\upsilon = \frac{2\,eV}{h} \qquad (2)$$

(h is Planck's constant) and is equal to 483.6 MHz for each microvolt of applied voltage. Recently, the existence of this AC supercurrent, now called the AC Josephson current, has been directly verified by observing the radiation associated with it.[10] Thus, although there are some potential device applications for the DC Josephson effect (for example as a fast computer switching element), it is the AC effect which appears to be the more promising for microwave devices.

Other Josephson-effect Structures

The predictions of Josephson pertain to

Fig. 5—Normal-electron I-V curves for a superconducting tunnel junction composed of the two different superconductors Sn and Pb. Note the negative resistance regions and their dependence on temperature.

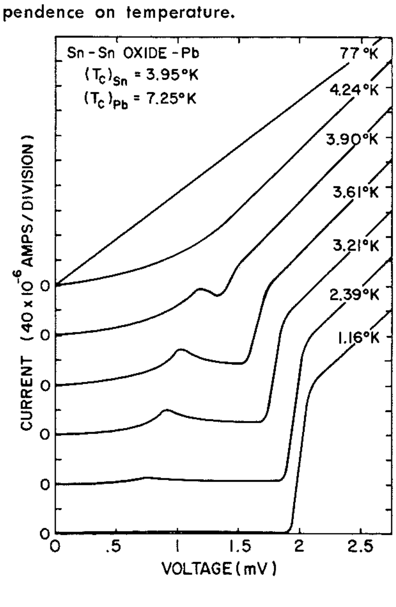

two superconductors weakly coupled together as in a superconducting tunnel junction. This type of coupling can also be achieved by connecting two superconductors via a small area contact—for example, by sharpening a fine point on one superconductor and pressing it against another superconductor, by laying two superconducting wires on top of one another, or by evaporating a pattern consisting of two large area films connected by a very short, narrow superconducting bridge (see Fig. 7). These "weak link" structures display many of the DC and AC Josephson-effect phenomena observed in oxide-layer junctions and will probably prove more useful for device applications because of their ease of fabrication. Such structures will be discussed in more detail below.

DEVICES—FILTERS AND DELAY LINES

The subject of superconducting microwave filters is discussed elsewhere in this issue and will not be elaborated on here. Let it suffice to say that, using the low-loss property of superconducting Pb, unloaded cavity Q's in excess of a billion have been attained at a frequency of 3 GHz.

A second passive device which can be greatly improved by the substitution of a superconductor for a normal metal is the microwave delay line. To appreciate the difficulty of attaining large delays with normal transmission lines, we need only contemplate the use of, for example, a standard RG-8 A/U coaxial cable for this purpose.[11] A wave propogating along such a cable (say at 3 GHz where the loss is $\cong$0.175 dB/ft) would be attenuated at the rate of 115 dB per microsecond of delay. For a large total delay, therefore, amplification would have to be provided. An additional consideration is that each microsecond of delay would require about eighty pounds of cable; miniaturization, while reducing size and weight, would aggravate the already intolerable loss problem. The use of a superconducting transmission line permits miniaturization while maintaining losses at a reasonable level. The use of one such line[12] (niobium wire center conductor and Pb-Sn solder outer conductor) resulted in a loss of only 1.9 dB per microsecond at 9 GHz and 3.2°K. While the volume required by the delay line was only 14 cubic inches per microsecond, additional space, of course, was needed to provide the cryogenic environment.

If the spacing, d, between conductors is made smaller than the superconducting penetration depth, λ, additional delay is achieved. This is so since the energy stored in the superconductor is no longer negligible compared to that stored between the conductors and the device becomes a slow wave structure. Also, since λ can be changed by applying a magnetic field, electronically-variable delay is possible. However, since $\lambda < 2{,}000$ angstroms for most specimens, a significant additional delay or variable delay would require conductor spacings of the order of tens of angstrom units. Such a structure in strip-line form, for example—would pose at least three problems. First, fabrication tolerances would be more critical. Second, losses would increase. Finally, since the line would have a very low characteristic impedance, coupling would be difficult. As we shall see, the problem of low impedance plagues most superconducting microwave devices.

PARAMETRIC AMPLIFIERS AND OSCILLATORS

Unique Nonlinear Properties

Since, as we have seen, a superconductor is characterized by a nonlinear inductance, it may be used, with proper circuitry, to provide parametric amplification. To an extent, the superconductor is the dual of the more familiar nonlinear reactance—the varactor. However, in a number of important respects, the two devices differ markedly. For example, the real part of the impedance which is essentially constant in most varactors is strongly nonlinear in superconductors. A second difference is that the capacitance-voltage curves of varactors show no symmetry. In a superconductor, on the other hand, the inductance in the presence of a current I is the same as that in the presence of $-I$. Thus the L—I (inductance-current) relation shows symmetry about the L axis. A third difference between the two devices is that the varactor is essentially a lumped element (the important interaction takes place at a junction, which is typically very small), while the superconductor is a distributed element. Also, as we have seen, the Q of a superconductor may be increased, essentially without limit, by lowering the temperature. In this sense, the behavior of a superconductor more closely resembles that of the ideal lossless nonlinear reactance treated by Manley and Rowe. Finally, the impedance of a superconductor is typically orders of magnitude less than that of a varactor.

Device Implications

Each of the above characteristics has significant implications, which are now discussed (for a more detailed treatment of some of this material, see Reference 13). The current dependence of the real part of a superconductor's admittance lowers the Q as the pump power is increased and also provides a small parametric action which complements that of the nonlinear inductance. The sym-

Fig. 6—I-V curve for a Pb-Pb oxide-Pb junction displaying the dc Josephson current. When the maximum dc Josephson current is reached, the junction switches along the circuit load line to the normal I-V curve (see Fig. 2).

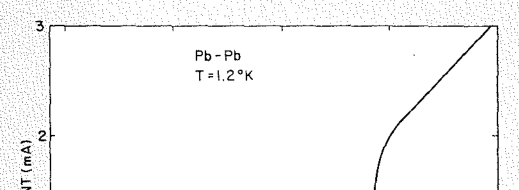

DR. A. S. CLORFEINE graduated magna cum laude with a BS in electrical engineering from the College of the City of New York in 1959. He received his MS in electrical engineering the following year from the Carnegie Institute of Technology and his PhD in EE from the same school in 1966. Since joining RCA Laboratories in 1961, he has been engaged in research in semiconducting and superconducting devices and circuits. His work with superconductors resulted in an "Industrial Research-100" award and an RCA Laboratories Achievement Award. Dr. Clorfeine has fifteen publications and patents issued or pending. He is a member of Eta Kappa Nu, Tau Beta Pi, Sigma Xi, and the IEEE Tunnel Diode Device Standards Committee.

DR. B. N. TAYLOR received the AB degree from Temple University in 1957, and the MS and PhD degrees from the University of Pennsylvania in 1960 and 1963, respectively, all in physics. From 1963 to 1966 he was an Instructor and Assistant Professor of Physics at the University of Pennsylvania where his research work centered around the general area of electron tunneling in superconductors. Recently, he has done work on the ac Josephson effect and the determination of e/h using this effect. Dr. Taylor joined RCA Laboratories in May of 1966 and is a member of the General Research Group. His immediate research plans include the investigation of various properties of superconducting thin films. Dr. Taylor is a member of the American Physical Society and the American Vacuum Society.

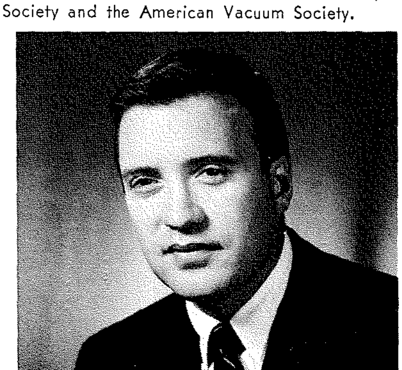

metry in the $L-I$ curves permits the easy establishment of what has been referred to[14] as "doubly degenerate" operation which is characterized by the fact that all pertinent frequencies—signal, idler, and pump—are very nearly equal. Whereas this mode of amplification has some disadvantage, it has the important virtue of great simplicity. Pump and signal may be introduced in the same waveguide and monitored with the same equipment. Only a singly-resonant circuit and one coupling mechanism are required. These simplifying features are especially welcome in a device that must operate in liquid helium.

The distributed nature of superconductors makes them ideally suited to traveling-wave structures. Thus, a truly-distributed wideband traveling-wave parametric amplifier, in principle, appears possible. Such a structure might take the form (and the problems) of the variable delay line previously discussed.

The distributed character of superconductors also makes accurate circuit calculations quite difficult since current, impedance, and nonlinear interactions vary from point to point. Except in simple TEM circuits, an equivalent circuit description of a superconductor yields information which, though useful, is limited. For example, edge effects which may occur in a film are not predicted if the film is represented by some spatially-averaged impedance. Such edge effects (e.g., edge nucleation of vortices) may be responsible for curious "jumps" or discontinuities which have been observed[15] in the absorption vs. frequency characteristics of a film irradiated with microwaves.

The pump power provided in parametric devices is dissipated primarily in the resistance associated with the device. Since superconductors exhibit extremely low loss, relatively little pump power is required. Low power requirements are advantageous in parametric digital circuits and in millimeter-wave amplifiers, where power is at a premium. A low pump power, however, is a disadvantage to the extent that it implies a low-signal saturation level.

Possibly the most serious problem associated with any attempt to make use of the internal impedance of a superconductor is its extremely low level. We have seen this to be true in the discussion of delay lines. Typically, a superconducting film at 10 GHz exhibits a primarily inductive impedance of less than 100 milliohms per square. As a rule of thumb, parametric amplification requires that the peak "swing" in reactance induced by the pump be of the order of the total circuit resistance. Thus, if the superconductor's impedance is small and its change is limited to a fraction of the total, the swing in reactance is indeed small. Consequently, even a slight amount of circuit loss is enough to prevent amplification. Minimization of such loss, therefore, is even more necessary than with other parametric devices.

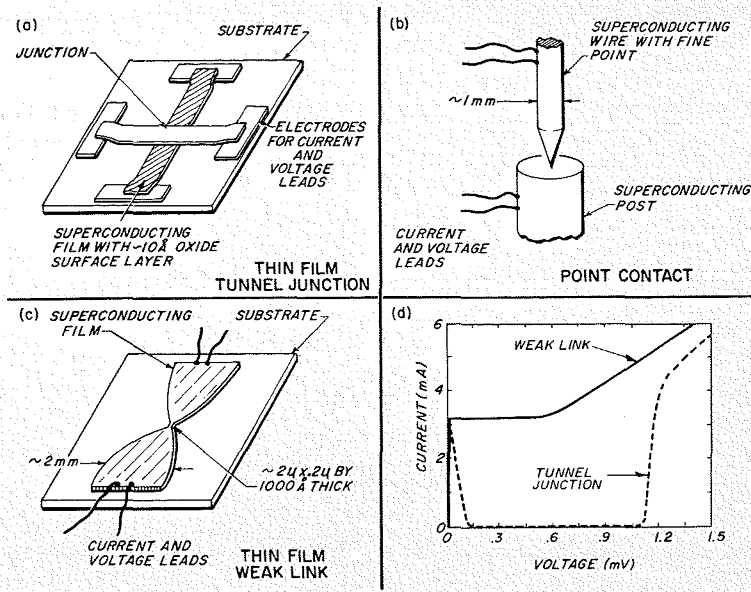

Fig. 7—Schematic diagrams depicting (a) a thin-film oxide-layer tunnel junction, (b) a point-contact weak-link junction, (c) a thin-film weak-link junction, and (d) the I-V curve of a weak link and the I-V curve of a tunnel junction displaying the dc Josephson current.

Experiments

The first demonstration of parametric amplification[16] in superconductors made use of the circuit illustrated in Fig. 8. A resonator consisting essentially of a rectangular specimen of rutile and a thin tin film on a crystal quartz substrate was mounted in a waveguide. The coupling to the resonator at its resonant frequency (6 GHz) was adjusted by means of a movable short-circuit plunger. Rutile was chosen because of its extremely small loss factor at cryogenic temperatures and its very high permitivity ($\varepsilon_{\parallel} = 255$, $\varepsilon_{\perp} = 130$) which can be shown to partially compensate for the low film impedance. The impedance, in principle, can be increased by the use of ultra-thin film superconductors. In a very thin film, however, uniformity and even continuity may be lost. As a compromise, the thickness of the film used in the experimental device was of the order of 250 angstroms. Fig. 9 illustrates the output and input spectra of the device operated in doubly-degenerate fashion. The lower trace shows pump and signal inputs of −37 dBm and −65 dBm. The upper trace is the output and illustrates the amplified (in this case, by 11 dB) signal, a reduced pump and three new frequencies. The response immediately to the left of the pump is the idler. The two smaller pips are attributed to higher order mixing processes in the film. The pump power required for amplification was only 0.2 microwatt. The minuteness of the required power is in accordance with expectations. Amplification has also been demonstrated in other superconducting film structures[15,17] and significant parametric effects have been observed at frequencies in the millimeter-wave range.[14]

JUNCTION MICROWAVE DEVICES

Normal Electron Tunneling Devices: Amplification and Oscillation

These applications may be viewed on the basis of the similarity between the *I-V* curves of Esaki diodes and those of superconducting tunnel junctions (Fig. 5). To date, work has been confined to frequencies of order 100 MHz or less, but simple extensions of the lower frequency techniques to microwave frequencies might be possible. Miles et al.[18] have constructed an RF oscillator operating at 72.5 MHz and with a modification of the circuit, have obtained 23 dB of gain at 50 MHz. That the analysis of the superconducting tunnel junction in such circuits follows very closely that of the Esaki diode is well born out by these experiments. Thus (according to Ref. 18), as an amplifier, the superconducting tunnel junction would be expected to have an excess noise figure lower than

Fig. 8—A superconducting parametric amplifier circuit.

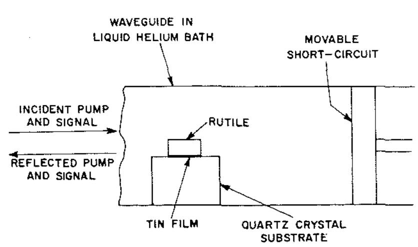

that of the Esaki diode by a factor of 20 or so because of the smaller current in the superconducting device (the major contribution to the noise is probably shot noise).

More recently, Scott[19] has considered theoretically some of the distributed device applications of the superconducting tunnel junction (again, as a negative resistance device but in transmission line form). He concludes that with Sn/Sn-oxide/Pb junctions, distributed amplifiers and oscillators operating at frequencies of the order of 1 GHz and at power levels of microwatts should be possible.

Fig. 9—Output and input spectra for the superconducting parametric amplifier.

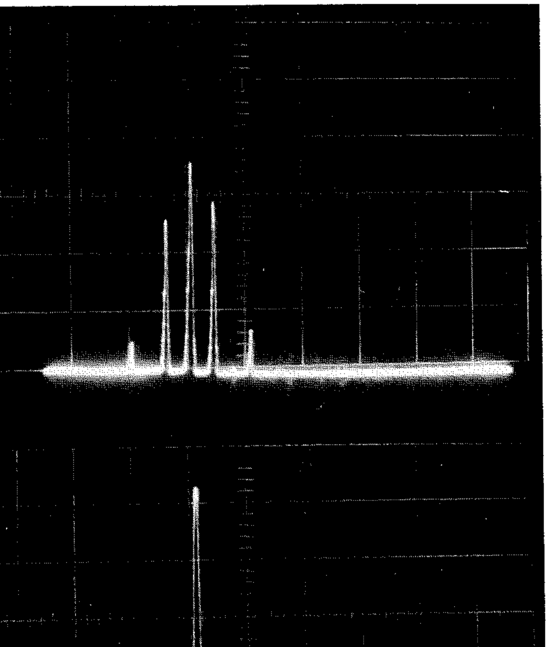

Fig. 10—I-V curves for a Sn-Sn Oxide-Sn junction irradiated with X band microwaves. The different curves are for four different power levels. The portion of the I-V curve in the dotted box is shown enlarged at the top of the figure. Note the vertical steps. The numbers under these steps correspond to the quantity n in the equation $V = nh\nu/2e$.

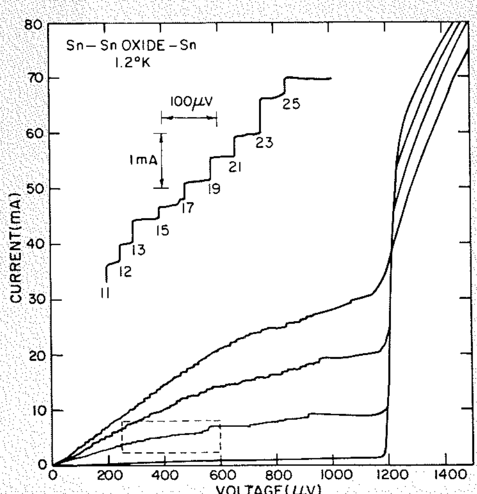

Detection and Mixing

Microwave detection as well as mixing can also be carried out with superconducting tunnel junctions. Using the highly nonlinear *I-V* curves of such junctions, Shapiro and McNiff[20] have video detected both CW and 1,000-Hz modulated X-band (9.3-GHz) and K-band (24-GHz) signals. For sufficiently small signals, the superconducting tunnel junction appeared to behave as a square law detector. Typical power levels used in these experiments were of order 30 microwatts. These same workers have also taken advantage of the nonlinear *I-V* curves of tunnel junctions for mixing. A 30 MHz IF frequency was observed from an Al/Al-oxide/Sn junction into which was fed two X-band microwave signals.

The superconducting tunnel junction is also a potential microwave and far infrared quantum detector. One would expect, for example, to observe a photocurrent when a junction is exposed to radiation of frequency ν such that the energy $h\nu$ of the incident photons is greater than or equal to the energy gap of the superconductors. This photoinjection of carriers by "optical" excitation across the energy gap of the superconductor resulting in additional tunneling current is analogous to the quantum detection of visible and near-infrared radiation by semiconductor *p-n* junctions. However, since the energy gaps of superconductors are only $\sim 10^{-3}$ that of semiconductors, the long-wavelength limits are in the millimeter and far infrared regions of the spectrum. For Al ($T_c = 1.2°K$) the long-wave length-limit λ_{max} as given by $\lambda_{max} = hc/2\Delta(0)$ is 3.9 mm while for Pb ($T_c = 7.2°K$), $\lambda_{max} = 460$ micrometers (formerly called micron). Such a detector has been analyzed theoretically by Burstein, Langenberg and Taylor.[21]

Josephson Effect Devices

In 1963, Shapiro[22] observed vertical current jumps (steps—see Fig. 10) in the DC *I-V* curves of Josephson tunnel junctions which were irradiated with X-band and K-band microwaves. The steps occurred at voltages V related to the frequency ν of the applied radiation by the generalized Josephson frequency-voltage relation $V = nh\nu/2e$ where n is an integer. They were interpreted as zero frequency sidebands arising from the frequency modulation of the AC Josephson currents in the junction by the applied microwave radiation. Similar step structure has also been observed in thin film and point-contact-type weak-link structures.

In 1964, Eck, Scalapino, and Taylor[23] observed step structure in Josephson tunnel junctions *without* any external radiation but with a small DC magnetic field applied. For this case the spacing of these self induced steps was determined by the junction dimensions and was interpreted as being due to the excitation of the characteristic modes of the junction (acting like an open ended resonator) by the AC Josephson currents in the junction.

Last year, two groups of workers[24,10,29] verified directly the existence of the AC Josephson current by detecting with a microwave receiver the radiation emitted by Josephson tunnel junctions. Using junctions with dimensions such that the self-induced steps were $\sim 20\mu V$ apart, radiation at X-band of order 10^{-11} to 10^{-12} watts was detected when the junctions were biased at the first step. The amount of DC power going into a typical junction used in these experiments was $\sim 10^{-7}$ watts and in principle, all of it was being converted into microwave radiation. However, the impedance of a Josephson tunnel junction is typically several milliohms; thus, the severe impedance mismatch between a junction and free space reduces the radiated power by a factor of 10^4 to 10^5.

Recently, Dayem and Grimes[25] have observed step structure in the *I-V* curve of a point contact weak link mounted in a coaxial cavity without applying external microwave radiation. The voltages V at which the steps occur are determined by the resonant frequencies ν of the cavity via the Josephson frequency-voltage relation $2\,eV = h\nu$. In this experiment, the *external* cavity determines the junction properties as contrasted with the oxide layer junctions in which the cavity formed by the *junction itself* determines its properties.

By biasing the point contact junction on its first step, which occurred at a voltage corresponding to a frequency of 9.2 GHz, Dayem and Grimes were able to detect better than 10^{-12} watts of radiation from the junction. The conversion efficiency—the ratio of radiated power to DC power fed into the junction—was $\sim 0.1\%$. This was an improvement of 10 to 100 over the efficiencies obtained with the oxide-layer junctions. By increasing the pressure on the point contact, they found that the step structure in the *I-V* curves could be made to disappear. At the same time, the resistance of the contact decreased by a factor of 40 (the current increased from $125\mu A$ to 5mA at a bias of $20\mu V$). However, more than 10^{-10} watts of 9.2-GHz radiation was observed coming from the junction when it was biased at a voltage corresponding to this frequency. This work has now been extended to 30 GHz with power levels of the order of 10^{-9} watts.

Another group of workers (Richards,

Grimes, and Shapiro)[26] have studied the sensitivity of point contact junctions to small amounts of externally applied microwave radiation. Using a far infrared spectrometer, it was found that typical point contacts could detect the presence of as little as 10^{-12} watts of radiation in the millimeter-wave range (by *detect* is meant measurable changes in the junction *I-V* curves). In another experiment, they have observed the effect of what was probably several hundred GHz radiation emitted by one point contact on the *I-V* curve of another in close proximity to the first.

Finally, we mention that Shapiro[27] has observed radiation at 12 GHz from weak link structures used as harmonic generators. The radiation was at the 2nd or 3rd harmonic of the input frequency. The structures used were formed by quick freezing a drop of low melting superconductor such as Sn, Pb or some Sn-Pb solders around an oxidized wire of Ta or Nb.

With the above experimental observations in mind, we are now in a position to enumerate and discuss some of the possible device applications of the AC Josephson effect. (In what follows, the word *junction* implies weak-link structures as well as Josephson-type oxide layer tunneling junctions).

1) *Direct generation of microwave radiation.* One of the most obvious applications for AC Josephson effect devices is the generation of coherent microwave radiation in the range 5 GHz to 1,000 GHz. The upper frequency will be limited by self absorption in the superconductors and will depend on the material used. The power available is small ($\sim 10^{-6}$ watts at most for one junction under optimum coupling conditions). However, arrays of junctions are possible and ten milliwatts at several hundred GHz is not inconceivable.
2) *Harmonic generation of microwave radiation.* Radiation may be generated harmonically using the AC Josephson effect in the following way. Radiation at some convenient frequency is applied to a junction. This radiation will generate a step pattern in the junction *I-V* curve at voltages corresponding to frequencies many times the frequency of the incident radiation. By biasing the junction on one of these higher voltage steps, radiation at higher harmonics can be obtained.
3) *Detection of microwave radiation.* Josephson junctions can also be used as detectors of radiation. Induced step structure has been observed in the *I-V* curves of point contact junctions when irradiated with as little as -70 dBm (10^{-10} watts) of X-band radiation while changes in the *I-V* curves of similar point contact junctions at power levels of -90 dBm (10^{-12} watts) in the millimeter range have also been observed.
4) *Combined local oscillator and mixer.* The highly nonlinear *I-V* curves of Josephson junctions suggest their possible use as a combination local oscillator and mixer. For example, with the junction biased on a given natural step and a small external signal incident upon the junction, an IF signal can be taken from the junction at a frequency equal to the difference between that of the incident radiation and that of the radiation corresponding to the junction bias voltage.
5) *Frequency meters.* By using the generalized frequency-voltage relation, $2eV = nh\nu$, Josephson junctions can be used as frequency meters. For example, a junction is irradiated with radiation of an unknown frequency ν and a step pattern induced in its *I-V* curve. By precisely measuring the voltages at which the steps occur, ν can be computed from the above equation to at least $\sim$10ppm.
6) *Frequency controlled reference voltages.* This application is operationally very similar to that given in (5) above. However, it is the frequency ν which must be accurately measured—for example, by counting techniques, and the voltage computed from the equation $2eV = nh\nu$.

MISCELLANEOUS DEVICES

Infrared radiation can be detected by means of superconductors used as bolometers. By maintaining a superconductor at a temperature sufficiently close to its transition temperature (for example, a temperature such that its resistance is half its normal state resistance) small changes in the temperature of the superconductor as would occur due to the absorption of radiation, give rise to large changes in resistance. In this manner, superconducting bolometers can detect 10^{-11} watts of thermal radiation under optimum conditions of operation.[28]

Finally, it should be mentioned that since superconductors are capable of providing large magnetic fields with a negligible expenditure of power, they are appropriate for use with microwave devices such as the maser.

CONCLUDING REMARKS

Superconductors are characterized by ultra-low loss factors at frequencies which extend, for some materials, into the far-infrared. Thus, the improved performance attainable in devices such as high-selectivity cavities and delay lines is marked. In systems which require cryogenic operation in any case (e.g., the maser) their use will likely be widespread. In other systems, the factors of performance, size and cost must all be weighed.

Other microwave devices—e.g., those which use parametric or Josephson phenomena—are relatively new and neither entirely understood nor developed. Thus, while near-term system application is not contemplated, interest in these areas is continuing.

BIBLIOGRAPHY

1. J. I. Gittleman and B. Rosenblum, "Microwave Properties of Superconductors," *Proc. IEEE*, Vol. 52, pp. 1138-1147, October 1964.
2. E. A. Lynton, *Superconductivity*, John Wiley and Sons Inc., New York, N. Y., Second Edition, 1964.
3. C. J. Gorter and H. B. G. Casimer, "Zur Thermodynamik des Supraleitenden Fustandes," *Phyz. z.*, Vol. 35, 963 (1934).
4. R. H. Parmenter, "Nonlinear Electrodynamics of Superconductors with a Very Small Coherence Distance," *RCA Review*, XXIII, 323 (1962).
5. V. L. Ginzburg and L. D. Landau, "On the Theory of Superconductivity," *J. Exp. Theor. Phys. (USSR)*, 20:1064 (1950).
6. J. Gittleman, et. al, "Nonlinear Reactance of Superconducting Films," *Phys. Rev.*, 137:A527 (1965).
7. A. S. Clorfeine and F. J. Young, "Inductance vs. Current Characteristics of Superconductors," *Proc. IEEE*, Vol. 54, 415 (1966).
8. For a more detailed discussion, see M. D. Fiske and I. Giaever, "Superconductive Tunneling," *Proc. IEEE.* Vol. 52, pp. 1155-1163, October 1964.
9. B. D. Josephson, "Supercurrents Through Barriers," *Advances in Physics*, Vol. 14, pp. 419-451, October 1965.
10. D. N. Langenberg, D. J. Scalapino, and B. N. Taylor, "Josephson Type Superconducting Tunnel Junctions as Generators of Microwave and Submillimeter Wave Radiation," *Proc. IEEE*, Vol. 54, pp. 560-575, April 1966.
11. This example was previously used; see I. Kaufman, "Microsecond Time Delay of Microwave Signals, Part I," *The Microwave Journal*, pp. 51-58, June 1966.
12. P. K. Shizume and E. Vaher, "Superconducting Coaxial Delay Line," *IRE International Convention Record*, ED, Part 3, MTT, pp. 95-99, 1962.
13. A. S. Clorfeine, *The Nonlinear Inductance of Superconductors and its Application to Parametric Amplification*, Ph.D. Thesis, Dept. of Elect. Eng., Carnegie Inst. of Tech., Pittsburgh, Pa., 1966.
14. A. S. Clorfeine, "Nonlinear Reactance and Frequency Conversion in Superconducting Films at Millimeter Wavelengths," *App. Phys. Lett.*, Vol. 4, pp. 131-132 (1964).
15. R. V. D'Aiello, "Parametric Amplification and Oscillations in Structured Superconducting Sn Films," *to be published.*
16. A. S. Clorfeine, "Microwave Amplification with Superconductors," *Proc. IEEE*, 52, 844 (1964).
17. P. Bura, "Parametric Amplification with Superconducting Films," *Proc. IEEE*, 54, 687 (1966).
18. J. L. Miles, P. H. Smith, and W. Schonbein, "Oscillation and Amplification at VHF Utilizing Electron Tunneling Between Superconducting Metals," *Proc. IEEE (Correspondence)*, Vol. 51, pp. 937-938, June 1963.
19. A. C. Scott, "Distributed Device Applications of the Superconducting Tunnel Junction," *Solid State Electronics*, Vol. 7, pp. 137-146, February 1964.
20. S. Shapiro and E. J. McNiff, Jr., *Superconductive Effects in Thin Films*, Technical Documentary Report No. AL-TDR-64-46, March 1964 (AF Avionics Laboratory, Research and Technology Division, Air Force Systems Command, Wright-Patterson Air Force Base, Ohio).
21. E. Burstein, D. N. Langenberg, and B. N. Taylor, "Quantum Detection of Microwave and Submillimeter Wave Radiation Based on Electron Tunneling in Superconductors," *Advances in Quantum Electronics*, J. R. Singer, Ed. New York: Columbia University Press, 1961, pp. 480-495.
22. S. Shapiro, "Josephson Currents in Superconducting Tunneling: The Effect of Microwaves and Other Observations," *Phys. Rev. Letters*, Vol. 11, pp. 80-82, July 1963.
23. R. E. Eck, D. J. Scalapino, and B. N. Taylor, "RF Tunnel Junction Modes Driven by The ac Josephson Current," *in Proc. IXth Internat'l. Conf. on Low Temperature Phys.*, J. G. Daunt, Ed. New York: Plenum, pp. 415-420, 1965.
24. D. N. Langenberg, D. J. Scalapino, B. N. Taylor, and R. E. Eck, "Investigation of Microwave Radiation Emitted by Josephson Junctions," *Phys. Rev. Letters*, Vol. 15, pp. 294-297, August 1965.
25. A. H. Dayem and C. C. Grimes, "Microwave Emission From Superconducting Point-Contacts," *Appl. Phys. Letters*, Vol. 9, pp. 47-49, July 1, 1966.
26. C. C. Grimes, P. L. Richards, and S. Shapiro, "Far Infrared Response of Point Contact Josephson Junctions," *Phys. Rev. Letters, 17*, Vol. 17, pp. 431-433, August 1966.
27. S. Shapiro, "Microwave Properties of a New Form of Josephson Junction," *Bull. Am. Phys. Soc.*, Vol. 11, p. 479, June 1966.
28. R. A. Smith, F. E. Jones, and R. P. Chasmar, *The Detection and Measurement of Infra-Red Radiation*, London: Oxford University Press, 1957.
29. I. K. Yanson, V. N. Svistunov, and I. N. Dmitrenko, Soviet Physics, JETP 21, 650 (1965).

SUPERCONDUCTING MICROWAVE FILTERS

This paper discusses the various aspects of using superconducting materials in microwave filters. The minimum theoretical filter insertion loss, and associated high resonator unloaded Q's (in excess of 10^8), are discussed as functions of the superconducting materials, the operating temperature, and the individual resonator modes. The maximum power that can be passed through a direct-coupled superconducting filter is analyzed theoretically with respect to the peak fields existing in a superconducting cavity resonator before threshold (i.e., a superconducting-to-normal transition at a critical peak magnetic field, or a breakdown due to a peak electric field). Several experimental cavities have been evaluated, and the actual attainable cavity Q's are compared with those predicted.

E. W. MARKARD and B. S. PERLMAN

Advanced Communications Laboratory
Communications Systems Division
DEP, New York City

THE use of ultra-low-noise microwave masers and parametric amplifiers, operating at cryogenic temperatures, has resulted in the development of additional cryoelectric microwave components. The overall receiver noise is dependent upon the insertion losses of any diplexer, circulator, or filter device introduced into the transmission system between the antenna and the low-noise amplifier. Of particular interest is the design of superconducting microwave preselectors, which are characterized by noise temperatures below those of the corresponding preamplifiers. Another consideration is the high isolation between transmitter and receiver possible with a diplexer which might use both a superconducting high-power transmitter filter and low-noise receiver filter.

Final manuscript received August 15, 1966.

NEED FOR LOW-NOISE SYSTEMS

The increasing need for ultra-low-noise receiving systems has resulted in the use of a cryogenic environment for parametric and maser amplifiers. Additional improvement in the over-all system noise figure may be achieved if the preselection filters are included in the cryogenic system. In particular, the use of superconducting cavities for the filter resonators would significantly decrease the contribution of the filter insertion loss to the effect system noise temperature.

The primary sources of noise, preceding the preamplifier comprise a combination of the antenna temperature and the equivalent noise temperatures resulting from the insertion losses between the antenna and the amplifiers. For a minimum noise system, it may be assumed that the feed-line losses are due primarily to the preselector or diplexer.

SYSTEM NOISE TEMPERATURE

In a microwave receiver system, where the receiver amplifier is operating in a cryogenic medium, a noise temperature T_R of 10 to 20°K is possible with state-of-art masers and paramps. The addition of a practical antenna system with noise temperatures, T_A, varying from 100°K

E. W. Markard

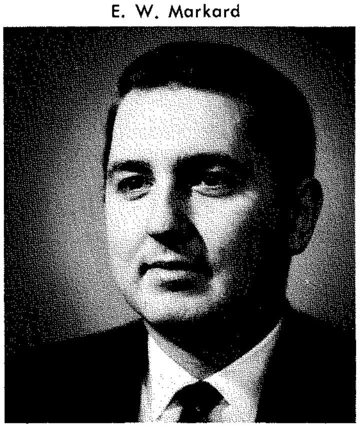

B. S. Perlman

EDGAR W. MARKARD received the BEE degree from the City College of New York in January 1961. He joined RCA in February 1961 in the Design and Development Training Program. In August 1961 he was assigned on a permanent basis to the Advanced Microwave Techniques Group at CSD-NY Laboratories, where he participated in the S-band, broadband paramp development program. At the completion of that program, he began working on the development of varactor frequency multipliers. He was responsible for the development of a high-power microwave varactor multiplier chain for the Solid State Radio Relay program which yielded two watts at C-band. In 1963 he was assigned (in cooperation with RCA Laboratories) to the CSD-NY Cryoelectric Program, which has as its objective the development of a parametric amplifier based on the superconducting properties of thin films. Here he helped develop a superconducting parametric amplifier which exhibited a net gain of 9 dB at S-band. In parallel with this program, he has worked on high-power tunable and broadband varactor frequency multipliers, and participated in the development of the theory of high nonlinearity (hyper-abrupt) varactor devices. In connection with the latter, he built an idler-less frequency octupler from 500 MHz to 4 GHz, with 25% efficiency. In 1965 he was responsible for setting up the CSD-NY Cryogenic Laboratory, and worked on the theory and design of superconducting and cooled microwave filters, and the theory and design of miniature microwave filters using high permittivity low-loss materials. His latest assignment is in the field of signal enhancement. Mr. Markard is a member of the IEEE, the American Institute of Aeronautics and Astronautics, and holds office in the N.Y. Alumni Chapter of Eta Kappa Nu.

B. S. PERLMAN received his BEE degree from CCNY in 1961, and an MSEE degree from the Polytechnic Institute of Brooklyn in 1964. In 1961, he joined RCA as a specialized trainee in DEP Applied Research where he was introduced to concepts of signal processing, radar receivers, and parametric amplifiers. In late 1961 he became an employee of Communications Systems Engineering in New York where work was continued in the development of active low-noise and broadband reactive devices. He developed several high-power varactor devices, among which was a 5 Gc converter with 50% efficiency for use in all-solid-state relay equipment. In 1963, Mr. Perlman studied various aspects of lasers at the RCA Laboratories, and returned to New York to develop a laser communication system; of primary interest was the development of efficient optical modulators. He has recently been concerned with intermodulation distortion in amplifiers, the development of broadband reactance devices, and a study of the use of superconducting materials at microwave frequencies. Mr. Perlman has published numerous papers related to his work and has several patent disclosures; he is a member of IEEE, PTGMTT and NYSSPE.

to 10°K for frequencies between 1 and 10GHz, respectively, in addition to the insertion loss of a normal microwave filter network, has a decided effect upon the system performance. The decrease of receiver range capability as a function of the losses attributed to the antenna and filter combination is shown in Fig. 1 where the relative range R' is plotted as a function of an effective filter loss $(T_F' + L)$, with T_A' as a parameter, where:

$$R' = \frac{\text{Range of System}}{\text{Range of Receiver Alone}}$$

$$= (T_F' + L + T_A')^{-1/2}$$

The primed variables are quantities normalized to the receiver characteristics (i.e., $T_A' = T_A/T_R$). The terms L and T represent the midband filter insertion loss and ambient temperature respectively. The area of interest, $0° \leq T_A \leq 1.0$, $T_R = 20°K$, $(T_F' + L) \leq 2.0$ represents a low-loss system. If the antenna

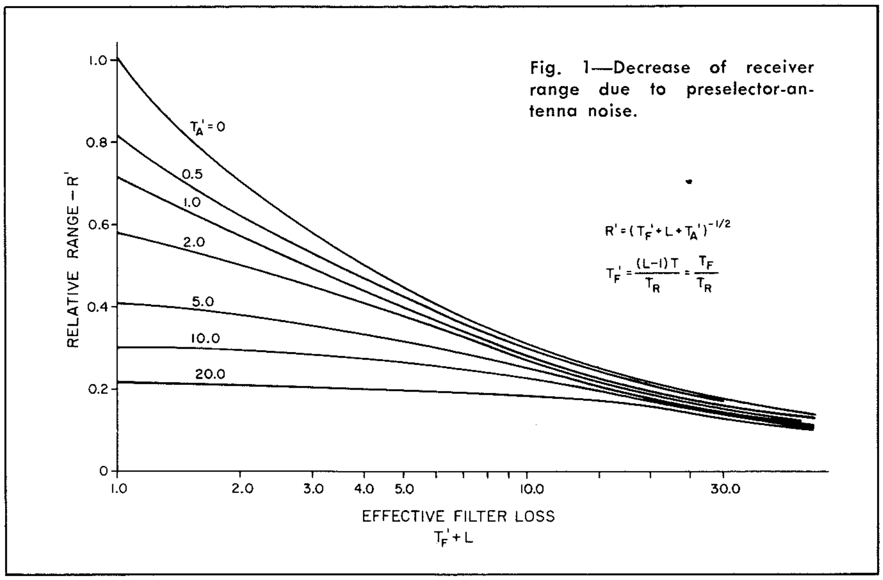

Fig. 1—Decrease of receiver range due to preselector-antenna noise.

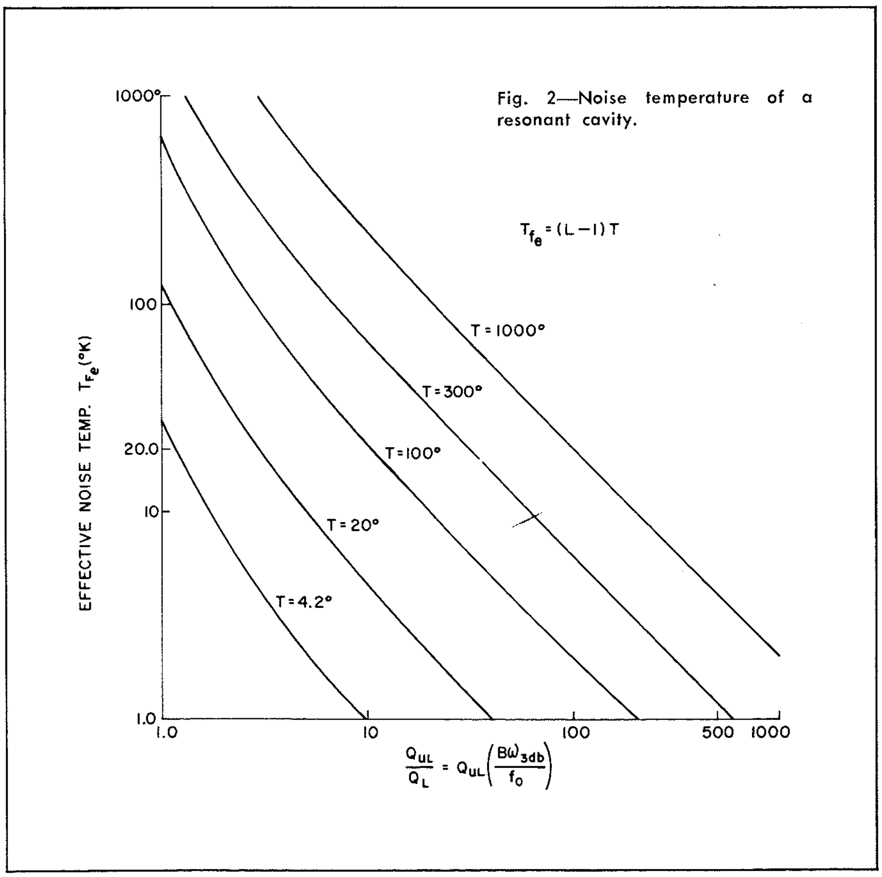

Fig. 2—Noise temperature of a resonant cavity.

or receiver noise was relatively higher, there would be no gain in improving the filter performance. With a low-noise antenna and receiver temperature, achieving a filter of less than 20°K for narrow bandwidths requires the use of superconductors.

Fig. 2 is a plot of the effective filter noise T_F for a single resonant cavity, as a function of Q_{UL}/Q_L and represents a *minimum loss* condition. At 300°K, a normal X-band cavity ($Q_{UL} = 10^4$) with a 10MHz bandwidth has $T_F = 65°$. Increasing the number of resonators would result[1,2] in an increase of T_F. A reduction in bandwidth to 10kHz is possible with $T_F = 2°K$ if $Q_{UL} = 5 \times 10^6$, a condition which is possible *only* with superconducting cavities. The cavity insertion loss would be 1.74 dB, resulting in an effective loss, relative to a 20°K receiver of $(T_F' + L) \cong 1.6$. The use of very-narrow-band systems, particularly for long-range telemetry, extends the relative range of Fig. 1 by a factor $(B')^{-1/2}$ where B' is the ratio of the superconducting filter bandwidth to the original receiver bandwidth. Another consideration in the use of narrow band receivers is the significant improvement in skirt selectivity. The use of superconducting resonators permits the use of a larger number of sections, in addition to obtaining increased values of Q_L, without a degradation of the low values of filter noise temperature.

PROPERTIES OF SUPERCONDUCTORS

A detailed study of superconductors is available in several references.[3,4,5] Figs. 3 and 4 demonstrate the relation between the surface resistance R_s and temperature for Type I and Type II superconductors operated below their critical temperatures T_c, relative to the normal resistance R_n, measured at a temperature slightly higher than T_c, with frequency as a parameter. An abrupt transition for R_s/R_n occurs only for DC excitation (curve A). At RF, the variation of R_s/R_n is gradual, curve B approaching a finite residual resistance R_o. A superconducting-to-normal electron transition occurs when an energy greater than:

$$h\nu_g = 3.52\,KT_c \qquad (2)$$

is absorbed by the superconductor, as shown by curve C. This normal transition usually occurs at submillimeter wavelengths as predicted by BCS theory.

The quantum energy ($h\nu_g$) is required to decouple a pair of superconducting electrons into two "normal" electrons. The value of ν_g is strictly true only for $T = 0°K$ but is a very good approximation up to operating temperatures of $T = 0.6\,T_c$.

At this point, it would do well to compare the physical properties that cause a superconductor to be classified as Type I or Type II. If the magnetization M and the resistive R_s/R_n transitions of superconductors are plotted as functions of applied magnetic field H, the resulting curves for pure Type I and pure Type II are as shown in Fig. 3 and Fig. 4, respectively. In Type I, which is exemplified by pure mercury or tin single crystals, magnetic induction and electrical resistivity change suddenly and reversibly at a well-defined critical field, commonly denoted as H_c. This is usually described as the "ideal case" in standard textbooks. The existence of pure Type II superconductivity has only been established within the last decade. In Type II materials, magnetic flux penetrates into the metal at a much lower field (H_{c1}) and that (H_{c2}) at which the resistance ceases to be zero. The region between H_{c1} and H_{c2} is known as the mixed state. In this case, instead of the material retaining zero induction until H_c is reached, the material tends to split up into superconductive and normal regions, beginning with $H = H_{c1}$. The superconductive regions act as zero-resistance short circuits across the normal regions and hence the DC resistance does not appear until $H = H_{c2}$, where the superconductive regions disappear. Type II behavior is exemplified by Nb single crystals, most superconductive alloys, and by pure lead at temperatures below $\frac{1}{2}$ T_c.

If the resistive transitions for the high-frequency case are considered, the situation is more like that pictured by the dashed curves in Figs. 3 and 4. Now it can be said that the behavior of a Type II superconductor below its H_{c1} is essentially the same as that for a Type I superconductor below its H_c. Hence, one can compare the H_{c1} of a Type II material to the H_c of a Type I material in order to determine the one that can sustain higher magnetic fields.

Before this comparison can be made on a quantitative basis, certain postulates must be stated. It is assumed now that the superconducting filters will operate at a temperature near 4.2°K. This is to make the operation of these filters compatible with existing and near future closed-cycle refrigerator technology. Therefore, the prime rival of niobium ($T_c = 9.46$°K) for this application is lead ($T_c = 7.18$°K) with a slim possibility also for tin ($T_c = 3.72$°K).

To obtain numerical values for the critical fields of lead and tin, a standard text on superconductivity can be used. Thus at 3°K, for tin, the $H_c = 100$ gauss, while at 4.2°K, the H_c for lead is 550 gauss. (At 4.2°K, it is valid to deal with lead in terms of H_c, since at this temperature it is a Type I material.) Consideration of these numerical values for H_c and the fact that lead has a consistently higher value than tin for all temperatures allows us to dispense with tin by saying that lead is better than tin.

Niobium Stannide (Nb_3Sn) has been considered as an exotic superconductor, the use of which would offer a high power handling capability in a superconducting microwave filter. This was due to the exceptionally high critical field (H_c) attributed to this material. However, a closer look at the magnetic field behavior of Nb_3Sn revealed that in order to avoid filter operation in regions where hysteresis and other nonlinear effects occur, the maximum applied H-field must be less than the lower critical field (H_{c1}) of the superconductor. Since the H_{c1} of the Nb_3Sn is comparable to the critical field of Sn, which in turn is less than that of Pb, the Nb_3Sn offers no real advantage over the more conventional lead and tin superconducting cavities insofar as power handling and linear operation is concerned. This factor and the fact that the fabrication of an experimental filter of Nb_3Sn is extremely difficult, has led to the shelving of Nb_3Sn for the present as a superconducting material.

The pure metal superconductor niobium has two distinct advantages over lead. First, Nb has a higher critical temperature ($T_c = 9.46$°K) than Pb ($T_c = 7.18$°K). Therefore, at standard liquid helium temperature (4.2°K), the Nb would be operating at a lower reduced temperature ($t = T/T_c = 0.444$) than Pb ($t = 0.588$) and this would help avoid non-linear operation.

Secondly, the H_{c1} for Nb is approximately 1,000 gauss. This again raises the possibility of higher-power superconducting filters. The fabrication problems associated with Nb are much less severe than those associated with Nb_3Sn. For example, Nb in pure bulk form has similar machining characteristics to copper, while Nb_3Sn is a very brittle material. As far as plating is concerned, there has been published the details of a process whereby Nb can be electrodeposited onto a base metal to obtain deposits that have a density almost 100% of theoretical and which at the same time are extremely pure. This process forms a metallic bond between the niobium and its substrate, thus reducing the temperature differential between the substrate and the cladding. This process, although more complex than conventional plating, is much simpler than the vapor transport process involved in depositing Nb_3Sn.

While superconducting materials show certain limitations when considered as low loss materials, i.e., the surface resistance does not completely disappear at high frequencies, they still represent an improvement of one or more orders of magnitude over conventional materials (copper, silver, etc.). It must be pointed out that conventional materials also have limitations, i.e., the anomalous skin effect. In materials such as copper, which normally obey the conduction relation $\bar{J} = \sigma\bar{E}$, the microwave $J(z)$ at a frequency f is found to penetrate the surface of the conductor according to the relation:

$$\frac{J(z)}{J(o)} = \exp(-z/\delta) \qquad (3)$$

where the skin depth $\delta = (\pi f \mu \sigma_n)^{-1/2}$. In copper at 10GHz, the room temper-

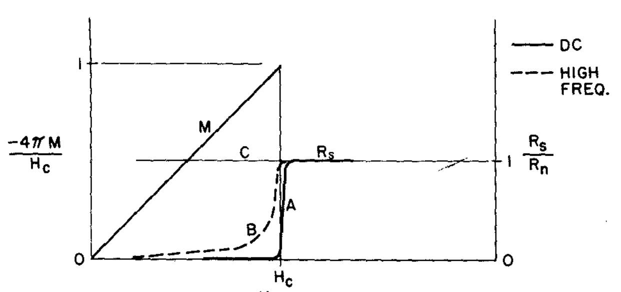

Fig. 3—Magnetization and resistive transitions for a type I superconductor.

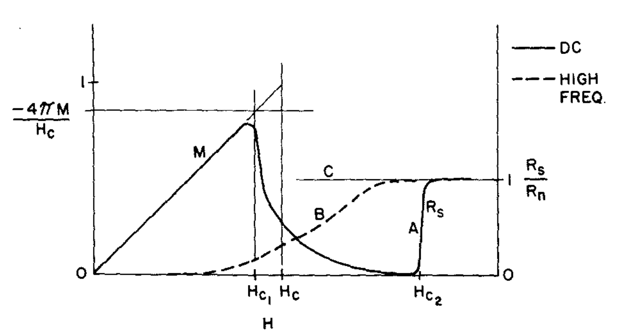

Fig. 4—Magnetization and resistive transitions for a type II superconductor.

ature skin depth δ is less than 10^{-4} cm. At cryogenic temperature (77°K), the mean free path l_c of the conduction electrons in the material can be made considerably larger than δ and the normal conduction relation no longer holds. In this condition, those electrons travelling in a path parallel to the surface in the region very near the surface will move through a uniform field between collisions, while those electrons travelling with any appreciable component of velocity normal to the surface will not remain long in the uniform field region. Only those of the total number of normal conduction electrons which closely approximate the travel of the former will be effective and hence the over-all conductivity will become anomalously low.

To evaluate this effect, a critically coupled copper cavity was constructed and tested. The object of this experiment was to measure Q_o as a function of temperature and to show that the increase in Q_o for operating temperatures below 77°K is small relative to the increase for a temperature change from room temperature to 77°K. The X-band measurements yielded an unloaded Q of 6,800 at room temperature, 12,000 at 77°K, and 13,000 at 4.2°K.

An important consideration in the use of very narrow bandwidth superconducting resonators is the effect of temperature changes on the stability of the center frequency. In a normal metal cavity, temperature variations would alter the physical dimensions of the cavity thus shifting the resonant frequency. This effect can be minimized by building the cavity using a base metal with a very small coefficient of expansion such as invar and then plating the base metal with a good conductor or a superconductor. However, in the case of a superconducting cavity, the effect of temperature on the penetration depth must be considered. This effect is:

$$\lambda_p = \frac{\lambda_f(0)}{\sqrt{1-\left(\frac{T}{T_c}\right)^4}} \qquad (4)$$

where λ_p (0) is the penetration depth at $T = 0$. As T varies, the penetration depth changes and alters the effective size of the cavity thus changing the resonant frequency.

FILTER CAVITY QUALITY FACTOR

The unloaded Q of the cavity is a function of the geometry, the mode configuration and conductivity of the walls. In general[6]:

$$Q_o = G\left(\frac{\lambda_o}{\delta}\right) = 1{,}185\,\frac{G}{R_s} \qquad (5)$$

where δ = skin depth, λ_o = resonant wavelength, G = geometric form factor, and R_s = real part of the surface impedance.

At temperatures well below T_c, the surface resistance of a superconductor is given by the following phenomonological relationship[7]:

$$R_s = A(\nu)\, f(t)\, R_n \qquad (6)$$

where A (ν) is a function of frequency only and $f(t)$ is a function of temperature only. Experimentally determined values of $A(\nu)$ for various materials are found in the literature.[8] At 9GHz, the $A(\nu)$ for lead is approximately 0.1. The $f(t)$ is given by:

$$f(t) = \frac{t^4\,(1-t^2)}{(1-t^4)} \qquad (7)$$

where $t = T/T_c$. The R_n can be determined from the expression for the surface impedance of a normal metal in the extreme anomalous limit. Hence,

$$R_n = \left(\frac{\sqrt{3}\,\pi\,\omega^2}{c^4}\right)^{1/3}\left(\frac{l}{\sigma}\right)^{1/3} \qquad (8)$$

From tabulated values[9] for l/σ, the R_n can be calculated for various materials.

For lead at 9 GHz, $R_n = 6.5 \times 10^{-3}\Omega$.

For $T = 4$°K, $t = 0.56$ and $f(t) = 0.073$.

Now R_s can be calculated for lead at 4°K:

$$R_s = (0.1)\ (0.073)\ (6.5)\ (10^{-3}) = 4.75 \times 10^{-5}\,\Omega$$

For a TE_{111} cavity mode, $G = 0.27$ and the expected unloaded Q is:

$$Q_o = 1{,}185\,\frac{0.27}{4.75 \times 10^{-5}} = 6.75 \times 10^6$$

and, for a TE_{011} mode configuration, may approach a maximum value of:

$$Q_{o_M} = 1.65 \times 10^7$$

The present state-of-the-art in closed-cycle cryogenic refrigeration makes it practical to operate near the boiling point of liquid helium (4.2°K). However, certain theoretical considerations make it desirable to consider operation of superconducting microwave cavities at lower temperatures for future application.

The first such consideration is that unloaded Q's in the order of 10^9 are theoretically possible for an X-band TE_{011} electroplated lead cavity at 2°K, compared with theoretical Q's of 2.4×10^7 when the same cavity is operated at 4°K. It has been reported[10] that a Q_o of 3.7×10^9 has been measured at 3GHz with a lead-plated cylindrical cavity operating at 2°K.

The second consideration is that when the liquid helium-4 bath is operated below its lambda point (2.17°K), the bath is a superfluid with a thermal conductivity much greater than copper at room temperature. This implies that the dissipated heat in the microwave filter can be conducted out through the bath without the creation of appreciable temper-

Fig. 5—Unloaded Q vs. temperature for X-band cylindrical cavities (f_o = 9Gc).

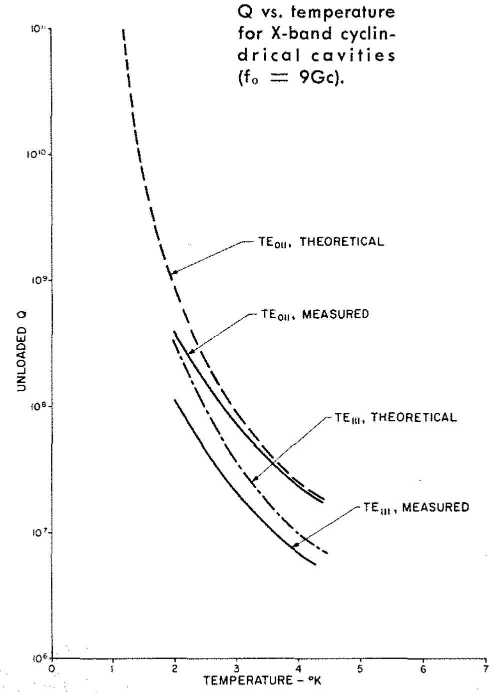

ature gradients. This is an important consideration in the stability of a microwave filter with considerable power dissipation, since the electrical stability is a function of the temperature stability of the bath.

For the case of a microwave cavity with superconducting boundaries operating at a frequency much less than the gap frequency, the unloaded Q is shown in Fig. 5 as a function of T for TE_{011} cylindrical cavity with lead boundaries operating at 9GHz. This result is based upon the microscopic theories of superconductivity.[11] The solid curve shows the results of the measurements on such a cavity mentioned above. A reentrant (one-port) and a two-port electroplated lead cavity are shown in Fig. 6. The two-port filter is shown assembled for cryostat operation in Fig. 7.

POWER HANDLING CONSIDERATIONS IN A SUPERCONDUCTING FILTER

The peak power which may be passed through a normal microwave filter is primarily limited by the maximum peak electric field which may be sustained before breakdown or field emission in either the cavities or coupling lines, for gas filled or evacuated guide, respectively. An additional peak power limitation exists when the normal metal cavity surfaces are replaced by a super-

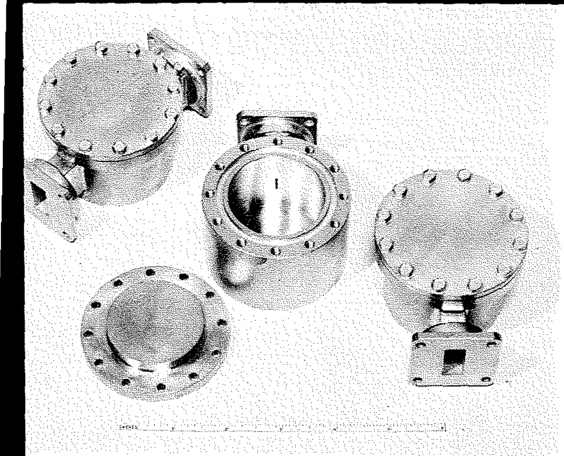

Fig. 6—A one- and a two-port X-band superconducting electroplated lead cavities.

conductor. The new mechanism is characterized by a superconducting-to-normal-mode transition in the presence of high peak magnetic fields. The threshold in this transition occurs when the peak H_{fld} becomes equal to the critical H_{fld} for the particular superconducting material used.

The maximum average power which can pass through a superconducting filter is limited by the thermal capacity of the cryogenic system. This capacity is related to the rate at which power is dissipated in the metallic cavity walls, and is related to the ratio of leaded to unleaded cavity Q's. Because of the increase in thermal conductivity of superconductors and the associated high Q ratio, large average powers may be handled in this type of filter. The power limitations of superconducting direct-coupled resonator filter are of a primary importance and are derived below.

An analysis of the pulse-power capacity of narrow bandpass direct-coupled filters[12,13] relates the fields that exist in any cavity of this type of filter to the field that would exist in a matched transmission line having the same geometrical cross-sectional characteristics as the individual cavities. A typical waveguide filter is shown schematically in Fig. 8.

Since each coupling element is characterized by an inversion impedance Z_{ck} and $\phi_{ck} = \pi/2$, the fields appearing at the center of each cavity may be readily found, in relation to the fields which exist in the terminating line of a similar cross-section. At the midband frequency, the field relationship becomes:

$$E_i = E_T \frac{\lambda_o}{\lambda_{go}} \sqrt{\frac{2 g_i \omega_1'}{n_i \pi B'}} \qquad (9)$$

where $B' = (f_2 - f_1)/f_o$, f_1 f_2 = band edge frequencies of filter response, ω_1' = normalized low-pass prototype frequency corresponding to band-edge frequencies f_1 and f_2, g_i = normalized element value, and n_i = number of half wavelengths of λ_{go} in the ith cavity.

In general, when ω_1' is set equal to unity, denoting a normalized low-pass prototype response cut-off frequency, a maximally flat filter is characterized by a 3dB, $(f_2 - f_1)$ bandwidth, whereas an equal ripple response requires $(f_2 - f_1)$ to correspond to the ripple, or A_m bandwidth.

Since the power is proportional to the square of the electric (or magnetic) field, the peak allowable cavity power must be reduced by the ratio (E_i/E_T) so that E_T remains the maximum guide field strength. Thus,

$$(P_i)_o = P_i' \left[\frac{\pi n_i B'}{2 g_i \omega_1'}\right] \left[\frac{\lambda_{go}}{\lambda_o}\right]^2 \qquad (10)$$

where P_i' is the pulse-power of a matched waveguide having the same cross-sectional dimensions as the cavity under consideration.

In general, for the Butterworth and Tchebychev responses, the values of g_k are not equal. Thus, the peak power that may be sustained by the multiple resonator filter is limited by that cavity having the largest g_i. However, if all the g's are equal, particularly to unity (equal resonator condition), the midband pulse power is maximized for a given off-channel selectivity. Although a minimum midband insertion loss exists for this type of filter, the inband ripple is quite appreciable. This type of filter construction is therefore restricted to central pass-band operation to avoid high reflections.

By introducing variable cross-sectional geometry, the unequal g_i condition with desired response characteristics may be used and still maintain an equal $(P_i)_o$ throughout the filter. The introduction of larger cavities would support higher modes which would tend to be suppressed by the smaller cavities. If this unequal cross-sectional geometry is undesirable, the power capacity may be extended by increasing the number of resonators. The increased insertion losses may be overcome by the high superconducting unloaded Q. An examination of the distribution of peak fields inside a multiple cavity device, indicates that within the pass-band, the fields are a minimum at the center frequency, rising to sharp peaks just outside each resonator passband.[14] The results computed for several filters indicate an increase in field strength by as much as 3:1 between the out-of-band field and midband field for several common filter cavity configurations. The highest increase of fields occurs generally in those cavities which are nearest the generator.

This increased field just outside of the filter passband must be considered

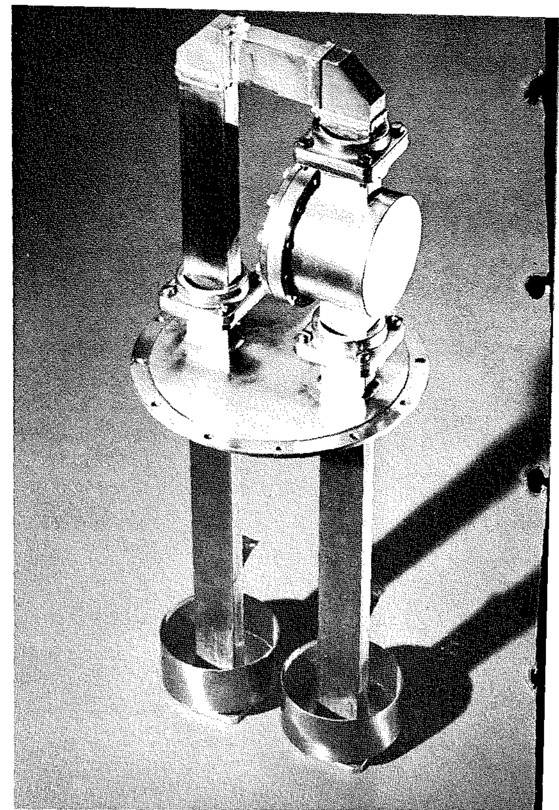

Fig. 7—An assembled X-band superconducting filter.

Fig. 8—Waveguide cavity filter.

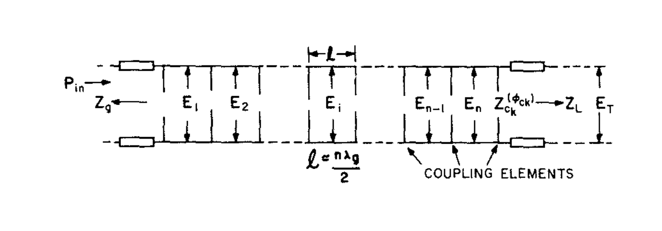

Fig. 9—Relative cross-sectional dimensions of several fundamental waveguide modes.

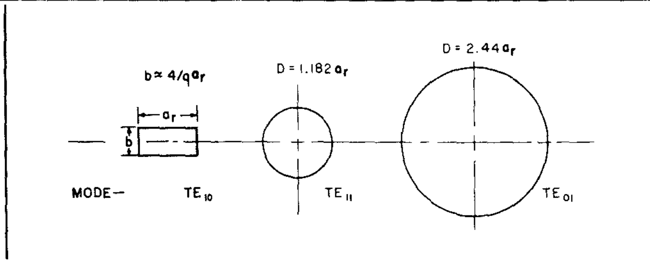

with regard to the separation in frequency between the transmit and receive filters of a superconducting diplexer. An excessive field due to the out-of-band transmitter could switch the receiver superconducting filter normal resulting in both detuning and increased insertion losses in the latter device.

A comparison of the maximum midband pulse power ratings of several types of matched waveguide, and the resulting midband cavity pulse power using Equation 10 is shown below. For the purpose of a practical comparison, assuming equal operating frequencies, the guide cut-off wavelengths have been chosen to be equal. Consequently, the cross-sectional dimensions of the various guides are different. Fig. 9 indicates the relative sizes of three distinct guides operating in their fundamental modes.

The relationships of Table I have been found for evaluating the midband pulse-power limitations of the three waveguides shown in Fig. 9, operating into a matched load.[6] In Table I, the maximum value of longitudinal H_Z field has been evaluated for $r = D/2$ at the waveguide wall which is operating in a superconducting mode. The maximum superconductor critical field H_c, is given in amperes/cm with the wavelengths in cm. The waveguide is assumed to be evacuated, and is characterized by an intrinsic impedance of 377 ohms.

Since the electric field gradient might cause a power limitation for certain types of cavities, it is desirable to express the values of P' in terms of the maximum attainable electric fields for each particular mode. Using $E_{max} = 350$ kV/cm as a design example for the maximum electric field that might exist in an evacuated section of waveguide before breakdown, the following limiting values for P_{max} are found, as shown in Table II. These results have been found by calculating the maximum electric field which could exist in each particular mode geometry. In order to compare these E_{fld} results with the critical field results in Table I, a value of 560 gauss for superconducting lead at 4.2°K has been used. These results indicate a rather close correspondence between the limiting pulse power based on either mechanism, particularly for the circular TE_{10} mode where a cutoff wavelength design of 1.44λ would result in a threshold condition for both breakdown mechanisms. A further increase in cutoff wavelength would permit the electric field to dominate in breakdown. It is also remembered that these results have been calculated for an evacuated matched section of waveguide. At atmospheric pressure ($E_m = 29$ kV/cm) the breakdown mechanism would, in general, always result from an electric field limitation.

A quantitative estimate of this power may be found for an example, where $P_E' = P_H'$ for TE_{01} circular mode. In this case, with $\lambda = 3.33$ cm (9GHz), the limiting power becomes $P' = 135\lambda^2 = 1.5 \times 10^3$MW. The limiting pulse-cavity power is readily found from these results by using Equation 10. Assuming a multiple cavity filter where the largest value of g_i is nominally equal to 2, $n_i = 1$, $w_1' = 1$, $(\lambda_g/\lambda_o) = 1.4$ and a loaded Q_L of 10^6, the resulting $(P_i)_o = 2.3$-kW peak power.

The primary limiting peak power variable in Equation 10 is the fractional bandwidth B'. A reduced bandwidth results in a reduced allowable pulse power. However, it will be shown that the reduction of B' will also allow small frequency separation between the transmitter and receiver filters. Normally, a severe reduction in filter bandwidth is associated with an increase in midband insertion loss, but in this case, operating in a superconducting mode, the inband loss may be kept at minimum.

The feasibility of using a superconducting filter in the transmitter arm of a diplexer is a function of the desired value of B'. A value of $Q_L = 10^3$ with $B' = 10^3$ would permit a transmitter pulse power of up to 2.3 MW to be used.

TABLE I—Maximum Matched Line Power

Mode	λ_c	P'_{max} (watts)	Longitudinal H_Z Distribution
TE_{10}	$2\,a_r$	$10.5\,H_c^2\left(\frac{\lambda_c^4}{\lambda\lambda_g}\right)$	$H_Z = H_{ZM}$
TE_{11}	$1.706D$	$35.9\,H_c^2\left(\frac{\lambda_c^4}{\lambda\lambda_g}\right)$	$H_Z = H_{ZM}\exp(i^\theta)\,J_1\,(3.68\,r/D)$
TE_{01}	$0.820D$	$222\,H_c^2\left(\frac{\lambda_c^4}{\lambda\lambda_g}\right)$	$H_Z = H_{ZM}\,J_o\,(7.66\,r/D)$

TABLE II—Comparison of E_{fld} and H_{cfld} Power Limitations

Mode	E_{fld} (350 kV/cm) LIMIT	$H_c = 446A$/cm = 560 gauss	Relative Power Limit $\frac{P_E'}{P_H'}$
	(P_E')	(P_H')	
TE_{10}	$9.1\left(\frac{\lambda}{\lambda_g}\right)\gamma_c^2$	$2.09\left(\frac{\lambda_c^4}{\lambda\lambda_g}\right)$	$4.35\left(\frac{\lambda}{\lambda_c}\right)^2$
TE_{11}	$21\left(\frac{\lambda}{\lambda_g}\right)\gamma_c^2$	$7.15\left(\frac{\lambda_c^4}{\lambda\lambda_g}\right)$	$2.94\left(\frac{\lambda}{\lambda_c}\right)^2$
TE_{01}	$91\left(\frac{\lambda}{\lambda_g}\right)\gamma_c^2$	$44.2\left(\frac{\lambda_c^4}{\lambda\lambda_g}\right)$	$2.06\left(\frac{\lambda}{\lambda_c}\right)^2$

CONCLUSIONS

The design of the actual filter may be based upon several standard procedures which have assumed a lossless prototype with a high degree of accuracy.[15,16] Achieving the specified performance is dependent upon the accuracy with which the coupling apertures are designed and the tolerance with which they are fabricated. The requirement for resonator alignment in a cryogenic system increases the complexity of the system design. The possibility of using remote tuning devices, both electrical and mechanical, has been considered for a multiresonator filter operating at X-band, with regard to the degradation of performance due to the tuning network.

The ultimate objective of providing extremely low noise, high selectivity preselectors for low-noise amplifiers, image and noise rejection filters for use with mixers and oscillators, or high-selectivity diplexers, operating in cryogenic system provides a basis for a trade-off study with regard to achieving the desired result at the expense of increased system complexity. The advanced development of these filters may ultimately result in their efficient use in many high-frequency communication systems.

BIBLIOGRAPHY

1. S. B. Cohn, "Dissipation Loss in Multiple-Coupled-Resonator Filters", *Proc. of IRE,* Aug. 1959, pp. 1342-1348.
2. E. G. Fubini, E. A. Guillemin, "Minimum Insertion Loss Filters", *Proc. of IRE,* Vol. 47, pp. 37-41, Jan. 1959.
3. E. A. Lynton, *Superconductivity* (1962), London: Methuen, New York: Wiley.
4. V. L. Newhouse, *Applied Superconductivity,* Wiley, 1964.
5. F. London, *Superfluids,* Vol. 1, Wiley, New York, 1950.
6. C. Montgomery, R. Dicke, E. M. Purcell, *Principles of Microwave Circuits,* MIT Radiation Lab. Rpt.
7. A. B. Pippard, *Proc. Roy. Soc.,* Vol. A 191 (1947).
8. P. B. Miller, *Phys. Rev.* 118:928 (1960).
9. G. Reuter and E. H. Sondheimer, *Proc. Roy. Soc.,* Vol. A 195, p. 336 (1948).
10. P. B. Wilson, H. A. Schwettman, *IEEE Trans. on Nuclear Science,* June 1965, p. 1045.
11. A. A. Abrikosov, L. P. Gorkov and I. M. Khalatnikov, Zh. Eksperim, *i Teor. Fiz. 35,* 265 (1958). Eng. Transl.: *Soviet Phys.—JET,* p. *8,* 182 (1959).
12. S. B. Cohn, "Design Consideration for High Power Microwave Filters", *IRE Trans. on MTT-7,* pp. 149-153, Jan. 1959.
13. S. L. Matthaei, L. Young and E. M. T. Jones, *Microwave Filters Impedance Matching Networks, and Coupling Structures,* McGraw-Hill, 1965.
14. L. Young, "Peak Internal Fields in Direct-Coupled Cavity Filters", *IRE Trans. PTG MTT-8,* pp. 612-616, Nov. 1960.
15. S. B. Cohn, "Direct Coupled Resonator Filters", *Proc. IRE,* Vol. 45, pp. 187-196, Feb. 1957.
16. W. W. Mumford, "Maximally Flat Filters in Waveguide", *BSTJ,* Vol. 27, pp. 648-714, Oct. 1948.

HIGH-FIELD SUPERCONDUCTORS AT ELEVATED TEMPERATURES

This paper discusses current experimental findings in high-field superconductor research. These are the type II superconductors, including niobium compounds, which remain partially superconducting while being impregnated by a high magnetic field beyond the thermodynamic critical field. Phenomena such as flux jumps are analyzed to develop more stable, high-field superconductors.

C. M. HARPER

Applied Research, DEP, Camden, N.J.

A CLASS of type II superconductors of practical importance is the one which contains those with high transition temperature ($T_c \geq 9°K$) and large current carrying capacity in high magnetic fields ($J_c \approx 10^5$ amperes/cm^2). These are known as *high-field superconductors*, and include niobium stannide (Nb_3Sn), niobium titanium (NbTi), and niobium zirconium (NbZr). The purpose of this experiment was to investigate the temperature and magnetic field dependency of the critical current density J_c and the pinning strength parameter α of these high-field superconductors.

Final manuscript received September 26, 1966.

EXPERIMENTAL PROCEDURE

High magnetic fields ($\approx$ 25 kilo-oersted) and cryogenic temperatures ($\approx$4.2°K) are required to perform experiments on high-field superconductors.

As seen in Fig. 1, a solenoid of superconducting wire (NbZr) encloses the heater cavity with the sample under test so that its magnetic field is applied parallel to the axis of the sample cylinder and thus is tangential to its wall. The sample was isolated from the liquid helium bath (4.2°K) by a thermally insulated heater cavity. The sample could be warmed to temperatures of about 20°K by a current passed through a heater element which surrounded it.

A Hall effect sensor was placed in the interior of the hollow sample to measure the internal magnetic field which penetrated the wall of the sample. The heater cavity was vacuum pumped to about 10^{-4} mm-Hg and then purged with dry helium gas before each experiment. The system was then vacuum pumped to about 10^{-1} mm-Hg during an experiment to minimize temperature gradients caused by convection currents. A germanium resistance thermometer monitored the sample temperature to within 0.1°K.

After being precooled in liquid nitrogen (77°K), the heater cavity with sample was centered in the solenoid and allowed to reach thermal equilibrium. As the applied field was increased, a

CHARLES M. HARPER received a BS in Physics from the University of Alabama in 1955. He is presently attending Drexel Institute of Technology studying for a MS degree in Physics. From 1955 to 1958 Mr. Harper served as a Special Weapons Electronics Officer in the U.S. Army Ordnance Corps. He trained and supervised enlisted technicians in the testing and maintenance of Special Weapons fuzing and firing devices. In November 1958, he was employed by RCA, Communications Systems Division, as an electrical engineer. He performed audio frequency electrical design and administrative duties on communications equipments such as the AN/GKA-5, Minuteman Cable Terminating Equipment, Solid State Microwave Radio Relay, and AN/TRC-97. In January, 1964, Mr. Harper began working for Applied Research as a physicist to develop practical applications of superconductivity phenomena. Mr. Harper is a member of Phi Beta Kappa, Sigma Pi Sigma, Phi Eta Sigma, and Pi Mu Epsilon.

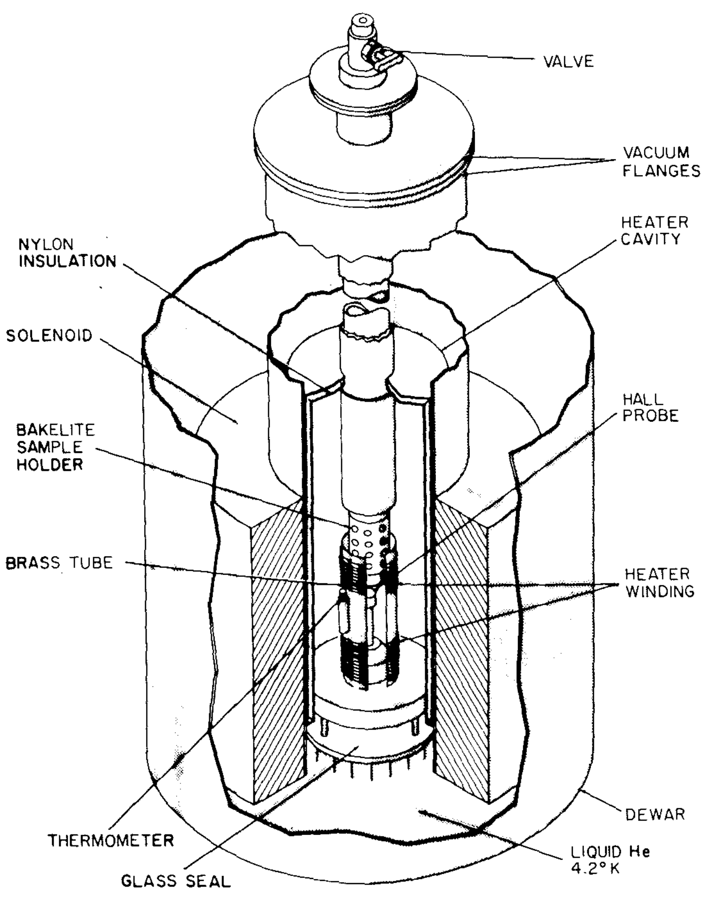

Fig. 1—Cross-sectional view of apparatus.

magnetization curve was plotted on an X-Y recorder with the internal magnetic field H' plotted against the applied field H. The plot was completed by running the magnetic field to a desired value, and then decreasing it to zero as the X-Y recorder plotted the hysteresis loop which is characteristic of type II superconductors.

Before another curve could be plotted, trapped flux had to be released from the superconducting sample by heating it to T_c. This was accomplished by activating the heater element briefly or by withdrawing the heater cavity momentarily from the helium bath.

To obtain characteristic curves at elevated temperatures, the heater element was first activated and held constant while the germanium thermometer was monitored to determine that a constant temperature was established in the sample. A magnetization curve could then be plotted for that temperature.

THE CRITICAL STATE

When magnetic flux reaches the inner wall of the sample and penetrates the interior of the hollow cylinder, the superconductor is in the *critical state.* This is brought about in the following manner.

According to Lenz's law, an induced current in a conducting loop will generate a magnetic field which opposes any change in the applied field. In the steady state, however, these induced currents are dissipated by the resistance in the wire so that the induced magnetic fields die and the applied field threads the conductor unopposed. If there is no resistance in the material (as in the case of a superconductor) the induced current will persist to shield the interior of the current carrying device.

Thus, for our hollow cylinder, as H is increased from zero, a sheet of current flows at the surface to shield the interior. As H gets larger, the sheet of current gets thicker until the entire wall is carrying a maximum current, which is specified as the critical current density J_c. The magnetization curve in Fig. 2 is typical of such an experiment. When the increasing H reaches the value of H_{c1}, the lower critical field, flux will begin to move across the wall of the sample. When the flux reaches the inner wall of the sample and penetrates the interior of the cylinder, the superconductor is then in the critical state. The critical current density is then the current which flows while the superconductor is supporting a maximum supercurrent and has flux lines throughout.

The critical current density of a type II superconductor may be enhanced by inducing defects into the material which act as pinning sites for flux lines. High-field superconductors have these pinning sites in sufficient concentrations and size to enable them to carry high supercurrents.

Kim's semi-empirical equation relates J_c to H for the hollow tube experiment[1]:

$$J_c = \frac{\alpha}{H^* + B_o}$$

where J_c is the critical current density in amps/cm^2, α is the pinning strength of the material, H^* is the mean magnetic field intensity in the wall of the sample, and B_o is a curve-fitting constant. Once α and B_o are known for a particular sample, the J_c for that sample can be calculated for any value of H^*.

To obtain the α and B_o for a sample, a relationship between J_c and the applied field H is derived from Ampere's law:

$$\overline{\nabla} \times \overline{H} = 0.4\pi \overline{J}_c$$

$$\int (\overline{\nabla} \times \overline{H}) \cdot d\overline{S} = 0.4\pi \int \overline{J} \cdot d\overline{S}$$

Since from Stoke's Law,

$$\int (\overline{\nabla} \times \overline{H}) \cdot d\overline{S} = \int \overline{H} \cdot d\overline{l}$$

then:

$$\int \overline{H} \cdot d\overline{l} = 0.4\pi \int_s \overline{J}_c \cdot d\overline{S}$$

integrating:

$$(\overline{H} - \overline{H}') = 0.4\pi J_c W$$

therefore, for infinite cylinders:

$$\overline{J}_c = \frac{\overline{H} - \overline{H}'}{0.4\pi W}$$

where W is the wall thickness in cm.

Thus only the knowledge of H and H' is needed to determine J_c for an annular cylinder of known dimensions. Our experiment was based on measuring these parameters for different values of temperature and applied field. Fig. 3 describes this derivation pictorially.

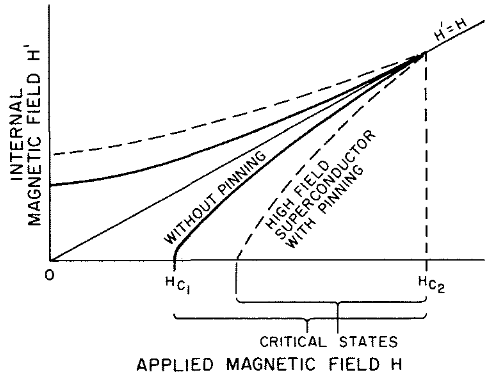

Fig. 2—Internal magnetic field (H') as a function of applied magnetic field (H) with and without pinning.

If a sufficient number of points can be obtained from critical state curves, a curve of magnetization (or J_c) versus H^* can be plotted, from which α and B_o can be determined for a particular sample. Once α and B_o are known, Kim's equation is then used to calculate the J_c for any value of H^*.

EXPERIMENT OBSERVATIONS

Samples of prime interest in this investigation were niobium stannide (Nb_3Sn). Fig. 4 depicts the typical magnetization curve for a sample of Nb_3Sn. For this sample, Nb_3Sn was vacuum deposited on hollow ceramic tubes to a thickness of about 80 micrometers.

This superconductor has a transition temperature of 18.2°K and an upper critical field of 220kOe. Since these are the highest T_c and H_{c2} known at this time, Nb_3Sn is of particular interest to engineers and scientists who require high magnetic fields in their work, or need magnetic shielding. Nb_3Sn vapor depos-

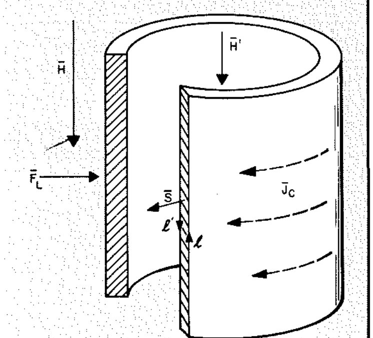

Fig. 3—An annular cylinder of known dimensions as used to determine J_c with H and H' known.

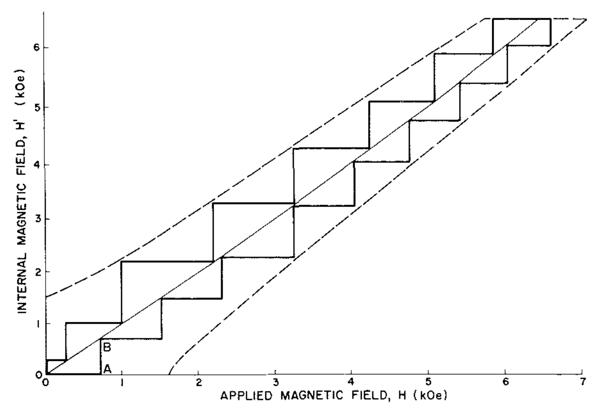

Fig. 4—Typical magnetization curve for a Nb_3Sn sample.

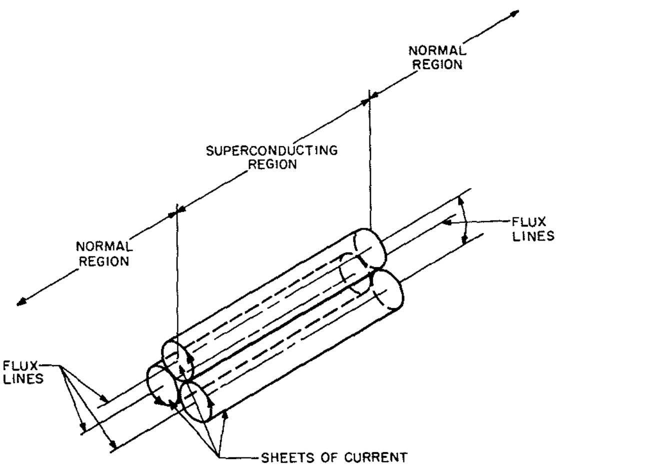

Fig. 5—Flux vortices—a flux vortex is visualized as a flux line in a narrow tube of normal material enclosed in a small cylindrical sheet of current.

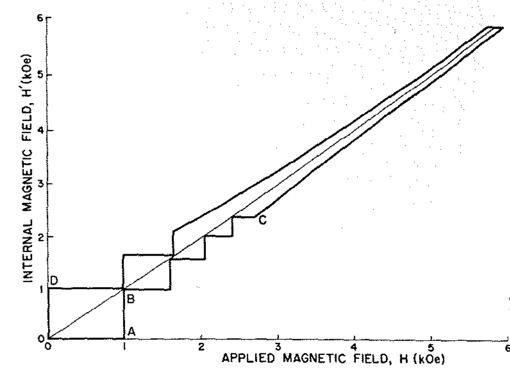

Fig. 6—Magnetization curve for Nb_3Sn at higher temperature.

ited onto narrow stainless steel ribbon was developed by RCA Laboratories in Princeton, N.J., and used to construct the first 100,000-gauss solenoid.

FLUX JUMP ANALYSIS

From Fig. 4, the effects of high magnetic fields and elevated temperatures on Nb_3Sn can be seen. The solid line was plotted with an applied field of 0 to 15 kOe, while the temperature was held constant at 4.2°K. As the applied field was increased from zero, supercurrents shielded the interior from magnetic flux. These flux lines (inclosed in vortices) were pinned by grain boundaries and dislocations in the material, which built up a flux gradient across the wall of the tube. When the Lorentz force ($\overline{F}_L = \overline{J} \times \overline{H}$) exceeds the pinning force at a point, it triggers flux motion with accompanying generation of heat which unpins other flux lines as it spreads. An avalanche of flux results. This phenomenon, called a *flux jump,* drives the superconductor normal as evidenced by point B on the curve. Since any point where the internal field equals the applied field (as along the line $H' = H$) describes normal flux penetration, it can be seen that flux jumps momentarily destroy the superconductivity of a material by causing a transition to the normal phase. Needless to say, this is a most undesirable aspect of high-field superconductors, and various safeguards are utilized to protect superconducting devices of this type, such as solenoids, which pass large currents.

Abrikosov has described how flux quanta may exist in a superconductor with his concept of *flux vortices.*[2] A flux vortex is visualized as a flux line in a narrow tube of normal material enclosed in a small cylindrical sheet of current. Thus magnetic flux lines may exist throughout a type II superconductor and by so doing establish the mixed state of superconducting and normal regions. Flux lines move through a superconducting region, the vortices enveloping new regions of normal material as they go, while the areas left behind become superconducting again. (See Fig. 5.)

As mentioned before, the group of high-field superconductors occupies a special position of interest because of their high J_c in large H fields, and their high T_c. The operation of superconducting devices at temperatures above 4.2°K permits the simplification of closed cycle refrigerator design and results in significant power savings. The phenomena of flux jumps mar the advantages of this group, however.

Flux jumps occur when there is a catastrophic reversion from the superconducting to the normal state, before critical state is achieved. Critical state performance (represented as a dotted line on Fig. 4) is not possible at low temperatures and low magnetic fields for Nb_3Sn. Flux jumps are associated with the pinning force which is characterized by high-field, high-J_c superconductors.

As the applied magnetic field (H) is increased from zero, a sheet of current is set into motion at the outer surface of the cylinder, in accordance with Ampere's Law, to shield the interior of the cylinder. This sheet of current thickens as H increases to provide additional shielding. At H_{c1}, flux vortices are formed throughout the current layer as it moves into the bulk of the material from the surface. Vortices move with the current layer until the wall is filled, at which point flux breaks through the inner wall and threads the tube's interior. The tube is now in the critical state. The motion of the flux through the bulk of the material or flux creep,[3] develops a *flux flow resistivity* which Kim has shown can be expressed as

$$\rho_s = \rho_n \frac{H}{H_{c2}} \qquad (3)$$

Thus, heat is generated within the bulk of a high-field superconductor associated with the flow of supercurrent across this flux flow resistivity.

Although flux jumps are not fully understood, the heat developed by the motion of flux through the superconductor is believed to be a determining factor in causing them. The poor thermal diffusivity of these superconductors at low temperatures causes hot spots to develop before heat can be dissipated, and an avalanche of flux motion results in a flux jump.

After the superconductor is driven normal (point B in Fig. 4), the flux gradient is zero, heat generated by the transition is dissipated, and since the thermal environment remains below the T_c of the superconductor, it reverts to the superconducting state. As the applied field continues to increase without interruption from point B, the supercurrents again shield the tube interior completely, repeating the cycle of flux jumps.

Large critical currents and the instability of flux jumps appear to go together. The higher the J_c, the more prevalent are flux jumps. Since J_c is inversely proportional to H and T, a reasonable expectation is that flux jumps would diminish with increasing fields and higher temperatures. Fig. 6 shows what happens at a higher temperature as H is increased. The flux jumps become more frequent and smaller (of course J_c is getting smaller, and it follows that the flux jumps must stay within the limits of the critical state curve). Finally a value of H is reached (point C) where the plot reverts to critical state performance, which continues until H_{c2} is reached, extinguishing the last vestiges of J_c. (The curve is not taken all the way to H_{c2} in

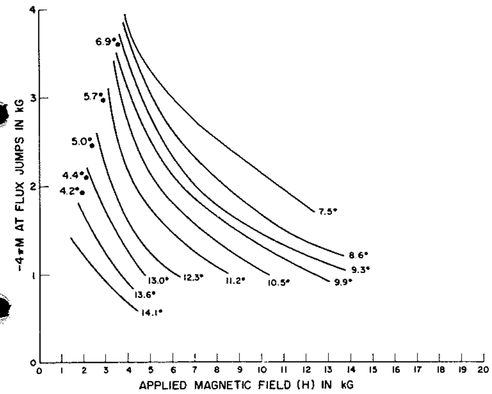

Fig. 7—"Practical" magnetization of Nb_3Sn tube.

Fig. 6.) If H is now decreased, a sheet of current (at the outer surface) is induced by the directional change in H which flows in the opposite direction, tracing the characteristic hysteresis curve of a magnetic body. The H' is greater than H above the $H' = H$ line, since flux is trapped in the tube. The same analysis can be applied to this region of the curve as was used before, but when $H = 0$ (point D) a remnant magnetization remains due to the trapped flux in the interior of the sample.

STABLE PERFORMANCE

If the temperature of the sample is raised to 15°K, the Nb_3Sn will plot a pure critical state curve, but the J_c will now be only about 20% of the value at 4.2K. (Of course at 18.2°K, $J_c = 0$). Thus the price to achieve stable conditions with pure Nb_3Sn is high. But our experiment with Nb_3Sn has revealed that there is an optimum temperature where flux jumps are minimized while J_c is not seriously impaired.

A practical critical current density for Nb_3Sn sample PM24#4 was derived from magnetization curves taken at fixed temperatures from 4.2°K to 14.1°K, the range in which flux jumps persist. Because of flux jumping, sample PM24#4 did not exhibit critical state performance at low T and H. Therefore no direct method of determining the critical current density could be devised. The use of the "practical critical current density" was an alternative. In order to use the information from flux jumps, the value of magnetization at a flux jump was plotted against the applied magnetic field for different values of temperature as seen in Fig. 7.

The value of magnetization at $H =$ 2kOe (an arbitrary choice of H) was converted to J_c and then plotted against temperature in Fig. 8. As can be seen, there is a maximum "practical J_c" at about 8°K. Since at low T and H the flux jumps prevent a determination of the true J_c, the "practical J_c" provides a reasonable approximation of the supercurrents which the Nb_3Sn tube can support.

This maximum value of J_c at 8°K for Nb_3Sn would be an important consideration where superconducting devices are used in closed cycle refrigerators. Power requirements and complexity of design would both be eased if the refrigerator could be operated at 8°K rather than some lower temperature such as 4.2°K.

Fig. 9 shows the region in which this Nb_3Sn sample PM24#4 exhibits stable performance. The area to the right of the shaded region represents the normal state, while in the area to the left flux jumps are manifest. Thus in the shaded region, the sample is in the superconducting state free of flux jumps.

FUTURE PLANS

Further experimentation with Nb_3Sn is planned to investigate how we may develop more stable high field superconductors. Heat treatment, surface treatment, doping with magnetic inclusion, and other attempts to enhance J_c while controlling and understanding flux jumps are possible approaches to this study.

ACKNOWLEDGEMENTS

The work herein reported was carried out with Dr. Richard Hecht of RCA Laboratories, Princeton, N.J., who served as chief investigator for this project.

The author would like to express his appreciation to David A. Gandolfo for many useful suggestions in the writing of this report.

BIBLIOGRAPHY

1. Y. B. Kim et al., *Phys. Rev.*, 131, 2486, 1962.
2. Abrikosov, A. A. Dokl. *Akad, Nauk SSSR*, 86, 43, 1952 (Russian).
3. P. W. Anderson, Phys. Rev. Ltr. 9, 309, October 1962.

Fig. 8—"Practical" J_c of Nb_3Sn tube.

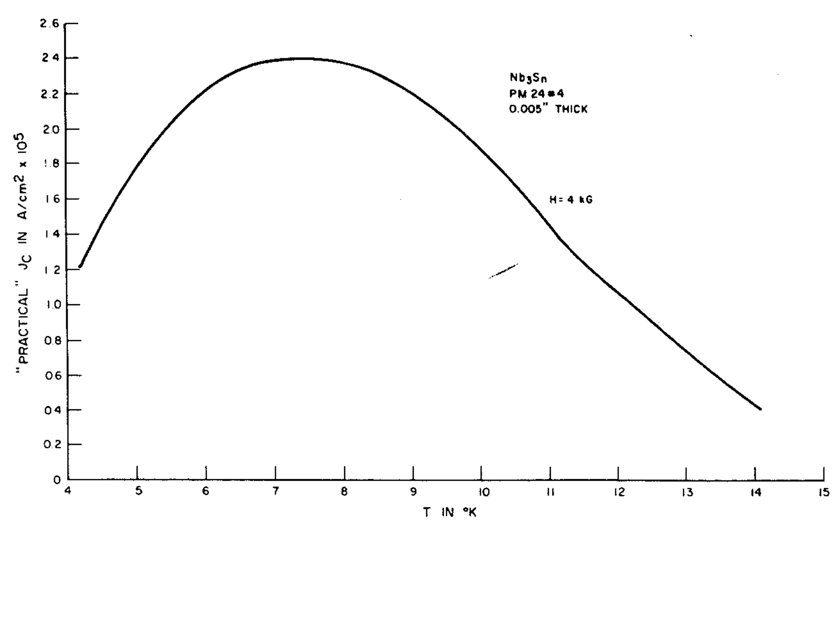

Fig. 9—Regions of critical state for Nb_3Sn and NbZr tubes.

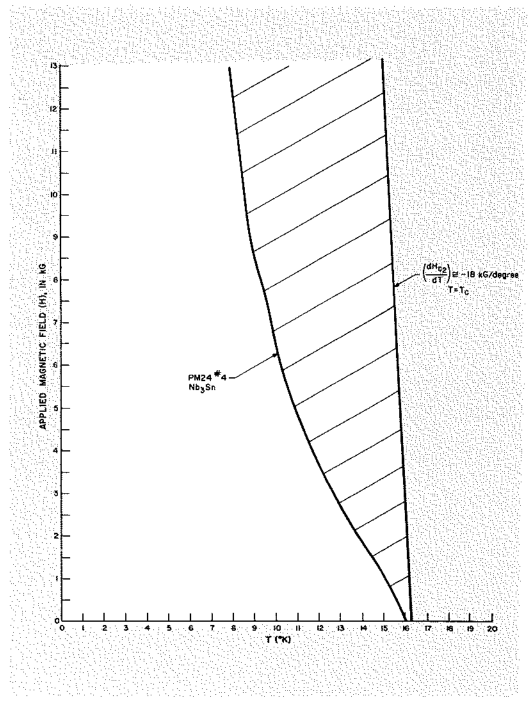

BALLOONS AS RELAY SYSTEMS FOR JUNGLE RADIO

Jungle foliage attenuates the signals of transceivers to a critical degree, in addition to the losses due to the curvature of the earth. The authors here propose the use of balloon-borne transponders as radio relay systems. Such a method is superior to the alternative of raising antennas above the jungle because it gives not only greater communications range, but also mobility.

S. M. PERLOW, P. TORRIONE, and B. B. BOSSARD

Advanced Communications Laboratory
Communications Systems Division
DEP., New York, N.Y.

BERNARD B. BOSSARD received the BSEE from the Virginia Military Institute in 1956. He was employed by Allied Chemical during 1956 through 1957 as a project engineer. Upon completion of a six month tour of active duty with the Army, he joined the Signal Corps Research and Development Laboratories in Belmar, New Jersey where he developed parametric and superregenerative devices. He received the Department of Defense Sustained Superior Performance Award in 1959. In 1960, he joined the New York Systems Lab of the DEP Surface Communications Division as a Member, Technical Staff where he was responsible for several state of the art military contracts. He became Senior Member, Technical Staff in 1961 and in 1962 became leader of the Microwave Techniques Group, where he is responsible for the advanced development of solid state devices. Mr. Bossard has published many papers in the microwave field and holds three patents.

PETER S. TORRIONE was graduated from CCNY in 1963 with a BEE degree. Following his graduation he joined RCA as a specialized trainee. His assignments as a specialized trainee included the design and testing of a wide-range tunnel diode VCO for an FM phase-lock loop, the development and testing of a vidicon television camera for the Apollo Space Project, the design and development of a Gallium Arsenide infrared injection-diode logic circuit, and the development of high-gain, broadband, DC coupled video amplifiers. Mr. Torrione then assumed his present position in the CSL microwave group. Here he has performed theoretical analyses and experimental measurements on X-band resistive frequency converters for an Interface Reduction contract. He has also done work on L-Band vacuum-tube VCOs for application in altimeters. In addition, he has done development work on broadband transistor amplifiers in the VHF and UHF bands, as well as developed transformer hybrids in these bands. Mr. Torrione has worked on an R&D miniature filter contract, using materials with high permittivities, and the design of bandpass and band-reject filters in waveguide. He has also done work on high-order, high-efficiency, step-recovery frequency multipliers. Mr. Torrione is a Member of the IEEE and the PTGMTT, the author/co-author of several published articles, and has made one patent disclosure.

STEWART M. PERLOW received his BEE degree from the City College of New York in June 1963. Upon graduation he joined RCA as a specialized trainee in RCA's Design and Development Training Program. His first two assignments were with the Aerospace Communications and Controls Division. While there he worked on an inertial guidance system study program. The second two assignments brought him to the NYSL of CSD. In November 1963, he joined the Advanced Solid State RF Techniques Group as an Associate Member of the Technical Staff. His work with parametric devices helped in the development of a highly efficient field tunable solid state modulated power source in the 4.4 to 5.0 GHz frequency band. This work, together with work on the Interference Reduction Study contract, led to his co-authoring a paper on the prediction of intermodulation distortion in parametric upconverters. He has also worked on correlation techniques for rejecting jamming signals in the HF and VHF bands, and has had design experience with RC active filters and has patent disclosures on several new filter concepts, one of which is a band-reject filter with an equivalent unloader Q of 50,000 at 1 MHz. Mr. Perlow is a member of IEEE and Eta Kappa Nu. He is currently enrolled in the evening graduate division of the Polytechnic Institute of Brooklyn pursuing his MSEE degree.

B. B. Bossard

P. Torrione

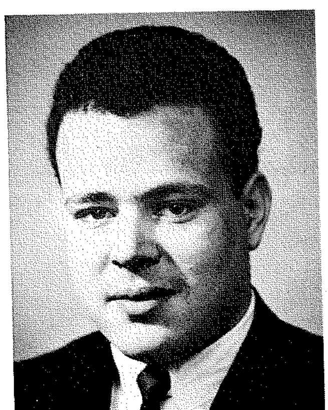

S. M. Perlow

THE maximum distance that a transmitter and receiver combination can be used for communications is determined not only by the minimum discernible signal of the receiver and the output power of the transmitter, but also by the path losses of the propagated radio wave. The ideal situation occurs when the field intensity is inversely proportional to the square of the distance from the source. This inverse square law is based on the assumption that the wave is propagated through a medium that does not absorb energy as the wave travels through it.

COMMUNICATIONS RANGE VS PATH LOSSES

Quantitatively, for the situation in which two isotropic antennas are located in free space, the path loss is given by:

$$\frac{P_t}{P_r} = 4.56 \times 10^3 f^2 d^2$$

where P_t and P_r are the transmitted and received powers in watts, f is the frequency in megahertz and d is the distance between antennas in miles. In decibels, the attenuation or path loss may be written as:

$$\alpha = 37 + 20 \log f + 20 \log d$$

If the earth was flat and had a perfectly conducting surface, this inverse square law would be a very good approximation for the path loss between short vertical antennas situated close to it. Since the earth's surface does not meet these requirements, ground losses do occur. The effect of these losses is to make the ratio of P_t to P_r proportional to d^4 instead of d^2.

In addition to the ground losses, ground wave communication further suffers due to absorption of the propagated wave by vegetation, foliage, and any other obstacles situated on the surface of the earth. In many instances, it is this absorptive loss which is the deciding factor in determining the communi-

Final manuscript received August 15, 1966.

cations range for any given set of equipment. An approximate formula for calculating this loss is:

$$a_a = 20 \log E^{d/\delta}$$

where the skin depth, δ, in meters is:

$$\delta = \frac{1}{2\pi}\sqrt{\frac{\lambda}{30\sigma}}$$

and σ is the conductivity of the medium in mhos/meter.

The conductivity of dense jungle foliage is in the order of 10^{-5} mhos/meter. The skin depth for this conductivity at a frequency of 50 MHz is 22.5 meters. The attenuation due to absorption is therefore:

$$\alpha = 63 \text{ db per } 0.1 \text{ mile}$$

This agrees very closely with the attenuation due to the jungle foliage measured in the rain forest of Panama[1].

The true meaning of a path loss of this magnitude is best seen by using it in a practical problem. The allowable path loss for any set of equipment is determined by the minimum discernible signal of the receiver and the output power of the transmitter. Suppose that the equipment used operates at 50 MHz and allows a path loss of 110 dB. This path loss is equivalent to having a 1 milliwatt transmitter and a receiver with a significant output for a 20μV signal input, both working with 50 ohm antennas. If used in free space, the communications range would be 95 miles. This same equipment used in dense foliage would have a range of approximately 250 feet. Naturally, the communications range will increase as the density of the foliage decreases, but it will be far less than the 95 miles of free space propagation.

INCREASING COMMUNICATIONS RANGE

The only solution to the problem of increasing the communications range is to decrease the distance through which the propagated wave must travel in order to get through jungle growth. This can be accomplished by raising the antennas above the foliage. This would eliminate the losses due to the growth but would not eliminate the ground losses. An even more severe handicap occurs if this solution is used. The communications equipment loses much of its mobility, since every time the equipment is moved, a new antenna must be constructed.

Another solution which will keep the equipment mobile and also approximate free space wave propagation, consists of using balloon-borne transponders as relays. In this case, the only additional attenuation is due to the foliage that the propagated wave must pass through, as shown in Fig. 1.

The configuration of Fig. 1 is the sample case under consideration. It was chosen because any drift of the balloon toward the right reduces the propagation distance between surface and balloon, while any drift to the left can be compensated for by launching a balloon from the other camp.

The communications range versus balloon height is shown in Fig. 2. The type of terrain is used as a parameter. The distance the wave must be propagated through the foliage depends upon the line of sight angle to the balloon as shown in Fig. 1. The losses for different types of jungle for various heights and ranges have been tabulated and will be found in Table I.

The jungles considered for Fig. 1 were the worst possible cases. That is, the 100 foot jungle was considered to be dense jungle from ground level up to 100 feet. This is rarely the case. Jungles can be divided into two major classes, primary and secondary. A primary jungle consists of large trees averaging 70 feet in height, but may be over 100 feet. These trees branch out at the top and form a canopy. This canopy shields the jungle floor from the sunlight and, consequently, there is comparatively little vegetation on the jungle floor. Therefore, a jungle which is 100 feet high may only have from 30 to 50 feet of really dense foliage.

The secondary jungle consists of small trees, tall grass and thick vines. The vegetation is not very high and usually does not exceed 25 feet.

Even in terrain where the jungle does not pose a severe problem, the mountains may severely handicap communications. Fig. 3 shows the attenuation of field strength and the profile of the land. If a balloon-borne transponder was used in a case like this, communication from one side of a mountain to the other side would present much less of a problem.

Fig. 1—Communications range.

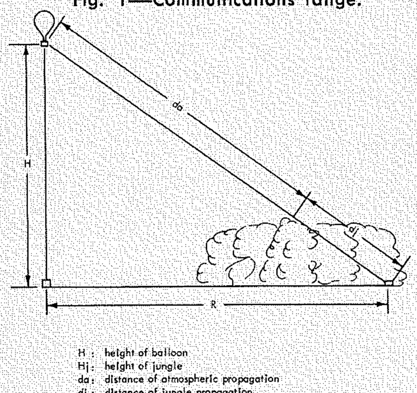

Fig. 2—Communication range vs. balloon height for an allowable path loss of 120 dB between balloon and receiver at 50 MHz.

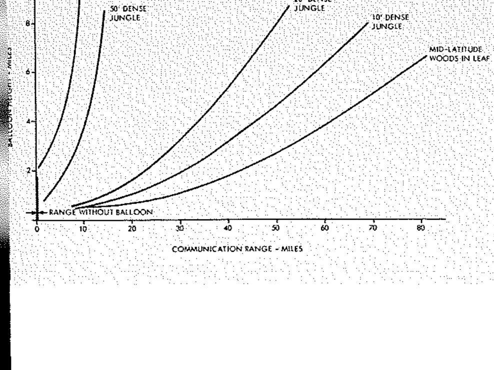

Fig. 3—Field strength profile.

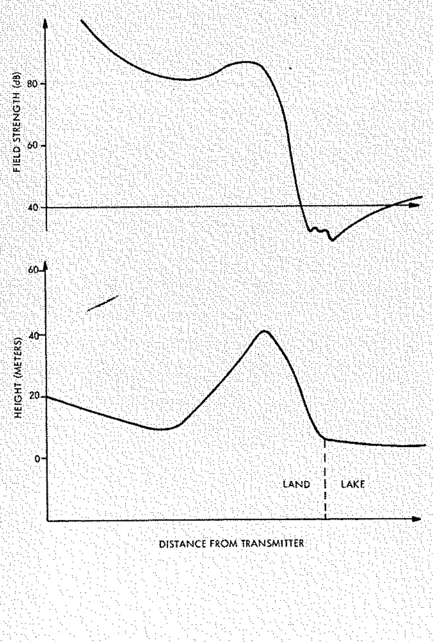

BALLOONS AND DRIFT

A balloon-borne transponder provides a very significant increase in communications range. However, an additional consideration must be taken into account when balloon transponders are compared to other methods of increasing communications range. This additional consideration is the velocity of the wind and its effect on the balloon's movements. To study these effects data have been taken at a location in southeast Asia.

Fig. 4 shows the average, maximum and minimum wind velocities as a function of the altitude over the selected location in the months of January and July of 1961. These plots indicate a very definite decrease in wind velocity at approximately 32,000 feet in January and 20,000 feet in July. Note that in both cases, the average wind speed in this

TABLE I—Path Loss

Balloon Height H (Miles)	Ground Distance R (Miles)	Path Loss No Jungle (dB)	Path Loss Dense Jungle 100 ft (dB)	Path Loss Dense Jungle 50 ft (dB)
0.5	5	85	185	165
1.0	5	85	150	125
1.0	10	90	190	155
2.0	5	85	131	115
2.0	10	91	156	131
2.0	20	97	197	162
4.0	5	86	116	106
4.0	10	91	137	121
4.0	20	97	162	137
4.0	30	100	180	155
4.0	40	103	203	168
8.0	5	90	110	104
8.0	10	93	123	113
8.0	20	97	143	127
8.0	30	100	160	136
8.0	40	103	168	143
8.0	50	105	175	150
8.0	60	106	186	161
8.0	70	108	218	168

region of decreasing wind velocity is approximately 10 knots. The decrease in wind speed is caused by the different directions of motion of the low and high altitude air masses. At the interface of these two air flows, the wind velocity is the vector sum of the wind velocity of the low and high-altitude winds.

A balloon designed to reach an altitude of 5,000 feet will attain that height in about 25 minutes, while it takes a balloon designed to reach an altitude of 15,000 feet 10 more minutes to attain an additional 10,000 feet. Since the low-altitude winds have relatively low velocities under normal conditions, the balloon can be expected to drift less than 6 or 7 miles in the first 35 or 40 minutes after launch. When the balloon reaches the high altitudes at which the wind interface occurs, this drift decreases. If the interface is passed, the balloon begins to drift back toward the launch area. This difference of wind direction greatly improves the available transmission time for a balloon.

The balloon should be designed so that it is not permitted to rise much above an altitude of 30,000 feet because the wind velocities at altitudes exceeding this height increases very rapidly. Hence, constant-altitude balloons, with the property of rising to and maintaining a constant altitude are most desirable. To be more precise, they maintain themselves at an altitude of constant ambient pressure. Using this type balloon, it is possible to avoid both the relatively swift low-altitude winds and the very much higher velocity high-altitude winds.

The forces acting on the balloon are shown in Fig. 5. The net lift L_N of the balloon is:

$$L_N = L_a - W_p - W_h - D$$

The lift due to the air, L_a, is equal to the weight of the volume of air displaced by the balloon:

$$L_a = \rho_a V$$

where ρ_a is the density of the air and V is the volume of a balloon. Similarly, the weight of the helium, W_h, is:

$$W_h = \rho_h V$$

The net lift now becomes:

$$L_N = (\rho_a - \rho_h)\ V - W_p - D$$

To maintain a constant altitude, the net lift must be zero. Since the drag is a function of the balloon's vertical velocity, it is reduced to zero when a constant altitude is reached. The only remaining forces on the balloon are the lift due to the displaced air, the weight of the helium, and the weight of the balloon and its payload. Since all these forces must be balanced:

$$(\rho_a - \rho_h)\ V = W_p$$

It is now seen that a balloon will remain at a constant altitude if its volume remains constant. To minimize changes in volume with changes in temperature (e.g., night and day temperatures), the balloon is initially inflated to a higher or super pressure with respect to the ambient pressure. The required super pressure of the helium is given by:

$$P_h = \left(\frac{T_w}{T_c} - 1\right) P_a$$

where P_h and P_a are the helium and ambient air pressures, and T_w and T_c are the warm and cold temperatures. When the balloon is inflated to this higher pressure, any temperature change will not cause it to go slack. For example, a super-pressure of 64 mbar will keep the volume of a balloon constant if it is flying at a pressure of 900 mbar with a daytime temperature of 300° ABS and a night time temperature of 280° ABS.

These balloons are usually tetrahedron shaped. This shape is chosen because it can be manufactured quite easily by using flat sheets of skin material and straight seams. Polyethylene is used as the skin material because it does not stretch appreciably under tension, and has a low density. The thickness of the skin varies between 0.5 and 1.5 mils.

Table II indicates payload, flying altitude, height, volume, and cost of constant altitude balloons. Correlation of the data in Table II with the communications range results in Fig. 6, communications range as a function of balloon cost for 8 and 23 ounce payloads. This plot was made on the basis of an allowable path loss of 120 dB and for the various types of terrain expected to be encountered in a jungle.

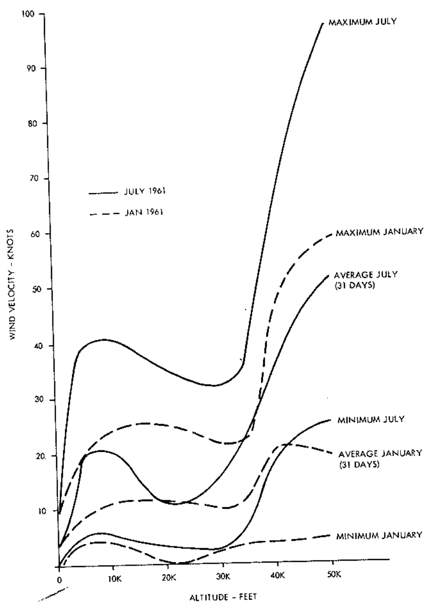

Fig. 4—Maximum, average, and minimum wind velocity vs. altitude, Southeast Asian jungle.

Fig. 5—Forces acting on balloon.

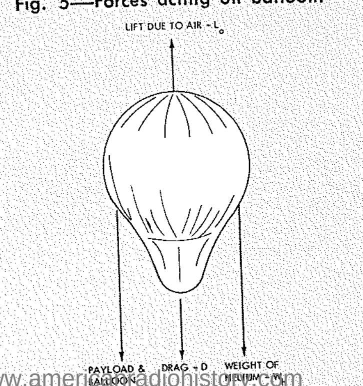

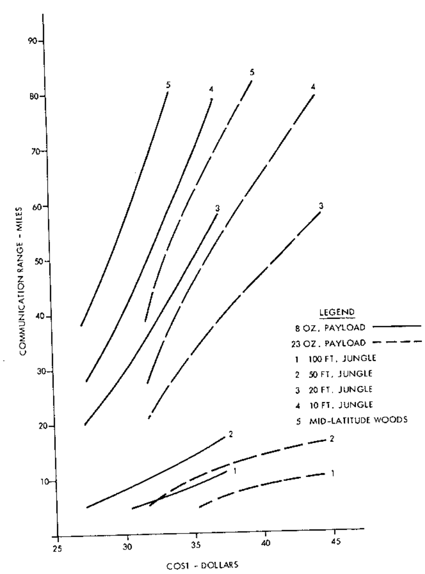

Fig. 6—Communication range vs. balloon cost.

TABLE II—Commercial Balloons

Payload (oz)	Altitude (1000 ft)	Height (inches)	Volume (ft³)	Approximate Price $
3	10	41	10	28
3	25	51	20	32
3	50	72	55	37
8	10	55	24	28
8	25	65	40	32
8	50	88	100	37
23	10	68	46	32
23	25	81	80	37
23	50	115	230	44

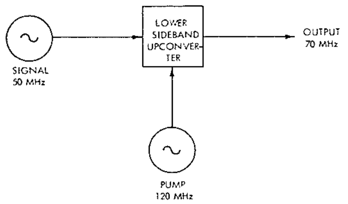

Fig. 7—Lower-sideband upconverter.

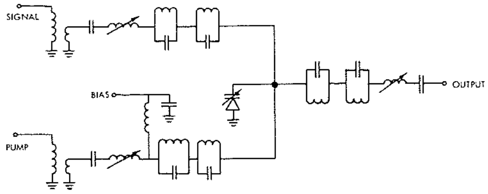

Fig. 8—Converter circuit configuration.

A significant advance in balloon technology was made recently by the Aerospace Instrumentation Laboratory, AFCRL. They demonstrated the feasibility of using a new balloon material which consists of Dacron threads laminated to a thin Mylar base film. This material is distinguished by variations in the pattern of the reinforcing Dacron threads over the surface of the balloon, thus providing added strength at the points of maximum stress. Balloons constructed of this new, extremely lightweight material are capable of carrying larger payloads to much higher altitudes.

TRANSPONDER

The heart of the communications system is the transponder itself. The transponder must meet two very important criteria: gain, and second isolation between input and output. The second criterion must be met to avoid any regenerative or degenerative behavior. Regeneration leads to general instability and oscillations, while degeneration results in a loss of gain.

If a conventional amplifier is used as the transponder, i.e., if the transponder receives and transmits exactly the same signal, the receiving and transmitting antennas must be isolated by at least the gain of the amplifier plus a margin of safety of about 10 dB. In the case of an amplifier with a gain of 80 dB, the antennas would have to provide 90 dB of isolation. This is a highly impractical figure; thus, other types of transponders must be considered for use in any practical system.

One method for achieving the required isolation can be found in the old technique of heterodyning. By using frequency conversion, isolation is obtained simply by proper filtering. Since gain is also very important, the frequency conversion should be as efficient as possible. These requirements suggest the use of a lower-sideband parametric upconverter, which has a pump or local oscillator frequency (ω_p) that is greater than twice the signal frequency (ω_s). The output frequency (ω_o) is the difference frequency, i.e.:

$$\omega_o = \omega_p - \omega_s$$

and it is greater than the signal frequency.

$$\omega_o = \omega_p - \omega_s > \omega_s$$

TABLE III—Power Consumption of Converter

Stage	Gain (dB)	Power Consumption (mW)
A	18	30
B	—	60
C	35	—
D	15	35
E	12	250
F	—	20
Total	80	395

For example, if a lower sideband upconverter is desired to convert a 50 MHz signal to 70MHz, the system to be used is shown in Fig. 7. The actual circuit configuration of this type of converter is shown in Fig. 8. Typical results using this circuit and a pump power of 20 mW at 120 MHz results in a converter with 35 dB gain and an information bandwidth of 100 kHz.

The application of the lower sideband upconverter to the balloon borne transponder is shown in Fig. 9. Block A consists of a 50 MHz high-gain transistor amplifier providing about 20 dB of gain to the incoming signal. The output of this amplifier is fed to the upconverter, block B, which derives its local oscillator power from a 120 MHz crystal controlled oscillator, capable of delivering 20 mW of power. Following the upconverter is an amplifier with 15 dB of gain and capable of 8 mW of output power. The output stage has 10 dB of gain and an output power capability of 100 mW. The overall gain of this system is 80 dB at about −60 dBm of input signal power. The power consumption of each element is listed in Table III.

The power pack for the system consists of nickel cadmium cells. They are particularly suited to rough handling, long periods of disuse and wide temperature ranges (−30° to +50°C.). A battery of ten 1.2-volt cells would weigh 0.6 pound and be capable of 34 mA or about 400 mW for slightly greater than 10 hours. At the end of this time, the individual cell voltage has dropped 0.1 volt to 1.1 volts giving a battery voltage of 11 volts. This 9% variation should have little effect on overall performance. The maximum altitude, limited by battery temperature, is about 25,000 feet.

The second method for achieving the required isolation while maintaining the high gain is to use superregenerative techniques. A typical example of a tunnel-diode superregenerative amplifier is given in Fig. 10. The *TD1* oscillates at 50 MHz and is quenched at a 100 kHz rate, which is determined by the values of *R* and *L*. Any frequency modulation produced by the tunnel diode superregenerative oscillator will have sidebands that are beyond the FM bandwidth of the desired signal. This method provides high gain at low power levels with very low power consumption. In addition, the size and weight of this package is very small, thus permitting a very inexpensive balloon.

A third possible transponder configuration is one in which a phase locked oscillator is used. This circuit has the same weight and size advantages that the superregenerative systems have, but its main disadvantage is that the locking range of the oscillator is decreased as the signal power decreases, thus giving reduced information bandwidth at low signal levels. In both the superregenerative and phase locked oscillator scheme, frequency and gain stability may be a problem.

Considering stability of frequency and gain as a criterion, the frequency converter scheme is far superior to the other two techniques. Its main drawback is its

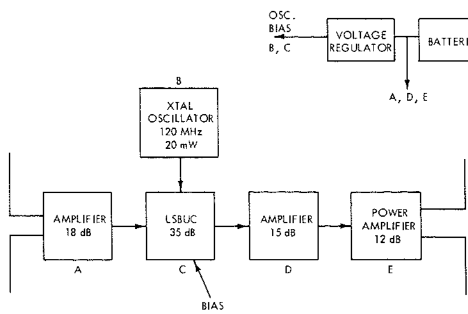

Fig. 9—Complete converter system.

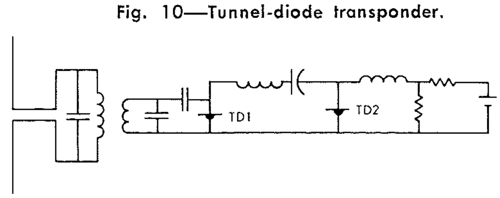

Fig. 10—Tunnel-diode transponder.

larger size and weight. Although it is not an extreme problem, it would be preferable to reduce both of these factors. A relatively newly developed technique, which involves both parametric and conventional amplification, allows these reductions in weight and size while still maintaining high efficiency performance of the converter. This technique makes use of a single transistor as the mixer, oscillator, and amplifier. Fig. 11 shows this transistor circuit along with the high frequency, and low frequency equivalent circuits. The principle of operation is as follows. The transistor in a common base configuration operates at high frequencies as a Hartley oscillator. Looking into the emitter, there is a nonlinear impedance for parametric amplification of the input signal (lower sideband). Since this lower sideband (oscillator frequency *minus* signal frequency) appears at the emitter, there is the possibility of gain through the transistor if the difference frequency is well below the cut-off frequency of the transistor.

The high-frequency equivalent circuit is that of a Hartley oscillator, the frequency of which is determined by the butterfly capacitor. The low-frequency equivalent circuit is that of a high-gain, narrowband amplifier. In addition to gain due to this low-frequency amplifier, there is also gain due to parametric amplification at the emitter.

Using this technique with a signal frequency of 450 MHz and a difference frequency of 2 MHz, a gain of 72 dB with a 20 kHz bandwidth and 50 dB with 750 kHz bandwidth was reported by Zuleeg and Vodicka.[2]

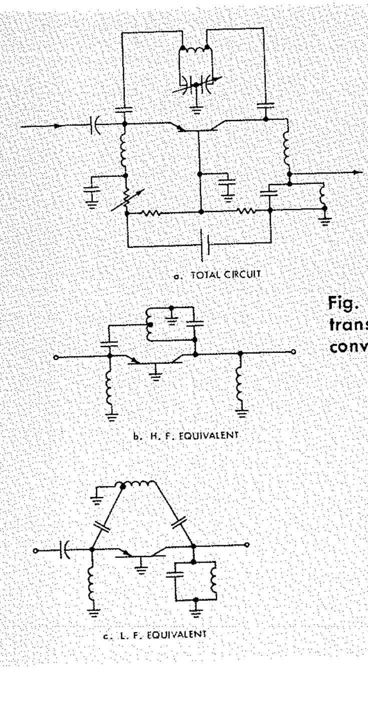

Fig. 11 — Single-transistor frequency conversion.

TACTICAL OPERATIONS

The need for mobility during tactical communications cannot be overemphasized. Communications equipment capable of penetrating a jungle environment requires large amounts of power and is therefore too bulky and cumbersome to be of any aid during small troop movements. However, small hand-held transceivers are ideal for this situation. Since they do lack the large amounts of power needed for jungle communications, they must be used in conjunction with the balloon transponder.

There are two basic ways in which a balloon transponder may be used for communications. The first is communications between individual units and a home base. In this case, the balloon can be launched over the home base. If this base, is for example, an air field, it could use a very high altitude balloon in conjunction with a relatively powerful transmitter and high gain antenna system.

Its second use would be as a means of communication between several patrols in the jungle. In this case, a balloon can be launched in two different ways. The patrols can carry the launching equipment themselves or a helicopter or other aircraft can release it in the general vicinity of the patrols. If there is cause to worry about giving the location of these patrols away, then high level aircraft can release the balloons at 20,000 feet within a 10 to 60 mile radius of the actual location. This method has the advantage that launching equipment need not be carried by the patrol.

If the patrol is to launch the balloon, it must carry the balloon and its launching equipment. With proper packaging, the balloon itself represents negligible weight addition. The helium pack is the major contributor of weight and bulkiness. A typical man-pack of helium consists of two tanks weighing a total of 20 pounds. Each is 18.5 inches long with an outside diameter of 4.24 inches. The helium is under 4,940 psi of pressure and has an equivalent volume of 81 ft^3 at one atmosphere. The number of fillings from such a man-pack for balloons capable of various altitudes and various payloads is shown in Fig. 12. It should be noted that the size of the man pack may be reduced. The actual size depends upon the required altitude, payload and number of balloon launches.

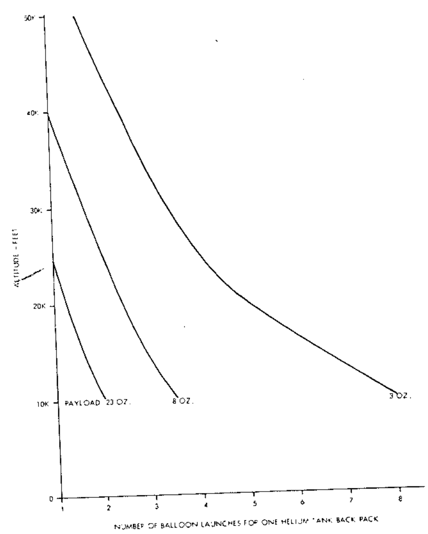

Fig. 12—Balloon altitude vs. number of launches for one helium pack (8 Ft^3) payload as parameter.

CONCLUSION

A balloon borne transponder significantly increases communications range in tropical and semi-tropical terrain. It has two major advantages over various other systems such as those requiring raising an antenna above the vegetation. First, the communications range is greater using a balloon transponder and, secondly, there is no need to construct an antenna at each new location. This second factor results in complete mobility of a patrol.

Even in regions where trees and other types of vegetation present no great problem, VHF communications is limited to line of sight distances. Mountainous terrain also limits communications range. In both of these situations, balloons produce very significant increases in the distance over which communications can be achieved.

A balloon-borne communication system has already been successfully demonstrated by the Aerospace Instrumentation Laboratory, AFCRL, on 16 November 1965 at Holloman AFB, N.M. The objective of this test was to demonstrate a technique available for solving some of the command and control problems associated with limited warfare. The balloon used reached an altitude of 80,000 feet and relayed voice and teletype communications between Ft. Huachuca, Arizona and Lubbock, Texas, a distance of approximately 500 miles, for several hours.

At the present state of the art, conventional balloons of reasonable size and cost can reach altitudes of 100,000 feet. A balloon floating at this altitude results in a communication range of approximately 780 miles. Greater distances can be obtained by using several balloons.

BIBLIOGRAPHY

1. S. Krevsky, *Tactical Jungle Communications Study*, RCA Report CR-63-419-11, Contract DA-36-039-AMC-00011(E), (Unclassified).
2. R. Zuleeg, V. W. Vodicka, "Parametric Amplification Properties in Transistors," *Proc. IRE (Correspondence)*, October, 1960.

A NOVEL SPACECRAFT ANTENNA ARRAY

Future space missions will require narrow-beam high-gain electronically steered communication antennas. The maximum scan angle will be small because the spacecraft will normally be stabilized. This paper describes a technique for realizing high aperture efficiency in an array consisting of an aperiodic arrangement of large elements. This technique provides a given small-scan coverage with a minimum number of phase-control elements.

Dr. W. T. PATTON, Ldr.
Advanced Microwave Technology
Missile and Surface Radar Division
DEP, Moorestown, N.J.

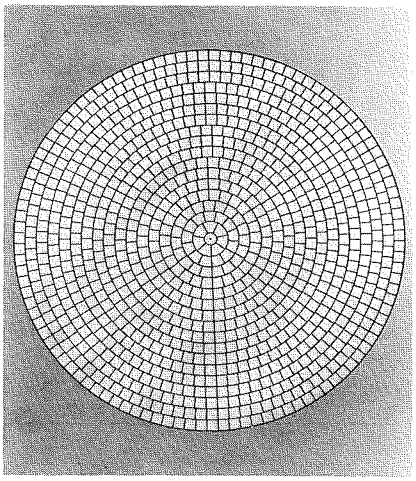

Fig. 1—Circular grid consisting of 18 concentric rings and 1048 antennules (30-foot diameter).

DR. WILLARD T. PATTON received his BSEE and MS degrees from the University of Tennessee in 1952 and 1958, respectively. He received his PhD in Electrical Engineering from the University of Illinois in 1963. While on the staff of the University of Tennessee Experiment Station, he did research on circular arrays. He was an instructor at the University of Illinois, and he conducted research on log-periodic and simple periodic antennas at the Antenna Laboratory; he also was a consultant with the Radio Direction Finding Laboratory. For 3 years he was Ship Superintendent for DER conversions at the Boston Naval Shipyard. Since joining RCA's M&SR Div., Moorestown, N.J. in 1962, he has done research on large phased arrays. Dr. Patton is the author or coauthor of several technical publications, and he is a member of the IEEE, AAAS, Sigma Xi, Tau Beta Pi, and Eta Kappa Nu.

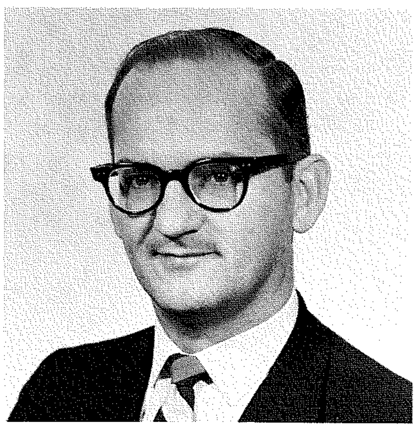

THE trend in space science is toward more sophisticated vehicles requiring higher telemetry data rates and toward more distant space missions. This trend must be anticipated in antennas and microwave technology by the development of techniques capable of producing even larger *effective radiated power*. Since, in a weight-limited system, maximum effective radiated power occurs when the weight is shared equally by the antenna and the power-generating equipment, this increase will be provided by larger antennas as well as by increased power input.

The trend to larger antennas with their narrower beams will produce a significant increase in antenna stabilization requirements. When the stabilization requirements for the antenna exceed that for navigation and for the scientific experiments, there is a need for electronic scanning. There is thus a requirement for a light electronic-scanning antenna providing only a small-scan coverage with a high aperture efficiency. The usual (periodic) array configuration is unattractive for this application because element size must be less than one square wavelength to avoid grating lobes and the resulting loss in aperture efficiency. The large number of phase control components resulting from this restriction on element size violates the primary requirement for low weight.

The problem then is to provide a highly efficient electronically scanned array with the minimum number of elements consistent with the scan coverage requirement.

Final manuscript received October 5, 1965

SOLUTION OF THE PROBLEM

An aperiodic arrangement of equal area elements on a circular grid allows the use of large elements without the formation of grating lobes. It is the aperiodic spacing which eliminates grating lobes. The circular grid provides a regular arrangement of elements that can be chosen to accommodate nearly identical elements at all locations. One such grid is shown in Fig. 1; this arrangement was designed so that all elements have equal area.

When electrically small elements (less than one square wavelength in area) are

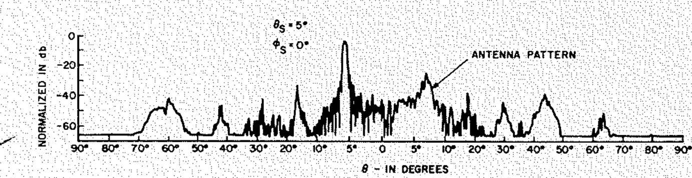

Fig. 2—Computed pattern (1000-element circular-grid array).

Fig. 3—Computed pattern (100-element circular-grid array).

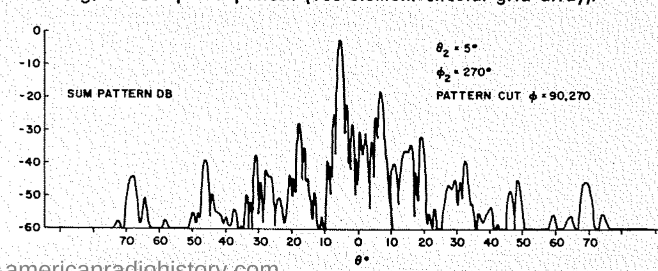

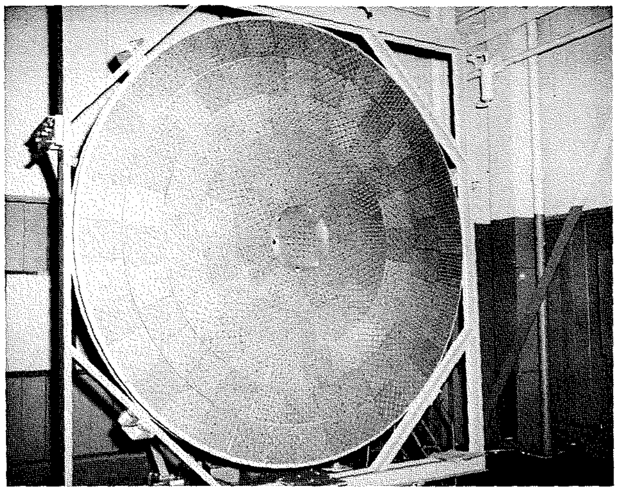

Fig. 4—Circular-grid array antenna model.

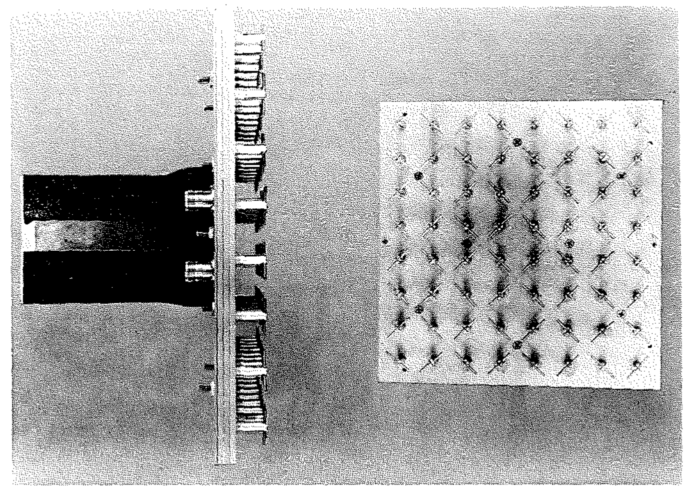

Fig. 5—Circular-grid array antenna element (antennule).

used in an array the current distribution on the element has little effect on the aperture efficiency of the array. The primary function of the element in this case is to effect an efficient impedance match between the feed network and the antenna aperture. When large elements are used in an array, however, the aperture efficiency of the element becomes a factor in the total array aperture efficiency. For this reason, it is essential that large array elements be uniformly illuminated so that their aperture efficiency is unity.

The maximum angle of scan that can be obtained with this array configuration is determined by the field of view of the radiating elements. The most convenient definition for element field of view is the angle between the 3-dB points on the element patterns. For comparison, the field of view of elements in a closely spaced periodic array is at best 120° and is usually somewhat less than this. At the edge of the field of view the array gain is down 3 dB from the broadside array gain. The field of view for uniformly illuminated elements is related to the length of the element by

$$\theta_3 = \frac{50.8\lambda}{L} \qquad (1)$$

Thus if a 10° field of view is required, elements having five wavelengths on a side or 25 square wavelengths in area can be used; for a 5° field of view, 100 square wavelength elements can be used.

Although the array is globally aperiodic it is approximately periodic locally of period equal to the element size. This local periodicity produces a vestige of a grating lobe. The level of the vestigial grating lobes depends upon the total number of elements in the array approximately as 10/N. The element pattern will appreciably reduce the level of the vestigial grating lobe except when the array is scanned to the limits of the field of the element.

The maximum element area in the circular grid array is determined by the scan coverage requirements. The total array area is determined by the broadside gain. The ratio of these areas determines the total number of elements and from this the vestigial grating lobe level can be estimated. When the level of the vestigial lobes is excessively high, more elements of smaller area may be used. This reduction in element area will tend to increase the gain at the scan limits and to decrease the effective level of the vestigial lobe at the scan limit.

CALCULATED RESULTS

Antenna patterns have been calculated for two configurations of the circular grid array designed to scan a 10° cone. One of these consisting of approximately 1,000 elements has the pattern at 5° scan shown in Fig. 2. A second array consisting of approximately 100 elements has the pattern at 5° scan shown in Fig. 3. The second array is actually the center 10% of the first. Both arrays are illuminated with a 10-dB Gaussian taper distribution function. The antenna pattern characteristics computed for these arrays are summarized in Table I.

EXPERIMENTAL RESULTS

A full-scale model of the smaller array has been built and tested. The element configuration is shown in Fig. 4. The final configuration has been modified from that shown in Fig. 1 to allow one basic element design to serve all stations. This has resulted in an effective aperture blockage which modified the effective illumination distribution across the array. The term *antennule* (small antenna) is used for an element of the circular grid array with the term *element* reserved for the smaller radiating components (dipoles) of which it is composed. The antennule shown in Fig. 5, is a dually polarized square array of 64 dipole elements measuring 9.5 inches on a side. If uniformly illuminated, the beamwidth (field of view) of this antennule would be 11°. In Fig. 6 we see that the beamwidth of this antennule is 12°. The

Fig. 6—Antennule typical pattern.

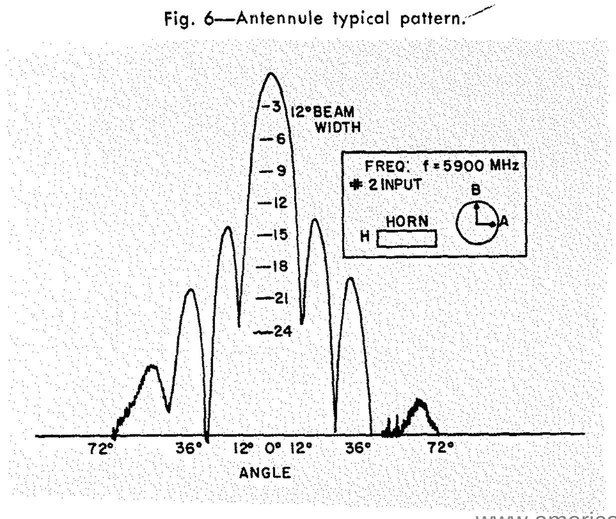

Fig. 7—Gain measurements on isolated antennule.

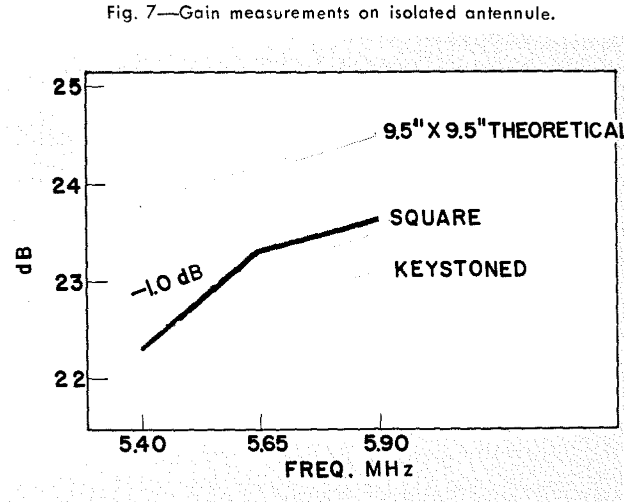

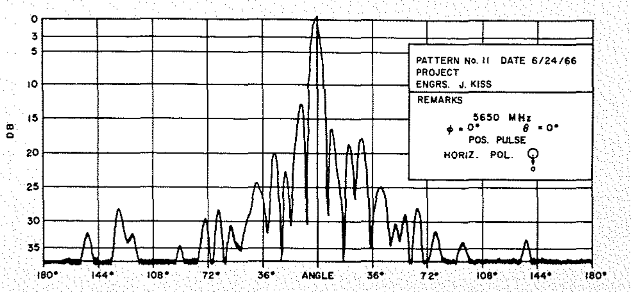

Fig. 8—Measured pattern, 100-element circular-grid array, scan angle 0 degrees.

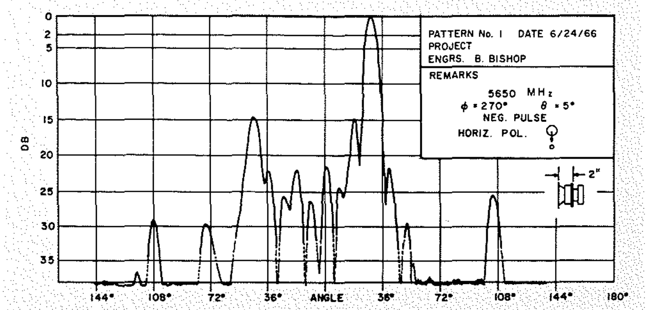

Fig. 9—Measured pattern, 100-element circular-grid array, scan angle 5 degrees.

broader pattern is caused by the illumination taper produced by mismatch of the edge elements.

The dipoles were designed to be matched in the array environment using a waveguide simulator technique. This minimizes loss in the power divider network and accounts for the high efficiency (80%) of the antennule. The gain of an isolated antennule is shown in Fig. 7.

The pattern of an antennule in the array has not been observed directly. However, the gain of the array was down 2.5 dB at 5° which indicates that the antennule had a beamwidth of 11° in the array. This is consistent with uniform illumination of the antennule and suggests that its efficiency is even higher than 80% when used in the array.

Typical patterns measured on the array model are shown in Figs. 8 and 9. It may be noted that the first sidelobes are higher than predicted because of the effective aperture blockage but that the vestigial grating lobe, Fig. 9, is substantially at the predicted level.

APPLICATION

The use of the circular grid array to reduce the number of phase shifters required for limited scan requirements has been emphasized. Phase shifters are used when the array is controlled by angle information from star or earth sensors, from the array using monopulse RF sensing, or from a stored program. This array technique also offers important advantages when used as a retrodirective antenna system.

The efficient operation of the phase conjugating networks or phased locked loops in a retrodirective antenna array depend upon the signal-to-noise ratio at each element of the array. The element gain is below the array gain by approximately the number of elements. When the number of elements is very large, narrowband noise filters must be used in the control loop to obtain an adequate signal-to-noise ratio for control, usually at the expense of response time. The use of large elements permits significantly larger control bandwidth and hence shorter response times.

Retrodirective transmitting antenna systems generally provide the final stage of RF power amplification at each element. The use of large array elements provides an increase in directive gain per amplifier unit. This provides the design flexibility needed to obtain a minimum weight antenna system.

By using active phase-conjugating circuits such as that shown in Fig. 10, the distribution of local oscillator and transmitter modulation information to the individual modules and the collection of the incoming command information can be accomplished by a single horn antenna located behind the array. This leads to the adaptive lens antenna concept shown in Fig. 11.

The active circuits in the lens array provides low noise amplification of signals arriving from any direction within the field of view of the antennules and focuses these signals for coherent summation at the pickup horn located on axis behind the lens. A local oscillator signal eminating from this horn is mixed with a pilot signal from a ground terminal to derive an intermediate frequency signal containing the conjugate phase information. This signal is amplified and transmitted from the array in the direction from which the pilot signal was received.

TABLE I—Antenna Pattern Characteristics

Scan Angles Θ_s	Φ_s	Worst Side Lobe Level (db)	position (deg)	Remarks
1000 Elements:				
2.5	160	—24	1.9	First side-lobe
5.0	133	20.9	—6.3°	Vestigial grating lobe
100 Elements:				
2.5	0	—21	4.5°	First side-lobe
5.0	90	—15	—7°	Vestigial grating lobe

Fig. 10—Retro-directive element circuit block diagram.

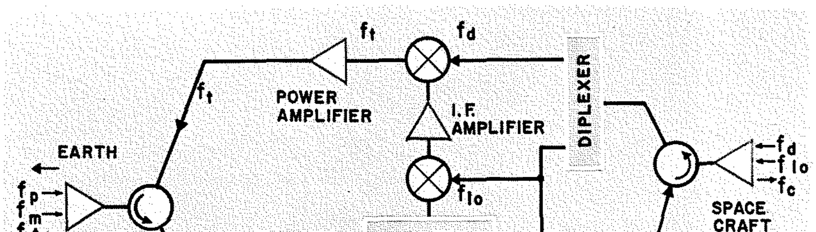

Fig. 11—Self-focusing circular-grid array.

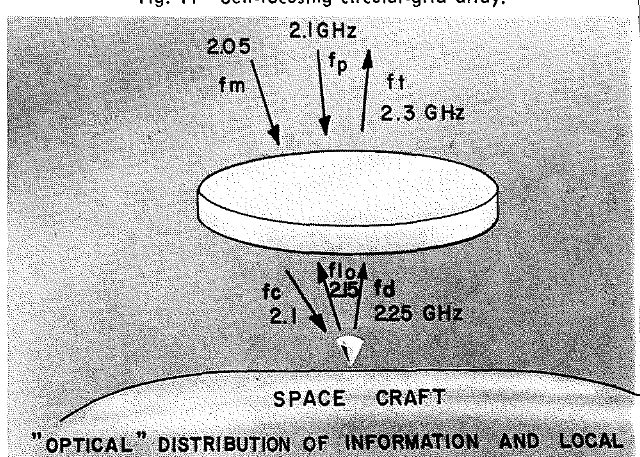

LOCOTAC

Design of a Low-Cost Tactical Radar

To dramatize the need for cost breakthroughs, a low-cost tactical radar (LOCOTAC) was constructed at RCA Missile & Surface Radar Division, Moorestown, N. J., as a company-sponsored project. Emphasis was placed on providing a serviceable, unsophisticated, frugal tactical device with moderate performance that could be transported by infantry and set up quickly without special tools. Its cost had to be low enough so that abandoning it or destroying it in the field would not involve a major financial decision. The use of commercially available components was stressed.

U. A. FRANK
Missile and Surface Radar Division
DEP, Moorestown, N.J.

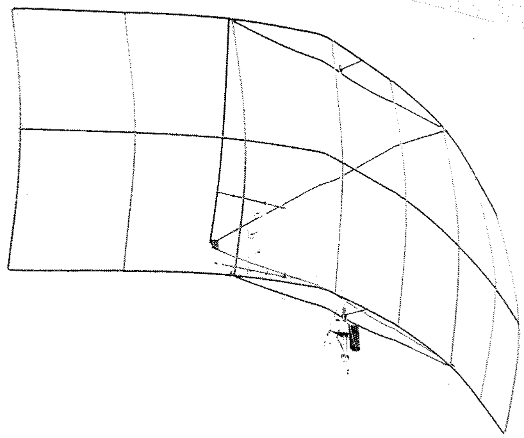

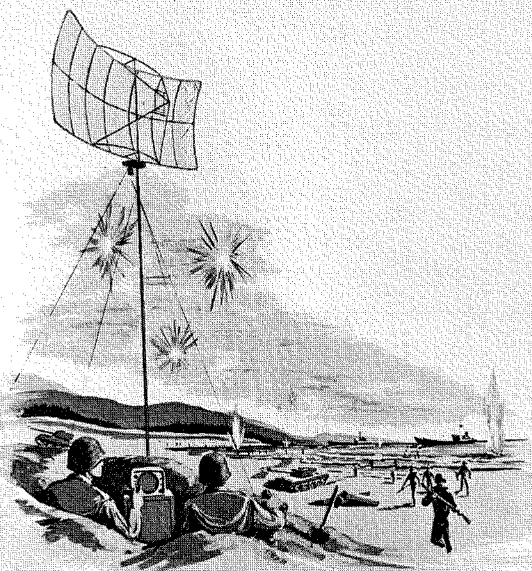

Fig. 1—Photo and sketch at left show the complete LOCOTAC radar unit.

ULRICH A. FRANK received his BSME from the University of N. H. in 1947 and did graduate work in instrumentation at Johns Hopkins University. His initial work was with NACA (now NASA) doing basic research on high temperature sensing and control. Other positions included assistant to Chief Engineer at Kaiser Metal Products in charge of automation and development programs. He has also been Assistant Chief Engineer with a vending machine company. Since joining RCA, M&SR, he was lead mechanical engineer on tactical radars such as AN/UPS-1 and AN/TPS-35. Other assignments included the design, building and installation at the site of Project Marshmallow, the instrumentation of an underground nuclear event, as well as principal project engineer on the "2 Pound Radar" during the R & D phase.

TABLE I—Measured Performance vs. Design Objectives

Characteristic	*Design Objective*	*Measured*	*Remarks*
Frequency	425 MHz	430 MHz	Good window through weather.
Pulse width	6 μs	6 μs	
PRF	1600 pps	900 pps	Lower because of delay between sweep start and transmitted pulse caused by circuit uniqueness in indicator.
Power, peak	30 kW	20 kW	Limited by tube operating parameters.
Antenna:			
Rotation	10 rpm 30 mph wind	10 rpm 30 mph wind	½ hp motor, motorcycle chain drive.
Beamwidth, az	5°	5.8°	13° vertical
Size	10′ x 25′	9′6″ x 24′6″	
Feed	Corner subreflector	Ground plane subreflector	Superior illumination of main dish.
Gain	18 dB	23 dB	As measured on two antennas.
Display	7″ CRT	7″ CRT	
Display range	50 nmi	48 nmi	

> **Editor's Note:** Good news that a contract was received for four radar systems based on the capabilities and product performance demonstrated on project LOCOTAC; the four systems are similar to the LOCOTAC transmitter-antenna system, two each operating at two different frequencies. Delivery of the two high-frequency units has already been accomplished within the time schedule and well within budget. Delivery of the two lower frequency units is proceeding according to schedule and within cost budget.

The design and building of the LOCOTAC radar represents an attempt to demonstrate the feasibility and utility of a low-cost, simple radar. As such, it provides a dramatic reversal in the continuing tendency to design toward greater sophistication, complexity, and the ultimate in long life and reliability (with attendant higher costs).

The need for a lightweight, limited-range, easily transportable and quickly erectable radar for use by ground troops is immediately apparent. Such a radar can be used for training purposes, or for personnel with a minimum of technical training. The requirements for portability, fast setup time, simple breakdown, unambiguous display, and ease of maintenance were emphasized during the LOCOTAC design, and were re-emphasized during recent design phases of such military radars as the AN/UPS-1 and AN/TPS-35.

Keeping this design philosophy in mind, design objectives were written and are listed in Table I; measured results obtained from the LOCOTAC model are also listed in Table I.

THEORY OF OPERATION

The completed LOCOTAC radar unit and the black-box diagram are shown in Figs. 1 and 2. Operationally, the transmitter trigger pulse is amplified by the driver amplifier and applied to the second grid of the transmitting tube by the pulse modulator. The RF pulse goes to the antenna through the circulator. The returning pulse goes from the antenna through the circulator, limiter, mixer, and the IF and video amplifiers to the scope. The CRT sweep is driven directly by the synchro output. The trigger for the sweep precedes the transmitter trigger to permit synchronization of the sweep-start and transmitted pulse.

The implementation of the basic mode of operation and design philosophy can best be demonstrated by giving a few examples of the approaches utilized in selecting the proper radar components.

THE ANTENNA

To achieve the required parabolic shape for the antenna, thin fiberglass tubes (1¼ inch OD × 1/16 inch wall) were

Final manuscript received July 28, 1966.

Fig. 2—Block diagram showing LOCOTAC operation.

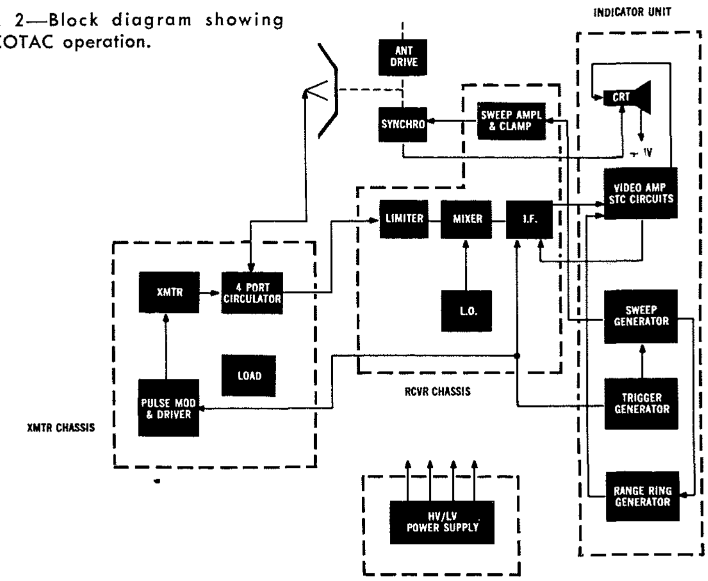

TABLE II—LOCOTAC Equipment Components

ANTENNA FEED

Primary feed—two fan-type dipoles spaced one wavelength apart and ⅓ wavelength over a ground plane (made from a charcoal grill in the model).

Transmission line feed—coax line from transmitter through a modified General Radio connector used as a rotary joint to a balun at base of antenna. Twin lead from balun via commercial TV lead to a variable-spacing, parallel-rod matching line between the dipoles.

MECHANICAL

½ HP gearhead motor—washing machine type—drive through ½ inch pitch motorcycle chain.
Reflector—10′ x 25′
Weight—150 pounds
Fiberglass tube size—1¼ ID, 0.06″ wall thickness
Aluminum mast tube size—3″ ID, ⅛″ wall thickness
Mesh—1-inch hex, galvanized chicken wire.
Fasteners on mesh—12 gauge steel feed bag ties
Reflector frame joints—angle, Reynolds tee joints, splices and crossovers for do-it-yourself projects with aluminum tubing.
Synchro: 3 phase, small marine type.

TRANSMITTER EQUIPMENT

Circulator—Coaxial, 4 port
20 dB isolation between transmitter and receiver
30 kW peak power handling capability
Insertion loss: 0.8 dB to receiver, 0.4 dB to transmitter
Limiter—Solid state
Limits at −35 dBm
30-dB insertion loss at high power levels
0.5-dB insertion loss at low power levels

RECEIVER

Mixer—Balanced diode, coaxial
Conversion loss—3 dB max.
Noise Figure—7.0 dB max.
IF amplifier—From RCA Radiomarine Radar model N3B
11 amplifier stages
100 dB gain
2.5 MHz bandwidth
Local oscillator—Xtal controlled (44.45833 MHz x 9) = 400.125 MHz

INDICATOR (RCA Radiomarine Model N3B)

Video amplifier—two stage
STC circuits—adjusted for recovery time equal to 2 miles or 25 μs.
Trigger and sweep generator—Free running multivibrator Trigger pulse delayed to permit sweep centering.
Range ring generator—self excited Colpitts oscillator 3 miles between rings

SWEEP CIRCUITS

Sweep amplifier and clamp—Uses 6DQ5 which is a standard TV horizontal amplifier tube.
Synchro—1:1 ratio, 3 phase output to deflection yoke.
No synchro amplifiers required.
Synchro unit identical to that used on N3-B radar
Deflection Yoke—3 phase circuit, 4 wire, original yoke as used in N3-B indicator

TRANSMITTER

Output Stage—Self-excited oscillator, grounded-grid, grounded-plate, screen pulse modulated.
6 μs pulse
20 kW pulse output peak
Full wave cavity
Constructed from off-the-shelf tubing
7651 tube, air cooled
5,000 volt plate supply
Modulator—6293 output tube; driver amplifier is a synchronized blocking oscillator

POWER SUPPLY

Conventional circuits
Solid state rectifiers

bowed within their elastic limit to the required curvature in both the horizontal and vertical planes. To minimize setup time, the hollow fiberglass tubes were joined together at both tee and elbow junctions by Reynold's "Do-It-Yourself Joints" obtained at the local hardware store. The straight joints were made by short fiber tubes with an outside diameter fitting snugly into the inside diameter of the longer tubes to be joined. No bolts were used, since each joint was *automatically locked* when the antenna structure was bowed into its parabolic curvature.

REFLECTOR

The reflector surface was made of 1-inch hexagonal galvanized chicken wire; initially, this was to be fastened onto the bowed reflector structure by spiraling a long wire between them. Setup time was greatly reduced by changing to wire ties such as those used by feed mills to close burlap and paper bags. By using a spiral Yankee screwdriver tool, these wire ties were placed on approximately 8-inch centers. The ties will probably rust through in a year's exposure to salt atmosphere and cannot be easily reused; however, at a unit cost of ⅕¢ this is not thought to be a problem. The reflector is shown in Fig. 3 and the antenna patterns in Fig. 4; excellent symmetry is apparent. The horizontal beamwidth is 5.8°, the vertical beamwidth is 13°, sidelobes are down 17 dB, and backlobes are down better than 25 and 27½ dB.

PULSED OSCILLATOR

Another area requiring detailed design attention was the connector and resonating cavity for the pulsed oscillator. An RCA-7651 air-cooled lighthouse tube was used, but no connector was available for this tube. A combined connector-resonating cavity was designed and constructed using standard copper plumbing pipes and pipe caps, supplemented by fingerstock, Mylar and Teflon sheets, and automotive hose clamps. By using wraparound sheets, the machining of solid stock was avoided.

The rotary joint was constructed by modifying a standard swivel coaxial connector. A small RCA Radiomarine indicator, modified slightly for range, was just sufficient to serve as our display and was thus utilized. Some off-the-shelf (local hardware store) components are shown in Fig. 5. The equipment parameters of other components are shown in Table II.

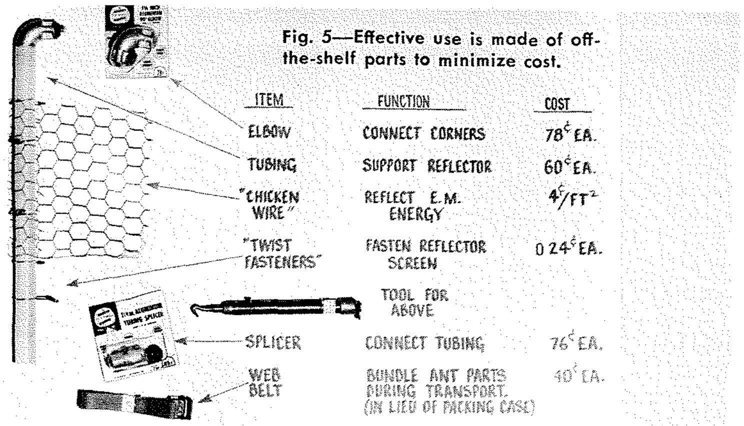

Fig. 5—Effective use is made of off-the-shelf parts to minimize cost.

CONCLUSION

The practical importance of the approach using common commercially available hardware was dramatically demonstrated when the assembled antenna was scheduled to be moved by truck. Unfortunately, the reflector got involved with an overhead structure and was destroyed. Starting Friday evening, and reusing the feed and driver mechanism, two engineers and one technician were able *to procure enough parts locally during the weekend to assemble completely a new reflector* and report completion of the task on Monday morning.

Here we have reversed the usual process by a simple, workable initial design which places the burden of justification or complexity on other subsequent specifications. A series of demonstrations of the LOCOTAC model was conducted for most engineering personnel at RCA Moorestown to show what uninhibited creativity can achieve. This project shows the way and provides a real challenge to apply just such a cost-conscious approach to designing and building models on other projects, even where more stringent military specifications make a choice of approaches more limited.

The validity of the frugal approach of "leaving-well-enough-alone"—of a critical examination of what is really required to achieve a low-cost tactical radar—has been proved by the performance of the unit.

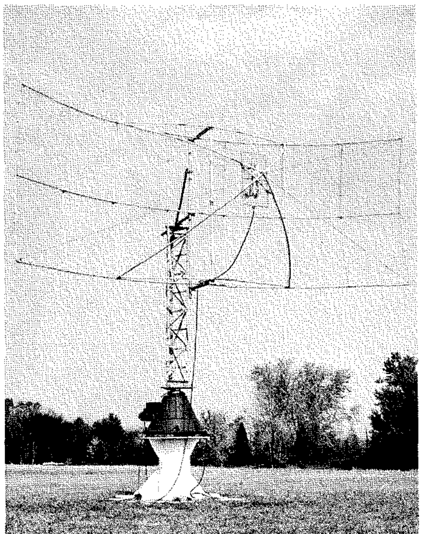

Fig. 3—The LOCOTAC unit showing reflector.

Fig. 4—LOCOTAC antenna patterns.

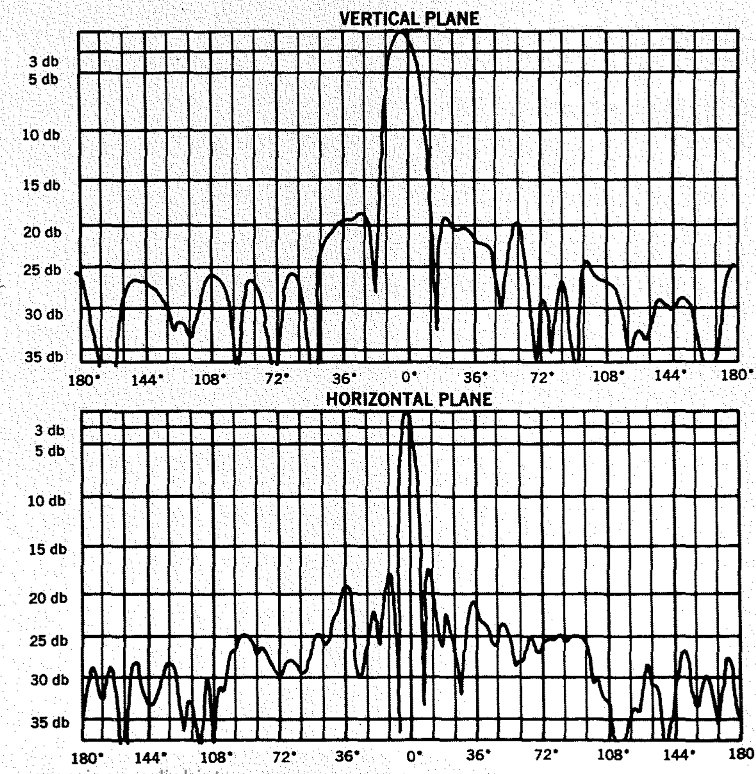

DIGITAL-SYNTHESIZER DESIGN WITH A SIMPLIFIED CHART

The simplified design chart presented here allows rapid derivation of parameters for a basic digital synthesizer, once given the requirements of frequency range, channel spacing, and any design constraints on the circuitry. Tradeoffs among critical parameters are more readily performed with the design chart than with the applicable mathematical relationships.

D. H. WESTWOOD, Mgr.
Light Equipment Technology
Communications Systems Division
Camden, New Jersey

Most frequency synthesizers which have been built over the past twenty years have consisted of multiple crystal oscillators, harmonic generators, mixers, filters, and other circuitry required from combining separate frequencies to obtain a single output. Frequency synthesis is often a determining factor in the ultimate complexity and costs of communications equipment.

Recently, the advent of low-cost high-speed digital microcircuits has revolutionized the approach to obtaining highly accurate discrete frequencies over any required band. This new technique, termed digital synthesis, is now competitive with the multiple-crystal and mixing technique, and has significant performance advantages if proper design methods are adopted.

The simplified design chart presented here (Fig. 3) allows rapid derivation of parameters for a basic digital synthesizer, once given the requirements of frequency range, channel spacing, and any design constraints on the circuitry. Tradeoffs among critical parameters are more readily performed with the design chart than with the applicable mathematical relationships.

Final manuscript received October 25, 1966.

Fig. 1 shows a digital frequency synthesizer. The voltage controlled oscillator (VCO) which supplies the output signal is divided by a fixed ratio K_1 and then supplied to a divide-by-N counter which is manually programmed by the channel selector. The factor N is an integer established by manually setting shafts which determine the counter logic. (In some applications, this may be performed by remotely programmed serial or parallel digital codes.) The output of the divide-by-N counter is fed to a phase comparator which has as its other input a fixed reference frequency F_c (obtained from a precision crystal oscillator through a fixed scaler counter having a dividing factor of K_2). The phase comparator output produces a correction voltage if the two phase comparator inputs are not identical in frequency and phase. Hence the VCO frequency is automatically set so that the divide-by-N input signal to the phase comparator is phase locked to the divide-by-K_2 input. At the end of each counting period of F_c, the counter N is reset and the counting process is repeated. Fig. 2 illustrates the basic waveforms associated with Fig. 1.

In a typical synthesizer, the input counting frequency F_N to the divide-by-N counter will be limited to a practical maximum frequency determined by the speed of the digital circuits selected. If, for example, the maximum F_N is chosen to be 15 MHz, a VCO with a required frequency range of 40 to 60 MHz would require a fixed scaler division of 4, which is the factor K_1.

One of the inherent drawbacks of digital synthesizers for some applications stems from the rate at which frequency corrections can be made to the VCO when F_c is at a low frequency. For example, when the phase comparator frequency of 1 kHz is used, the error corrections to the VCO cannot be at a rate in excess of 1 kHz and any disturbances of the VCO at approximately the above rate, or higher cannot be electronically corrected through the action of this feedback loop. Thus, it is to the interest of the designer to raise the F_c to the maximum possible comparison frequency,

D. H. WESTWOOD received his BSEE in 1943 from the University of Minnesota, and his MS degree from the University of Pennsylvania in 1953. He joined RCA in 1943 and was assigned circuit development for airborne radars, radar altimeters and multichannel UHF communication equipments. He was promoted to Leader in 1951 and was placed in charge of development of the APN-42 Pulse Radar Altimeter. In 1955 he was promoted to Manager responsible for terrain clearance radar techniques development and system studies. Since 1957 Mr. Westwood has had design and development management responsibility for programs which include AN/ARC-62, 3500-channel Air Force Command Set; the Dyna-Soar (X-20) Vehicle Communications Equipment; the design stage of the Project Ranger Television Transmitter; the telemetry transmitter for Project Relay; the Gemini Data Transmitter; and the Lunar Excursion Module and Apollo VHF Communications Equipment development phase. In addition, during this period he has been heavily involved in numerous new techniques development programs for transmitters, receivers and frequency synthesizers employing advanced state-of-the-art solid-state and microwave techniques. Currently, he is Group Manager in the Advanced Communications Technology Activity of the Communications Systems Division. Mr. Westwood holds four U.S. patents in the field of airborne electronics and has published several technical papers. He is a member of IEEE, Beta Kappa Nu and Tau Beta Pi.

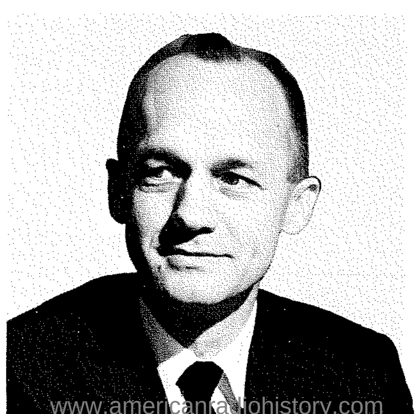

thus enabling a wideband loop for improved short-term stability.

The following mathematical relationships exist in the frequency synthesizer:

$$\frac{F_o}{K_1} = F_N \qquad (1)$$

$$\frac{F_N}{N} = F_c \qquad (2)$$

$$\frac{F_R}{K_2} = F_c \qquad (3)$$

where F_o = output frequency, F_N = input frequency to divide-by-N counter, F_c = output of divide-by-N counter after lock-up and also output of divide-by-K_2 counter, F_R = reference crystal oscillator frequency, K_1 = fixed scaler counter factor following VCO, K_2 = fixed scaler counter factor following reference crystal oscillator, and N = counter factor which is programmable.

Equations 1 and 2 may be combined to obtain the output frequency as a function of K_1, N, and F_c:

$$F_o = K_1 \, N \, F_c \qquad (4)$$

When the divide-by-N count is changed by the smallest integer increment of 1, the output frequency is incremented by its minimum amount of ΔF_o, as follows:

$$\begin{aligned} F_o + \Delta F_o &= K_1 \, (N+1) \, F_c \\ &= K_1 \, N \, F_c + K_1 \, F_c \qquad (5) \\ &= F_o + K_1 \, F_c \end{aligned}$$

It is evident from Equation 5 above that:

$$\Delta F_o = K_1 \, F_c \qquad (6)$$

And by combining Equations 4 and 6:

$$\Delta F_o = \frac{F_o}{N} \qquad (7)$$

The above equations are important for obtaining precise values of K_1, N, F_c, and K_2, when F_R, F_o, and ΔF are known. It is useful, however, to employ shortcuts in the form of a design chart to obtain the approximate values and derive tradeoffs among the various values prior to employing a desk calculator to obtain the precise numbers. Fig. 3 is the design chart which readily yields the set of dependent parameters having been given a set of independent parameters.

Consider the following typical problem of a frequency synthesizer having the following requirements:

1) Output Frequency, F_o . . . . .100 to 400 MHz
2) Incremental Frequency Spacing, ΔF_o . . . . .50 kHz
3) Reference Crystal Oscillator, F_R . . . . .5 MHz
4) Design constraint: the frequency feeding the programmable counter N shall not exceed 20 MHz.

It is desired to find the range of the divide-by-N factor N, the range of frequency F_N which feeds the divide-by-N counter, the phase comparator frequency F_c, and the fixed scaler factors K_1 and K_2. Following the instructions on the digital synthesizer design chart of Fig. 3, a diagonal line is drawn for each of the following frequencies: ΔF_o, F_R, and the minimum and maximum values of F_o. The vertical line is drawn at ΔF_o = 50 kHz and a second vertical line is drawn from the upper K scale intersecting the maximum F_o line at a frequency below 20 MHz (the design constraint). This factor, K_1, is established at the value of 32 being a binary number and readily obtainable in a simple divider. The intersection of the vertical K_1 line with the F_o diagonal lines yields the divide-by-N counter input frequency read on the right hand scale. This range is noted to be from 3 MHz to approximately 12 MHz.

It may be noted that if the scaler factor K_1 were chosen to be 16, the F_N would have a maximum value of 24, which exceeds the desired counter input frequency. The extension of the K_1 vertical line intersects the ΔF_o diagonal line at a reading of 1.6 kHz on the right hand scale. This is the value of F_c and the horizontal dashed line is drawn through the K_1 and the ΔF_o intersection until it intersects the diagonal F_R line. The vertical dashed line from this intersection yields the fixed scaler factor K_2 on the upper scale. This value is read as approximately 3200. Thus, the following approximate information has been obtained through the simple graphical construction:

$$K_1 = 32$$
$$K_2 = 3200$$
$$F_N = 3 \text{ to } 12 \text{ MHz}$$
$$F_c = 1.6 \text{ kHz}$$
$$N = 2{,}000 \text{ to } 8{,}000$$

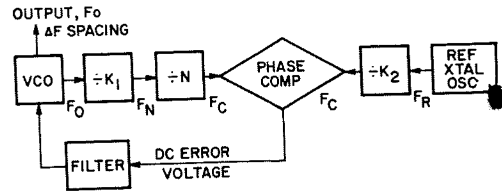

Fig. 1—Frequency synthesizer basic block diagram.

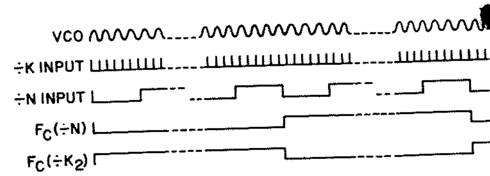

Fig. 2—Voltage waveform in frequency synthesizer.

From these values, the designer must evaluate the expected performance of his synthesizer. It will be noted that the phase comparator frequency of 1,600 Hz will limit the loop bandwidth to some value below this frequency. Vibrational effects which are experienced in the VCO in the form of incidental FM noise will not be removed by the feedback action at frequencies above the loop bandwidth.

By moving the K_1 line to the right to a value of 10, for example, raises the phase comparator frequency F_c to 5 kHz, but at the same time requires an input frequency to the programmable counter of 40 MHz. The designer must weigh the benefits of having a higher phase comparator frequency against the added difficulty of performing his counting and reset logic in the divide-by-N counter at the higher frequency of 40 MHz.

Similarly, with a straight edge he may choose to examine the effects of shifting other lines in the chart over which he has design control.

Several digital synthesizers have been designed, fabricated and tested. In general, these units, in breadboard form, are substantially smaller than previous assemblies constructed along the lines of multiple crystals, filters and mixers. The ultimate reduction of the flatpack assemblies to a multilayer printed board mounting assures uniformity in construction and the elimination of all the alignment adjustments associated with conventional frequency synthesizers.

Fig. 3—Digital synthesizer design chart.

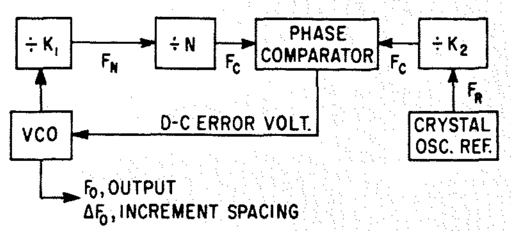

INSTRUCTIONS:

DRAW AND LABEL THE FOLLOWING LINES:
DIAGONAL LINES FOR F_0, ΔF_0 & F_R
VERTICAL LINES FOR ΔF_0 & K_1
READ N AT INTERSECTION OF F_0 & VERT. ΔF_0
READ F_N AT INTERSECTION OF K_1 & F_0
READ F_C AT INTERSECTION OF K_1 & DIAG. ΔF_0
READ K_2 AT INTERSECTION OF F_C & F_R

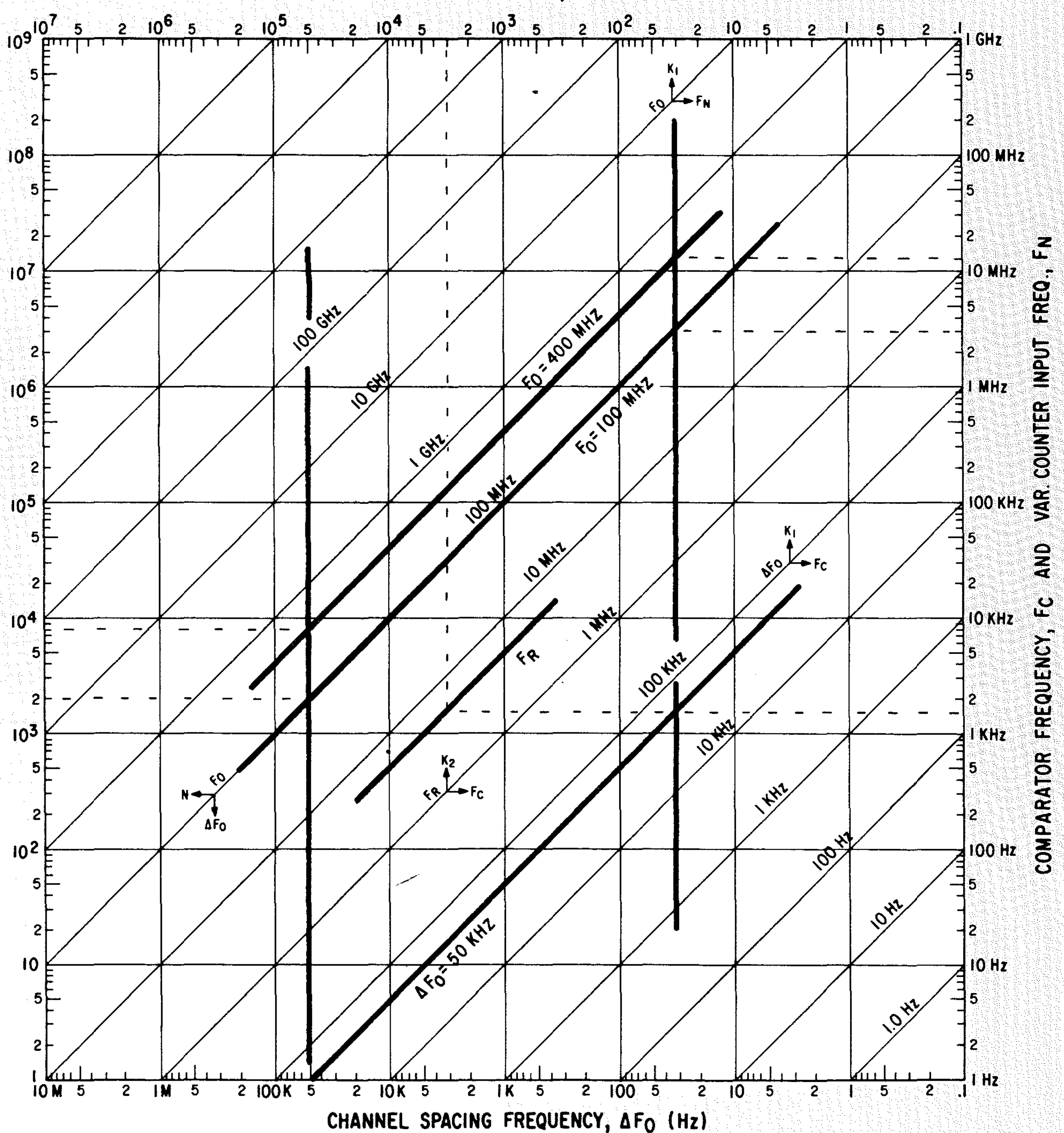

A PRACTICAL METHOD OF HEAT COMPUTATIONS IN ELECTRONIC EQUIPMENT

Disregard of a thermal analysis during the design of electronic equipment may lead to inadequate thermal design, yet time schedules and cost aspects often exclude construction of thermal laboratory models. This paper describes a relatively simple method for manual thermal computations, particularly useful for electronic equipment where all types of heat transfer must be taken into account. The method involves construction of a simplified thermal network diagram for the equipment. When good judgment is used, predicted temperature values approach actual ones.

G. REZEK
Communications Systems Division
DEP, Camden, N.J.

The omission of preliminary thermal analysis in the design of electronic equipment may lead to severe financial penalties. In some instances such analysis is bypassed for reasons of its complexity. Design parameters are then not optimized, leading to possible thermal deficiencies in performance of the equipment. In other cases computations are made, but they are presented in bits and pieces, lacking in clearness and sweep of concept, posing a disadvantage in contracting bids.

ANALOGY

The method of thermal computation described in this paper makes use of the affinity between thermal and electrical networks and thus appeals also to electrical engineers. A known analogy exists between thermal and electrical quantities as shown in Fig. 1. Heat flow is represented in the electrical analog scheme by current flow, temperature potential is represented by voltage potential and a thermal resistor by an electrical resistor. For the transient heat flow, the analogy is extended in representing heat absorbed and stored in a mass by an electrical current stored and absorbed in a capacitor. Differential equations bear out the mathematical similarity between thermal and electrical quantities (Fig. 1.)

GENERAL APPROACH

As a practical consequence of this analogy, the entire mechanical equipment can be visualized as a thermal network comprised for steady state, of equivalent thermal resistances and heat generators. The flow of heat through the thermal resistances causes temperature differences. For the transient computation, thermal capacitors can be added to the network.

By using experience and some ingenuity the equipment network can often be simplified and so arranged as to lend itself to manual arithmetic computation. Exceptional complexity may dictate the use of a digital computer with node-equation capability, or the use of an analog computer.

DERIVATION OF THERMAL RESISTANCE NETWORK

First, heat flow by conduction, radiation and convection at different locations within the equipment is computed as was done in the past. Then, according to the thermal Ohm's law, thermal resistance is defined as the ratio of computed temperature elevation divided by generated heat power. Some typical equivalent thermal resistances are compiled in Fig. 2.

Note that certain less tangible quantities such as coefficient of heat transfer for radiation and convection, or cooling air mass, hydraulic flow resistance and fan power are not directly, but in some indirect manner incorporated in the thermal resistance diagram: e.g.:

1) For forced-air flow, compute pressure head losses, then determine air mass delivered into the equipment, and compute resultant air temperature rise from inlet to outlet.
2) For heat transfer by natural convection, substitute the buoyance of the air "chimney effect", for pressure head losses.
3) The heat flow of radiation is expressed in the classical Stefan-Boltzmann law, a fourth power relationship between heat power and Kelvin temperatures. It can be mathematically shown that only a small error is incurred when we assume a linear relationship, because the temperature changes very little in our limited temperature range.
4) Values for the heat transfer coefficient of convection can be taken from known graphs.

Once the equivalent thermal resistances have been determined, by one of these methods, they are incorporated into the overall equipment diagram.

DERIVATION OF EQUIVALENT THERMAL EQUIPMENT DIAGRAM

To the thermal resistances add amperages representing heat generators for the steady-state computation of the temperatures. Then add heat capacitors for the transient computation. Temperature elevations are then computed and are entered into this diagram and/or into a summary Table.

This graphic presentation can serve to aid in various evaluations such as:

1) Locations of largest thermal resistance causing high temperatures and calling for means of reduction.
2) Effect of reduction of generated heat power where possible, or effect of change of design parameters.
3) Expected thermal behaviour at sea level or at higher altitudes.

Final manuscript received October 14, 1966

Fig. 1—Thermal and electrical analogies.

Thermal	Electrical
heat generator Q [BTU/H]	current generator I [amp]
temperature difference Θ [°F]	voltage potential V [volt]
thermal resistor $R_{th} = \Theta / Q$ = [°F/(BTU/h)]	resistor R = V/I = [Volt/amp] = [ohm]
heat capacitor = C_{th} = weight x specific heat = $W c_p$ [BTU/°F]	capacitor C hr/Ohm
time constant $\tau_{th} = R_{th} W c_p$ [hr]	time constant $\tau = R C$ = [hr]
heat flow from ambient stored in mass: of material of specific heat c_p 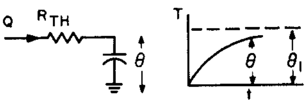 for $R_{th} = \frac{1}{A(h_r + h_c)}$ $C_{th} = W c_p$ $dQ = W c_p \, d\Theta = A(h_r + h_c)(\Theta_1 - \Theta)\, dt$ $\frac{d\Theta}{\Theta_1 - \Theta} = \frac{1}{R_{th} C_{th}} dt$ $\Theta = \Theta_1 (1 - e^{-t/\tau})$	current flow through resistor stored in capacitor 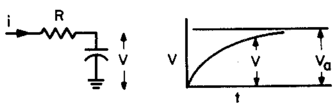 $dq = i\,dt = C\,dV$ and $i = \frac{V_a - V}{R}$ $\frac{dV}{V_a - V} = \frac{1}{R C} dt$ $V = V_a (1 - e^{-t/\tau})$
one dimensional transient heat flow through bar 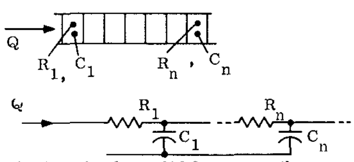 (Analogy is also valid for two or three dimensional networks)	one dimensional current flow through RC networks 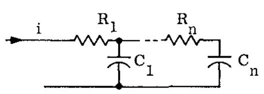

Fig. 2—Some equivalent thermal resistances Θ = Q R, Q = generated heat power, R = equivalent thermal resistance, Θ = temperature elevation, and A = surface area.

$\Theta = Q R$

Q = generated heat power
R = equivalent thermal resistance
Θ = temperature elevation.
A = surface area

For radiative heat transfer

$$R_{rad} = \frac{1}{A h_r}$$

h_r = heat transfer of coefficient of radiation

For convective heat transfer:

$$R_{conv} = \frac{1}{A h_c}$$

h_c = heat transfer of coefficient of convection.

Equivalent thermal resistance of airmass for air flow:

$$\Theta = \frac{Q}{W c_p} \quad \text{therefore} \quad R = \frac{1}{W c_p}$$

W = weight of air mass
c_p = specific heat of air

Equivalent thermal resistance for flow of heat through bar:

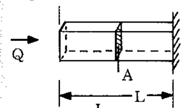

A = area of the cross section perpendicular to flow of heat
L = length of bar
K = thermal conductivity of material of bar

$$R_{th} = \frac{L}{A K} \quad \text{and} \quad \Theta_{max} = R_{th} Q$$

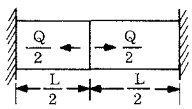

Equivalent thermal resistance for heat flow of heat power Q to two heat sinks

$$R_{th} = \frac{L}{4 A K}$$

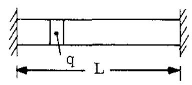

For equally distributed heat generation within bar; and also two heat sinks:

$$R_{th} = \frac{L}{8 A K}$$

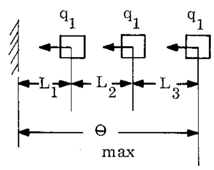

For heat flow from modules on p. c. boards to edge of p. c. board as heat sink.

$$\Theta_{max} = \frac{3q_1 L_1}{A K} + \frac{2q_1 L_2}{A K} + \frac{q_1 L_3}{A K}$$

$$R_{th} = \frac{\Theta_{max}}{3q_1} = \frac{1}{3A K}(3L_1 + 2L_2 + L_3)$$

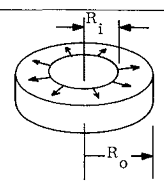

For radial heat transfer within cylinder

$$R_{th} = \frac{1}{2\pi t K} \ln\left(\frac{R_o}{R_i}\right)$$

SIMPLIFICATION OF THERMAL EQUIPMENT DIAGRAM

Simplification in the layout of the diagram, such as lumping of large numbers of individual heat generators and heat flow paths help simplify calculations but at some sacrifice of accuracy.

In practical examples, accuracies in temperature prediction have been found to stray from 10% to 25%. An element of challenge in this art remains, requiring some experience and intuitive judgment. To use manual computation methods, the user must construct a relatively simple thermal diagram. It is important upon preliminary thermal evaluation to implement such changes in concepts or dimensions as to achieve optimized thermal performance with the simplest means possible.

EXAMPLE: CONSTRUCTION OF A THERMAL DIAGRAM OF A PORTABLE ELECTRONIC EQUIPMENT

Fig. 4 is a typical diagram from application of the principle. Components in this equipment (shown in Fig. 3) are cooled by radiation and conduction to the case. The case is cooled by radiative and convective heat flow to ambient. When a fan is added for air recirculation within the case, heat transfer from the components to the equipment case is improved as shown in the schematic of Fig. 5. To construct the thermal diagram, individual thermal resistances were (with allowance for approximations) computed in detail. Then heat generators were added and the temperature elevations were computed using thermal Ohm's law.

Referring to Fig. 4, there are three levels of heat transfer. These are outlined by the dotted quadrangles, as follows:

1) The first level of heat transfer is by conduction from the integrated circuit module junction (ICM junction) to ICM case, or to the surface of the printed-circuit board (PC board) respectively, since both are thermally joined together. The conduction resistance from ICM junction to PC board is R_1, the heat generated is Q_{icm}.

2) The second level of heat transfer is from printed circuit board to equipment case. Three parallel pathways, representing thermal resistances from an individual printed-circuit board to the equipment case were computed for radiation heat:

$$R_2 = \frac{1}{A_2 h_r}$$

heat conduction through air:

$$R_3 = \frac{\Sigma L}{AK_{air}}$$

and heat conduction through materials of board:

$$R_4 = \frac{\Sigma L}{AK_{board}}$$

via guide springs R_5, and via side structures to case:

$$R_6 = \frac{\Sigma L}{AK_{metal}}$$

The heat generated is $Q_{pc\text{-}board}$.

3) The third level of heat transfer is

Fig. 3—Isometric sketch of electronic equipment cooled by conduction, radiation, and convection.

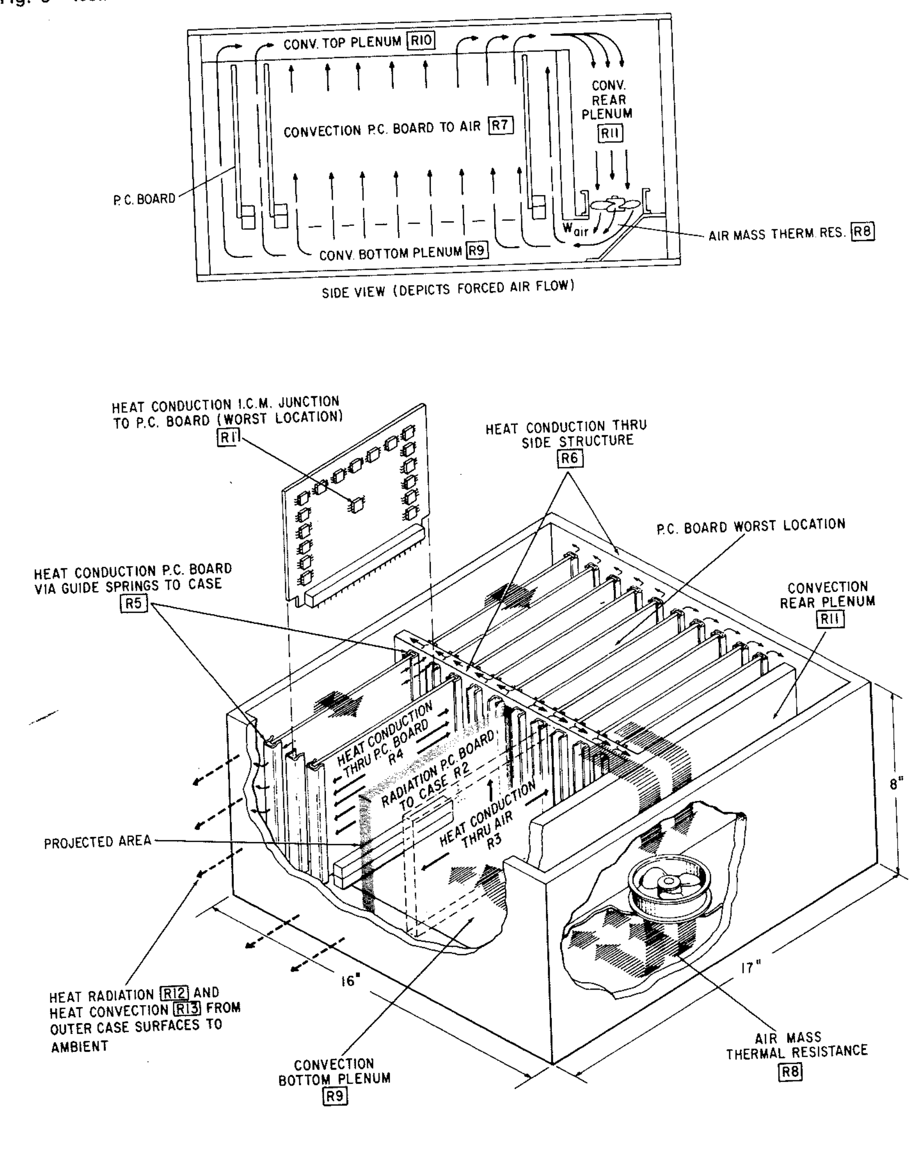

GERARD REZEK graduated in 1940 from the Swiss Federal Institute of Technology, Zurich, as a Mechanical Engineer and in 1948 as an Electrical Engineer from the same Institute. Between 1949 and 1951, Mr. Rezek was employed as a development Engineer by the H. K. Porter Co. in Pittsburgh and Fox Products Company in Philadelphia. Since 1951, he has been employed by RCA. He has done mechanical and also electrical development and design work on computers, mainly on input-output devices and random access memories. Since 1958, he has been associated with the Micromodule program, having participated in the design of the Micropac and Microrac Computer and also designed a thermoelectric refrigerator. He has made studies on miniaturized packaging techniques and was also assigned to various other design projects. Mr. Rezek authored a number of papers, all on thermal subjects. He holds or is coinventor, in 6 U.S. patents and was granted Senior membership by the IEEE.

from surface case to ambient air via radiation:

$$R_{12} = \frac{1}{A_{12}h_r}$$

as well as by free-air convection:

$$F_{13} = \frac{1}{A_{13}h_c}$$

The heat generated is the equipment heat power:

$$Q_{equ} - Q_{board}$$

In comparing the resultant temperature elevations θ_1, θ_2, and θ_3 for the three levels, we find θ_2 (between board and equipment case) is relatively large. It can be reduced by forced air flow recirculation within the case. Referring to Fig. 5, an added path of heat flow is then created. This path represents:

1) convective resistance from the board to air flow (boundary layer resistance):

$$R_7 = \frac{1}{A_7h_o}$$

2) then a thermal resistance of the air mass:

$$R_8 = \frac{1}{W_{air}c_p}$$

where W_{air} is the recirculating air mass;

3) and finally, the convective resistances R_9, R_{10}, and R_{11} between the air mass and inside surface of the equipment case:

$$R_9 = \frac{1}{A_9h_o} \text{ for bottom plenum}$$

$$R_{10} = \frac{1}{A_{10}h_o} \text{ for top plenum}$$

$$R_{11} = \frac{1}{A_{11}h_o} \text{ for rear plenum}$$

For simplicity of computation the thermal resistances R_2 to R_6 in Fig. 5 are not referenced to the power source Q_{po} of one individual printed circuit board, but rather to the total heat power ($Q_{equ} + Q_{fan}$) generated inside the equipment case. To obtain correct temperature elevations, R_2 to R_6 in Fig. 5 were therefore multiplied by a ratio factor:

$$x = \frac{Q_{po\text{-}board}}{Q_{equ} + Q_{fan}}$$

We find that the addition of forced air recirculation (Fig. 2) notably reduced the former predicted total temperature elevation shown in Fig. 4.

BIBLIOGRAPHY

1. *Heating and Ventilating and Air Conditioning*, The American Society of Heating and Ventilating Engineers, Vol 30, 1952. (Published by ASHVE, New York)
2. W.H. Carrier, R.E. Cherne, W.A. Grant and W.H. Roberts *Modern Air Conditioning Heating and Ventilating*, 3rd ed. p 251 to 264, Pittman Pub. Corp., N.Y.
3. G. Rezek and P.K. Taylor; "Thermal Design Solutions for Micromodular Equipment," *IRE Transactions on Product Engineering and Production*, June, 1961.
4. G. Rezek, "Temperature Evaluation in Microelectronic Structures Using Analog Networks" *IEEE Transactions on Product Engineering and Production*, April, 1965; Vol. 9-1.
5. G. Rezek; Design and Analog of a Thermoelectric Refrigerator for the Micropac Computer Core Memory RCA Engineer Oct.-Nov. 1963.

Fig. 4—Thermal diagram of equipment cooled by conduction, convection and radiation.

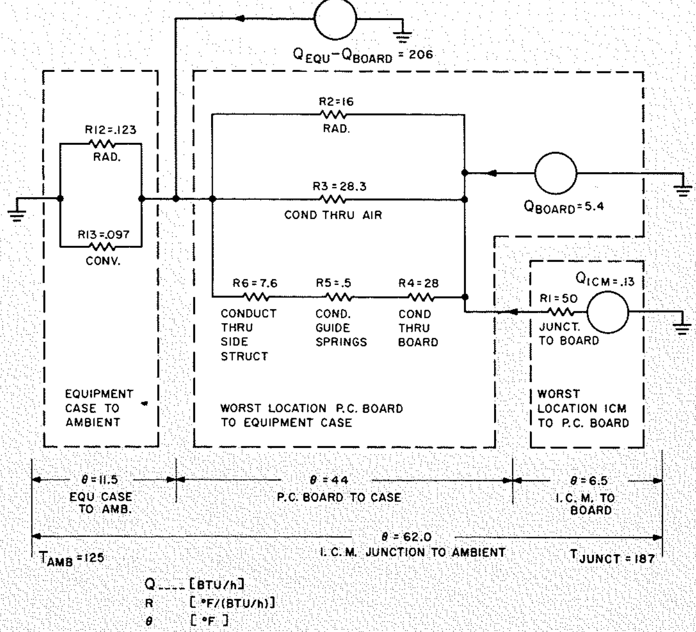

Fig. 5—Thermal diagram of equipment when forced air recirculation inside of equipment case is added.

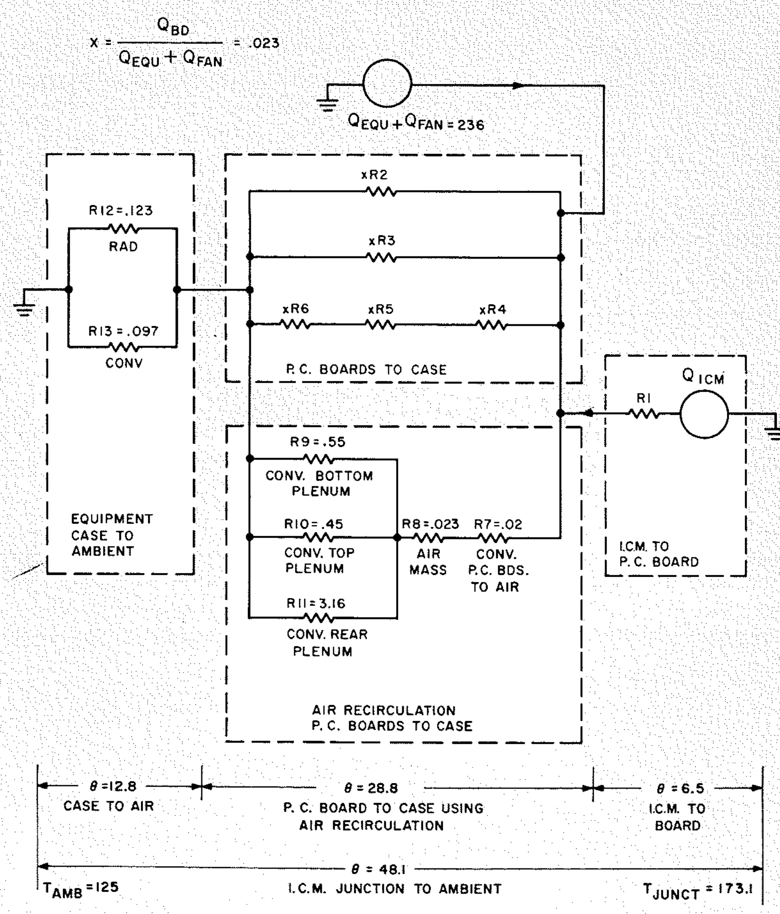

THE DESIGN OF A PCM ENCODER FOR THE ISIS-A SATELLITE

This paper describes a low-power PCM encoder which generates 8-bit words at 1440 words/second. Logical functions are performed by integrated circuits. The analog commutator uses field-effect transistor switches. The analog-to-digital converter, a cascaded type employing differential amplifiers and limiters, is preceded by an accurate sample-and-hold circuit employing overall negative feedback. A reliability figure of approximately 98% is estimated for one year's operation.

Dr. R. G. HARRISON

Research Laboratories

RCA Victor Company, Ltd., Montreal, Canada

The Isis-A Satellite is the third of a series of scientific satellites being designed and constructed in Canada under a joint Canadian government-NASA program. The responsible Canadian agency is the Defence Research Telecommunications Establishment (DRTE).

Telemetry equipment for the first two Canadian Satellites, Alouette I and Alouette II, was designed and constructed by RCA Victor Company, Ltd., which also assisted DRTE with the engineering design of Aloutte II. The company now has the prime contract, with DeHavilland Aircraft as associate contractor, for the complete Isis-A Satellite.

This paper describes a PCM encoder designed for Isis-A by RCA Victor's Research Laboratories in Montreal. Two of these PCM encoders, which incorporate an unusual analog-to-digital conversion technique, will be used in the satellite.

The encoder handles 16 analog, 4 serial digital, and 2 parallel digital channels. Two other channels are provided for synchronization purposes. The output consists of 8-bit words at a rate of 1440 words/second.

High reliability and accuracy over a wide range of temperatures together with low weight and power consumption have been primary design objectives.

Final Manuscript received March 30, 1966.

INPUT AND OUTPUT SIGNALS

The satellite carries 11 on-board experiments, 10 of which have outputs that must be telemetered to the ground. In addition to these, 180 critical voltages must be monitored periodically.

The encoder must accept the various analog and digital signals derived from the experiments and other equipment and time-multiplex them into a prescribed sequence of 22 channels. A complete frame consists of 24 channels, two of which are occupied by internally-generated synchronization signals.

The output consists of 24 eight-bit words read out in series. Thus the analog signals must be converted into serial digital code, whereas the serial and parallel inputs must be read out serially at the appropriate times. NRZ-C and split-phase outputs are provided simultaneously at 60 frames/second, so that information is fed to the transmitters at 11.52 kilobits/second.

DESIGN PHILOSOPHY

Logical operations are performed by standard diode-transistor-logic (DTL) integrated circuits to conserve space and to promote reliability. Certain parts of the encoder, e.g. the analog-to-digital converter (ADC) require DC differential amplifiers. However, commercially available linear integrated-circuit ampli-

Fig. 1—System diagram.

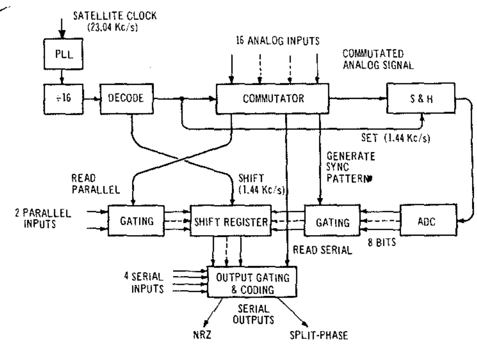

Fig. 2—The commutator.

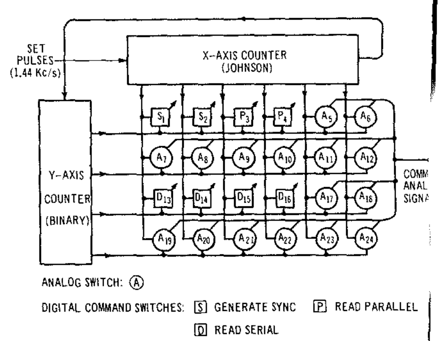

fiers did not fulfill the following requirements:

1) high voltage gain, (> 65 dB),
2) large input impedance, ($> 1\,\text{M}\Omega$),
3) sufficient common-mode range (-0.5 to $+6.5$ volts), and
4) low power consumption (< 30 mW).

It was therefore necessary to design discrete-component amplifiers specifically for this application.

Discrete components were used in the analog switches, sample-and-hold circuit, interface circuitry, and reference and supply voltage regulators.

Field-effect transistors (FET) were used extensively where high input impedance amplifiers or zero-offset switches were required.

All circuits were designed to use the least power consistent with reliability in a radiation environment and to maintain accuracy over a wide range of temperatures ($-50°$ to $+70°$C). Detailed stability analyses of all critical circuits were carried out to determine worst-case sensitivity to temperature, voltage fluctuations, and ageing of components. In addition, all significant sources of error in the encoder were analyzed. The design goal of $\pm 0.5\%$ accuracy for the temperature range $-5°$ to $+40°$C was found to be feasible and has been realized in practice.

ROBERT G. HARRISON received his B.A. in Electrical Engineering from the University of Cambridge in 1956 and an M.A. in the same subject in 1960. He was awarded a Ph.D. by London University and the Diploma of Imperial College (D.I.C.) in 1964 for research on steady-state and transient phenomena in parametric subharmonic oscillators. From 1956 to 1957 he was with Computing Devices of Canada Ltd., Ottawa, specializing in semiconductor circuit design. In 1957 he joined the Canadian Defence Research Board where he worked on high-speed logic systems for operation in the nanosecond range. In 1960 he was a consultant on color TV circuitry to Central Dynamics Ltd., Montreal. Dr. Harrison joined RCA Victor Research Laboratories in 1964 and is currently engaged in the design of analog/digital systems for a space-research satellite.

TIMING

All timing pulses used by the encoder are derived from a phase-locked loop (PLL) synchronized to the 23.04-kHz satellite clock. The output of the PLL is divided by 16 and decoded into PCM clock pulses at 11.52 kHz and set and shift pulses, both at 1.44 kHz.

SYSTEM DESCRIPTION

A simplified block diagram of the complete encoder is shown in Fig. 1. The 1.44-kHz set pulses step the commutator so as to switch the 16 analog inputs to a common output line in the correct sequence and also to provide the gating pulses for the digital inputs and the generation of the *wired-in* synchronization pattern.

The commutated analog signal is sampled at 1.44 kHz and held at a constant amplitude during the process of analog-to-digital conversion.

The ADC, an asynchronous type, is based on an idea due to B. D. Smith.[1] Eight bits appear on 8 parallel outputs, the most significant digit first. The rate of generation of bits depends only on the transient response of the converter circuits. After the eighth (least significant) digit has appeared, the entire word is gated in parallel into the output shift register. The contents of the register are read serially at 11.52 kilobits/second into the output gating and coding circuits.

The parallel digital inputs are read into the shift register under the control of the *read parallel* pulses; the serial inputs are fed directly into the output circuitry under the control of the *read serial* pulses.

The Commutator

As shown in Fig. 2, the 24-channel commutator is arranged in four rows of six switching elements. The digital switches are DTL *nand* gates and are symbolized by squares; the analog switches are logic-driven FET switches and are indicated by circles. The synchronization channels are marked *S*, the parallel channels *P*, the serial digital channels *D*, and the analog channels *A*. The numbers show the order of scanning.

The commutator is scanned by a 6-counter for the X-axis and a 4-counter for the Y-axis. The X-counter is driven by the 1.44-kHz set pulses. Every 6th count is fed to the Y-counter so that the next row of the matrix may be scanned. All analog channels are switched sequentially directly to the encoding circuitry. The other channels provide the command pulses which control the gating of the digital inputs and the generation of the synchronization words.

One of the analog switches used in the commutator is shown in Fig. 3. When both X and Y inputs of the *and* gate are high, the bipolar transistor saturates, turning the FET switch on. The two series diodes provide noise immunity, since the X and Y signals must overcome two diode-drops before the switch closes. The analog signals normally lie between ground and a voltage $< E_4$; a limiter prevents malfunctions due to abnormal voltage excursions. The FET switch exhibits no offset voltage; its series resistance, which is a few hundreds of ohms, is unimportant here since the *load* is an FET gate, a very-high-impedance point.

Fig. 3—Analog switching element.

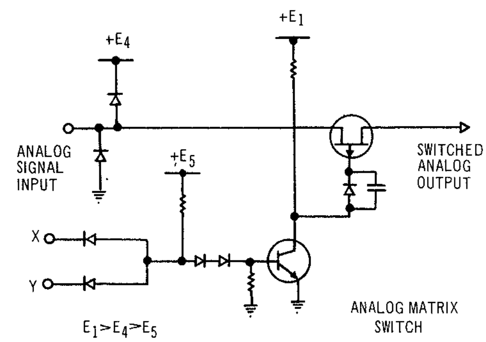

Fig. 4—Principle of the sample-and-hold circuit.

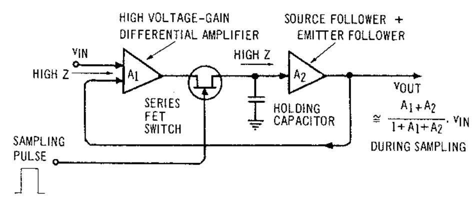

Fig. 5—Realization of the sample-and-hold circuit.

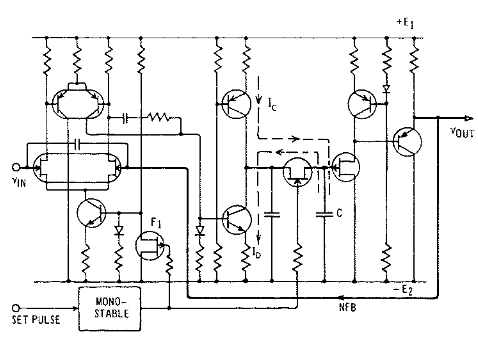

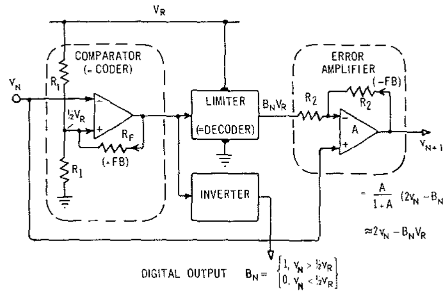

Fig. 6—One-bit encoder/decoder pair with error-detecting amplifier.

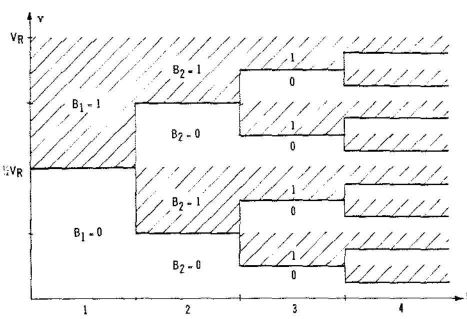

$$\frac{V}{V_R} = \tfrac{1}{2}B_1 + \tfrac{1}{4}B_2 + \tfrac{1}{8}B_3 + \ldots = \sum_{N=1}^{8} 2^{-N} B_N$$

Fig. 7—Diagram illustrating the process of straight binary coding.

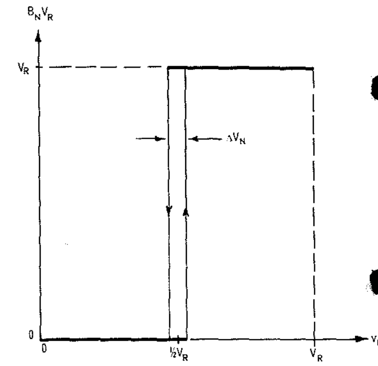

Fig. 8—The (v_N, $B_N V_R$)—transfer function.

The Sample-and-Hold Circuit (S&H)

The commutated analog signal is fed to an S&H circuit and thence to the ADC (Fig. 1). The S&H circuit is necessary because the switched sequence of waveform-segments may contain voltage rates of change (up to 2kV/second) rapid enough to preclude the use of any but an extremely high-speed ADC. The input to the ADC must not change by more than ½ a quantization step during the coding process, otherwise errors will occur.

The principle of the S&H circuit is illustrated in Fig. 4. The analog voltage V_{in} is applied to the noninverting input of a high-gain differential amplifier, A_1. The forward path is completed by a series FET switch and by a high-input-impedance/low-output-impedance amplifier, A_2, of approximately unity gain. A holding capacitor is provided across the input of A_2. Negative feedback is returned from the output to the inverting terminal of the input amplifier.

During sampling, the output follows the input with an accuracy governed by the open-loop gain and the input offset voltage of A_1. When the sampling pulse is removed, the FET switch is pinched off. The holding capacitor now "sees" only reverse-biased junctions, so that a holding time-constant of minutes is obtained. This is to be compared with an 8-bit encoding time of approximately 50 μsec.

Details of the actual S&H circuit are shown in Fig. 5. The input amplifier consists of a closely matched pair of FET's connected as a long-tailed pair, followed by a bipolar differential amplifier that drives a high-gain unbalanced stage. This unbalanced stage provides constant-current charging and discharging of the holding capacitor. The paths I_C and I_D of the charging and discharging currents are indicated.

The output isolation amplifier is an efficient source-follower and emitter-follower in series.

To save power, amplifier A_1 is switched off during the holding interval by shorting the base-emitter junction of the input current-sink transistor via the FET F_1.

The Analog-to-Digital Converter (ADC)

The steady output from the S&H circuit must be encoded to 8 bits, giving $2^8 = 256$ quantization levels. Each level corresponds to a different binary-coded number.

The asynchronous ADC is a sequence of similar stages, each consisting of a one-bit encoder/decoder pair with an error-detecting amplifier (Fig. 6). A one-bit encoder is a device that generates a *1* digit if the analog sample v_N (which in this case lies between 0 and V_R) is greater than ½ V_R, and a *0* digit if less. Decoding is accomplished by converting a *1* digit to the full-scale reference voltage V_R and a *0* digit to zero volts. The error-detecting amplifier transmits the difference between twice v_N and the one-

Fig. 9—The (v_N, v_{N+1})—transfer function of one complete stage.

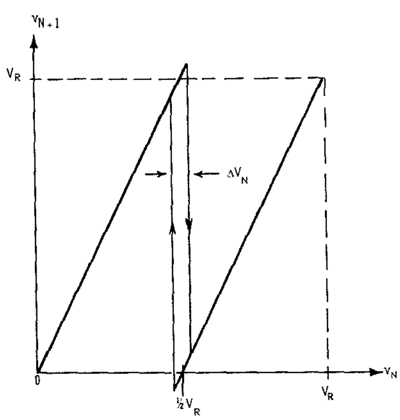

Fig. 10—One complete stage of the analog-to-digital converter.

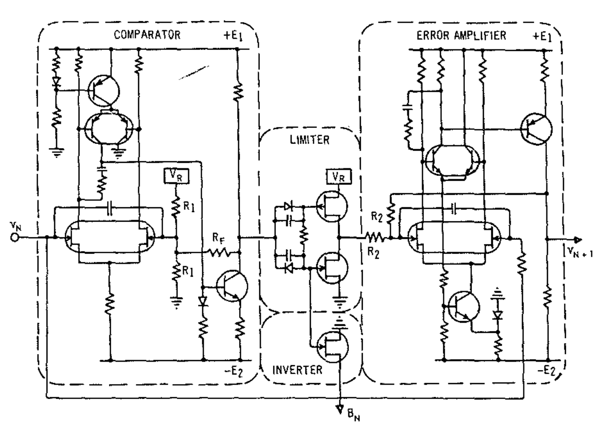

Fig. 11—Photograph of the engineering model of the complete encoder in its case.

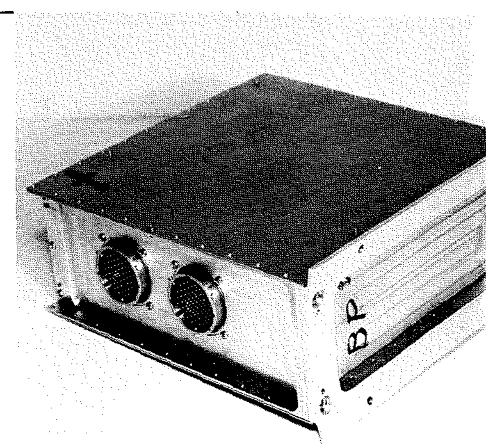

bit approximation $B_N V_R$ (where B_N is *1* or *0*) to the next stage. Two advantages are associated with the amplification of v_N by 2:

1) The same reference voltage V_R may be used for all stages,
2) Each stage need only be half as accurate as the preceding one. In principle, any desired accuracy could be obtained by cascading a sufficient number of such stages.

The encoding process is illustrated in Fig. 7. If $v_1 > \frac{1}{2} V_R$, $B_1 = 1$, but if $v_1 < \frac{1}{2} V_R$ then $B_1 = 0$. Suppose $B_1 = 1$. Then the next stage decides whether v_1 is $>$ or $<\frac{3}{4} V_R$ (i.e. whether $2v_1 - V_R \gtrless \frac{1}{2} V_R$). Similarly if $B_1 = 0$, the decision is whether $v_1 \gtrless \frac{1}{4} V_R$. One or other of these decisions determines B_2. When eight such decisions have been made, a digital word is available which gives the coded value of v_1 accurate to 1 part in 255 (assuming that no errors greater than the quantization error of 0.39% are present).

As shown in Fig. 6, the function of the one-bit encoder is performed by a positive-feedback comparator amplifier. Because of this feedback, the $(v_N, B_N V_R)$ — transfer function (Fig. 8) exhibits a hysteresis loop, the width of which is determined by the resistors R_1 and R_F. This loop provides a measure of noise-immunity. Since the N-th comparator is "seen" by v_1 through a gain of 2^N, the width ΔV_N of the N-th hysteresis loop is made twice as great as that of the previous one, ΔV_{N-1}. This ensures that a regular $(v_1, B_8 V_R)$ — transfer characteristic (which has $2^8 - 1 = 255$ transitions) is obtained. Thus the noise-immunity of each comparator is twice that of the previous one. In the present design ΔV_1 is made 10 mV ($\sim\frac{1}{2}$ a quantization level), ΔV_2 is 20 mV and so on. (These values are for $V_R = 5.100$ volts.)

Fig. 12—Encoder with seven printed-circuit boards partially removed to show method of assembly.

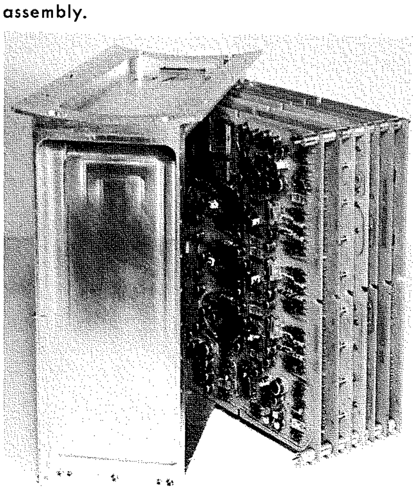

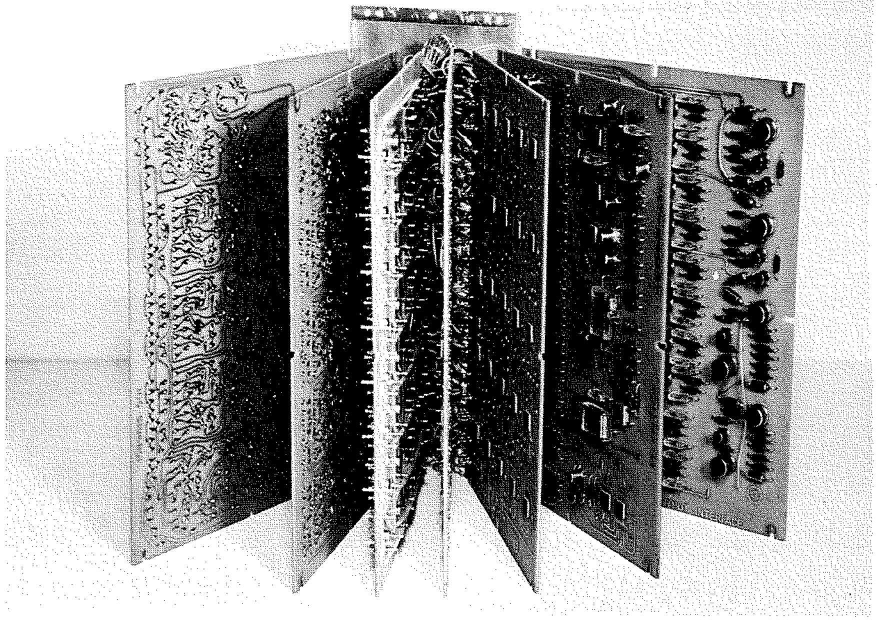

Fig. 13—Printed-circuit boards removed from case.

In general, the width of the N-th hysteresis loop in an S-bit encoder of this type should be

$$\Delta V_N = 2^{N-S-2} V_R.$$

The error amplifier is a DC differential amplifier with negative feedback arranged so that

$$v_{N+1} = \frac{A}{1+A}(2v_N - B_N V_R),$$

If the open-loop voltage gain, A, is large enough, then

$$v_{N+1} = 2v_N - B_N V_R$$

i.e., the inverting gain is unity and the noninverting gain is 2.

Including the effect of hysteresis, the ideal (v_N, v_{N+1}) — transfer function of a complete stage (Fig. 9) is given by the last equation with

$$B_N = \begin{Bmatrix} 0, 0 \leq V_N < \frac{1}{2}(V_R + \Delta V_N) \\ 1, \frac{1}{2}(V_R - \Delta V_N) < v_N \leq V_R \end{Bmatrix}$$

The $(v_1, B_8 V_R)$—transfer function of the complete 8-bit ADC can be found by an obvious iteration. Such expressions, however, become very complicated when the influences of the various error-sources are included.

A practical realization of a complete stage of the ADC is shown in Fig. 10. The comparator employs a matched pair of FET's as a high input-impedance differential input stage, which is followed by a second differential amplifier composed of a pair of bipolar transistors. Thermal stability considerations dictate that the *second* amplifier rather than the first should be provided with a constant-current source. One collector of this stage drives an unbalanced amplifier; positive feedback from the output of this amplifier is taken via the large resistor R_F to the noninverting input gate. Note that the use of FET's enables a large input impedance to be maintained over a wide dynamic range of v_N.

The limiter takes advantage of the zero offset voltage of an FET in the ohmic region. When the input to the limiter is high, the N-channel device is *on* and presents a channel resistance of a few hundreds of ohms to ground. The other device is *off*. When the input is low, the roles of the two FET's are reversed and the output is connected to $+V_R$ through a similar resistance. Since the load presented by R_2 is some hundreds of kilohms, there is negligible offset.

The error amplifier is similar in some respects to the comparator, but since large common-mode (CM) signals are encountered, CM feedback is employed to increase CM range and rejection ratio. The high-stability resistors, R_2, provide unity-gain negative feedback to the inverting input.

The open-loop voltage gain of both amplifiers is about 70 dB and their rise times are less than 1 μsec.

CONCLUSIONS

An unusual PCM encoder has been designed which takes advantage of some recently-developed components, particularly integrated logic circuits and matched pairs of field-effect transistors.

The total power consumption of the encoder—including voltage regulators—is about 3 watts, of which the ADC accounts for only 0.72 watt. The overall weight is under 3.5 pounds.

The completed encoder is shown in Fig. 11. As can be seen in Figs. 12 and 13, all components are mounted on seven printed circuit boards; two of these contain integrated circuits and five contain discrete components. Current design changes should reduce the total to six boards.

On the basis of one year's operation, the reliability of the encoder is estimated to be approximately 98%.

REFERENCE

1. B. D. Smith, "Pulse-Code Modulation Method", M. S. Thesis, Massachusetts Institute of Technology, 1948. (See also, R. P. Sallen, "A Method of Pulse Code Modulation", M. S. Thesis, M.I.T., 1949.)

MARS VOYAGER-LANDER DIRECT-LINK COMMUNICATIONS SYSTEM

This paper describes the direct communications link between a space probe landing on the surface of Mars and an Earth station. This study includes the system performance trade-offs of coherent and noncoherent binary and non-binary modulation systems. Some of the characteristics considered were the signal design, bandwidth, data rate, error probability, etc. The frequency and time acquisition and tracking problems for these systems are discussed. The system constraints were imposed by the near-future facilities of the Deep Space Instrumentation Facility and near-future realizable design conditions for the Lander.

DR. A. B. GLENN, Staff Engineer

Systems Engineering, Evaluation, and Research

DEP, Moorestown, N. J.

A BASIC limitation of the Mars VOYAGER-LANDER communications system is the marginal effective radiated transmitted LANDER power. Further work is required on the implementation problems concerned with a high-gain antenna on the LANDER.

The use of a nondirectional antenna on the Lander will result in signal fading. An analysis of the scattering of electromagnetic waves from irregular surfaces is needed so an accurate evaluation of system margin may be made for some satisfactory probability of system performance. This rather complex subject is now under investigation.

Final manuscript received October 5, 1966.

ALVIN B. GLENN received his BEE degree from Polytechnic Institute of Brooklyn in 1938, his MSEE from MIT in 1941, and his PhD in Electrical Engineering from Syracuse University in 1952. As an adjunct Professor at Drexel Institute of Technology, he teaches graduate courses in statistical theory of communications, information theory, and modulation theory. While with Sperry Gyroscope and Western Electric, he specialized in radio receiver design and UHF and microwave tube development. For 5 years he did advanced development and product design of TV receivers for General Electric. Since joining RCA in 1954, he has been engaged in the synthesis, analysis, and evaluation of communication systems. He is presently concerned with high-survivability satellite communication systems and interplanetary communications. Dr. Glenn is a member of Sigma Xi, Tau Beta Pi, Eta Kappa Nu, and IEEE. As staff Engineer of SEER, he acts as a consultant on communications systems for DEP. He has served on and was chairman of several IEEE committees since 1959. He is listed in "American Men of Science." He has published or presented more than 40 technical papers.

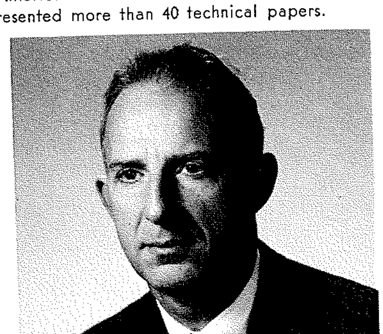

MODULATION AND DETECTION

Selection of Waveforms

In a binary modulation system, the selection of waveforms to represent the two symbols are chosen so that the receiver can easily distinguish between them. Common choices of signals used in binary systems are two different frequencies or phases (as in FSK and PSK) or a signal and no signal (as in *on/off* keying).

With nonbinary modulation, the choice of signals must be carefully chosen if they are to be easily distinguished from one another by the receiver. Consider a nonbinary modulation scheme in which any one of $M > 2$ possible signals $[s_1(t), s_2(t), \ldots, s_M(t)]$ is transmitted during a given interval T. One of the signals is selected during each successive interval in accordance with a symbol to be transmitted. Assume the receiver for this M'ary system contains a set of filters, each matched to a corresponding waveform $s_i(t)$.

The use of matched filters will ensure that the signals are most easily distinguishable one from another. In the absence of noise, the response of the j^{th} filter to the i^{th} transmitted signal at the instant $t = T$ is given by:

$$g_{ji} = k \int_0^T s_j(t)\, s_i(t)\, dt \qquad (1)$$

If the signals are chosen so that

$$\int_0^T s_i(t)\, s_j(t)\, dt = \begin{cases} O \text{ when } i \neq j \\ E \text{ when } i = j \end{cases} \qquad (2)$$

then, at the instant the matched filter output is a maximum $(t = T)$, the outputs of the nonmatched filters $(i \neq j)$ will be zero if the signals are chosen to be mutually orthogonal on $[0, T]$. In a coherent system, the optimum choice of waveforms should have the property that the filter matched to the transmitted signal attains its maximum positive output at the same instant that the remaining filters have large, equal, and negative outputs. However, for values of M larger than 8, operation within ½ dB of the

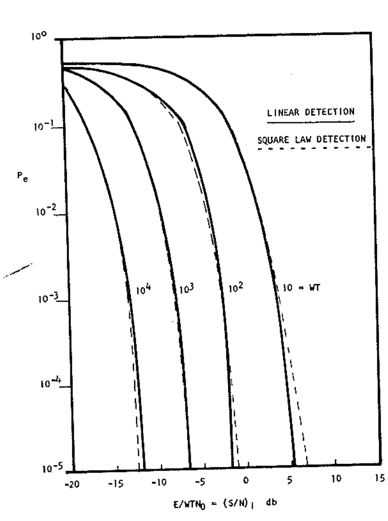

Fig. 1—Comparison of linear and square law envelope detection for wideband FSK systems.

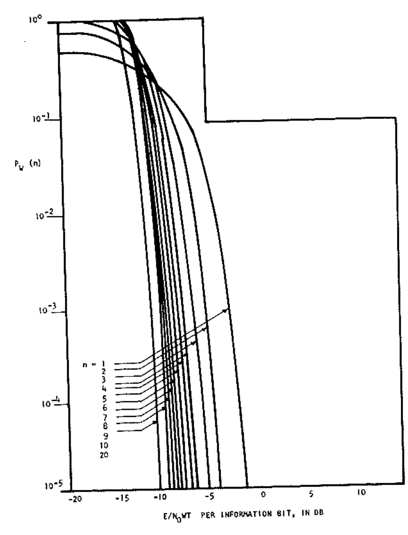

Fig. 2—Word error probability P_W (n) versus channel SNR per information bit for FSK systems using square law detectors.

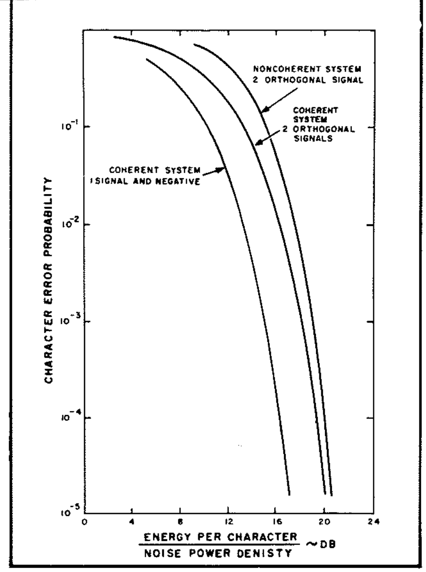

Fig. 6—Comparison of binary modulation-decision systems for 5-bit character transmission.

ideal can be achieved from the use of a set of orthogonal signals.

In a noncoherent system, where the precise phase of the transmitted signal is unknown, the received signal is indistinguishable from its negative. For this system the input to the decider is a set of non-negative values. Similar to the coherent system, it is desirable that the nonmatched filter outputs be as small as possible. Thus, for noncoherent systems, a set of orthogonal waveforms gives the optimum reliability.

Wideband Noncoherent FSK Systems

When the frequency uncertainty of the carrier is comparable to the bandwidth required by the data, the bandpass filter before the envelope detector is not matched to the data signal. Under these conditions, the matched filter follows the envelope detector.

Analyses[1] were made for noncoherent binary and nonbinary frequency shift keyed systems under the conditions that the predetection bandwidth was at least ten times the post detection bandwidth. With post detection filters matched to the transmitted signal expressions for information bit error probability as a function of channel input (predetection) signal to noise ratios were derived for square law and linear envelope detectors.

A comparison of error probability performance of a wideband noncoherent binary FSK system using linear and square law detectors is shown in Fig. 1. In these curves W is the predetection channel bandwidth, T is the signal duration, E is the signal energy, and N_o is the single-sided noise power spectral density. It is seen that at SNR above 0 dB, the linear detector is better than the square law detector. This difference increases to a maximum of 3 dB as the SNR increases. At SNR below -2.5 dB the square law detector is about 0.5 dB better than the linear detector.

Fig. 2 shows a plot of the word error probability $P_W(n)$ for wideband nonbinary noncoherent FSK systems versus the channel signal-to-noise ratios (this is the input SNR at the envelope detector) E/N_oWT required per unit of bit information. These curves are for systems using square-law detectors and for a WT of 100. The factor n represents n bits of information, or there must be 2^n words available at the transmitter. An $n = 1$ represents the binary FSK system. Thus, for $n = 1$ and $P_W(n) = 10^{-3}$, the required E/N_oWT is -2.7 dB. When n is increased to 5 and for the same $P_W(n)$, the required SNR per unit of bit information is -8.5 dB.

Fig. 3 shows a comparison for a 5-bit information word using *32*-ary and binary systems for an FSK system using square-law detectors. The 5-bit word for the binary system has five times, or 7 dB more, energy than each binary information bit. Since $WT \geq 10$, the channel bandwidth W for all values of n are practically equal. The WT product varies from 10 to 10^4. It is seen that the *32*-ary system, which has 2^5 different frequencies, requires about 6 dB less E/N_oWT than an equivalent 5-bit binary system. This improvement basically arises because the duration of a *32*-ary signal is 5 times larger than the duration of a binary signal.

Fig. 4 shows the basic system. The transmitter stores 2^n messages and a

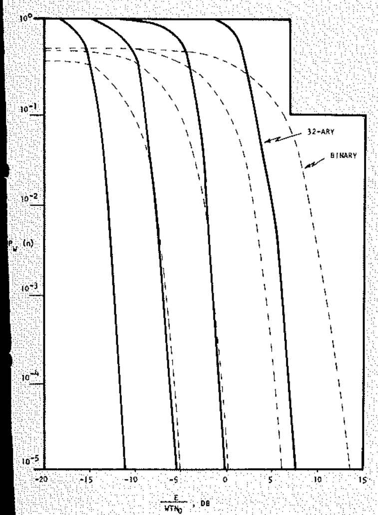

Fig. 3—5 bit word error probability versus input SNR for wideband FSK using square law detection. n = 5 bits/word
32-ary
binary (5 bits/word)

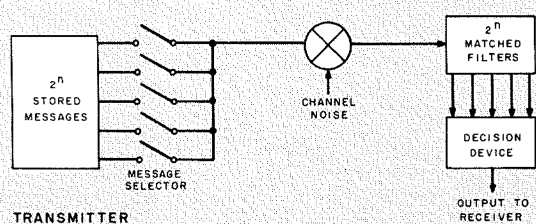

Fig. 4—Basic system.

Fig. 5—Receivers for non-coherent FSK.

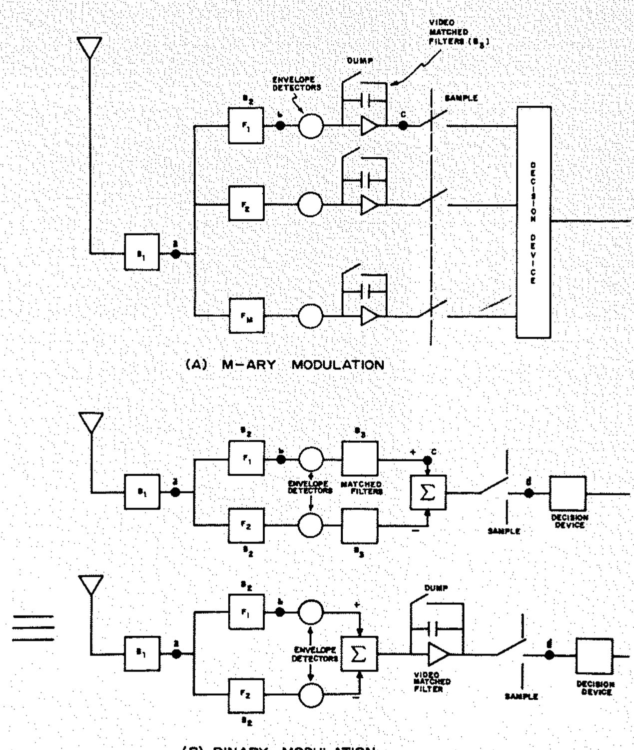

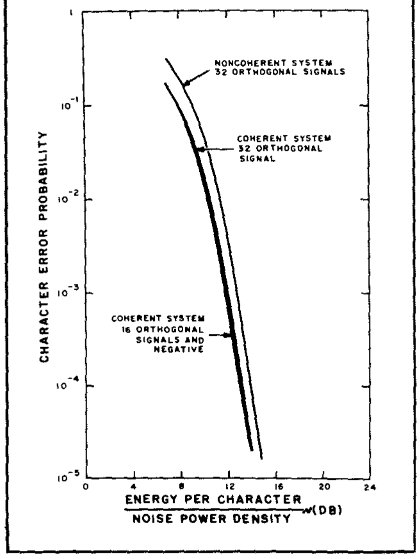

Fig. 7—Comparison of 32-ary modulation decision systems for 5-bit character transmission (ref. 14)

message selector will select one of the 2^n messages. The channel adds thermal noise to the transmitted signal. The receiver which has 2^n matched filters will decide which of the 2^n messages received is the most probable. If $n = 5$, then a character in the binary case will be composed of 5 information bits. The information bits will be transmitted at either frequency f_1 or f_2 for the noncoherent binary FSK modulation. For the equivalent information rate, a 32-ary system utilizes a choice of 32 frequencies. Each waveform will be 5 times the length of the information bit waveform for the binary case.

Fig. 5 shows the block diagrams for the M-ary and binary receivers.

Coherent M-ary Systems

The derivation for the probability of error for M-ary systems using M orthogonal signals and both coherent and noncoherent detection is given by Viterbi[2] and Lindsey[3].

Figs. 6 and 7 show the probability of error in receiving a 5-bit character for coherent binary and 32-ary modulation-decision systems. Note that while the difference between the best coherent and noncoherent detection systems is 4 dB when the binary alphabet is used, the difference is less than 1 dB with the 32-ary alphabet. Also the 32-ary alphabet with noncoherent detection yields a gain of 2 dB over the coherent detection of one binary signal and its negative.

The following general observations may be made:

1) The highest reliability is obtained by coherent detecting $M/2$ orthogonal signals and their negatives.
2) The difference between the coherent detection systems is substantial for binary transmission, but becomes negligible as the order of modulation used in the system is increased.
3) For example, at $P_e = 10^{-4}$, a comparison of curves in Figs. 6 and 7 show that the noncoherent 5-bit binary FSK system requires 6 dB more power than the noncoherent 32-ary FSK system.

TABLE 1—LANDER System Constraints

P_T	20 W
G_T	0 dB
f	2,300 MHz
Range	2×10^8 km
System Margin (99% time, $\gamma^2 = 10$)	9 dB
Freq. Stability	4 parts in 10^8
G_R	61 dB
T_e	35°K
SNR_o	10.8 dB

TABLE 2—Information Rates

Results:	
Information per Word	5 bits
P_e	10^{-3}
T_{AF} (90% prob.)	10 min.
T_{AT}	85 sec.
System	*Data Rate*
FSK binary noncoherent	90 bits/hr
FSK 32-ary noncoherent	360 bits/hr
FSK 32-ary coherent	12,000 bits/hr

LANDER SYSTEM CONSTRAINTS

The system constraints for the direct communication link between the LANDER on Mars and an Earth station is shown in Table I. (Gamma squared (γ^2) which characterizes the channel is defined as the ratio of the direct power to the reflected power.)

Table II shows the information rates for the three systems. This Table shows that there is a 15-dB increase in information rate for the coherent 32-ary FSK system compared to the wideband noncoherent 32-ary system. In addition, the frequency stability used for the noncoherent system is very difficult to realize for this mission.

COHERENT 32-ARY FSK SYSTEM

A coherent 32-ary system using orthogonal waveforms requires about 6 dB less signal power than an equivalent noncoherent binary system. The transmitting facilities required for a nonbinary system need be no more complex than those required for a binary system. The additional complexity of the nonbinary system is in the Earth receiver. Therefore, the proposed system for the direct link between a LANDER on Mars and an Earth station is the coherent 32-ary FSK system. The next two sections will discuss the implementation required for frequency acquisition and time synchronization.

Frequency Acquisition and Tracking

Fig. 8 shows the block diagram for the frequency acquisition and tracking circuits plus the information channel. At the start of transmission, an unmodulated signal (say at f_1), is sent for a duration sufficient for the phase locked loop (PLL) to acquire the signal. The switches are thrown to the 1 position. After frequency acquisition is accomplished, the switches are placed in position 2, the transmitted signal is phase modulated with a pseudonoise (PN) coded signal. During this mode, the receiver must acquire the frame sync for timing synchronization while at the same time track the signal frequency.

The receiver consists of 32 quadrature detectors for the 32 frequencies. The output of the in-phase detector is the information while the output of the quadrature phase detector contains the frequency error signal. The decider makes the decision which one of the 32 channels contains the signal. The error signal from the correct channel is then applied to the PLL and the frequency of the reference signal is thereby corrected.

Fig. 8—Frequency acquisition and tracking.

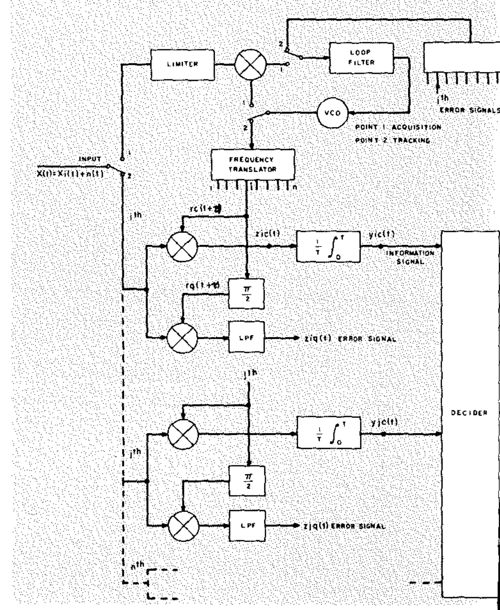

Fig. 9—Noisy demodulation reference SN loss curve. (ref. 27)

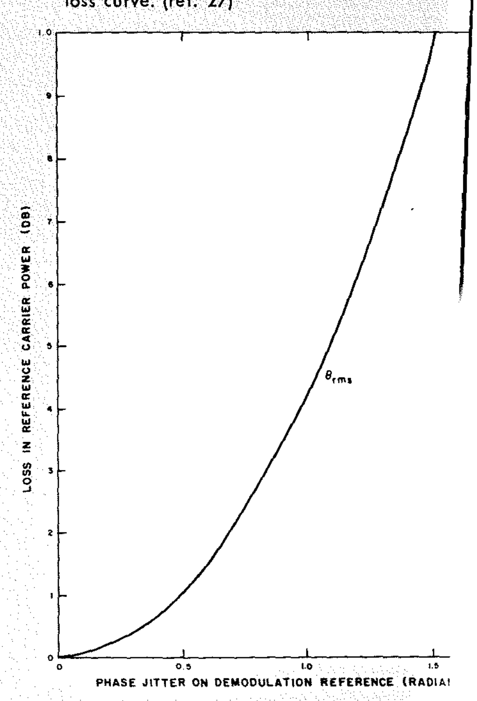

An important characteristic of the reference signal is phase jitter. Since the performance of a PLL in the presence of noise is very difficult to predict theoretically, many results have been arrived at experimentally. Results have shown that a *SNR* in a loop noise bandwidth $2B_{LO}$ of about 9 dB gives satisfactory performance. This *SNR* causes a phase jitter of 15°. The amount of phase jitter on the reference signals may very significantly degrade the performance of the data channel[4]. If the loss introduced by the phase jitter is independent of the data channel noise and that the phase jitter noise is gaussian distributed, the performance loss may be calculated by means of weighted statistical averages. The basic problem is to obtain the statistical average of a sine wave which is phase modulated by gaussian noise and a sine wave of the same frequency and phase but free of noise.

Fig. 9 shows the results of this analysis. For an RMS phase jitter of about 30° the loss in the reference carrier power is about one dB. The variance of the phase jitter is related to the *SNR* in the PLL bandwidth of $2\ B_L$ by:

$$\sigma_n^2 \doteq \frac{1}{2\left(\frac{S}{N}\right)} \qquad (3)$$

Thus, an *SNR* of 9 dB corresponds to a σ_n of 15° or a loss in performance of about 0.4 dB.

A far more significant reason for low phase jitter is the probability of unlock.[5] Fig. 10 shows the time in seconds for less than a one jitter. It is seen that for a 15° phase jitter that the time for less than 1% of probability of unlock is 650 seconds. A decrease in *SNR* to 3 dB results in an increase in phase jitter to 30°. This change results in a very significant decrease of the time to unlock to only 2 seconds. This curve demonstrates that the practical threshold *SNR* for satisfactory phase lock loop performance is about 6 dB.

Time Synchronization and Tracking

The basic system for time synchronization is shown in Fig. 11. For frequency synchronization a pure carrier at frequency f_i is transmitted. As explained in the preceding paragraph on this subject, the VCO in the Earth receiver is frequency locked to this signal. After the frequency of the received signal has been acquired, it will be necessary to synchronize the timing generator for the telemetry data in the LANDER and the timing generator in the Earth receiver.

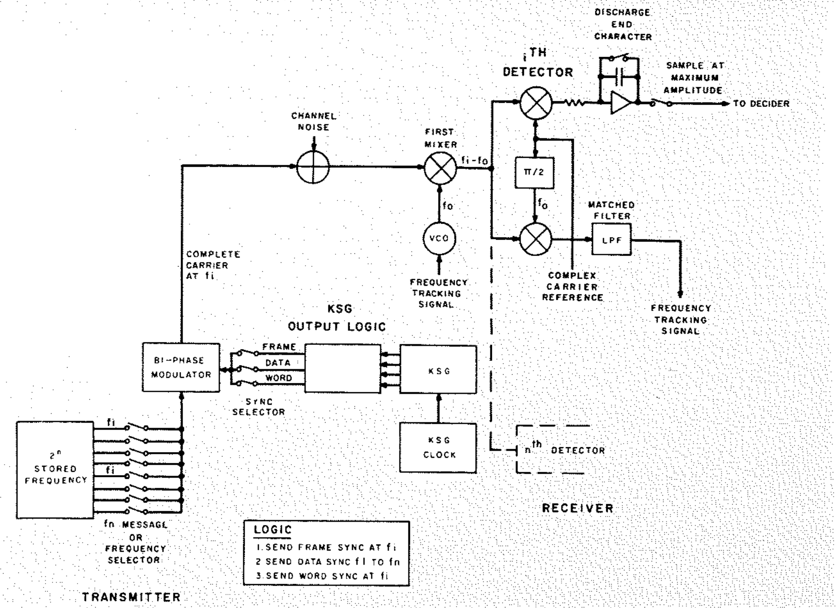

Fig. 11—Pseudo-noise signal transmission system.

Fig. 10—Mean time to unlock vs. phase jitter.

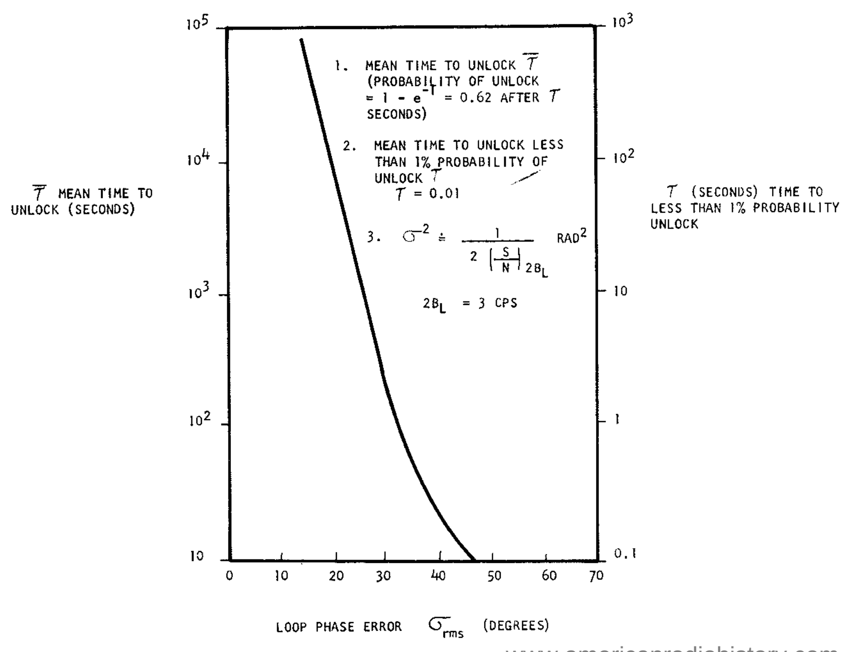

This may be accomplished by using maximal length or PN codes. The PN code will angle modulate the carrier at f_i. The resulting signal is a complex carrier. The received signal is the transmitted signal plus additive thermal noise. The phase of this received signal is compared with similar reference signals in the correlation detector. When the reference signals and the received signals are in phase the *SNR* at the output of the correlation detector will be high. At this point timing synchronization is obtained. Tracking circuits will then keep the received and reference signals in synchronization. In the synchronization process, the reference signal slides past the received signal at about one PN bit per integration time. This integration time should be sufficient to make a decision for some required error probability. The approximate keying rate of the timing generator in the LANDER may be obtained from the conditions (such as temperature, voltage, etc.) existing in the LANDER before ejection from the spacecraft and during the descent mode.

A tracking technique known as early-late tracking is recommended. This technique has the advantage of requiring negligible power from the signal but has the disadvantage that twice as many detectors are required. Since the received power is very marginal there appears to be no other choice. Fortunately, the complexity in the LANDER for this type of sync system is relatively small.

A tracking-loop diagram is shown in Fig. 12. The received signal is correlated against complex local oscillator signals which are early and late in time with respect to the desired position. These signals are obtained by tapping from the outputs of appropriate stages of an n-stage feedback shift register and then feeding them back to the input through a module-2 adder. This produces a linear minimal-length sequence at the shift register whose length is $(2^n - 1)$ digits and whose duration is $(2^n - 1)\Delta$ seconds where Δ is the keying interval. The same sequence appears at each of the taps but it is advanced in time by Δ for each tap further from the output. The late sequence is taken from tap N while the early sequence is obtained from tap $(N - 2)$. At synchronism, the sequence will come from the $(N - 1)$ tap. These PN binary waveforms will then phase modulate a carrier resulting in a complex reference signal. Cross-correlations are then performed between the input waveform and the two local reference waveforms which are separated by 2Δ.

Figs. 13a and 13b show the signal characteristics at the output of the integrators as a function of the delay time Δ. These are the cross-correlation functions for rectangular PN waveforms. The tracking error signal is derived directly as the early correlator output minus the late correlator output. Fig. 13c shows this error signal as a function of the keying element Δ. This error signal, which has a shape similar to a discriminator transfer function, hence the name *tracking discriminator*, has a total duration of four keying periods and the null point of the error signal is midway between the two correlations.

As seen from the synchronization tracking loop, it is possible to maintain synchronization (i.e. keep the relative position of the received and local PN waveforms constant) by a non-ambiguous tracking error signal. This signal is driven to zero when the local and received complex signals are synchronized. The response time of this tracking loop must be adequate to tracking any transmission path changes. The performance of this type of tracking loop has been confirmed in the laboratory. Implementation is within the state of the art.

CONCLUSIONS

A study was made of the direct link between the LANDER on the surface of Mars and Earth for the telemetry link. The results of this study are:

System Constraints

Total transmitter power	20 W
Transmitter antenna gain	0 dB
Transmitter frequency	2300 MHz
Range	2×10^8 km
Total system margin	9 dB
Receiving antenna gain	61 dB
Receiver effective noise temperature	35°K
Received signal power to noise power spectral density	10.8 dB

Proposed System

1) *Modulation and Detection:* A comparison of the 5-bit binary and *32*-ary coherent FSK systems for a word error probability of 10^{-3} is the following:

System	Data Rate bits/hour
binary noncoherent	90
32-ary noncoherent	360
32-ary coherent	12,000

The above data shows that the coherent *32*-ary FSK system has a 15-dB increase in data rate over the noncoherent *32*-ary wideband FSK system. In addition, the required frequency stability for the noncoherent system is 4 parts in 10^8, which at the present time is extremely difficult to obtain in the LANDER.

2) *Frequency and Time Acquisition Logic:* Signal is transmitted at frequency f_1 and receiver sweeps through uncertainty until acquisition. Transmitted signal at frequency f_1 is phase-modulated with a 63-bit pseudo noise code for frame synchronization. The signal frequency is continuously tracked after frequency acquisition. After frame synchronization is accomplished, the receiver continuously tracks both the frequency and time variations. Time tracking is accomplished by an early-late type tracker.

The data is now transmitted with a choice of one of 32 frequencies. A 15-bit PN code which phase modulates the signal is used for data synchronization. Since the 32 frequencies are related to each other, frequency tracking is realized by sensing the frequency variation of any one of the transmitted signals. A 31-bit PN coded signal which phase-modulates the transmitted signal is used for word synchronization. This signal is transmitted at a frequency f_1.

3) *Frequency Acquisition and Probability of Unlock:* A trade-off of a bank of n-phase lock loops vs. the frequency stability for an acquisition time of ten minutes with a 90% probability of success and a $(SNR)_L$ of 6 dB into a PLL bandwidth of 3 Hz are:

n	Stability 1 part in	Input bandwidth Hz PLL
1	6×10^8	277
17	10^6	4,600

For the resultant 20° phase jitter, the time to unlock for less than 1% probability is 90 seconds.

4) *Time Acquisition for Keying Rate of 10 bits/second:*

	Period bits	T_A (seconds)
Frame	63	85
Data	15	0.11
Word	31	0.12

Most of the basic techniques for realizing the proposed system have been experimentally verified.

BIBLIOGRAPHY

1. A. B. Glenn, "Analysis of Non-coherent FSK Systems with Large Ratios of Frequency Uncertainties to Information Rates," *RCA Review*, June 1966.
2. A. J. Viterbi, *On Coded Phase Coherent Communications*, JPL Report 32-25, August 1960.
3. W. L. Lindsey, "Coded Non-coherent Communications," *IEEE Trans. Space Electronics and Telemetry*, March 1965.
4. J. C. Springett, *Telemetry and Command Techniques for Planetary Spacecraft*, JPL Report 32-495, January 1965.
5. R. W. Sanneman and J. R. Rowbotham, "Unlock Characteristics of the Optimum Type Z Phase-Locked Loop," *IRE Trans. Aerospace and Navigational Electronics*, March 1964.

Fig. 12—Time tracking and data.

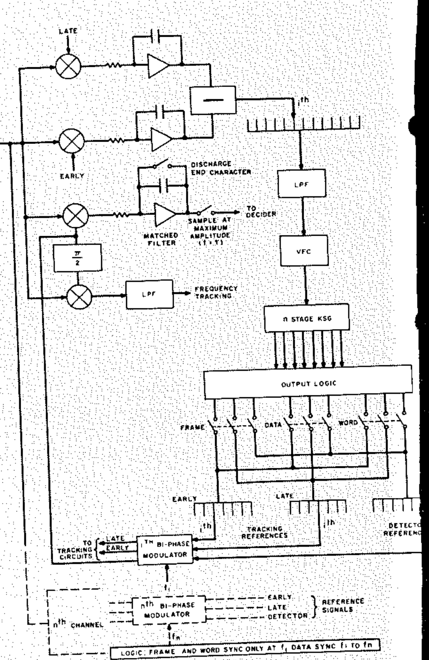

Fig. 13—Tracking loop correlation characteristics

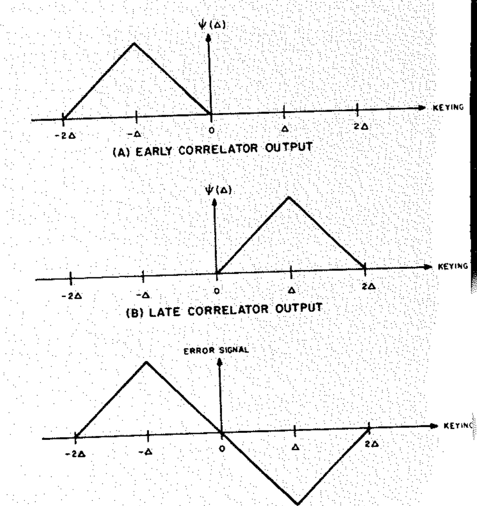

HYDRAULIC TEST SYSTEM

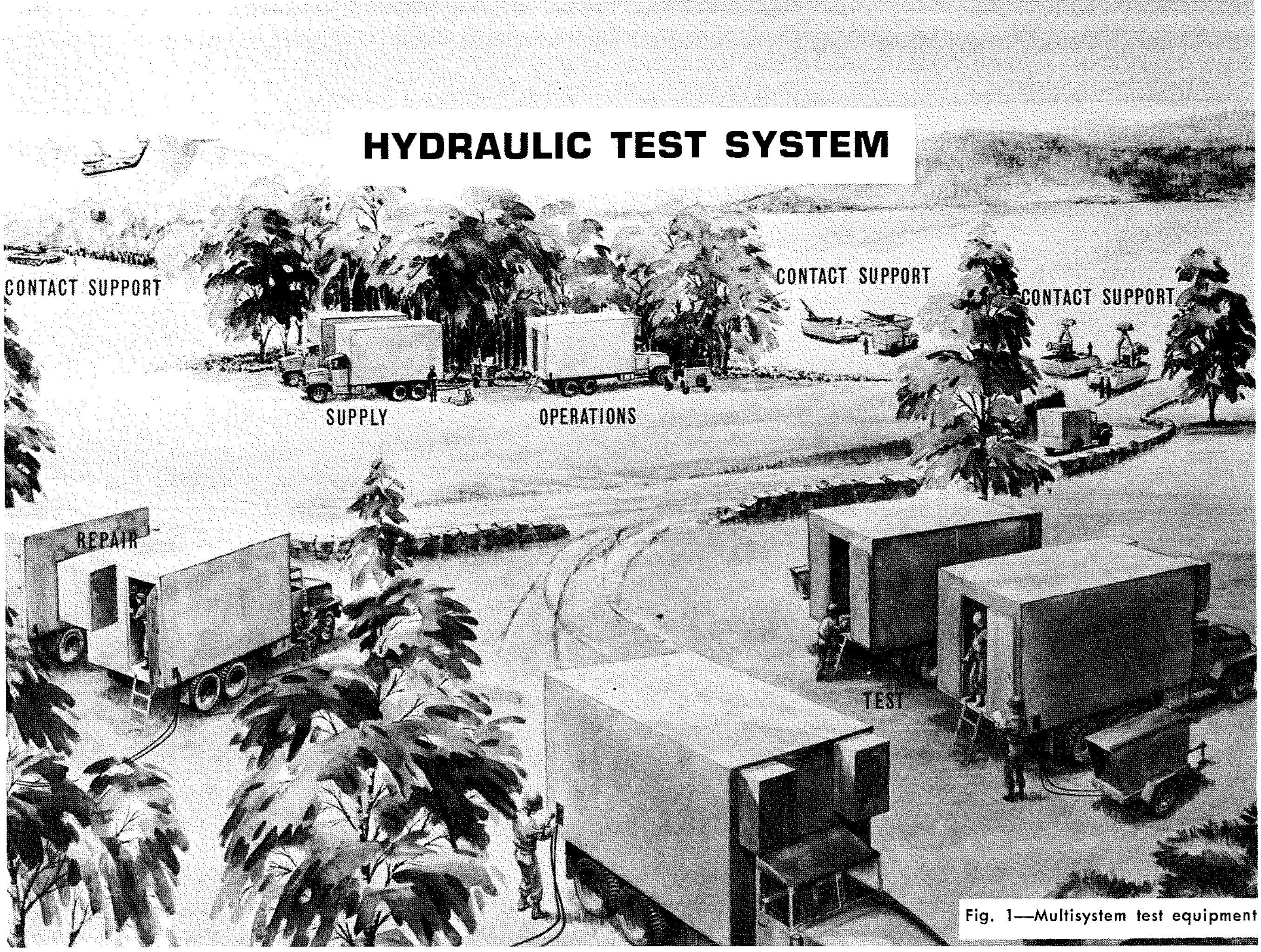

Fig. 1—Multisystem test equipment

J. H. GROFF
Systems Support Program
Management Office
Aerospace Systems Division
Burlington, Mass.

Since the mid-1950's, RCA has been developing a series of test equipments based on a broad standardization approach encompassing system and test techniques down to component selection. These are predominately electronic test systems, which include the Electronic Test Systems 1 and 2 (ETS-1 and ETS-2) which test dc and microwave electronics, respectively, of ground-to-air missile systems; the Electronic Test System 3 (ETS-3) testing smaller, tactical ground-to-ground missile system electronics; and DIMATE series of systems, testing military communications units. Unique among these systems, as well as among mobile hydraulic test equipment, is the Hydraulic Test System (HTS). The HTS couples the advanced electronic control systems available with a compactly designed, servo-controlled hydraulic test stand to provide automatic, field mobile testing of hydraulic and electro-hydraulic systems and components. The operational and system level function of the support equipment is described, as well as a schematic description of the hydraulic test stand.

J. HERBERT GROFF is a graduate of the Pennsylvania State University having received his BSME in 1951. He has attended Drexel Institute of Technology in the Graduate Physics Program and is presently attending Northeastern University in the Graduate Engineering Management Program. From 1951 to 1955, Mr. Groff was employed by Lockheed Aircraft Corporation as a design engineer. He contributed to the design of the YC-130 Hercules transport and the XF-104 and F-104 fighter aircraft. This included all phases of aircraft structure analysis and design, particularly as applied to exits, mechanisms, cockpit and landing gears. In 1955, Mr. Groff worked for the Vertol Corporation on the redesign of the cockpit console of the H-16 helicopter to reduce excessive vibration. He has been associated with RCA since 1955, with design responsibility on the MA-10 airborne radar system, and preliminary design effort on the F-108 radar system, the Dyna Soar packaging concepts, and Dyna Soar microwave design. Later assignments included design responsibilities on the Television Feasibility Demonstration System launched from a Redstone rocket, the Integrated Submarine study and associated Under Sea Warfare studies. For the past four years, Mr. Groff has been responsible for the design and management of various aspects of Ground Support Equipment. He is presently responsible for the Service Test Model Phase of the Land Combat Support System within the Automatic Test Equipment Program Management Office. Mr. Groff is a member of IEEE.

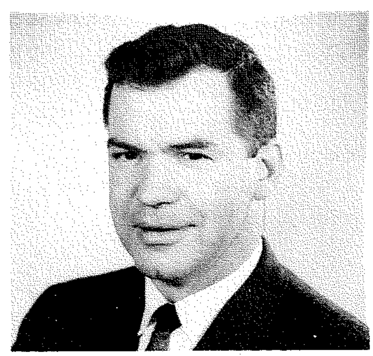

THE Hydraulic Test System (HTS) is one of a family of test facilities providing fully mobile field level support for Army missile systems (Fig. 1). Inherent in the HTS design is the capability to test a major portion of missile hydraulic components in present usage, as well as those in development. This was due largely to the design parameters established by the initial technical requirements analysis. This analysis took into account not only the prime weapon system requirements (in this case, MAULER), but also the requirements of large missile hydraulic systems (PERSHING, for example) and anticipated state-of-the-art future requirements such as higher temperature fluids and more complex servo systems. The result was the hydraulic-pneumatic capability listed on Table I. It is capable of testing the following types of units:

1) linear actuators
2) rotary actuators
3) servo valves (and systems)
4) hydraulic pumps (and systems)
5) hydraulic motors
6) relief valves
7) flow regulators
8) accumulators
9) solenoid valves
10) pressure transducers
11) manual selector valves
12) pressure regulators
13) pneumatic hot gas servos
14) hydraulic subsystems
15) full weapon system tests (when slaved to electronics controlled testing units ETS-1)
16) check valves

The HTS can be utilized to perform field and depot level maintenance on components and is limited only by input power. However, higher power pumps and motors may still be tested, first at maximum pressure and then at maximum flow. The HTS (as shown in Fig. 2) provides:

1) capability for test and repair of hydraulic and pneumatic components of missile and similar weapon systems;
2) capability for either internal or external testing;
3) remote control by other units, when computer capability is required;
4) limited pneumatic capability (as described in Table I);
5) assembly and spares interchangeability with other Army test equipments;
6) self-contained repair station.

Faulty or suspected faulty hydraulic assemblies are received by the HTS. The operator is directed by appropriate test procedures to select specific cables, tools, and test tapes. He is then given instructions to partially disassemble the unit before testing (if required) and given hook-up instructions. If the unit lends itself to the automatic testing operation, this mode will be preferred because of three important advantages:

1) No human error is introduced in reading or interpreting test results.
2) A higher degree of operator safety is realized.
3) Free time is available for the operator to set up work on the next unit.

Operator participation is required to the extent of making test unit adjustment and alignment or, in some instances, rearrangement of hydraulic stimulus and measurement points at the test unit.

Repair is not normally carried out at the test positions; instead, a repair position is provided in the shelter. The actual repair is performed manually, but the repair procedures may be presented to the operator semi-automatically. The instructions for repair are printed out at the test position when a faulty part has been isolated. The instructions contain information such that pictures and schematics can be quickly addressed and displayed on a viewer. By these means, the quantity of manuals and other data required in the HTS is kept to a minimum, even when many missile systems are assigned to a test group.

Due to the close similarity between the HTS control system and the ETS-1 and ETS-2, operator training is greatly simplified. Other cost advantages exist, due to the commonality built into the test equipment family. These include a standardized: 1) shelter configuration, 2) rack and chassis size, 3) power source, 4) air-conditioning, 5) operator control console (with the exception of the status monitor panel), 6) controller subsystem, 7) stimulus subsystem (with an added servo stimulus drawer), 8) measurement subsystem, 9) as well as numerous lesser level hardware items. Fig. 3 schematically depicts the HTS. Fortunately for the HTS development costs, the basic electronics system of ETS-1 and ETS-2 was directly applicable to the HTS. The gross system design characteristics of the HTS are demonstrated if a hydraulic test stand is connected to the *stimulus-measurement input-output* points of an ETS-1. The HTS was system analyzed with the basic requirement of making maximum use of existing missile test equipment hardware, thus applying the principles of standardization to the system level. This resulted in a configuration composed of all "standard" items, plus a hydraulic test stand, and peculiar wiring installation hardware and test fixtures.

TEST SYSTEM FUNCTION

Briefly, the system function is as follows. Following hook-up of the test unit, the heart of the system—the *controller*—provides the sequencing, selection, and routing of stimulus and measurement to the selected test unit. In a test system capable of automatic, semiautomatic, or

Final manuscript received September 1, 1966

Fig. 2—Hydraulic test system

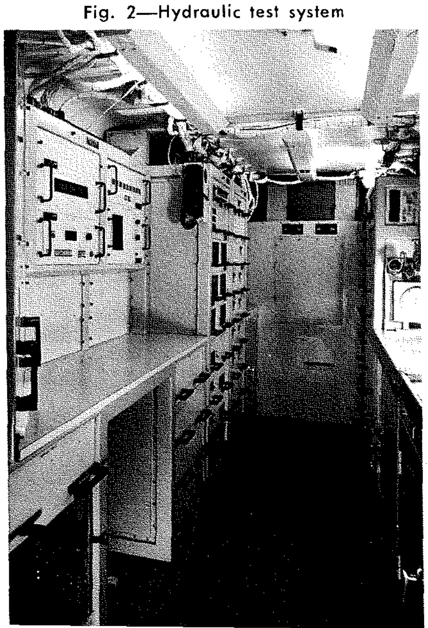

Fig. 3—Hydraulic-pneumatic—functional block diagram

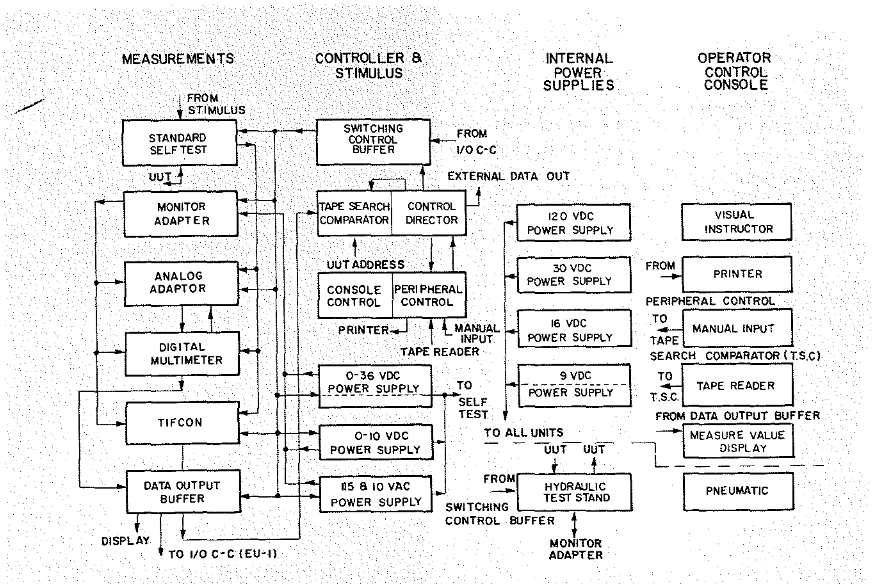

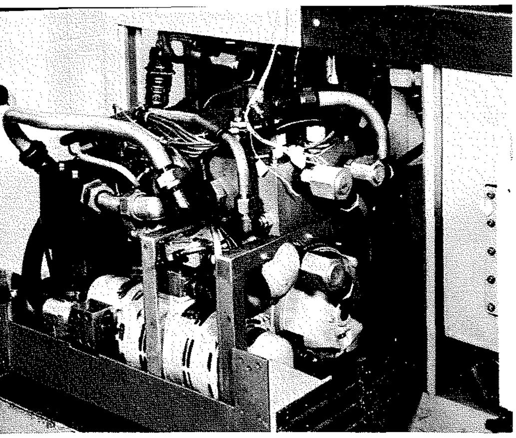

Fig. 6—Hydraulic test stand - power supply module

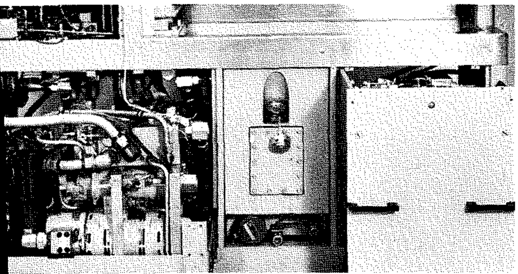

Fig. 5—Hydraulic test stand—power supply (left) and pneumatic modules (right)

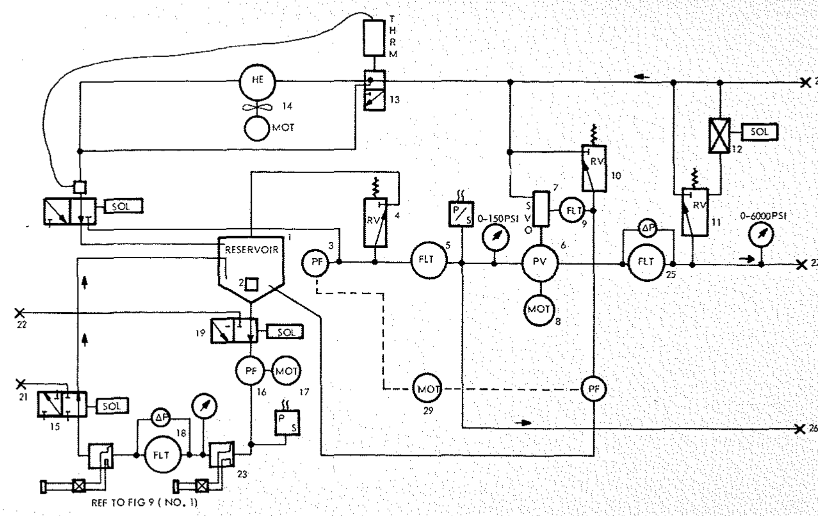

ITEM NO	NO REQD	NOMENCLATURE	ITEM NO	NO REQD	NOMENCLATURE	ITEM NO	NO REQD	NOMENCLATURE
29	1	MOTOR & ELECTRIC	20	1	CHECK VALVE	9	1	FILTER
28	1	PORT 3/4'' QUICK DISCON RETURN	19	1	VALVE-SOLENOID 1 POSITION-3 WAY	8	1	MOTOR-ELECTRIC
27	1	PORT 1/2'' QUICK DISCON HIGH PRESS	18	1	FILTER-LOW PRESS 10 MICRON	7	1	PUMP-SERVO
26	1	PORT QUICK DISCONNECT 1/4 STATIC	17	1	MOTOR ELECTRIC INTEGRAL WITH 16	6	1	PUMP-VARIABLE DISPLACEMENT
25A	1	DIFFERENTIAL PRESS SWITCH	16	1	DUMP FIXED DISPLACEMENT	5	1	FILTER
25	1	FILTER HP	15	1	VALVE 2 POSITION-3WAY-SOLENOID	4	1	RELIEF VALVE
24A	1	THERMO SWITCH	14	1	HEAT EXCHANGER UNIT	3	1	PUMP-FIXED DISPLACEMENT
24	1	HEATER (RESERVOIR)	13	1	THERMAL MIXING VALVE	2	2	STRAINER-SUBMERG TYPE
23	1	VALVE-RESERVOIR DRAIN	12	1	VALVE SOLENOID	1	1	RESERVOIR 20 GAL CAP ALUM.
22	1	PORT (RETURN)	11	1	RELIEF VALVE			
21	1	PORT	10	1	RELIEF VALVE			

Fig. 7—Hydraulic schematic—power supply module

manual operation, the controller receives inputs from a tape reader, or manual keyboard, and directs appropriate stimulus or measurement events to occur. It also directs the operation of the readout devices. These instructions may be commands which:

1) select and set up particular stimuli,
2) select desired measurement test points,
3) order measurements to be performed,
4) perform comparisons of measurements results to limit values, or
5) order a change to a new series of tests.

In addition, the instructions may contain time delay or print commands, or they may select a particular measurement range and function. At all times, the control director, along with the instructions, controls the flow of data to and from the various units of the system. The *electronic stimulus subsystem* receives selection and ranging information from the controller and provides DC and AC voltages to the unit under test (UUT) through the "monitor adapters," as well as a DC reference voltage to the *hydraulic test stand.* Each of the stimuli have program control which allow either side to be grounded. Each stimulus is also protected against overload, and possesses remote sensing of load variations, thereby insuring voltage accuracies at the load well within regulation limits. The hydraulic stimulus parameters are also set electronically to the required value by the controller. Set values are maintained by internal servo systems which also provide self-check information to the controller.

Fig. 4—Hydraulic test set - test stand

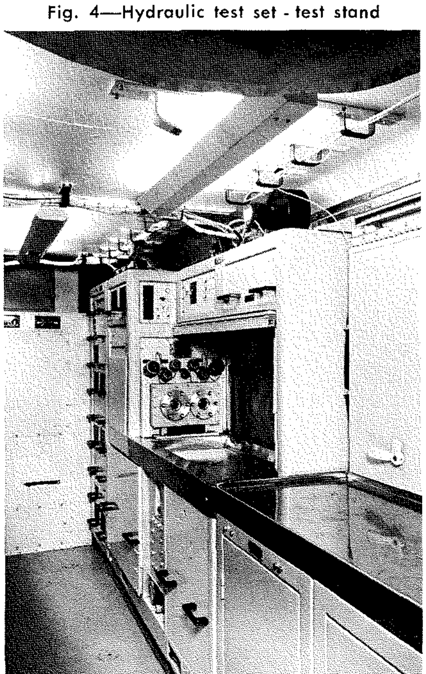

Transducers, provided in ranges to assure the greatest accuracy, are included as feedback elements of the servo systems. They provide confirmation signals to the controller and measure the qualifications of a UUT in a defined test. All pertinent *hydraulic-pneumatic test stand* functions provide malfunction indications to the controller. These indicate any conditions that might contribute to operator safety, potential damage to the stand or UUT, or the need for maintenance. The function of the *measurement subsystem* is to select the proper monitoring point on the UUT, route the selected incoming signal to the proper measurement device, scale the incoming signal to the proper value, and convert the scaled signal to a digital value for transmission to the controller for processing and display.

After testing has been accomplished, the UUT will be turned over to the repair station for repair, or replaced on the spot and reverified. If the UUT is complicated or composed of numerous components, the faulty component is isolated and either turned over to the repair station for repair or replacement, or the UUT may be alloted to the *repair support set.* Whenever allocations of UUT repairs are made to the *repair support set,* appropriate instructions will accompany the work. After repairs are effected, operation will be reverified in the hydraulic test set.

TEST STAND PHYSICAL CONFIGURATION

The hydraulic-pneumatic test stand contains the major functional element peculiar to this system. Some of its unique features include: 1) compactness, 2) functional modularization, 3) solid block manifolding, and 4) environmental in-

TABLE I—Hydraulic-Pneumatic Stimulus

pressure range	250 to 5,000 lbf/in²
flow range	2 to 20 gal/min (to 3000 lbf/in²)
	2 to 11.5 gal/min (to 5000 lbf/in²)
leakage detection	1 to 500 cm³/min
hydraulic fluid temperature	160°F maximum (Provisions for 250° operation)
mechanical drive	30 hp delivered to shaft
low speed shaft	100-4000 rev/min
speed increaser	200-8000 rev/min
high speed shaft	150-6000 rev/min
speed increaser	300-1200 rev/min
torque measurement	Up to 1000 in•lbf
filtration	
Super Clean Loop	3 μm nominal
Operating Loop	5 μm nominal
pneumatic	1500 lbf/in² air, 19 ft³/min, for 15 minutes (5000 lbf/in² source)

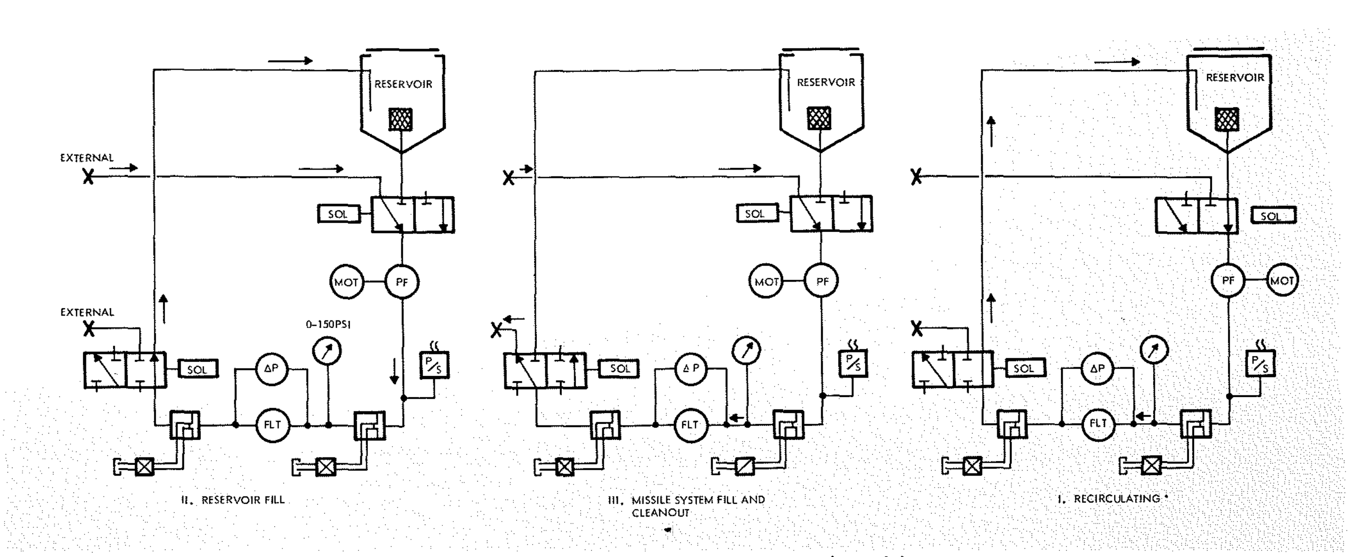

Fig. 8—Fill and filtering section—power supply module

ITEM NO	NO REQD	NOMENCLATURE
45	1	PORT (RETURN)
44	1	PORT (RETURN)
43	1	PORT, HIGH PRESSURE
42	1	PORT, HIGH PRESSURE
41	1	PORT BOOST PRESSURE
40	1	VALVE CHECK
39	1	VALVE CHECK
38	1	VALVE - SOLENOID
37	1	VALVE, 2 POS, 2 WAY SOLENOID
36	1	VALVE, 2 POS, 2 WAY SOLENOID
35	1	PRESSURE TRANSDUCER
34	1	TEMPERATURE TRANSDUCER
33	1	RELIEF VALVE
32	1	PORT (RETURN)
31	1	PORT
30	1	PORT

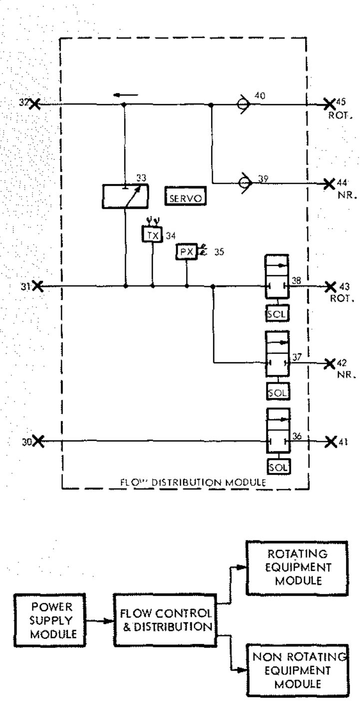

Fig. 9—Hydraulic schematic–flow distribution module

tegrity. The test stand envelope is 66 inches high x 22 inches deep x 72 inches long. This does not include the hydraulic heat exchanger or pneumatic compressor which are located on the wall behind the repair bench such that they can be swung out during operations to reduce interior acoustical noise and swung inside and locked in place for the transportation environment. The overall envelope does include one full and two half-depth electronic drawers, in addition to an area 32 inches high x 22 inches deep x 24 inches long containing the pneumatic controls and reservoir. Therefore, the actual hydraulic system occupies a space (of approximately 1½ standard racks) 66 inches high x 22 inches deep x 24 inches long, including a 20-gallon hydraulic reservoir. When compared with the stimulus provided (Table I), the compactness is clearly evident. The right hand side of Fig. 4 shows the test stand in its shelter installed position.

TEST STAND MODULARIZATION

Because of the desired flexibility necessary in the test equipment, where weapon system changes or expanded testing may require rapid test equipment modifications, the test stand, like the electronic equipment, is fully modularized. The modules include the: 1) *power supply module;* 2) *flow distribution module;* 3) *rotating equipment module;* 4) *static test module;* 5) *pneumatic module;* 6) *structure assembly;* 7) *electrical power distribution assembly;* 8) *hydraulic-pneumatic control assembly,* and 9) *hydraulic stand control assembly.* Items 1, 5, 8, and 9 are slide-out drawer mounted. Fig. 5 shows the power supply module (developmental model) with the front panel removed, the centrally located hydraulic reservoir, and the slide-out pneumatic module. The hydraulic modules make extensive use of solid-block manifolding to greatly reduce component

Fig. 10—Hydraulic schematic–nonrotating equipment test module

ITEM NO	NO REQD	NOMENCLATURE
66	1	PORT STATIC
65	1	PORT
64	1	PORT (RETURN)
63	1	PORT (RETURN)
62	1	PORT HIGH PRESSURE
61	1	PORT - STATIC SYSTEM
60	1	PRESSURE TRANSDUCER
59	1	VALVE CHECK
58	1	PRESSURE TRANSDUCER
57	1	PRESSURE TRANSDUCER
56	1	VALVE, 2 POS., 4 WAY-SOLENOID
55A	1	VALVE FLOW CONTROL
55	1	INTENSIFIER, HYDRAULIC
54	1	VALVE - SOLENOID
53	1	VALVE, THROTTLING-SERVO
52	1	LEAKAGE TRANSDUCER
51	1	VALVE, BLEED - SOLENOID
50	1	FLOW TRANSDUCER
49	1	VALVE, SHUTOFF - SOLENOID
48	1	FLOW TRANSDUCER
47	1	PORT (RETURN)
46	1	PORT HIGH PRESSURE

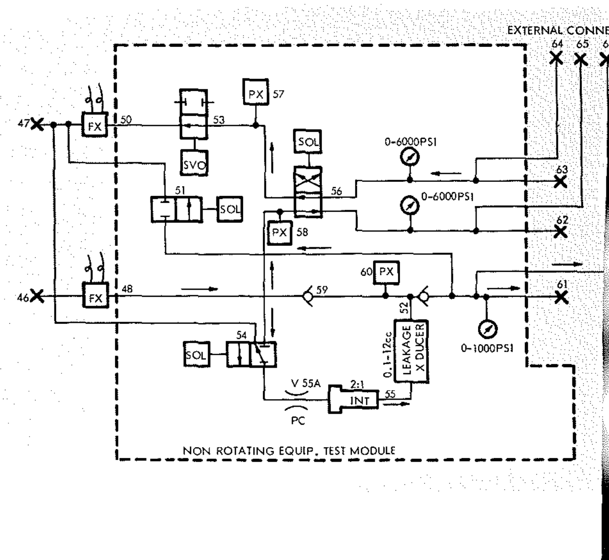

interconnections and tubing. Servo units, valves, etc., with their outer housing removed are screwed directly into a solid aluminum block bored to duplicate their original enclosure. These units are interconnected by bored holes functionally located with the "block."

Thus, a highly rugged subassembly is developed with all possible components operating at a common pressure manifolded within a solid block. The block minimizes leakage and results in a considerably more compact and maintainable system. Fig. 6 shows a close up of the power supply module and its block manifold prior to final wiring assembly. The power supply module consists of a reservoir (20-gallon capacity), a complete filtration circuit, main pump and its auxiliary boost, and servo pumps and manifolded control elements. Fig. 7 shows the details of this module. The filtration system was designed to handle contaminants from a number of sources: 1) test stand generated, 2) debris due to new parts, 3) new fluid contaminants, 4) maintenance contaminants, 5) UUT contaminants, 6) UUT system level cleanout requirements. Fig. 8 shows several filtration loops. The output of the hydraulic power supply is directed, as required, to a rotating equipment module or a static test module. This is accomplished via a manifolded group of hydraulic valves called the flow distribution module (Fig. 9). The static test module is used for all nonrotating UUT's and contains the means of controlling fluid flow and direction, and oil pressure as required by the UUT's. The external connections from the shelter are connected to the static test module in such a fashion that all functions performed by this module may be duplicated outside the shelter. Fig. 10 gives the details of this portion of the test stand. The rotating-equipment test module is essentially a variable speed hydrostatic transmission. A choice of speed increaser driving pads (Table I) was established by the speed and torque requirements of various missile system rotational components. The drive system is designed to transmit a maximum of 60 hp, although in actual practice the power available for the test stand has been limited to 30 hp because of the electrical power source and size limitations. Fig. 11 conservatively depicts the available horsepower and torque.

The pneumatic test module provides the necessary air pressure and flow rates to test the various types of pneumatic components and subsystems found in applicable missile systems. Air supplied to the various UUT's is conditioned to a dew point of −65°F and is filtered to insure that 95% of contaminants do not exceed five microns. Such components as pneumatic servo systems, gas servo valves, flow regulators, relief valves, transducers, gauges, actuators and similar devices can be tested with the facility supplied. Fig. 12 depicts schematically the pneumatic module. The equipment is designed to meet the requirements listed in MIS-5710.

TRUCK-MOUNTED CONFIGURATION

The truck-mounted configuration (Fig. 13) shows the right wall of the HTS containing the hydraulic test stand, repair bench with hydraulic cooler and pneumatic compressor shown in the transport configuration. The measurement rack is also located on this side. The other truck shows the opposite side wall of an ETS-1 which approximately depicts what is found in an HTS: a *control console*, *control and stimulus rack*, *power supply rack*, and *power distribution and storage area*, in that order.

Fig. 11—Available horsepower and torque characteristics

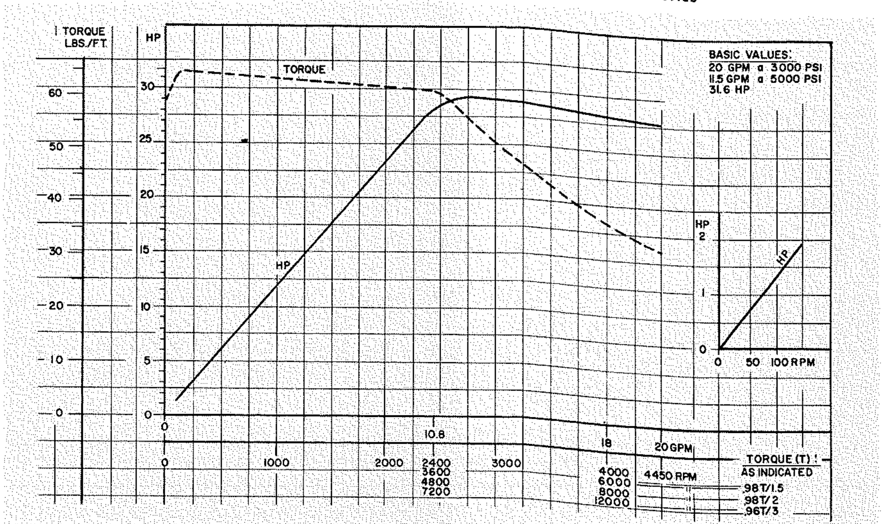

Fig. 12—Hydraulic test stand–pneumatic schematic

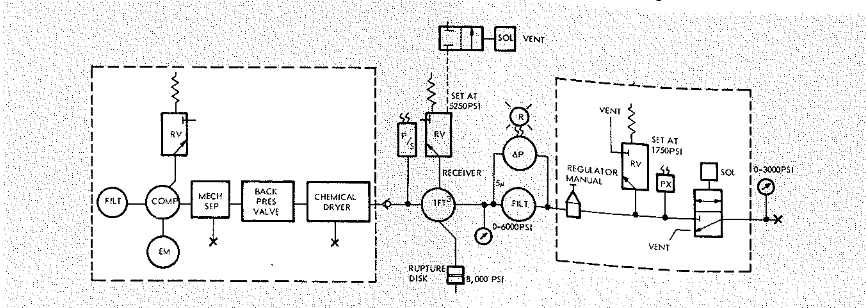

Fig. 13—Hydraulic test system–truck-mounted configuration

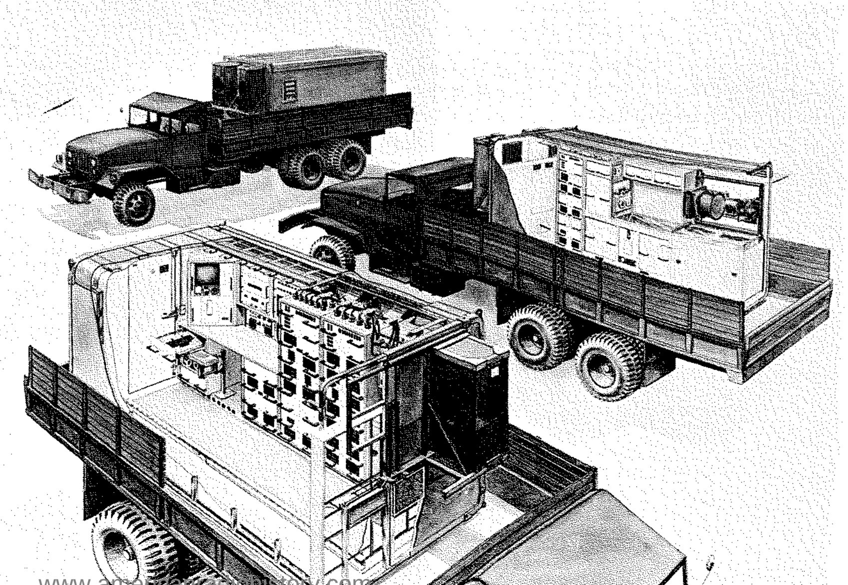

ALL-SOLID-STATE TRANSMITTERS FOR MOBILE TWO-WAY RADIOS USE OVERLAY POWER TRANSISTORS

The recent developments in RF power transistors using the overlay technique have resulted in all-solid-state transmitter designs for mobile two-way commercial radio service in the 25-to-50, 148-to-174, and 450-MHz bands. The rugged transistor construction and improved reliability provide more consistent performance in critical applications. The resultant long-term savings in maintenance costs more than offset the increase in present initial costs over equivalent hybrid equipments. Reliability is further improved by replacing magnetic relays by solid-state circuits, except in the 450-MHz transmitter where a long-life coaxial antenna relay is used.

N. G. RICHARDS and F. A. BARTON
Communications Products Engineering
Broadcast and Communications Products Division
Meadow Lands, Pa.

Fig. 1—A typical mobile transmitter package and accessories.

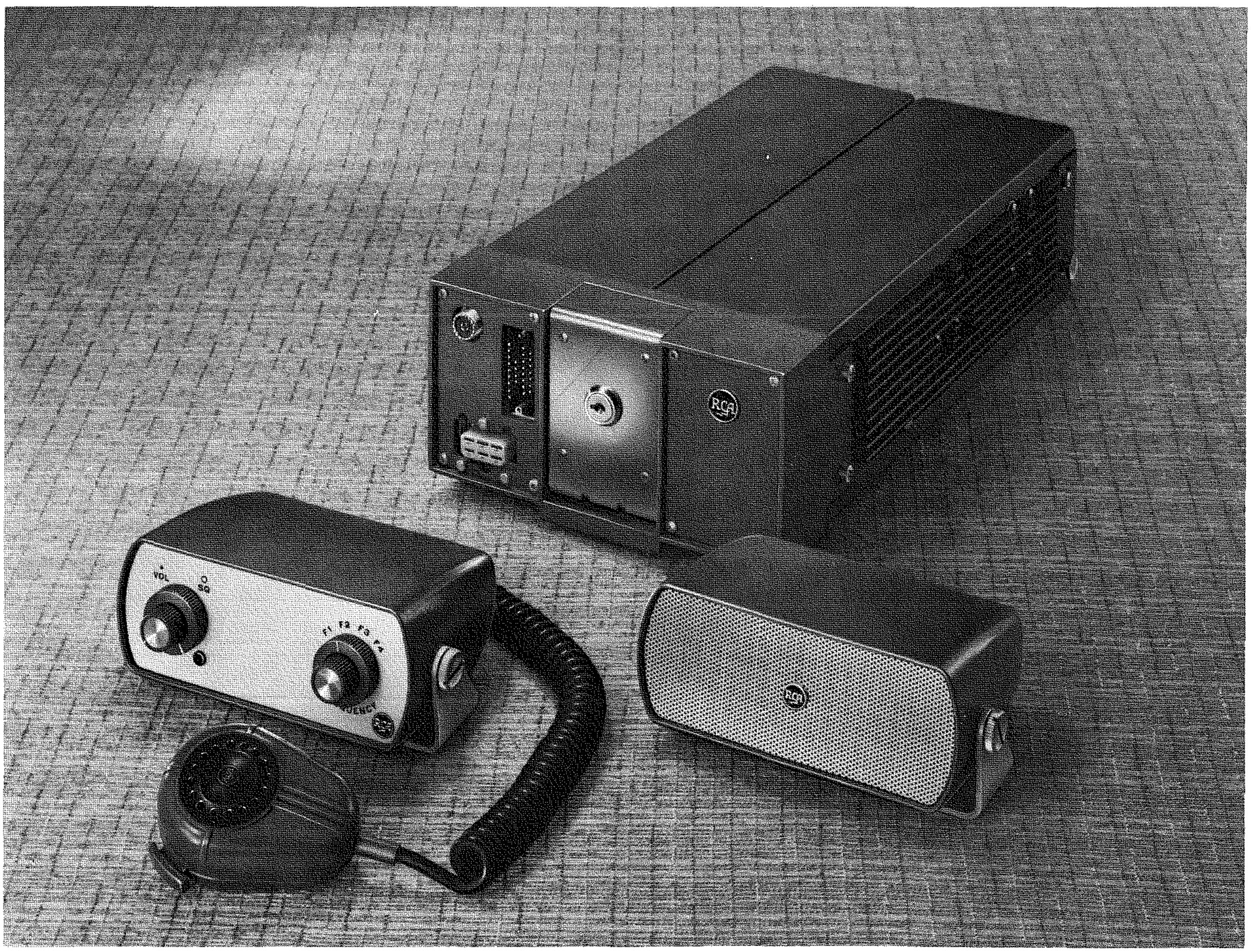

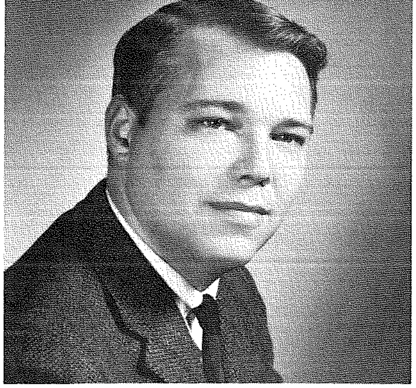

NICHOLAS G. RICHARDS received his BSEE from the Pennsylvania State University in 1958. He joined the Broadcast and Communications Division of RCA in January 1961, after serving 2 years as an officer in the United States Army. Since joining RCA, he has been engaged in the design of solid state transmitters for the Super Fleetfone Line of Mobile Communications Systems.

FREDERICK A. BARTON received an HNCEE degree from the Borough Polytechnic, London, England in 1944. He served as a Radar Officer with the Royal Indian Navy from 1945 to 1947. From 1948 until 1955, he was a development engineer in the Communications Department of Redifon Ltd., London. After two years with Central Rediffusion Services as a CATV Systems Engineer in the field, he rejoined Redifon Ltd., as Section Leader in charge of HF Transmitter Design. In 1960, he joined the Mobile Communications Engineering Department of RCA. From 1961 to date he has been an Engineering Leader responsible for Mobile Transmitter design in Meadow Lands, Pa.

To design a high-power transmitter employing solid-state devices exclusively, the problem of "second breakdown" must be overcome to avoid a collector-to-emitter short circuit. The power amplifier stages of transmitters are subject to the voltage and current conditions which cause second-breakdown failure, particularly during the tuneup procedure or when a load fault occurs. Load fault is said to occur if, for example, the antenna is accidentally broken off. To prevent second-breakdown failure, it is necessary that the transistor manufacturer specify interrelated voltage-current limits which define a safe-operating range as a guide to the design engineer. Some of the earlier high-frequency transistors had a very limited safe-operating range which greatly restricted the use of transistors in practical mobile radio equipment.

The development of the overlay transistor has made possible, for the first time, reliable high power at high frequencies for use in the land mobile-radio service. Because of the overlay transistor's rugged design and resistance to second breakdown, elaborate power-supply protective circuits and automatic mismatch sensors are *not* required.

Another major design problem is that of providing adequate cooling for the high-frequency, high-power transistors. The RF power transistors require efficient conduction cooling to maintain junction temperatures within the safe limits specified by the manufacturer. An aluminum diecast chassis, with a large radiating surface area, provides an economic solution to the heat-conduction problem.

Fig. 1 shows a typical mobile transmitter package with accessories. The transmitter and power supply are located in the righthand section and the exciter and receiver in the lefthand section. The front portion (combiner) contains the interconnection wiring, provides a heat sink for the power-supply transistors, and supplies connections to the car bat-

Final manuscript received September 21, 1966

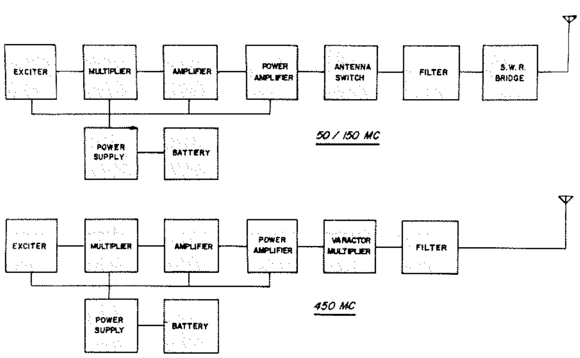

Fig. 2—Solid-state transmitters based on modular arrangements.

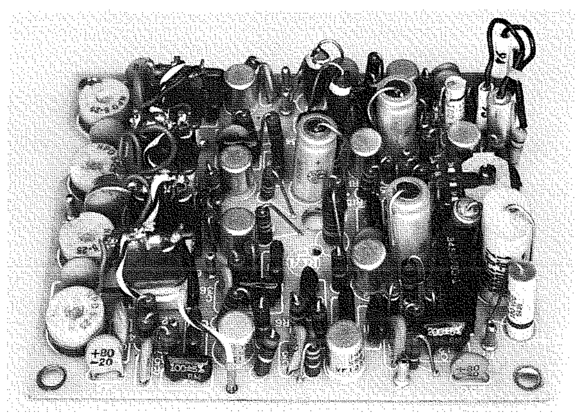

Fig. 4—High-band exciter printed-board assembly.

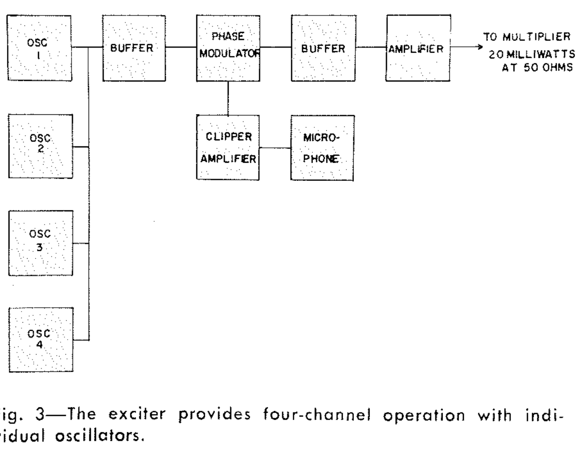

Fig. 3—The exciter provides four-channel operation with individual oscillators.

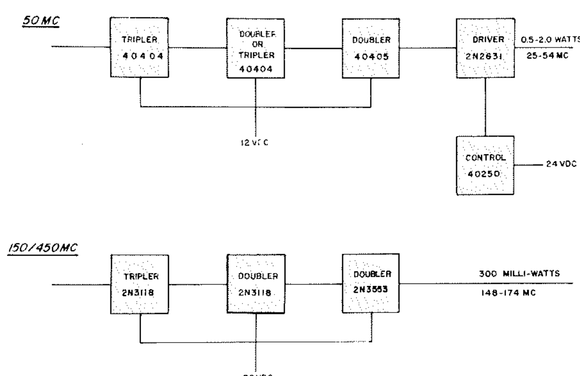

Fig. 5—The 150-MHz and 450MHz multipliers.

tery and to the control equipment and accessories. The transmitter housing is an aluminum casting with fins on one side to provide adequate cooling for the overlay transistors.

For ease of construction, testing and maintenance, each transmitter was designed in a modular form, each with input and output impedances of 50-ohms nominal. The block diagrams of Fig. 2 show a 50-, 150-, and 450-MHz solid-state transmitter based on the modular arrangement.

EXCITER

The exciter (Fig. 3) consists of four individual oscillators for 4-channel operation followed by a buffer, a phase modulator, a second buffer, and an amplifier. The proper audio pre-emphasis, amplification, clipping, filtering, and de-emphasis needed to obtain the desired audio response is provided by a single stage. The high-band exciter printed-board assembly is shown in Fig. 4; crystal frequency trimmers and modulation level control are easily accessible for adjustment. Power output from the exciter is approximately 20 mW into a 50-ohm load. Exciter output frequency is 2 to 3 MHz for the 25-to-50-MHz transmitter and 12.33 to 14.5 MHz for the 148-to-174-MHz and 450-to-470-MHz transmitters.

MULTIPLIER

The multiplier module provides power gain. It multiplies the exciter output frequency to the carrier frequency in the 50- and 150-MHz transmitters, and to one-third of the carrier frequency in the 450-MHz transmitter. The 150- and 450-MHz multipliers have an output of 300 mW (see Fig. 5). The 50-MHz multiplier incorporates an additional amplifier stage and provides a power output of up to 2 watts into a 50-ohm load. A gain control stage is also provided on the 50-MHz multiplier to adjust the drive level at different output frequencies.

The 50- and 150-MHz multipliers are designed as printed-circuit modules (see Fig. 6). Double-tuned, top-capacitance-coupled circuits are used between each stage to obtain the harmonic and subharmonic rejection required. One control on the 50-MHz multiplier adjusts the multiplier power output during normal operation, and the other control adjusts the power output for reduced power operation when the unit is operated continuously under abnormally high temperature or prolonged fault conditions. Switching between modes of operation is accomplished automatically by a thermal switch.

AMPLIFIER STAGES

The driver power-amplifier for the 50- and 150-MHz transmitters is shown in Fig. 7. The 50-MHz driver uses a 2N2876 transistor to provide up to 10-watts drive for three 40341 overlay transistors in parallel in the power amplifier assembly. The 150-MHz driver uses two transistors; the first (a 2N3553) provides a 2.5-watt drive for the second (a 2N3632 overlay transistor), which in turn provides 12 watts to drive the three final amplifier 2N3632 transistors in parallel.

The 50-MHz and 150-MHz power amplifier modules are shown in Fig. 8. The three amplifier transistors are mounted on an aluminum casting which is bolted to the finned wall of the main transmitter casting. Power output at 50 MHz is 60 watts, and at 150 MHz is 40 watts.

A simplified power amplifier schematic is shown in Fig. 9. Series-tuned input and output circuits provide good harmonic rejection and low loss, and facilitate both tuning and loading. Variable series base inductance provides a convenient method of balancing the individual currents. Small value resistors in each emitter provide gain stabilization

Fig. 6—The 50 MHz and 150 MHz multipliers are printed-circuit modules.

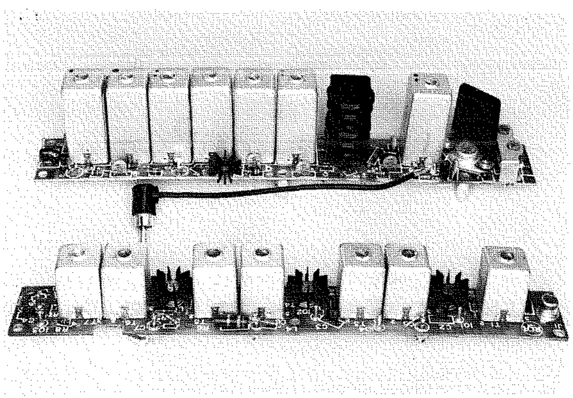

Fig. 8—The 50-MHz and 150-MHz power amplifier modules.

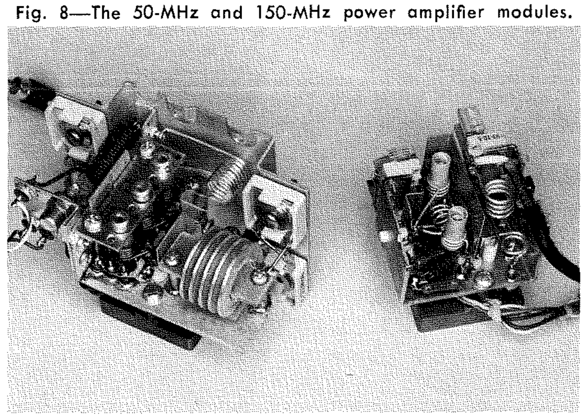

Fig. 7—The driver-power amplfier for the 50- and 150-MHz transmitters.

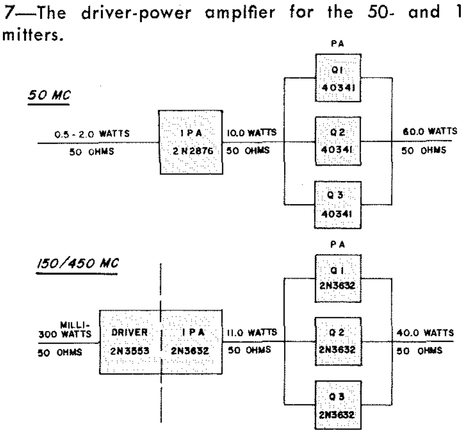

Fig. 9—Power amplifier simplified schematic.

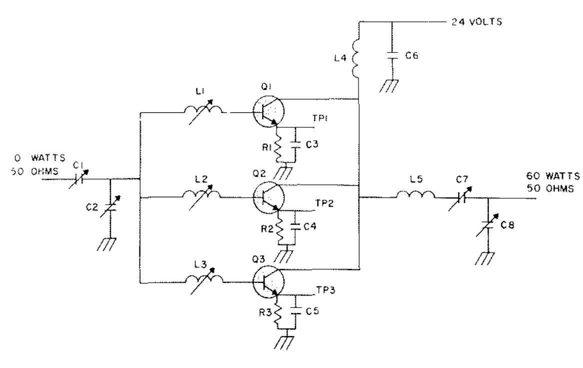

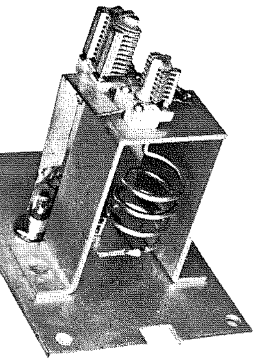

Fig. 10—Varactor multiplier.

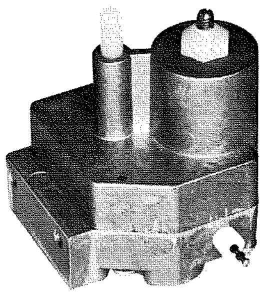

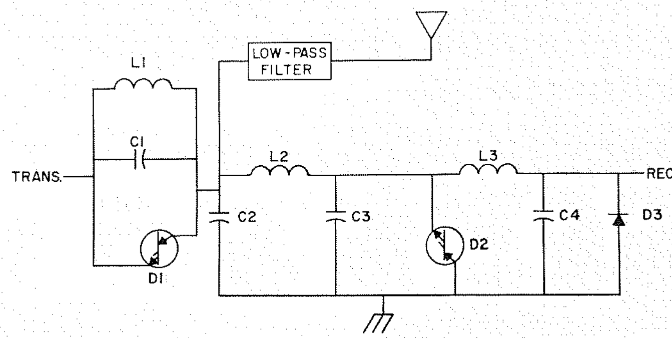

Fig. 11—RF activated antenna switch.

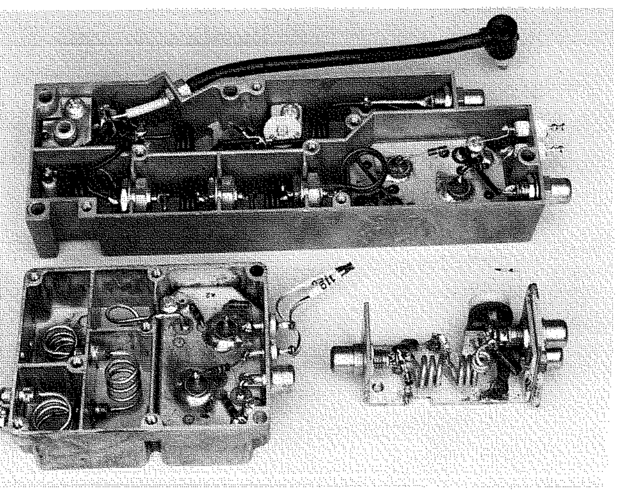

Fig. 12—Antenna switch, filter and reflectometer circuit.

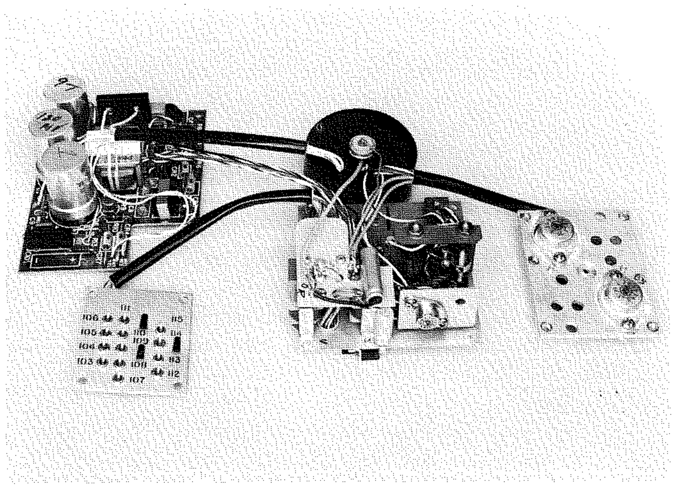

Fig. 13—The 50 MHz transmitter power supply.

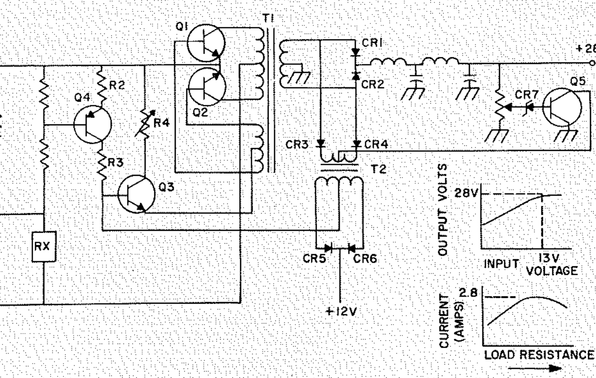

Fig. 14—Conventional square-wave DC-to-DC inverter circuit.

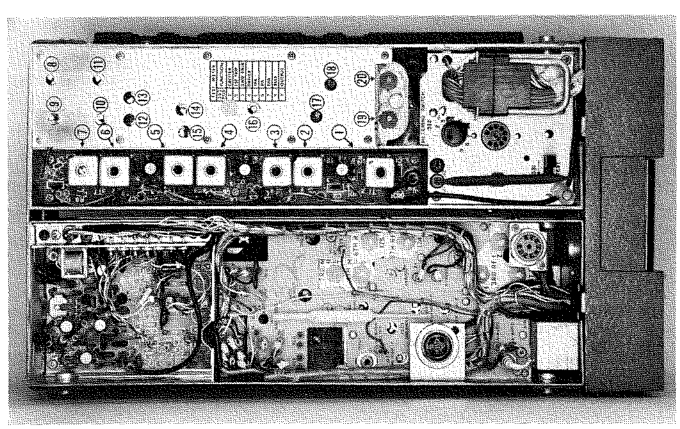

Fig. 15—The 150 MHz mobile unit with all modules in place.

and an accurate way to measure each transistor's current. Broadband ferrite chokes in the base circuit and broadband decoupling in the collector supply circuit prevent low-frequency, spurious oscillation due to the very high transistor gain at low frequencies.

450-MHz VARACTOR STAGE

In the 450-MHz transmitter, power output is obtained by adding a varactor stage to the output of the 150-MHz power-amplifier module; the varactor multiplier (Fig. 10) delivers over 20 watts of output at 450 MHz with a 40-watt drive at 150 MHz.

The lefthand module is the input matching network for the varactor multiplier assembly shown on the right (Fig. 10). A coaxial line filter reduces conducted spurious output frequencies to 80-dB below carrier level.

ANTENNA SWITCH

Recent advances in solid-state technology have made electronic antenna switches practical for 50- and 150-MHz mobile radios; essential elements of the RF-activated antenna switch are shown in Fig. 11. When the transmitter is *off*, energy picked up by the antenna reaches the receiver via filter network L_2, C_2, and C_3. The L_1 and C_1 are in parallel resonance at the receiver frequency to provide isolation from transmitter loading. When the transmitter is activated, the first cycle of RF voltage exceeds the diode breakdown voltage; this causes D_1 to conduct heavily, which in turn shorts out elements L_1 and C_1 and causes diode D_2 to short out C_3. Power is thus transmitted to the antenna, and receiver isolation is accomplished by the voltage divider effect of L_2 and D_2. Diode D_3 is a low-power switching diode that protects the rceiver before D_2 breaks down.

The 50-MHz and 150-MHz antenna switch, filter and reflectometer circuit are shown in Fig. 12. The 50-MHz antenna switch is located in a casting with the transmitter lowpass filter and reflectometer circuit. The lowpass filter and reflectometer circuit for the 150-MHz transmitter are located in a casting separate from the 150-MHz antenna switch.

POWER SUPPLY

The power supply (Fig. 13) delivers 24 volts at 5 amperes for the 50-MHz transmitter, and 28 volts at 3.3 amperes for the 150-MHz transmitter. Overall voltage regulation and current limiting provide adequate circuit protection against damage from high battery voltages or antenna faults should the antenna become disconnected, broken, or shorted.

The network of Q_1, Q_2, and T_1 in Fig. 14 forms a conventional square-wave DC-to-DC inverter circuit. Transistor Q_3 is in series with the base-return circuit of transistors Q_1 and Q_2. During the receive condition, transistor Q_4 is biased to cutoff; hence, transistor Q_3 is also biased to cutoff. During the *transmit* condition, the push-to-talk switch shorts out the receiver DC supply and turns on transistor Q_4 and, in turn, transistor Q_3. The inverter thus operates, and the main DC output is rectified by diodes CR_1 and CR_2. The bias for transistor Q_5 is the difference in voltage developed at the slider of a variable potentiometer and the zener diode CR_7. Transistor Q_5 controls the rectified push-pull current through the primary of transformer T_2. The rectified output voltage produced in the secondary of T_2 provides a controlling bias to transistor Q_3, which in turn controls the base current drive level to the inverter transistors Q_1 and Q_2. This feedback loop provides a regulated voltage output from the inverter. The maximum current delivered by the inverter is limited by the adjustment of R_4 which limits the base drive current to Q_1 and Q_2. Transformer T_2 provides DC isolation in the feedback loop between the grounded DC output circuit and the battery-input connections for operation in either positive or negative grounded vehicles.

METERING AND TUNING

The 150-MHz mobile unit with all modules in place is shown in Fig. 15; all significant tuning controls are accessible from the top surface of the transmitter. Metering of the various test points if provided by a nine-pin test socket for use with an RCA CX35 test meter. Alternatively, any simple 50-microampere meter can be plugged into the two jacks adjacent to the test sockets.

The built-in reflectometer circuit enables antenna length trimming and the measurement of approximate power output without the use of an external wattmeter.

DUTY CYCLE

In tube equipment, mobile transmitters have traditionally been rated only for intermittent duty-cycle operation. This system has provided an economic compromise between cost and life for the tubes. When the rated duty cycle for the tube equipment is exceeded, power output will degrade more rapidly but rarely results in catastrophic failure.

Mobile transmitters using RF power transistors differ in two respects:

1) There is no significant degradation in power output with life when the transistor is operated within rated values at all times.
2) The transistor manufacturer does not offer the transmitter designer the luxury of an ICAS rating. Catastrophic failure is the most likely result of rating abuse. Hence, a sound transmitter design which benefits from the inherent reliability of the transistor must be rated for continuous duty under all predictable environmental conditions, even though the service involved rarely has a need for this duty cycle.

In these transistorized equipments, full power output is maintained at all times unless very high environmental temperatures and/or prolonged antenna fault conditions are experienced. In such extremes, a thermostat will operate to reduce the drive to the driver and final amplifier stages; power output is then reduced approximately 2:1.

LIFE TESTS

Continuous-duty life tests have been in operation on 150-MHz and a 450-MHz transmitters since July 1965; the power output of 34 watts has been maintained without incident on the 150-MHz unit (8,700 hours). The 450-MHz unit had a varactor diode failure after 4,000 hours due to a bonding fault in the diode; however, the test has continued since then without further problems. All production transmitters are subjected to a two-hour continuous life test followed by a worst-case antenna fault condition to ensure reliable field operation.

FIELD PERFORMANCE

The performance characteristics of the three groups of transmitters are summarized in Table I. Successful field experience has been established with the 150- and 450-MHz equipments for over a year in various mobile and repeater applications. Although the 50-MHz equipment has been available for a shorter period, we have equal confidence in its performance, since its design has been based on the well established techniques used in the other bands.

BIBLIOGRAPHY

1. K. W. Angel; "An RF-Activated Antenna Switch," *IEEE Transactions on Vehicular Communications, March, 1966.*

TABLE I—Performance Data

	Super Fleetfone 50 MHz	*Super Fleetfone 150 MHz*	*Super Fleetfone 450 MHz*
Frequency Range, MHz	25 - 50	148 - 174	450 - 470
Transmitter Power output, W	30 & 50	30	15
Quieting Sensitivity, μV	0.3	0.45	0.5
Usable Sensitivity, μV	0.25	0.35	0.4
Receive Battery Drain, mA	200	200	200
Transmit Battery Drain, A	12.5 @ 50 W 9.2 @ 30 W	10	10
Transmit Duty Cycle	continuous	continuous	continuous
Operating Temperature Range, °C	−30 to +60	−30 to +60	−30 to +60

TWO RCA MEN NAMED IEEE FELLOWS

The two RCA men cited herein have been honored for their professional achievements by being elected **Fellows of the Institute of Electrical and Electronic Engineers.** This recognition is extended each year by the IEEE to those who have made outstanding contributions to the field of electronics.

LESLIE L. BURNS
. . . for contributions to superconductive computer memories and to color television.

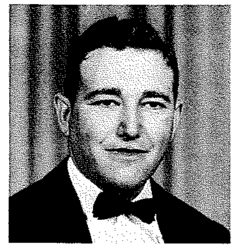

ROBERT M. COHEN
. . . for significant contribution to the application of electron tubes and semiconductor devices in radio and television receivers.

Leslie L. Burns attended Texas A & M University where he received the BS degree in 1943, and Princeton University where he received the MS degree in 1952. He joined RCA Laboratories in 1946, where his initial work was on solid state phenomena and integrated devices. Later he worked on color television with responsibility for developing the color synchronizing circuits now used in color television broadcasting. He has published over 15 papers on integrated devices, superconductive computer devices, and color television, and holds over 40 U.S. patents. He received RCA Laboratories Achievement Awards in 1949, 1960, and 1963. Mr. Burns is Head, Cryoelectric Computer Group of the Computer Research Laboratory at the RCA Laboratories. He is a member of the APS and Sigma Xi, and was a member of IEEE prior to being named a Fellow.

Robert M. Cohen joined the RCA Receiving Tube Applications Laboratory at Harrison, New Jersey in 1940. He studied at the evening school of Newark College of Engineering and Stevens Institute of Technology, receiving the BS in EE and ME in 1949. Mr. Cohen became Manager of the RCA Semiconductor Applications Laboratory in 1953 and in 1963 assumed his present position as Manager of Engineering for RCA's Commercial Receiving Tube and Semiconductor Operations. In 1957, he was one of eight employees to receive an RCA Award of Merit. He had authored a number of papers on tube and transistor applications and was a Senior Member of the IEEE prior to being named Fellow.

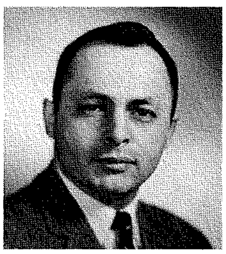

DR. M. H. LEWIN RECEIVES HIGHEST ETA KAPPA NU HONOR

The Eta Kappa Nu Jury of Awards has selected Dr. M. H. Lewin as the **Outstanding Young Electrical Engineer of 1966.** He will receive the award (the first time that this honor has been bestowed on an RCA engineer) at the IEEE Convention in New York in March 1967. Dr. Lewin is a Member, Technical Staff, of the Computer Research Laboratory, RCA Laboratories, Princeton, N.J. He was honored for his contributions to computer research in the areas of logic memories and input-output devices, and for his dedication to community activities. Dr. Lewin is the 31st engineer to receive this award since it was established in 1936. Winners must be no more than 35 years old, with a BSEE or equivalent held no more than 10 years, and outstanding professional achievements, civic activities, and cultural pursuits.

Dr. M. H. Lewin received his BSE from Princeton University in 1957, during which he worked part-time as a Staff Member in Forrestal Research Center, Princeton, N.J. on the early "Stellarator" experimental machines. He was awarded the IRE Student Prize as the outstanding EE senior at Princeton University, and was also recipient of the Jersey Central Power and Light Company Scholarship. He continued his education at Princeton with a Sayre fellowship and received the MSE in 1958. He was awarded the Charles Ira Young Memorial Medal and Plaque (the highest EE research honor at Princeton) for his Master's thesis work. In 1958 he joined the RCA Laboratories, while he continued his studies at Princeton for the Doctorate. His first work involved the use of negative-resistance elements as digital computer components, using as a vehicle the newly-developed tunnel diode. This work was the basis for his Ph.D. dissertation at Princeton, for which he received a second Charles Ira Young Medal, and for which he was a member of a team which was awarded the David Sarnoff Outstanding Achievement Award in Science. He was awarded the Ph.D. in 1960. Dr. Lewin continued in research on new solid-state devices as memory and logic elements, including pioneering work in ultra-high-speed switching circuits, and memory arrays fabricated by vacuum deposition and silk-screening. He was particularly concerned with read-only and associative memory realizations and made significant contributions to both fields. In particular, he directed a research group which constructed a prototype read-only memory using novel fabrication materials and interconnection methods. He also conceived a content-addressed-memory information-retrieval algorithm which is currently widely referenced in the literature. This work led to his receiving two RCA Laboratories Achievement Awards in 1959 and in 1963. Recently, Dr. Lewin has been engaged in research in time-sharing systems and in computer-aided-design. He was responsible for the conception and development of a magnetic "pen and tablet" to allow a computer user to input graphic information directly to a machine. He has also devised a portable "electronic keyboard" to allow input of messages to a remote time-sharing machine via conventional telephone. He is presently responsible for the hardware and software development of a computer-controlled cathode-ray-tube display system, to be used as a research tool for further work in man-machine communication and design automation. Dr. Lewin has authored many papers and reports, and has 9 issued U.S. patents and a number of additional patent applications awaiting action. He has been Assistant Review Editor for the IEEE Transactions on Electronic Computers and has been a reviewer for this publication as well as for numerous other computer and solid-state journals and conferences. He is a member of the IEEE Committee 4.10 on Solid-State Circuits. In addition, he has been an invited panel member at numerous computer conferences and has given several invited colloquium talks to university and IEEE groups. Dr. Lewin holds the rank of Adjunct Professor at Drexel Institute of Technology, Philadelphia, where he has been teaching graduate courses for a number of years in solid-state circuits, switching theory and computer systems. He has also been a Visiting Lecturer in the E.E. Department of Princeton University. Further, he is teaching courses at some of the RCA Product Divisions and has also served as an MIT nonresident instructor for MIT summer cooperative students working at RCA Laboratories. In addition to Sigma Xi membership, Dr. Lewin is a member of IEEE and ACM.

Engineering and Research NOTES

BRIEF TECHNICAL PAPERS OF CURRENT INTEREST

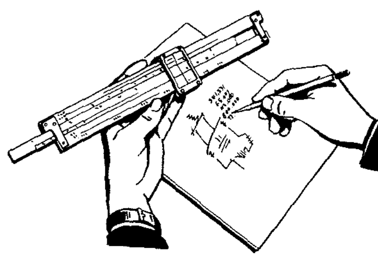

Problems Looking for Solutions: Five Related Questions on Radio Signal Propagation

H. Goodman, *Communications Systems Div. Camden, N.J.*

Final manuscipt received October 10, 1966

Editor's Comment: This Note, instead of reporting an accomplishment, presents five related problems on radio signal propagation, in the form of questions to which the author is seeking answers. Interested RCA engineers who can provide answers (or leads to answers) are invited to contact the author (**H. Goodman, Bldg. 16-3, Camden.**) Such answers will also merit consideration for publication in a future issue of the RCA ENGINEER.

The five problems in radio signal propagation discussed below in this *Note* are as follows:

1) *What is a reasonable nonconcentric model of the structure and density of the ionosphere for long range point-to-point communications?*
2) *What are the orthogonal reactions to refractivity due to transmission through temperature inversions and storm cells?*
3) *How do the dielectric properties of a conically shaped hill effect the intensity of the diffracted field?*
4) *What is the effect of absorptive material contiguous to the propagation path upon the field intensity?*
5) *What are the short term scintillation effects of the ionosphere to signals traversing at various angles?*

Accurate analysis of the propagation characteristics of electromagnetic energy is classically accomplished by using Maxwellian equations. Here, the degree of accuracy attainable depends upon the existence of distinctive boundaries between homogeneous, isotropic media. The accuracy of these equations is well demonstrated by optical experiments performed under controlled laboratory conditions, where the boundaries can be distinctive and time stable while the media are microscopically uniform. Under non-laboratory-controlled conditions, such as when the earth's atmosphere is the propagating medium, mathematical analysis becomes more difficult, since the medium does not have large scale homogeneity and the boundaries are often obscure and time variable.

The usual procedure for analyzing these types of media is to synthesize a propagation model which is laboratory reproducible in toto or in part and produces results which approximate field observations. The discrepancies between field and laboratory results are usually rationalized on a statistical basis and attributed to the time variations of the media.

Two related methods for solving radio propagation have been developed from the Maxwellian equations to permit simplified analyses. These are the ray and phase front methods. Each has its advantage depending upon the specific propagation characteristic to be disclosed. The usual propagation characteristics considered are the time delay, polarization, absorption, and refraction. These are best viewed by the ray method such that this has become the more popular approach. However, these same parameters can be visualized as coupling co-efficient and phase delay and are more often handled by the phase front method.

Models developed to explain certain propagation phenomena were based upon a spherical earth surrounded by radially stratified homogeneous media. This concept provided a reasonably accurate replica of the performance observed in the field for the class of transmitting frequencies, modulation and service range for broadcast service which carried the greatest motivation for these predictions. As the utilization of radio communication service expanded, the need for this predictability at different frequencies, modulation types, and ranges was forced to expand. Current knowledge of the ionospheric structure has ruled out the concentric stratification concept. Therefore a question is raised as to *what is a reasonable model for the ionospheric structure as a function of local time and latitude plus the direction and distance of propagation as a function of frequencies below MUF?*

Time variability of the atmosphere lead to additional modes of propagation rather than a constraint to others. Thus, the models were modified to exploit these anomalies. Stratification was not applicable for diffracted paths such as created by meteorological conditions affecting the dielectric properties of the medium at relatively low altitudes and those created by interceding mountains.

Extreme meteorological perturbations within the troposphere have generally been excluded from statistical performance data. Apparently this phenomenon is complex when attempting to predict the coupling of specific terminals. However, in the case of earth-space transmissions this type of disturbance, going beyond the work of Millman, could produce unnecessary outages unless a reasonable model is developed. Thus, it is desired to learn *what are the orthogonal reactions of refractivity created by temperature inversions or storm cells as a function of frequency above the MUF and of the incident angle?*

The diffraction mode of propagation beyond interceding mountains have been developed based upon an infinite wedge. However, the field results have not been restricted to mountain ridges, e.g., NBS use of Pike's Peak. These results apparently give close approximation to the wedge theory that revisions were not considered. However, this infinite dimension of the wedge should preclude polarization variations that should have been observed for the conical mountain. Polarization shift due to signal leakage around the slopes of the mountain should depend upon the dielectric properties at the point of grazing. However, these reactions lack reporting in the field data. The questions is thus raised to *what effect the dielectric properties along the surface of a conically shaped hill have upon the intensity of the diffracted field?*

Extensive analyses and evaluations are currently being conducted to determine the absorptive effect of tropical vegetation upon the propagation of radio waves. These cover two specific areas. First, when the vegetation becomes a portion of the dielectric in the propagation path, and second, when the vegetation is contiguous to the propagation path. The absorptive quality for the first case, although rather high, is amenable to propagation theory such that the field intensity can be predicted as a function of polarization wave and path length. However, the absorptive effects of a dielectric contiguous to the propagation path could disturb the Huygen concept of a continuous wave front since the field strength along the wave front would be a variable of this absorptive property and the phase summation would be a function of the electromagnetic viscosity of the dielectric. These characteristics are sensitive to polarization, wave and path length, and Fresnel clearance. The question is then raised as to *what are the predictable effects of absorptive material located contiguous to the propagation path upon the field intensity of an electromagnetic wave?*

Above MUF, little concern was found for the structure of the atmosphere until the advent of satellites and space communications. With propagation intended to pass through the troposphere and ionosphere, certain investigations have been made with respect to absorption, noise, temperature, refraction, scintillation, and Faraday shift. In most cases, the models have resorted to concentric stratification, low-angle observation, and long term integration. The traffic requirements for future space communication systems preclude these quasi-monochromatic conditions. In these cases, microscopic homogeneity must be available. However, it is known that the ionosphere is specifically not homogeneous nor truly isotropic. Thus the scintillation effects upon high-data transmissions between earth-bound terminals and non-stationary satellites must be recognized. This does not appear available to date. Thus the question is raised as to *what are the scintillation effects upon space communications due to inhomogeneity and non-concentric structure of the ionosphere as a function of frequency, elevation angle, local time and latitude, and satellite altitude?*

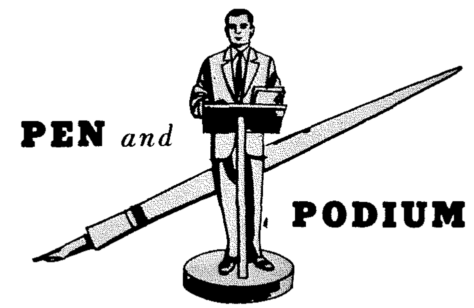

COMPREHENSIVE SUBJECT-AUTHOR INDEX
to
RECENT RCA TECHNICAL PAPERS

Both published papers and verbal presentations are indexed. To obtain a published paper, borrow the journal in which it appears from your library, or write or call the author for a reprint. For information on unpublished verbal presentations, write or call the author. (The author's RCA Division appears parenthetically after his name in the subject-index entry.) For additional assistance in locating RCA technical literature, contact: **RCA Staff Technical Publications, Bldg. 2-8, RCA, Camden, N. J. (Ext. PC-4018).**

This index is prepared from listings provided bimonthly by RCA Division Technical Publications Administrators and Editorial Representatives—who should be contacted concerning errors or omissions (see inside back cover).

Subject index categories are based upon the Thesaurus of Engineering Terms, Engineers Joint Council, N. Y., 1st Ed., May 1964.

SUBJECT INDEX

Titles of papers are permuted where necessary to bring significant keyword(s) to the left for easier scanning. Authors' division appears parenthetically after his name.

ACOUSTICS
(theory & equipment)

AUDIO LEVEL CONTROL, Automatic—D. C. Connor (BCD, Meadow Lands) Audio Engrg. Soc., October 1966; *AES preprint*

STEREOPHONIC LOUDSPEAKERS, Unitized Omnispatial—H. F. Olson (Labs, Pr) Audio Engrg. Soc., October 1966

AIRCRAFT INSTRUMENTS

AIRBORNE TV DISPLAYS, Human Factors in—B. Hillman (ASD, Burl) Soc. for Info. Display, Boston, Mass., October 1966

AMPLIFICATION

AUDIO AMPLIFIERS, Silicon Transistors in—J. C. Sondermeyer (ECD, Som) Nat'l Elec. Conf., Chicago, Ill., October 1966; *Conv. Record*

AUDIO HI-FI POWER AMPLIFIERS Using Silicon Transistors, Design of—R. D. Gold, J. C. Sondermeyer (ECD, Som) *Electronics World*, Sept., Oct., Nov. 1966

HIGH-POWER AMPLIFIERS in Satellite Communications Systems—G. M. Koch (RCA Ltd., Montreal) 6th Int'l Conf. on Microwave Generation & Amplification, Univ. of Cambridge, Eng., September 1966

PARAMETRIC AMPLIFIER (SELF-PUMPED), The Avalanche Transit-Time Diode as a—A. S. Clorfeine (Labs, Pr) IEEE Int'l Conf., Elec. Devices, Washington, D.C., October 1966

SMALL-SIGNAL RF AMPLIFICATION of MOS Devices—F. M. Carlson, E. F. McKeon (ECD, Som) Nat'l Elec. Conf., Chicago, Ill., October 1966; *Conf. Record*

ANTENNAS

ANTENNA SURFACES (BEST-FIT), Total Parameter Variation Yields—T. Szirtes (RCA Ltd., Montreal) *Microwaves*, September 1966

DIPOLE ANTENNA IMPEDANCE Measurements in an Isotropic Laboratory Plasma—K. A. Graf, D. Jassby (RCA Ltd., Montreal) Amer. Phys. Soc., Div. of Plasma Phys. Ann. Mtg., Boston, Mass., November 1966

MONOPULSE ANTENNA FEED System, A High-Efficiency Dual-Frequency Multimode—C. E. Profera, L. H. Yorinks (MSR, Mrstn) 1966 IEEE Aerospace & Electronics Sys. Conv., Washington, D.C., October 1966; *Supplement to IEEE Trans. on Aerospace*, Vol. 2, No. 6, November 1966

OPTICAL TUNNEL BEAMFORMER for Transmitting Arrays, Experimental Evaluation of an—L. W. Martinson (MSR, Mrstn) 24th U.S. Navy Symp. on Underwater Acoustics, 11/66; *Proc. of the Symp.*

PHASE ARRAY RADAR MAINTENANCE, Application of Queing Theory for—W. J. O'Leary (MSR, Mrstn) 1966 Aerospace & Elec. Sys. Conv. in Washington, D.C., October 1966; *Supplement to IEEE Trans. on Aerospace*, Vol. 2, No. 6, November 1966

RADIOTELESCOPE HORN, Manual Drive Aims Half-ton—T. Szirtes (RCA Ltd., Montreal) *Machine Design*, July 1966

SPACECRAFT ANTENNA ARRAY, A Novel—W. T. Patton (MSR, Mrstn) Dallas Chapter, IEEE. Also: WESCON 1966, Los Angeles, Calif., August 1966; *Convention Record*

BIONICS

TIME-DIVISION MULTIPLEXING as Possible Explanation for Short-Term Memory—W. H. Buchsbaum (CSD, Cam) 19th IEEE Engrg. in Medicine & Biology Conf., San Francisco, Calif., November 1966

CHECKOUT
(& maintenance)

AUTOMATIC TESTING, Computer-Controlled—B. Joyce, E. Stockton (ASD, Burl) *Electro Technology*, October 1966

COMPUTERS & Computation in Automatic Test Equipment—R. E. Turkington (ASD, Burl) ISA, New York City, N.Y., October 1966

PATCHBOARD WIRING DESIGNS (LCSS) for Shared Adapter Optimization—F. E. Liguori, P. M. Toscano (ASD, Burl) IEEE Automatic Support Sys. Symp., St. Louis, November 1966; *Symp. Record*

CIRCUIT ANALYSIS
(& theory)

GENERATOR MATRICES for Doubly-terminated Ladder Networks—T. Marshall (AED, Pr) Allerton Conf. on Circuit & System Theory, Monticello, Ill., October 1966; *Conf. Proc.*

CIRCUITS, INTEGRATED

AUDIO APPLICATIONS, Integrated Circuits for—J. T. Heizer (CSD, Cam) Audio Engrg. Soc., New York City, New York, October 1966

BINARY COUNTER, An Integrated Complementary MOS 12-Stage—H. Borkan, A. K. Rapp, L. P. Wennik (DME, Som) Timers for Ordnance Symp., November 1966; *Conf. Proc.*

CONTROL INSTRUMENTATION, Linear Integrated Circuits for—R. H. Pollack, B. A. Jacoby (ECD, Som) Instrument Soc. of Amer. Mtg., New York City, October 1966

ESSA II SATELLITE, Microelectronics in the—R. Callais (AED, Pr) 2nd Int'l Symp. on Microelectrons, Munich, Germany, October 1966; *Conf. Proc.*

INTEGRATED CIRCUITS—I. H. Kalish (ECD, Som) IEEE Pennsylvania Student Branch, October 1966

INTEGRATED CIRCUITS Yesterday, Today and Tomorrow—R. D. Lohman (Labs, Pr) Naval Air Development Ctr., Johnsville, Penna., October 1966

ISOLATION TECHNIQUES for Integrated Circuits—A. I. Stollar, N. E. Wolff (Labs, Pr) Second Int'l Symp. on Microelectronics, Munich, Germany, October 1966

LARGE-SCALE ARRAYS — A. H. Medwin (ECD, Som) Working Committee on Electron Devices, Washington, D.C., November 1966

LINEAR INTEGRATED CIRCUITS—B. V. Vonderschmitt, R. L. Sanquini (ECD, Som) *Electronics World*, November 1966

MICROWAVE INTEGRATED CIRCUITS, Impact of—H. Sobol (Labs, Pr) IEEE Int'l Conf., Electron Devices, Washington, D.C., October 1966

THIN-FILM Integrated Arrays—W. Y. Pan (CSD, Cam) 1966 CIE Sem. on Mod. Engrg. & Tech., Taiwan, China, June 1966

TRANSISTOR (THIN FILM), An Adaptive—S. S. Perlman, K. H. Ludewig (Labs, Pr) 1966 IEEE Int'l Conf., Electronic Devices, Washington, D.C., October 1966

TRANSISTORS (THIN FILM), Recent Advances in—R. L. Schelhorn, M. L. Topfer (DME, Som) 2nd Int'l Microelectronics Symp., Munich, Germany, October 1966; *Conf. Proc.*

TRANSISTORS (THIN FILM), Stability of—J. J. Fabula, R. L. Schelhorn, M. L. Topfer (DME, Som) 5th Ann. Symp. Phys. of Failure, Elec., Dayton, Ohio, November 1966; *Conf. Proc.*

UHF AND MICROWAVE Microelectronics Techniques—Dr. W. Y. Pan (CSD, Cam) IEEE N.J. Coast Chapter Comm. Tech. Group, Little Silver, N.J., October 1966

CIRCUITS, PACKAGED

(COOLING): Suction vs. Pressure Forced-Air Cooling—Part II—G. Rezek (CSD, Cam) *IEEE Trans. on Parts, Materials and Packaging*, Mar/June 1966, Vol. PMP-2, No. 1 & 2

MICROSTRIP TRANSMISSION LINES for Microwave Integrated Circuits, Measurements on the Properties of—M. Caulton, J. J. Hughes, H. Sobol (Labs, Pr) *RCA Review*, Vol. XXVII, No. 3, September 1966

MULTILAYER BOARDS for Printed Circuits—A. Levy (CSD, Cam) Inst. of Printed Circuits, New York City, June 1966; *Electronic Products*, December 1966

SHIELDING Effectiveness—A. DiMarzio (ASD, Burl) *Electronic Design News*, September 1966

COMMUNICATION, DIGITAL
(equipment & techniques)

ADCOM 70 PROGRAM, A Progress Report—W. F. Bell (CSD, Cam) Lecture to RCA Engrs. at Camden, September 1966

DIGITAL TV Data Compression—W. Bisignani (AED, Pr) Rutgers Univ. IEEE Student Chapter, New Brunswick, N.J., October 1966

OPTIMUM CODE WORD ASSIGNMENT to Telemetry Data by Integer Programming—P. Hahn (MSR, Mrstn) 4th Canadian Symp. on Comm., Montreal, Canada, October 1966

PCM TELEMETRY Burst Retransmission Format, Design of a—H. W. Trigg (MSR, Mrstn) 1966 Aerospace & Elec. Sys. Conv., Washington, D.C., October 1966; *Supplement to IEEE Trans. on Aerospace*, Vol. 2, No. 6, November 1966

COMMUNICATIONS COMPONENTS
(equipment subsystems)

MICROWAVE BRANCHING NETWORKS for Surface and Space Communication Systems—M. V. O'Donovan, J. A. S. Hansen, N. K. M. Chitre (RCA Ltd., Montreal) IEEE Canadian Symp. on Comm., Montreal, October 1966

MULTIPLE-SIGNAL FM DETECTION System, Analysis of—T. Murakami (MSR, Mrstn) *RCA Review*, Vol. XXVII, No. 3, September 1966

OSCILLATOR, CW Three-Terminal GaAs—K. Petzinger, A. Hahn, A. Matzelle (Labs, Pr) IEEE Conf., Electron Devices, Washington, D.C., October 1966

PHASED-ARRAY TRANSMITTER Modules, The Application of Grid-Controlled Tubes in—M. V. Hoover (ECD, Lanc) IEEE Electron Devices Mtg., Washington, D.C., October 1966

SHIELDING Effectiveness—A. DiMarzio (ASD, Burl) *Electronic Design News*, September 1966

TWO-METER CONVERTER, All-Transistor—R. M. Mendelson (ECD, Som) New Providence Radio Club, N.J., September 1966

TWO-METER CONVERTER, Transistors and Nuvistors in a—R. M. Mendelson (ECD, Som) Bell Telephone Labs, Murray Hill, N.J., September 1966

VARACTOR SELECTION for Voltage Tuning—D. J. Blattner (ECD, Pr) *Electronic Communicator*, Sept/Oct 1966

VIDEO SWITCHERS, New Techniques in Transition Control of—W. L. Hurford (BCD, Cam) IEEE 16th Broadcast Symp., Washington, D.C., September 1966

COMMUNICATIONS SYSTEMS

PLANT COMMUNICATIONS System — E. J. Tomko (CSD, Cam) Amer. Management Assoc. Sem., San Francisco, Calif., October 1966

TELEPHONE SWITCHING THEORY (Elementary) Applied to the Design of Message Switching Systems — Stambler, L. (CSD, Cam) Fall Joint Computer Conf., San Francisco, Calif., November 1966; *Conf. Record*

TRC-97: Portable Communications System for the Marines—G. Davis (CSD, Cam) Beth El Synagogue, Camden, N.J., December 1966

COMMUNICATION, VOICE
(equipment & techniques)

AUDIO LEVEL CONTROL, Automatic—D. C. Connor (BCD, Meadow Lands) Audio Engrg. Soc., October 1966; *AES preprint*

HIGH-EFFICIENCY VOICE COMMUNICATION System, Research Towards A—H. F. Olson, H. Belar, E. S. Rogers (Labs, Pr) *Journal of the Audio Engrg. Soc.*, Vol. 14, No. 3, July 1966

INTEGRATED CIRCUITS for Audio Applications—J. T. Heizer (CSD, Cam) Audio Engrg. Soc., New York City, October 1966

TWO-METER CONVERTER, All-Transistor—R. M. Mendelson (ECD, Som) New Providence Radio Club, N.J., September 1966

COMPUTER APPLICATIONS

AUTOMATIC TEST EQUIPMENT, Computers & Computation in—R. E. Turkington (ASD, Burl) ISA, New York City., N. Y., October 1966

AUTOMATIC TESTING, Computer-Controlled—B. Joyce, E. Stockton (ASD, Burl) *Electro Technology*, October 1966

COMPUTER and the Engineer—G. Smoliar (EDP, Cam) New York Univ., November 1966

DATA ABBREVIATION to Actual Range Telemetry Data, A Report on the Application of—N. Maestre (MSR, Mrstn) Int'l Telemetering Conf., Los Angeles, Calif., October 1966; 1966 *ITC Proc.*

ELECTRONIC COMPOSITION System — J. S. Greenberg (GSD, Pr) Magazine Pub. Assoc. Mtg., August 1966

PRINTING, Automation in—J. S. Greenberg (GSD, Pr) Assoc. of Publication Production Mgrs., November 1966

COMPUTER COMPONENTS
(subsystems & peripheral equipment)

BINARY COUNTER, An Integrated Complementary MOS 12-Stage—H. Borkan, A. K. Rapp, L. P. Wennik (DME, Som) Times for Ordnance Symp., November 1966; *Conf. Proc.*

LARGE-SCALE INTEGRATION, System Utilization of—H. S. Miiller, G. B. Herzog (Labs, Pr) 1966 Aero/Space Computer Symp., Santa Monica, Calif., October 1966

MULTITHREADING DESIGN of a Reliable Aerospace Computer — E. Miller, R. Hassett (ASD, Burl) Pres. at IEEE Aerospace & Electronics Sys. Conv., Washington, D.C., October 66; *Supplement to IEEE Trans. on Aerospace,* Vol. 2, No. 6, November 1966

SYNCHRONOUS SWITCHING of SCR's and Triacs—G. D. Hanchett (ECD, Som) IEEE Subsection Mtg., Peoria, Ill., November 1966

COMPUTERS, PROGRAMMING

VARIABLE INSTRUCTION Computer, Reliability Aspects of the RCA/USAF—R. P. Hassett, E. H. Miller (ASD, Burl) Symp. on Aerospace Computers, Santa Monica, Calif., October 1966

VARIABLE INSTRUCTION Computer Software—A. Spence (ASD, Burl) USAF Aerospace Symp. on Spaceborne Computer Software Systems, Los Angeles, Calif., September 1966

COMPUTER STORAGE

MONOLITHIC FERRITE MEMORY for Space—R. Ricci, P. Truscello (AED, Pr) Nat'l Elec. Conf., Chicago, Ill., October; *Conf. Record*

CONTROL SYSTEMS
(& automation)

CONTROL INSTRUMENTATION, Linear Integrated Circuits for—R. H. Pollack, B. A. Jacoby (ECD, Som) Instrument Soc. of Amer. Mtg., New York City, October 1966

DISPLAYS

AIRBORNE TV DISPLAYS, Human Factors in—B. Hillman (ASD, Burl) Soc. for Info. Display, Boston, October 1966

ELECTROLUMINESCENT DIODES (GaAs), Degradation Phenomena of Operating Life in—M. F. Lamorte, W. Agosto, G. Kupsky, N. Pennucci, H. W. Becke (ECD, Som) GaAs Device Conf., Univ. of Reading, Eng., September 1966

ELECTROLUMINESCENT DISPLAYS, Ferroelectric-Controlled—B. J. Lechner, A. G. Samusenko, G. W. Taylor, J. Tults (Labs, Pr) 1966 Aerospace Electronics Conf., Dayton, Ohio, May 1966; *Conf. Record*

(ELECTRON MICROSCOPE TV DISPLAYS): On the Possible Use of Data Correlation Techniques for Extracting Phase Contrast Information from TV-Displayed Electron Microscope Images—Dr. J. W. Coleman, J. M. Gottschalk (BCD, Cam) EMSA, San Francisco, Calif., August 1966

DOCUMENTATION
(& information science)

ENGINEERING WRITING—The Editor's View—D. B. Dobson (ASD, Burl) Boston Univ. Graduate School of Communications, November 1966

INFORMATION RETRIEVAL as a Problem in Packaging—L. Rosenberg (AED, Pr) 1966 ADI Mtg., Los Angeles, Calif., October 1966; *Conf. Proc.*

PROPOSAL REVIEW as a Feedback Mechanism—T. E. Altgilbers (CSD, Cam) IEEE Engrg. Writing & Speech Group, Phila., Penna., November 1966

EDUCATION
(& training)

(CURRICULUM): Dialogue of Unequals—R. F. Ficchi (CSD, Cam) *IEEE Phila. Section Almanack,* November 1966

ELECTROMAGNETIC WARFARE

OZONE CONCENTRATION at Early Times Subsequent to the Blue Gill Burst, The Computed Modification of the—Dr. K. Sittel (SEER, Mrstn) *Nuclear Weapons Effect Review,* August 1966

TEAK ATTENUATION ANOMALY Interpreted by Residue Debris—Dr. K. Sittel (SEER, Mrstn) *Nuclear Weapons Effect Review,* December 1966

ELECTROMAGNETIC WAVES
(theory & phenomena)

EFFICIENT SEQUENTIAL DETECTION in the Presence of Strong Localized Signal Interference—H. M. Finn, R. S. Johnson (MSR, Mrstn) *RCA Review,* Vol. XXVII, No. 3, September 1966

MAGNETO-IONIC MEDIA, The "Infinity Catastrophe" Associated with Radiation in—H. Staras (Labs, Pr) *Radio Sci.* Vol. 1, No. 9, September 1966

MULTIPLE-SIGNAL FM DETECTION SYSTEM, Analysis of—T. Murakami (MSR, Mrstn) *RCA Review,* Vol. XXVII, No. 3, September 1966

OZONE CONCENTRATION at Early Times Subsequent to the Blue Gill Burst, The Computed Modification of the—Dr. K. Sittel (SEER, Mrstn) *Nuclear Weapons Effect Review,* August 1966

TEAK ATTENUATION ANOMALY Interpreted by Residue Debris—Dr. K. Sittel (SEER, Mrstn) *Nuclear Weapons Effect Review,* December 1966

UNDERWATER TRANSMISSION Characteristics for Laser Radiation—H. Okoomian (ASD, Burl) *Applied Optics,* September 1966

ELECTROMAGNETS

NIOBIUM-TIN MAGNETS, Technology of—E. R. Schrader (ECD, Hr) URSI Conf., Munich, Germany, September 1966

OPTIMIZED DESIGN of Large-Bore High-Field Magnets, The Use of Superconductors with Varied Characteristics for the—E. R. Schrader, P. A. Thompson (ECD, Hr) *IEEE Trans. on Magnetics,* September 1966

RIBBON-TYPE MAGNETS, Nb_3Sn — H. C. Schindler (ECD, Hr) Brookhaven Nat'l Lab, Long Island, New York, November 1966

ELECTRO-OPTICS
(systems & techniques)

ELECTROLUMINESCENT DIODES (GaAs), Degradation Phenomena of Operation Life in—M. F. Lamorte, W. Agosto, G. Kupsky, N. Pennucci, H. W. Becke (ECD, Som) GaAs Device Conf., Univ. of Reading, Eng., September 1966

MODULATOR (Gallium Arsenide Electro-Optic) for the 10.6-Micron CO_2 Laser —T. E. Walsh (ECD, Pr) IEEE Electron Devices Mtg., Wash., D.C., October 1966

MODULATORS, Gallium-Arsenide Electro-Optic—T. E. Walsh (ECD, Pr) *RCA Review,* Vol. XXVII, No. 3, September 1966

ENERGY CONVERSION
(& power sources)

AVALANCHE DIODES, Harmonic Power Output for—S. G. Liu, J. J. Risko (Labs, Pr) 1966 Electron Devices Mtg., Washington, D.C., October 1966

CESIUM PRESSURE, The Development of a High-Temperature Reservoir for Automatic Control of—W. E. Harbaugh, A. Basiulis (ECD, Lanc) Thermionic Converter Specialists Conf., Houston, Texas, November 1966

CHARGE RECTIFIERS, Device Applications of—T. F. Dwyer, R. A. Shahbender (Labs, Pr) Nat'l Electronics Conf., Chicago, Ill., October 1966; *Conf. Record*

HEAT-PIPE Work at RCA, Review of—D. M. Ernst (ECD, Lanc) Thermionic Converter Specialists Conf., Houston, Texas, November 1966

POWER SYSTEMS for Space — G. Barna (Astro-Pr) Naval Reserve Research Co., Princeton, 4-1, September 1966

SOLAR CELLS, Lithium-Doped Radiation-Resistant Silicon—J. J. Wysocki, P. Rappaport, E. Davison, R. Hand, J. J. Loferski (Labs, Pr) *App. Phys. Letters* Vol. 7, No. 4, July 1966

SOLAR CELLS Today—P. Rappaport (Labs, Pr) Intersociety Energy Conversion Engrg. Conf., Los Angeles, Calif., September 1966

SOLID-STATE HIGH-FREQUENCY Power Generation—Dr. W. Y. Pan (CSD, Cam) 1966 CIE Sem. on Modern Engrg. & Tech., Taiwan, China, June 1966

SUN MACHINE: (RCA Space ARC Model 12-17)—W. Schacht (BCD, Cam) Audubon High School, November 1966

THERMIONIC-CONVERTER/HEAT-PIPE Assembly, The Development of an Insulated—W. E. Harbaugh, R. W. Longsderff (ECD, Lanc) Thermionic Converter Specialists Conf., Houston, Texas, November 1966

THERMIONIC-CONVERTER/HEAT-PIPE System, Thermal Measurements of a—P. K. Shefsiek (ECD, Lanc) Thermionic Converter Specialists Conf., Houston, Texas, November 1966

THERMIONIC FOSSIL-FUEL Energy Converters at RCA, Review of—D. M. Ernst, W. B. Hall, S. W. Kessler, R. C. Turner (ECD, Lanc) Thermionic Converter Specialists Conf., Houston, Texas, November 1966

THERMIONIC-ISOTOPE Space-Power Generator, The Development of an Advanced—R. J. Buzzard, A. Basiulis, P. K. Shefsiek (ECD, Lanc) AIAA Conf. on Non-conventional Energy Conversion Applications, Los Angeles, Calif., September 1966

THERMIONIC-ISOTOPE Space-Power Technology, The Development of—R. J. Buzzard, A. Basiulis, P. K. Shefsiek (ECD, Lanc) Thermionic Converter Specialists Conf., Houston, Texas, November 1966

THERMOELECTRIC DEVICES, Silicon-Germanium—G. S. Lozier (ECD, Hr) AIAA Conf. on Non-Conventional Energy Conversion Applications, Los Angeles, Calif., September 1966

ENVIRONMENTAL ENGINEERING

SHOCK SPECTRA of Practical Shaker Shock Pulses—J. R. Fagan, A. S. Baran (AED, Pr) Shock & Vibration Symp.—Air Force, Los Angeles, Calif., October 1966; *Conf. Proc.*

FILTERS, ELECTRIC

COMB-LINE BANDPASS Filters, Design of—R. M. Kurzrok (CSD, Cam) *IEEE Trans. PTGMTT,* Vol. MTT-14, No. 7, July 1966

FILTER DESIGN, Photographic Information Recording Techniques Aid—L. Slaven, S. Shek (RCA Ltd., Montreal) *Elec. & Comm.,* August 1966

GENERAL FILTER, Single Component Changes Bandpass into—R. M. Kurzrok (CSD, Cam) *Electronics,* April 1966

GENERAL FOUR-RESONATOR Filters at Microwave Frequencies, Correction to—R. M. Kurzrok (CSD, Cam) *IEEE Trans. PTGMTT,* Vol. MTT-14, No. 10, October 1966

GRAPHIC ARTS

AUTOMATION in Printing—J. S. Greenberg (GSD, Pr) Assoc. of Publication Production Mgrs., November 1966

ELECTRONIC COMPOSITION System—J. S. Greenberg (GSD, Pr) Magazine Pub. Assoc. Mtg., August 1966

PRINTING COSTS, Studies of—J. S. Greenberg (GSD, Pr) Amer. Univ. Inst. on Managerial Implications of Elec. in Publishing, January 1966

HUMAN FACTORS
(physiological & psychological)

AIRBORNE TV DISPLAYS, Human Factors in—B. Hillmann (ASD, Burl) Soc. for Info. Display, Boston, October 1966

LSD by Engineers, Use of—C. W. Fields (CSD, Cam) *IEEE Phila. Section Almanack,* October 1966

NIGHT VISION, Electronic Aids to—R. W. Engstrom (ECD, Lanc) Amer. Business Club Mtg., Lanc., Pa., November 1966

INFORMATION THEORY

PSEUDO RANDOM SEQUENCE, A Method of Obtaining all Phases of a—R. Curry (AED, Pr) Nat'l Electronics Conf., October 1966; *Conf. Proc.*

TELEPHONE SWITCHING THEORY (Elementary) Applied to the Design of Message Switching Systems—L. Stambler (CSD, Cam) Fall Joint Computer Conf., San Francisco, Calif., November 1966; *Conf. Record*

INTERFERENCE
(& noise)

EFFICIENT SEQUENTIAL DETECTION in the Presence of Strong Localized Signal Interference—H. M. Finn, R. S. Johnson (MSR, Mrstn) *RCA Review,* Vol. XXVII, No. 3, September 1966

SHIELDING Effectiveness—A. DiMarzio (ASD, Burl) *Electronic Design News,* September 1966

LABORATORY EQUIPMENT
(& techniques)

AUTOMATIC PLOTTING of Conductance and Capacitance of Metal-Insulator-Semiconductor Diodes or Any Two-Terminal Complex Admittance—J. Shewchung, A. Waxmann (Labs, Pr) *Review of Scientific Instru.,* Vol. 37, No. 9, September 1966

ELECTRICAL TEST METHODS as Analyticel Tools—L. R. Weisberg (Labs, Pr) *Annuals of the N.Y. Academy of Sci.,* Vol. 137, Article I, January 1966

(ELECTRON MICROSCOPE): A Very Low Disturbance Semiconductor Power Supply for the Objective Lens of a 1-MeV Electron Microscope—R. L. Libbey (BCD, Cam) EMSA, San Francisco, Calif., August 1966

(ELECTRON MICROSCOPE TV DISPLAYS): On the Possible Use of Data Correlation Techniques for Extracting Phase Contrast Information from TV-Displayed Electron Microscope Images—Dr. J. W. Coleman, J. M. Gottschalk (BCD, Cam) EMSA, San Francisco, Calif., August 1966

ION PRODUCTION and Analysis: Fundamentals and Instrumentation—R. E. Honig (Labs, Pr) Symp. on Spark Source Mass Spectrometry ACS, N.Y. Mtg., September 1966

IONS from Solids, The Production of—R. E. Honig (Labs, Pr) *Mass Spectrometric Analysis of Solids* Chapter II (Edited by A. J. Ahearn)

MASS SPECTROSCOPY as an Analytical Tool—R. E. Honig (Labs, Pr) *Annals of the N.Y. Academy of Sci.,* Vol. 137, Article I, January 1966

MASS SPECTROMETRY in the Manufacture of Color Television Tubes, Chemical Applications of—J. J. Moscony (ECD, Lanc) LaSalle College Sem., Phila., Penna., November 1966

MIS CAPACITANCE VS. BIAS Characteristics, Automatic Display of—K. H. Zaininger (Labs, Pr) *RCA Review,* Vol. XXVII, No. 3, September 1966

PRESSURE SINTERING, Die Design for—H. I. Moss, W. P. Stollar (Labs, Pr) *The Amer. Ceramic Soc. Bulletin,* Vol. 45, No. 9, September 1966

PURE MATERIALS ANALYSIS, Electrical Measurements for—L. R. Weisberg (Labs, Pr) *Analytical Chemistry* Vol. 38, No. 1, January 1966

SHOCK SPECTRA of Practical Shaker Shock Pulses—J. R. Fagan, A. S. Baran (AED, Pr) Shock & Vibration Symp.—Air Force, Los Angeles, Calif., October 1966; *Conf. Proc.*

LASERS

CONTINUOUS ARGON LASERS, High-Pressure High-Magnetic-Field Effects in—I. Gorog, F. W. Spong (Labs, Pr) *App. Phys. Letters* Vol. 9, No. 1, July 1966

ION LASERS, Mechanisms of Electron Beam Excitation of—J. M. Hammer, C. P. Wen (Labs, Pr) 6th Int'l Conf. on Microwave and Optical Generation and Amplication, Cambridge Univ., September 1966

MODULATOR (Gallium Arsenide Electro-Optic) for the 10.6-Micron CO_2 Laser—T. E. Walsh (ECD, Pr) IEEE Electron Devices Mtg., Washington, D.C., October 1966

ORIENTATION EFFECT in GaAs Injection Lasers—M. S. Abrahams, J. I. Pankove (Labs, Pr) *J. of App. Phys.*, Vol. 37, No. 7, June 1966

RARE EARTHS in Solid-State Laser Materials, The Determination of—S. J. Adler (Labs, Pr) Symp. on Trace Characterization—Chemical and Physical, Nat'l Bureau of Standards, Washington, D.C., October 1966

ROOM TEMPERATURE GaAs Lasers at High Pulse Repetition Rates (50Kc/s), Performance of—G. C. Dousmanis, H. E. Gross (Labs, Pr) *Proc. of the IEEE* Vol. 54, No. 7, July 1966

ULTRAVIOLET ZnO LASER Pumped by an Electron Beam—F. H. Nicoll (Labs, Pr) *App. Phys. Letters* Vol. 9, No. 1, July 1966

UNDERWATER TRANSMISSION Characteristics for Laser Radiation—H. Okoomian (ASD, Burl) *App. Optics*, September 1966

LINGUISTICS (& speech recognition)

HIGH-EFFICIENCY VOICE COMMUNICATION System, Research Towards a—H. F. Olson, H. Belar, E. S. Rogers (Labs, Pr) *J. of the Audio Engrg. Soc.*, Vol. 14, No. 3, July 1966

SPEECH RESEARCH at RCA Laboratories—P. W. Ross (Labs, Pr) Talk at Belle Meade Rotary Club, Belle Meade, N.J., October 1966

LOGIC ELEMENTS

MAGNETIC LOGIC (High-Speed) for Radiation-Resistant Applications—D. Hampel (CSD, Cam) Nat'l Electronics Conf., Chicago, Ill., October 1966; *Conf. Proc.*

MULTITHREADING DESIGN of a Reliable Aerospace Computer — E. Miller, R. Hassett (ASD, Burl) Pres. at IEEE Aerospace & Elec. Systems Conf., Washington, D.C., October 1966; *Supplement to IEEE Trans. on Aerospace*, Vol. 2, No. 6, November 1966

MANAGEMENT

CONFIGURATION CHANGE CONTROL — G. Offenbacher, D. Gilloly (ASD, Burl) ASQC Mtg., Phila., Pa., November 1965

ENGINEERING ASSIGNMENTS in the Space Program—T. E. Kupfrian (ASD, Burl) Symp. on Aero. Computers, Santa Monica, Calif., October 1966

IDEA LAB, RCA's—D. Shore (CSD, Cam) WFLN Radio Phila., Pa., Part I on September 24 and Part II, October 1966

MANAGEMENT DECISIONS on the Way to the Moon—F. J. Gardiner (ASD, Burl) Soc. for Advancement of Management, Boston Univ., November 1966

MOTIVATION of Engineers through a Program of Technical Excellence—G. R. Field (MSR, Mrstn) 4th Ann. Conf. of Prof. Engrs. in Ind., NSPE, St. Louis, Mo., October 1966; *preprint*

PH.D. INTERVIEW, Reflections on the—J. A. VanRaalte (Labs, Pr) *Research Management*, September 1966

PROPOSAL REVIEW as a Feedback Mechanism—T. E. Altgilbers (CSD, Cam) IEEE Engrg. Writing & Speech Group, Phila., November 1966

REVIEW: "Cost Estimating and Contract Pricing" (by T. F. McNeill & D. S. Clark; Amer. Elsivier Pub. Co. N.Y., 1966)—W. A. Parkinson (CSD, Cam) *Standards Engrg.*, October 1966

VALUE ANALYSIS—A Purchasing Concept—R. F. Morhart (ECD, Hr) Amer. Management Ass. Mtg., N.Y.C., November 1966

MASERS

MONOPULSE RADARS, A Traveling Wave Maser for—S. B. Adler, A. J. Haraburda (MSR, Mrstn) IEEE Aero. & Elec. Sys. Conv., Washington, D.C., October 1966; *Supplement to IEEE Trans. on Aero.*, Vol. 2, No. 6, November 1966

MATHEMATICS

GENERAL SPHERICAL HARMONIC TENSORS in the Boltzmann Equation—T. W. Johnston (RCA Ltd., Montreal) *J. of Mathematical Phys.*, August 1966

PSEUDO RANDOM SEQUENCE, A Method of Obtaining All Phases of a—R. Curry (AED, Pr) Nat'l Elec. Conf., October 1966; *Conf. Proc.*

MECHANICAL DEVICES

AIR DAMPING EFFECT on Structural Fatigue Failure—J. R. Fagan (AED, Pr) Shock & Vibration Symp., Air Force, Los Angeles, Calif., October 1966; *Conf. Proc.*

ASBESTOS-CEMENT PIPE in Structural Engrg., New Use for—Y. H. Dong (MSR, Mrstn) *Civil Engrg.*, October 1966

CIRCULAR ADJUSTER—T. Szirtes (RCA Ltd., Montreal) ASME Mechanisms Conf., Lafayette, Ind., October 1966

(COOLING): Suction vs. Pressure Forced-Air Cooling—Part II—G. Rezek (CSD, Cam) *IEEE Trans. on Parts, Materials & Packaging*, Mar/June 1966, Vol. PMP-2, No. 1 & 2

HYDROSTATIC BEARING for Instrumentation Radar—J. C. Spracklin, G. M. Robinson (MSR, Mrstn) ASME Winter Mtg., New York, 11/66; Pub. in: *Deep Space and Missile Tracking Antennas*, ASME, 12/66

RADAR TOWER and Foundation Analysis—P. Pschunder (MSR, Mrstn) ASME Winter Mtg., New York, 11/66; Pub. in: *Deep Space and Missile Tracking Antennas*, ASME, 12/66

RADIOTELESCOPE HORN, Manual Drive Aims Half-ton—T. Szirtes (RCA Ltd., Montreal) *Machine Design*, July 1966

THREADED FASTENERS, Joints Designed for—P. Guay (ASD, Burl) *Design News*, August 1966

MEDICAL ELECTRONICS

BIOLOGICAL ENGINEERING, Twenty Years of Medical and—L. E. Flory (AED, Pr) 1st Can. Medical & Biological Engrg. Conf., Radio & Elec. Engrg., Ottawa, Canada, September 1966

TIME-DIVISION MULTIPLEXING as Possible Explanation for Short-Term Memory—W. H. Buchsbaum (CSD, Cam) 19th IEEE Engrg. in Medicine & Biology Conf., San Francisco, Calif., November 1966

PARTICLE BEAMS

ELECTRON BEAM EXCITATION of Ion Lasers, Mechanisms of—J. M. Hammer, C. P. Wen (Labs, Pr) 6th Int'l Conf. on Microwave and Optical Generation & Amplification, Cambridge Univ., September 1966

ULTRAVIOLET ZnO LASER Pumped by an Electron Beam—F. H. Nicoll (Labs, Pr) *App. Phys. Letters*, Vol. 9, No. 1, July 1966

PLASMA PHYSICS

ANISOTROPIC PLASMA MEASUREMENTS Using a Turnstile Multiple-Probe Polarimeter—M. P. Bachynski, F. J. F. Osborne, B. W. Gibbs (RCA Ltd., Montreal) *Can. J. of Phys.*, July 1966

DIPOLE ANTENNA IMPEDANCE Measurements in an Isotropic Laboratory Plasma — K. A. Graf, D. Jassby (RCA Ltd., Montreal) Amer. Phys. Soc., Div. of Plasma Phys. Ann. Mtg., Boston, November 1966

GENERAL SPHERICAL HARMONIC TENSORS in the Boltzmann Equation—T. W. Johnston (RCA Ltd., Montreal) *J. of Mathematical Phys.*, August 1966

LINEARLY POLARIZED WAVES in Plasmas in the Region of the Electron Cyclotron Frequency—M. P. Bachynski, B. W. Gibbs (RCA Ltd., Montreal) *Plasma Phys. (J. of Nuclear Energy, Pt.C)* August-October 1966

PINCH INSTABILITY in Magnetic Fields — K. Ando, M. Glicksman (Labs, Pr) Mtg. of the Phys. Soc. of Japan, Niigata, October 1966

PLASMA SHEATH (V-B INDUCED) Formed Around a Satellite, An Experiment on the—F. J. F. Osborne, M. A. Kasha (RCA Ltd., Montreal) Amer. Phys. Soc., Div. of Plasma Phys., Ann. Mtg., Boston, November 1966

SATELLITE-PLASMA INTERACTION in the Laboratory, Simulation of—T. W. Johnston, M. A. Kasha (RCA Ltd., Montreal) Amer. Phys. Soc., Div. of Plasma Phys. Ann. Mtg., Boston, November 1966

UNBOUNDED PLASMAS, Sources in — M. P. Bachynski (RCA Ltd., Montreal) XVth Gen. Assembly of URSI, Germany, September 1966

UNIVERSAL INSTABILITY in Alkali-Metal Plasmas—H. Hendel (AED, Pr) Columbia Univ. Plasma Phys. Sem., N.Y., November 1966; *Conf. Proc.*

UNIVERSAL INSTABILITY in Non-Isothermal Plasmas—H. Hendel (AED, Pr) Amer. Phys. Soc. Mtg. Plasma Phys. Div., Boston, Mass., November 1966; *Conf. Proc.*

PROPERTIES, ATOMIC

ACOUSTICAL PHONON Interaction with Strongly Temperature-Dependent Optical Phonons—E. F. Steigmeier, R. Klein (Labs, Pr) Swiss Phys. Soc. Mtg., Solothurn, September 1966

AVALANCHE AND TUNNELING Currents in Gallium Arsenide—R. Williams (Labs, Pr) *RCA Review*, Vol. XXVII, No. 3, September 1966

BAND STRUCTURE DETERMINATION, Optical Reflection Techniques in—D. L. Greenaway (Labs, Pr) Conf. on the Phys. of Semiconductor Compounds, Swansea, Wales, September 1966

CIRCULAR DICHROISM in the Absorption Bands of Divalent Rare Earth Ions, Survey of the—C. H. Anderson, H. A. Weakliem (Labs, Pr) Johns Hopkins Conf. on Optical Properties of Ions in Crystals, Baltimore, Maryland, September 1966

CURRENT-CONTROLLED INSTABILITY in GaAs, Infrared and Microwave Radiations Associated with a—S. G. Liu (Labs, Pr) *App. Phys. Letters*, Vol. 7, No. 6, July 1966

ELECTROREFLECTANCE of Barium Titanate—C. Gahwiller (Labs, Pr) Swiss Phys. Soc. Mtg., Solothurn, October 1966

ENERGY LEVELS of Ho^{2+} and Tm^{2+} in CaF_2 and $SrCl_2$—Z. J. Kiss, H. A. Weakliem (Labs, Pr) Conf. on Optical Properties of Ions in Crystals, Johns Hopkins Univ., September 1966

HALL COEFFICIENT (High-Temperature) in GaSb-InSb Alloys—I. Kudman, T. Seidel (Labs, Pr) Conf. on the Phys. of Semiconductor Compounds, Swansea, Wales, September 1966

ION PRODUCTION and Analysis: Fundamentals and Instrumentation—R. E. Honig (Labs, Pr) Symp. on Spark Source Mass Spectrometry ACS, N.Y. Mtg., September, 1966

IONS from Solids, The Production of—R. E. Honig (Labs, Pr) *Mass Spectrometric Analysis of Solids Chapter II* (Edited by A. J. Ahearn)

METASTABLE EXCITONS in CdI_2 and PbI_2—D. L. Greenaway & G. Harbeke (Labs, Pr) Int'l Conf. on the Phys. of Semiconductors, Kyoto, Japan, September 1966

MICROWAVE PHASE SHIFT due to a Magnetoplasma Resonance—R. Hirota, K. Suzuki (Labs, Pr) Kyoto Int'l Conf. on Phys. of Semiconductors, Kyoto, Japan, September 1966

PARAMAGNETIC - RESONANCE ABSORPTION in the Optically Populated State $^2F_{5/2}$ $E_{5/2}$ of Tm^{2+} in CaF_2—E. S. Sabisky, C. H. Anderson (Labs, Pr) *Phys. Review* Vol. 148, No. 1, August 1966

PHOTOEMISSION of Electrons from Metals Into Silicon Dioxide — A. M. Goodman, J. J. O'Neill, Jr. (Labs, Pr) *J. of App. Phys.*, Vol. 37, No. 9, August 1966

RADIATIVE RECOMBINATION TEMPERATURE Behavior in p-n Junctions, Spontaneous and Stimulated—M. F. Lamorte, S. Caplan, T. Gonda (ECD, Som) GaAs Device Conf., Univ. of Reading, England; September 1966

SPACE-CHARGE LIMITED CURRENTS in an MOS System—R. Schilling (Labs, Pr) Conf. on the Phys. of Semiconductor Compounds, Swansea, Wales, September 1966

SPIN-LATTICE RELAXATION Times of Cr^{3+}, Field Dependence of—N. Rumin (RCA Ltd., Montreal) *Can. J. of Phys.*, July 1966

TRANSPORT PHENOMENA In InSb at High Electric and High Magnetic Field—K. Ando (Labs, Pr) *J. of the Phys. Soc. of Japan*, Vol. 21, No. 7; 7/66

TRANSPORT (THERMAL AND ELECTRICAL) in InAs—GaAs Alloys—E. F. Hockings, I. Kudman, T. E. Seidel, C. M. Schmelz, E. F. Steigmeier (Labs, Pr) *J. of App. Phys.*, Vol. 37, No. 7, June 1966

TUNNELING (Microwave Phonon-Assisted) in Superconducting Diodes—B. Abeles, R. W. Cohen (Labs, Pr) 10th Int'l Conf. on Low Temperature Phys., Moscow, August-September 1966

VALANCE BAND of Bismuth-Antimony Alloy—A. Anith (Labs, Pr) Int'l Conf. on the Physics of Semiconductors, Kyoto, Japan, September 1966

PROPERTIES, MOLECULAR (& crystallography)

CIRCULAR DICHROISM in the Absorption Bands of Divalent Rare Earth Ions, Survey of the—C. H. Anderson, H. A. Weakliem (Labs, Pr) Johns Hopkins Conf. on Optical Properties of Ions in Crystals, Baltimore, Maryland, September 1966

CRYSTAL PHASE CHARGE in Phthalocyanines, Conductivity and — S. E. Harrison, K. H. Ludewig (Labs, Pr) *J. of Chem. Phys.* Vol. 45, No. 1, July 1966

ENERGY LEVELS of Ho^{2+} and Tm^{2+} in CaF_2 and $SrCl_2$—Z. J. Kiss, H. A. Weakliem (Labs, Pr) Conf. on Optical Properties of Ions in Crystals, Johns Hopkins Univ., September 1966

LATTICE SOFTENING in Single Crystal Nb_3Sn—K. R. Keller, J. J. Hanak (Labs, Pr) *Phys. Letters*, Vol. 21, No. 3, May 1966

LITHIUM-DEFECT INTERACTION in Silicon by Electron Paramagnetic Resonance Measurements, Direct Observation of—B. Goldstein (Labs, Pr) *Phys. Review Letters*, Vol. 17, No. 8, August 1966

NUCLEATION AND GROWTH of Large Crystals by Chemical Transport. III: Iodine Transport and Sublimation of CdS—E. Kaldis (Labs, Pr) German Chem. Soc., Munich, Germany, October 1966

PHASE TRANSFORMATION of Antimony Triselenide—M. D. Coutts, E. R. Levin (Labs, Pr) 6th Int'l Congress for Electron Microscopy, Kyoto, Japan, September 1966

PRESSURE-SINTERED Gallium Arsenide, Densification Mechanisms of—W. P. Stollar, H. I. Moss (Labs, Pr) Amer. Ceramic Soc. Basic Sci. Div., Univ. Park, Pa., October 1966

PRESSURE SINTERING of GaSb—P. R. Sahm (Labs, Pr) AIME Fall Mtg., Chicago, Ill., October-November 1966

ULTRASONIC MEASUREMENTS in Single Crystal Nb_3Sn—K. R. Keller, J. J. Hanak (Labs, Pr) 10th Int'l Conf. on Low Temperature Phys., Moscow, August-September 1966

PROPERTIES, SURFACE (& thin films)

ANODIC OXIDATION of Silicon, Mechanism of—A. G. Revesz (Labs, Pr) Electrochemical Soc. Mtg., Phila., Pa., October 1966

ANODICALLY OXIDIZED Silicon, Interface Properties of—A. G. Revesz (Labs, Pr) Electrochemical Soc. Mtg., Phila., Pa., October 1966

DECORATION of Semiconductor Surfaces for Electron Microscopy by Displacement of Gold—M. D. Coutts, A. G. Revesz (Labs, Pr) *J. of App. Phys.*, Vol. 37, No. 8, July 1966

DEFECT STRUCTURE on Silicon Surfaces After Thermal Oxidation—A. W. Fisher, J. A. Amick (Labs, Pr) *J. of the Electrochemical Soc.*, Vol. 113, No. 10, October 1966

DEPOSITION (LOW-TEMPERATURE) of Si_3N_4—J. Scott, J. Olmstead (ECD, Som) Electrochemical Soc. Mtg., Phila., Pa., October 1966

ELECTROMAGNETIC BEHAVIOR of Thin-Film Structures—J. Pearl (Labs, Pr) *J. of App. Phys.*, Vol. 37, No. 8, July 1966

SHIELDING PROPERTIES of the Superconducting Surface Sheath—R. Klein, G. Fischer, J. P. McEvoy (Labs, Pr) *Solid State Comm.* Vol. 4, No. 7; July 1966

(SURFACE CONCENTRATION): Nondestructive Measurement of Surface Concentration by Plasma Resonance: (II) P-Type Silicon—L. A. Murray, N. Goldsmith, R. Duclos (ECD, Som) Electrochemical Soc. Mtg., Phila., Pa., October 1966

PROPERTIES, CHEMICAL

BISMUTHIOL II, Improved Procedure for Determining Tellurium with—B. L. Goydish, K. L. Cheng (Labs, Pr) *Talanta*, Vol. 13

CESIUM PRESSURE, The Development of a High-Temperature Reservoir for Automatic Control of—W. E. Harbaugh, A. Basiulis (ECD, Lanc) Thermionic Converter Specialists Conf., Houston, Texas, November 1966

DIVALENT LANTHANIDE IONS as Dilute Solutes in Alkaline Earth Halide Solid Solutions, Preparation and Identification of — P. N. Yocom (Labs, Pr) Amer. Chem. Soc., N.Y.C., September 1966

FRACTIONATION of Antimony Triselenide—A. Efstathiou, D. Hoffman, E. Levin (AED, Pr) 13th Nat'l Vacuum Symp., San Francisco, Calif., October 1966

GAS PERMEATION Studies of Some High-Purity Ceramic Materials—J. A. Fox (ECD, Lanc) Tube Tech. Conf., N.Y.C., September 1966

PURE MATERIALS ANALYSIS, Electrical Measurements for—L. R. Weisberg (Labs, Pr) *Analytical Chemistry*, Vol. 38, No. 1, January 1966

RARE EARTHS in Solid-State Laser Materials, The Determination of—S. J. Adler (Labs, Pr) Symp. on Trace Characterization-Chem. and Phys., Nat'l Bureau of Standards, Washington, D.C., October 1966

SELECTIVE EDTA TITRATION of Gallium or Aluminum in the Presence of Other Metals—K. L. Cheng, B. L. Goydish (Labs, Pr) *Talanta*, Vol. 13

PROPERTIES, ELECTRICAL

CONDUCTANCE AND CAPACITANCE of Metal-Insulator-Semiconductor Diodes or Any Two-Terminal Complex Admittance, Automatic Plotting of—J. Shewchung, A. Waxmann (Labs, Pr) Review of Scientific Instru., Vol. 37, No. 9, September 1966

CONDUCTIVITY and Crystal Phase Change in Phthalocyanines—S. E. Harrison, K. H. Ludewig (Labs, Pr) *J. of Chem. Phys.*, Vol. 45, No. 1, July 1966

CURRENT-CONTROLLED INSTABILITY in GaAs, Infrared and Microwave Radiations Associated with a—S. G. Liu (Labs, Pr) *App. Phys. Letters*, Vol. 7, No. 6, July 1966

C-V CURVES for Metal-Insulator-Semiconductor (MIS) Structures, Automatic Display of—K. H. Zaininger (Labs, Pr) *Proc. of the IEEE* Vol. 54, No. 7, July 1966

DOCTOR-BLADED FERROELECTRIC CERAMICS, Processing Parameters and Electrical Properties of—C. Wentworth, G. W. Taylor (Labs, Pr) West Coast Regional, Amer. Ceramic Soc., Portland, Oregon, October 1966

GALLIUM PHOSPHIDE, Electrical and Optical Properties of High-Resistivity—B. Goldstein, S. S. Perlman (Labs, Pr) *Phys. Review* Vol. 148, No. 2, August 1966

ISOLATION TECHNIQUES for Integrated Circuits—A. I. Stollar, N. E. Wolff (Labs, Pr) Second Int'l Symp. on Microelectronics, Munich, Germany, October 1966

NEUTRON-INDUCED DEFECTS Effects on the Current-Carrying Behavior of Vapor-Deposited Niobium Stannide—G. W. Cullen, R. L. Novak (Labs, Pr) *J. of App. Phys.* Vol. 37, No. 9, August 1966

TAXONOMY OF ELECTRIC CHARGES in Metal-Insulator-Semiconductor Systems—A. G. Revesz (Labs, Pr) *Proc. of the IEEE* Vol. 54, No. 7, July 1966

PROPERTIES, MAGNETIC

DOCTOR-BLADED FERROELECTRIC CERAMICS, Processing Parameters and Electrical Properties of—C. Wentworth, G. W. Taylor (Labs, Pr) West Coast Regional, Amer. Ceramic Soc., Portland, Oregon, October 1966

PINCH INSTABILITY in Magnetic Fields—K. Ando, M. Glicksman (Labs, Pr) Mtg. of the Phys. Soc. of Japan, Niigata, October 1966

PROXIMITY EFFECTS in a Magnetic Field—C. Fischer, R. Klein (Labs, Pr) Swiss Phys. Soc. Mtg., Solothurn, September 1966

PROPERTIES, MECHANICAL

AIR DAMPING EFFECT on Structural Fatigue Failure—J. R. Fagan (AED, Pr) Shock & Vibration Symp., Air Force, Los Angeles, Calif., October 1966; *Conf. Proc.*

PRESSURE SINTERING, Die Design for—H. I. Moss, W. P. Stollar (Labs, Pr) *The Amer. Ceramic Soc. Bulletin*, Vol. 45, No. 9, September 1966

PROPERTIES, OPTICAL

CATHODOLUMINESCENCE of P-Type GaAs—J. I. Pankove (read by M. Glicksman) Int'l Conf. on the Phys. of Semiconductors, Kyoto, Japan, September 1966

DEGRADATION PHENOMENA of Operating Life in Electroluminescent Diodes (GaAs)—M. F. Lamorte, W. Agosto, G. Kupsky, N. Pennucci, H. W. Becke (ECD, Som) GaAs Device Conf., Univ. of Reading, Eng., September 1966

ELECTRON BEAM EXCITATION of Ion Lasers, Mechanisms of—J. M. Hammer, C. P. Wen (Labs, Pr) 6th Int'l Conf. on Microwave & Optical Generation and Amplification, Cambridge Univ., September 1966

ELECTROREFLECTANCE of Barium Titanate—C. Gahwiller (Labs, Pr) Swiss Phys. Soc. Mtg., Solothurn, October 1966

FAR-INFRARED OPTICAL PROPERTIES of Fluoride Crystals—D. R. Bosomworth (Labs, Pr) Molecular Spectroscopy Symp., Columbus, Ohio, September 1966

ORIENTATION EFFECT in GaAs Injection Lasers—M. S. Abrahams, J. I. Pankove (Labs, Pr) *J. of App. Phys.*, Vol. 37, No. 7, June 1966

SILICON NITRIDE, Optical Properties of Deposited—L. A. Murray, J. H. Scott (ECD, Som) Electrochemical Soc. Mtg., Phila., Pa., October 1966

RADAR

ADAPTIVE DETECTION in Clutter—H. M. Finn (MSR, Mrstn) 5th Symp. on Discrete Adaptive Processes; Nat'l Electronics Conf. Proc.

DECOY RADAR SIGNATURES as Obtained by a Variety of Sensors, A Comparison of—A. Gold (MSR, Mrstn), R. S. Raffine (Labs, Pr) AMRAC Proc., October 1966

HYDROSTATIC BEARING for Instrumentation Radar—J. C. Spracklin, G. M. Robinson (MSR, Mrstn) ASME Winter Mtg., New York, 11/66; Pub. in: *Deep Space and Missile Tracking Antennas*, ASME, 12/66

MONOPULSE ANTENNA FEED System, A High-Efficiency Dual-Frequency Multimode—C. E. Profera, L. H. Yorinks (MSR, Mrstn) 1966 IEEE Aerospace & Elec. Sys. Conv., Washington, D.C. October 1966; *Supplement to IEEE Trans. on Aerospace*, Vol. 2, No. 6, November 1966

MONOPULSE RADAR, The Use of "Complex Indicated Angles" to Locate Unresolved Targets in—Dr. S. Sherman (MSR, Mrstn) Nat'l Elec. Conf., Chicago, Ill., October 1966; *Conf. Record*

MONOPULSE RADARS, A Traveling Wave Maser for—S. B. Adler, A. J. Haraburda (MSR, Mrstn) IEEE Aero. & Elec. Sys. Conv., Washington, D.C., October 1966; *Supplement to IEEE Trans. on Aero.*, Vol. 2, No. 6, November 1966

OPTICAL TUNNEL BEAMFORMER for Transmitting Arrays, Experimental Evaluation of an—L. W. Martinson (MSR, Mrstn) 24th U.S. Navy Symp. on Underwater Acoustics, 11/66; *Proc. of the Symp.*

PHASE ARRAY RADAR MAINTENANCE, Application of Queing Theory for—W. J. O'Leary MSR, Mrstn) 1966 Aero. & Elec. Sys. Conv. in Washington, D.C., October 1966; *Supplement to IEEE Trans. on Aero.*, Vol. 2, No. 6, November 1966

RADAR TOWER and Foundation Analysis—P. Pschunder (MSR, Mrstn) ASME Winter Mtg., New York, 11/66; Pub. in: *Deep Space and Missile Tracking Antennas*, ASME, 12/66

RADIATION DETECTION
(& measurement)

PHOTOMULTIPLIER with a Porous Transmission Dynode, Performance of a—H. Smith, J. E. Ruedy, G. A. Morton (ECD, Pr) *IEEE Trans. on Nuclear Sci.*, June 1966

PHOTOMULTIPLIERS, Afterpulses in—G. A. Morton, H. M. Smith, R. Wasserman (ECD, Pr) Nuclear Sci. Symp., Boston, Mass., October 1966

PHOTOMULTIPLIERS (Ceramic-Metal) for Scintillation Counting in Severe Environments—R. M. Matheson, F. A. Helvy (ECD, Lanc) Nuclear Sci. Symp., Boston, Mass., October 1966

PHOTOMULTIPLIERS, Extraneous Light Emission from—H. R. Krall (ECD, Lanc) Nuclear Sci. Symp., Boston, Mass., October 1966

RADIATION EFFECTS

MAGNETIC LOGIC (High-Speed) for Radiation-Resistant Applications—D. Hampel (CSD, Cam) Nat'l Elec. Conf., Chicago, Ill., October 1966; *Conf. Proc.*

MAGNETO-IONIC MEDIA, The "Infinity Catastrophe" Associated with Radiation in—H. Staras (Labs, Pr) *Radio Sci.* Vol. 1, No. 9, September 1966

NEUTRON-INDUCED DEFECTS Effect on the Current-Carrying Behavior of Vapor-Deposited Niobium Stannide—G. W. Cullen, R. L. Novak (Labs, Pr) *J. of App. Phys.*, Vol. 37, No. 9, August 1966

(NUVISTORS): Response of Low-Power Nuvistors to Pulsed Nuclear Radiation—I. F. Stacy, F. J. Feyder (ECD, Som) *RCA Review*, September 1966

OZONE CONCENTRATION at Early Times Subsequent to the Blue Gill Burst, The Computed Modification of the—Dr. K. Sittel (SEER, Mrstn) *Nuclear Weapons Effect Review*, August 1966

SOLAR CELLS, Lithium-Doped Radiation-Resistant Silicon—J. J. Wysocki, P. Rappaport, E. Davison, R. Hand, J. J. Loferski (Labs, Pr) *App Phys. Letters*, Vol. 7, No. 4, July 1966

TEAK ATTENUATION ANOMALY Interpreted by Residue Debris—Dr. K. Sittel (SEER, Mrstn) *Nuclear Weapons Effect Review*, December 1966

RADIO RECEIVERS
(mass-media)

AUDIO AMPLIFIERS, Silicon Transistors in—J. C. Sondermeyer (ECD, Som) Nat'l Elec. Conf., Chicago, Ill., October 1966; *Conf. Record*

AUDIO HI-FI POWER Amplifiers Using Silicon Transistors, Design of—R. D. Gold, J. C. Sondermeyer (ECD, Som) *Electronics World*, September-October-November 1966

STEREOPHONIC LOUDSPEAKERS, Unitized Omnispatial—H. F. Olson (Labs, Pr) Audio Engrg. Soc., October 1966

RECORDING, AUDIO
(equipment)

MAGNETIC TAPE CARTRIDGE and Player, Some Design Considerations of the 8-Track Endless-Loop—L. C. Harlow, H. E. Roys (REC, Indpls) AES Conv., October 1966; *AES Journal*, January 1967

STEREO PHONOGRAPH PICKUPS, High-Frequency Intermodulation Testing of—J. G. Woodward, R. E. Werner (Labs, Pr) Audio Engrg. Soc. Conv., N.Y.C., October 1966

RECORDING, IMAGE
(equipment)

DIELECTRIC TAPE CAMERA System for Meterological Applications—F. J. Bingley (AED, Pr) SMPTE 100th Tech. Conf., October 1966

NIMBUS B Satellite, The Development of a Tape Recorder for the—S. P. Clurman (AED, Pr) 1966 AES Conv., Los Angeles, Calif., October 1966

TAPE RECORDERS, A Paradox in Modern—R. N. Hurst (BCD, Cam) SMPTE Conv., Los Angeles, Calif., October 1966

RELIABILITY
(& quality control)

CONFIGURATION CHANGE CONTROL—G. Offenbacher, D. Gilloly (ASD, Burl) ASQC Mtg., Phila., Pa., November 1965

SAMPLING PLANS (Using)—E. Shecter (AED, Pr) Rutgers Univ., New Brunswick, September 1966

SOLID-STATE DEVICES

AVALANCHE AND TUNNELING Currents in Gallium Arsenide—R. Williams (Labs, Pr) *RCA Review*, Vol. XXVII, No. 3, September 1966

AVALANCHE DIODES, Harmonic Power Output for—S. G. Liu, J. J. Risko (Labs, Pr) 1966 Electron Devices Mtg., Washington, D.C., October 1966

CHARGE RECTIFIERS, Device Applications of—T. F. Dwyer, R. A. Shahbender (Labs, Pr) Nat'l Electronics Conf., Chicago, Ill., October 1966; *Conf. Record*

METAL-INSULATOR-SEMICONDUCTOR (MIS) Structures, Automatic Display of—K. H. Zaininger (Labs, Pr) *Proc. of the IEEE*, Vol. 54, No. 7, July 1966

METAL-INSULATOR-SEMICONDUCTOR Systems, Taxonomy of Electric Charges in—A. G. Revesz (Labs, Pr) *Proc. of the IEEE*, Vol. 54, No. 7, July 1966

MIS CAPACITANCE VS. BIAS Characteristics, Automatic Display of—K. H. Zaininger (Labs, Pr) *RCA Review*, Vol. XXVII, No. 3, September 1966

MODULATORS, Gallium-Arsenide Electro-Optics—T. E. Walsh (ECD, Pr) *RCA Review*, Vol. XXVII, No. 3, September 1966

MOS DEVICES, Small-Signal RF Amplification of—F. M. Carlson, E. F. McKeon (ECD, Som) Nat'l Elec. Conf., Chicago, Ill., October 1966; *Conf. Record*

MOS TETRODE, High-Frequency Characteristics of the—M. M. Mitchell, N. Ditrick, R. Dawson (ECD, Som) NEREM, Boston, Mass., November 1966; *NEREM Digests*, November 1966

NONDESTRUCTIVE SECOND-BREAKDOWN TESTING, Detection Techniques for—P. Schiff, R. L. Wilson (ECD, Som) *IEEE Trans. on Electron Devices*, November 1966

OSCILLATOR, CW Three-Terminal GaAs—K. Petzinger, A. Hahn, A. Matzelle (Labs, Pr) IEEE Conf., Electron Devices, Washington, D.C., October 1966

PARAMETRIC AMPLIFIER (SELF-PUMPED), The Avalanche Transit-Time Diode as a—A. S. Clorfeine (Labs, Pr) IEEE Int'l Conf., Elec. Devices, Washington, D.C., October 1966

POWER-AMPLIFICATION-BANDWIDTH PRODUCT of an Active Device, Physical Significance of the—E. O. Johnson (ECD, Hr) *Proc. of the IEEE* (Correspondence), October 1966

SOLID-STATE SOURCES—F. Sterzer (ECD, Pr) IEEE Panel Discussion, Boston, Mass., September 1966

TRANSISTOR (THIN FILM), An Adaptive—S. S. Perlman, K. H. Ludewig (Labs, Pr) 1966 IEEE Int'l Conf., Electronic Devices, Washington, D.C., October 1966

(TRANSISTORS): Design of Silicon Transistors for UHF Applications—H. S. Veloric, R. Johnson, W. Bailey (ECD, Som) NEREM, Boston, Mass., November 1966; *NEREM Digests*, November 1966

TRANSISTORS (DOUBLE-DIFFUSED): Emitter Sidewall Junction Capacitance in—N. Rumin, H. Lawrence (RCA Ltd., Montreal) *Proc. IEEE*, Vol. 54, No. 11, November 1966

TRANSISTORS, GaAs Insulated-Gate Field-Effect—H. W. Becke, J. P. White (ECD, Som) GaAs Device Res. Conf., Univ. of Reading, Eng., September 1966

TRANSISTORS (MOS), TV Applications of RCA—D. M. Griswold, W. M. Austin, W. M. Dean, O. P. Hart (ECD, Som) Nat'l Elec. Conf., Chicago, Ill., October 1966; *Conf. Record*

TRANSISTORS (THIN FILM), Recent Advances in—R. L. Schelhorn, M. L. Topfer (DME, Som) 2nd Int'l Microelectronics Symp., Munich, Germany, October 1966; *Conf. Proc.*

TRANSISTORS (THIN FILM), Stability of—J. J. Fabula, R. L. Schelhorn, M. L. Topfer (DME, Som) 5th Ann. Symp. Phys. of Failure, Elec., Dayton, Ohio, November 1966; *Conf. Proc.*

VARACTOR SELECTION for Voltage Tuning—D. J. Blattner (ECD, Pr) *Elec. Comm.*, September-October 1966

(VARACTORS): A Comparison of the Theoretical and Observed Cutoff Frequency of High-Voltage GaAs Varactors—G. Kupsky, H. Kressel (ECD, Som) *Proc. of the IEEE (Correspondence)*, September 1966

SPACE COMMUNICATION
(mass-media & scientific)

DATA ABBREVIATION to Actual Range Telemetry Data, A Report on the Application of—N. Maestre (MSR, Mrstn) Int'l Telemetering Conf., Los Angeles, October 1966; 1966 *ITC Proc.*

DIPOLE ANTENNA IMPEDANCE Measurements in an Isotropic Laboratory Plasma—K. A. Graf, D. Jassby (RCA Ltd., Montreal) Amer. Phys. Soc., Div. of Plasma Phys. Ann. Mtg., Boston, November 1966

HIGH-POWER AMPLIFIERS in Satellite Communications Systems—G. M. Koch (RCA Ltd., Montreal) 6th Int'l Conf. on Microwave Generation & Amplification Univ. of Cambridge, Eng., September 1966

ISIS-A TELEMETRY and Command System—L. A. Keyes, P. T. Caden et al (RCA Ltd., Montreal) IEEE Can. Symp. on Comm., Montreal, October 1966

MICROWAVE BRANCHING NETWORKS for Surface and Space Communication Systems—M. V. O'Donovan, J. A. S. Hansen, N. K. M. Chitre (RCA Ltd., Montreal) IEEE Can. Symp. on Comm., Montreal, October 1966

OPTIMUM CODE WORD ASSIGNMENT to Telemetry Data by Integer Programming—P. Hahn (MSR, Mrstn) 4th Can. Symp. on Comm., Montreal, Canada, October 1966

PCM TELEMETRY Burst Retransmission Format, Design of a—H. W. Trigg (MSR, Mrstn) 1966 Aero. & Elec. Sys. Conv., Washington, D. C., October 1966; *Supplement to IEEE Trans. on Aero.*, Vol. 2, No. 6, November 1966

PLASMA SHEATH (V-B INDUCED) Formed Around a Satellite, An Experiment on the—F. J. F. Osborne, M. A. Kasha (RCA Ltd., Montreal) Amer. Phys. Soc., Div. of Plasma Phys., Ann. Mtg., Boston, November 1966

SATELLITE-PLASMA INTERACTION in the Labo- Pr) IEEE 16th Broadcast Symp., Washington, D.C., September 1966; *Conf. Proc.*

SATELLITE-PLASMA INTERACTION in the Laboratory, Simulation of—T. W. Johnston, M. A. Kasha (RCA Ltd., Montreal) Amer. Phys. Soc., Div. of Plasma Phys. Ann. Mtg., Boston, November 1966

SPACEPORT COMMUNICATIONS—Present and Future—B. E. Keiser (SvcCo, Kennedy Space Ctr., Florida) Nat'l Elec. Conf., Chicago, October 1966; *Conf. Record*

TV SATELLITE Systems—S. Gubin (AED, Pr) Engineers Club, Phila., Pa., October 1966

SPACE ENVIRONMENT

MOON, Layman's Journey to the—C. Drewery (CSD, Cam) Willowdale Civic Assoc., Erlton, November 1966

SPACE NAVIGATION
(& tracking)

ADAPTIVE DETECTION in Clutter—H. M. Finn (MSR, Mrstn) 5th Symp. on Discrete Adaptive Processes; Nat'l Elec. *Conf. Proc.*

DECOY RADAR SIGNATURES as Obtained by a Variety of Sensors, A Comparison of—R. S. Raffine (Labs, Pr) A. Gold (MSR, Mrstn) *AMRAC Proc.*, October 1966

DIELECTRIC TAPE CAMERA System for Meteorological Applications—F. J. Bingley (AED, Pr) SMPTE 100th Tech. Conf., October 1966

UNRESOLVED TARGETS in Monopulse Radar, to Locate the Use of "Complex Indicated Angles"—Dr. S. Sherman (MSR, Mrstn) Nat'l Elec. Conf., Chicago, Ill., October 1966; *Conf. Proc.*

SPACECRAFT
(& space missions)

APOLLO Lunar Mission Profile—D. P. Campbell (CSD, Cam) Springmill School, Whitemarsh, Pa., November 1966

ENGINEERING ASSIGNMENTS in the Space Program—T. E. Kupfrian (ASD, Burl) Symp. on Aerospace Computers, October 1966, Santa Monica, Calif.

GEMINI II, The Flight of—D. P. Campbell (CSD, Cam) Chestnut Hill Academy, Phila., Pa., November 1966

LEM RENDEZVOUS, Design Maturity Demonstration of the—M. Weiss (MSR, Mrstn) ASME Winter Mtg., New York, 11/66; Pub. in: *Research Simulation*, ASME, 12/66

MANAGEMENT DECISIONS on the Way to the Moon—F. J. Gardiner (ASD, Burl) Soc. for Advancement of Management, Boston Univ., November 1966

SATELLITE METEOROLOGY and the World Weather Watch—L. Krawitz (AED, Pr) Earth Sci. Section N.J. Teachers Assoc., Atlantic City, N.J., November 1966

SPACECRAFT INSTRUMENTATION

AIRBORNE TV DISPLAYS, Human Factors in—B. Hillmann (ASD, Burl) Soc. for Info. Display, Boston; October 1966

MICROELECTRONICS in the ESSA II Satellite—R. Callais (AED, Pr) 2nd Int'l Symp. on Microelectrons, Munich, Germany, October 1966; *Conf. Proc.*

MONOLITHIC FERRITE MEMORY for Space—R. Ricci, P. Truscello (AED, Pr) Nat'l Elec. Conf., Chicago, Ill., October 1966; *Conf. Proc.*

MONOPULSE ANTENNA FEED System, A High-Efficiency Dual-Frequency Multimode—C. E. Profera, L. H. Yorinks (MSR, Mrstn) 1966 IEEE Aero. & Elec. Sys. Conv., Washington, D.C., October 1966; *Supplement to IEEE Trans. on Aero.*, Vol. 2, No. 6, November 1966

POWER SYSTEMS for Space—G. Barna (AED, Pr) Naval Reserve Research Co., Princeton, 4-1, September 1966

RETURN BEAM VIDICON, Space Applications of the—J. Dishler, P. Godfrey (AED, Pr) SMPTE 100th Tech. Conf., Los Angeles, Calif., October 1966; *Conf. Proc.*

SPACECRAFT ANTENNA ARRAY, A Novel—W. T. Patton (MSR, Mrstn) Dallas Chapter, IEEE. Also: WESCON 1966, Los Angeles, Calif., August 1966; *Conv. Record*

TAPE RECORDER for the Nimbus B Satellite, The Development of a—S. P. Clurman (AED, Pr) 1966 AES Conv., Los Angeles, Calif., October 1966

SUPERCONDUCTIVITY
(& cryoelectrics)

LARGE-BORE HIGH-FIELD MAGNETS, The Use of Superconductors with Varied Characteristics for the Optimized Design of—E. R. Schrader, P. A. Thompson (ECD, Hr) *IEEE Trans. on Magnetics*, September 1966

NEUTRON-INDUCED DEFECTS Effect on the Current-Carrying Behavior of Vapor-Deposited Niobium Stannide—G. W. Cullen, R. L. Novak (Labs, Pr) *J. of App. Phys.* Vol. 37, No. 9, August 1966

NIOBIUM-TIN MAGNETS, Technology of—E. R. Schrader (ECD, Hr) URSI Conf., Munich, Germany, September 1966

SUPERCONDUCTING CONTACTS, New Effect at—J. I. Pankove (Labs, Pr) *Phys. Letters* Vol. 21, No. 4, June 1966

TUNNELING (Microwave Phonon-Assisted) in Superconducting Diodes—B. Abeles, R. W. Cohen (Labs, Pr) 10th Int'l Conf. on Low Temperature Physics, Moscow, August-September 1966

VORTEXES are Creating a Stir in the Superconducting Field—J. Pearl (Labs, Pr) *Electronics*, Vol. 39, No. 12, June 1966

TELEVISION BROADCASTING
(mass-media)

COLOR FILM for Color TV, Processing and Utilization of—Dr. H. N. Kozanowski (BCD, Cam) IEEE 16th Broadcast Symp., Washington, D.C., September 1966

SATELLITE BROADCASTING—S. Gubin (AED, Pr) IEEE 16th Broadcast Symp., Washington, D.C., September 1966; *Conf. Proc.*

TAPE RECORDERS, A Paradox in Modern—R. N. Hurst (BCD, Cam) SMPTE Conv., Los Angeles, California, October 1966

VIDEO SWITCHERS, New Techniques in Transition Control of—W. L. Hurford (BCD, Cam) IEEE 16th Broadcast Symp., Washington, D.C., September 1966

TELEVISION EQUIPMENT
(non-mass-media)

AIRBORNE TV DISPLAYS, Human Factors in—B. Hillmann (ASD, Burl) Soc. for Info. Display, Boston, October 1966

DIELECTRIC TAPE CAMERA System for Meteorological Applications—F. J. Bingley (AED, Pr) SMPTE 100th Tech. Conf., October 1966

(ELECTRON MICROSCOPE TV DISPLAYS: On the Possible Use of Data Correlation Techniques for Extracting Phase Contrast Information from TV-Displayed Electron Microscope Images—Dr. J. W. Coleman, J. M. Gottschalk (BCD, Cam) EMSA, San Francisco, Calif., August 1966

ELECTRONIC ZOOM for Varying Raster Size—R. C. Kee, D. F. Dion (ASD, Burl) 11th SPIE Tech. Symp., St. Louis, August 1966; *Symp. Minutes*

RETURN BEAM VIDICON, Space Applications of the—J. Dishler, P. Godfrey (AED, Pr) SMPTE 100th Tech. Conf., Los Angeles, Calif., October 1966; *Conf. Proc.*

TELEVISION SENSOR PANEL, Development of a Thin-Film Solid-State Line-Scan—R. Callais (AED, Pr) 1966 Int'l Electron Devices Mtg., Washington, D.C., October 1966

TV SATELLITE Systems—S. Gubin (AED, Pr) Engrs. Club, Phila., Pa., October 1966

VIDICON PERFORMANCE in Extreme Thermal Environments—R. E. Johnson (ECD, Lanc) *RCA Review*, Vol. XXVII, No. 3, September 1966

TELEVISION RECEIVERS
(mass-media)

AUDIO AMPLIFIERS, Silicon Transistors in—J. C. Sondermeyer (ECD, Som) Nat'l Elec. Conf., Chicago, Ill., October 1966; *Conf. Record*

RF AND IF STAGES in TV Receivers, A Comparison of State-of-the-Art Devices for—S. Reich, L. Baar (ECD, Som) Nat'l Elec. Conf., Chicago, Ill., October; *Conf. Proc.*

SYNC TUBE and Circuit, A New Video and Noise-Immune—T. E. Deegan, E. Kashork (ECD, Som) Nat'l Elec. Conf., Chicago, Ill., October 1966; *Conf. Record*

TRANSISTORIZED COLOR TV Receiver, A Developmental 15-inch—W. E. Babcock (ECD, Som) *IEEE Trans. on Broadcast & TV Receivers*, July 1966

TRANSISTORIZED TV RECEIVER, An AC/DC Line-Operated—C. F. Wheatley (ECD, Som) Nat'l Elec. Conf., Chicago, Ill., October 1966; *Conf. Record*

TRANSISTORS (MOS), TV Applications of RCA—D. M. Griswold, W. M. Austin, W. M. Dean, O. P. Hart (ECD, Som) Nat'l Elec. Conf., Chicago, Ill., October 1966; *Conf. Record*

TRANSMISSION LINES
(& waveguides)

MICROSTRIP TRANSMISSION LINES for Microwave Integrated Circuits, Measurements on the Properties of—M. Caulton, J. J. Hughes, H. Sobol (Labs, Pr) *RCA Review* Vol. XXVII, No. 3, September 1966

WAVEGUIDES with a Semiconductor Side Wall, Characteristics of—R. D. Larrabee (Labs, Pr) *IEEE Trans. on Microwave Theory and Tech.* Vol. MTT-14, No. 7, July 1966

TUBES, ELECTRON
(design & performance)

GRID-CONTROLLED TUBES in Phased-Array Transmitter Modules, The Application of—M. V. Hoover (ECD, Lanc) IEEE Electron Devices Mtg., Wash., D.C., October 1966

KLYSTRON OUTPUT CAVITY, A Theoretical and Experimental Analysis on a Double-Gap π-Mode-Operated—C. Sun (ECD, Pr) IEEE Elec. Devices Mtg., Washington, D.C., October 1966

PHOTOMULTIPLIER with a Porous Transmission Dynode, Performance of a—H. Smith, J. E. Ruedy, G. A. Morton (ECD, Pr) *IEEE Trans. on Nuclear Sci.*, June 1966

PHOTOMULTIPLIERS, Afterpulses in—G. A. Morton, H. M. Smith, R. Wasserman (ECD, Pr) Nuclear Science Symp., Boston, Mass., October 1966

PHOTOMULTIPLIERS (Ceramic-Metal) for Scintillation Counting in Severe Environments—R. M. Matheson, F. A. Helvy (ECD, Lanc) Nuclear Sci. Symp., Boston, Mass., October 1966

PHOTOMULTIPLIERS, Extraneous Light Emission from—H. R. Krall (ECD, Lanc) Nuclear Science Symp., Boston, Mass., October 1966

TRAVELING-WAVE TUBES: Can They be Scaled?—M. J. Schindler (ECD, Hr) *The Microwave Journal*, October 1966

VIDICON PERFORMANCE in Extreme Thermal Environments—R. E. Johnson (ECD, Lanc) *RCA Review*, Vol. XXVII, No. 3, September 1966

TUBE COMPONENTS
(materials & fabrication)

BRAZED CATHODE Construction for Color Picture Tubes—C. H. Mattson (ECD, Lanc) Tube Techniques Conf., N.Y.C., September 1966

GAS PERMEATION Studies of Some High-Purity Ceramic Materials—J. A. Fox (ECD, Lanc) Tube Techniques Conf., N.Y.C., September 1966

MASS SPECTROMETRY in the Manufacture of Color Television Tubes, Chemical Applications of—J. J. Moscony (ECD, Lanc) LaSalle College Sem., Phila., Pa., November 1966

NONDESTRUCTIVE SECOND-BREAKDOWN TESTING, Detection Techniques for—P. Schiff, R. L. Wilson (ECD, Som) *IEEE Trans. on Elec. Devices*, November 1966

PHOSPHORS for Color TV—A. L. Smith (ECD, Lanc) Reading Chemists Club, Pa., October 1966

VACUUM
(techniques)

VACUUM PHYSICS and Space Simulation—J. T. Mark (ECD, Lanc) High-School Sci. Sem., Clearfield, Pa., November 1966

AUTHOR INDEX

Subject listed opposite each author's name indicates where complete citation to his paper may be found in the subject index. Where an author has more than one paper, his name is repeated for each.

DEFENSE MICROELECTRONICS

Borkan, H. circuits, integrated
Fabula, J. J. circuits, integrated
Rapp, A. K. circuits, integrated
Schelhorn, R. L. circuits, integrated
Schelhorn, R. L. circuits, integrated
Topfer, M. L. circuits, integrated
Topfer, M. L. circuits, integrated
Wennik, L. P. circuits, integrated

RCA SERVICE COMPANY

Keiser, B. E. space communication

ELECTRONIC DATA PROCESSING

Smoliar, G. computer applications

RCA VICTOR RECORD DIVISION

Harlow, L. C. recording, audio
Roys, H. E. recording, audio

SYSTEMS ENGINEERING, EVALUATION, AND RESEARCH

Sittel, Dr. K. electromagnetic warfare

GRAPHIC SYSTEMS DIVISION

Greenberg, J. S. computer applications
Greenberg, J. S. computer applications
Greenberg, J. S. graphic arts

BROADCAST AND COMMUNICATIONS PRODUCTS DIVISION

Coleman, Dr. J. W. displays
Connor, D. C. acoustics
Gottschalk, J. M. displays
Hurford, W. L. communications components
Hurst, R. N. recording, image
Kozanowski, Dr. H. N. television broadcasting
Libbey, R. L. laboratory equipment
Schacht, W. energy conversion

MISSILE AND SURFACE RADAR DIVISION

Adler, S. B. masers
Dong, Y. H. mechanical devices
Field, G. R. management
Finn, H. M. radar
Finn, H. M. electromagnetic waves
Gold, A. radar
Hahn, P. communication, digital
Haraburda, A. J. masers
Johnson, R. S. electromagnetic waves
Maestre, N. computer applications
L. W. Martinson, antennas
Murakami, T. communications components
O'Leary, W. J. antennas
Patton, Dr. W. T. antennas
Profera, C. E. antennas
P. Pschunder, mechanical devices
Raffine, R. S. radar
G. M. Robinson, mechanical devices
Sherman, Dr. S. radar
J. C. Spracklin, mechanical devices
Trigg, H. W. communication, digital
M. Weiss, spacecraft
Yorinks, L. H. antennas

ASTRO-ELECTRONICS DIVISION

Baran, A. S. environmental engineering
Barna, G. energy conversion
Bingley, F. J. recording, image
Bisignani, W. communication, digital
Callais, R. television equipment
Callais, R. circuits, integrated
Clurman, S. P. recording, image
Curry, R. information theory
Dishler, J. spacecraft instrumentation
Efstathiou, A. properties, chemical
Fagan, J. R. mechanical devices
Fagan, J. R. environmental engineering
Flory, L. E. medical electronics
Godfrey, P. spacecraft instrumentation
Gubin, S. space communication
Gubin, S. space communication
Hendel, H. plasma physics
Hendel, H. plasma physics
Hoffman, D. properties, chemical
Krawitz, L. spacecraft
Levin, E. properties, chemical
Marshall, T. circuit analysis
Ricci, R. computer storage
Rosenberg, L. documentation
Shecter, E. reliability
Truscello, P. computer storage

AEROSPACE SYSTEMS DIVISION

DiMarzio, A. circuits, packaged
Dion, D. F. television equipment
Dobson, D. B. documentation
Gardiner, F. J. management
Gilloly, D. management
Guay, P. mechanical devices
Hassett, R. P. computers, programming
Hassett, R. computer components
Hassett, R. computer components
Hillmann, B. aircraft instruments
Joyce, B. checkout
Kee, R. C. television equipment
Kupfrian, T. E. management
Liguori, F. E. checkout
Miller, E. computer components
Miller, E. H. computers, programming
Offenbacher, G. management
Okoomian, H. electromagnetic waves
Spence, A. computers, programming
Stockton, E. checkout
Toscano, P. M. checkout
Turkington, R. E. checkout

COMMUNICATIONS SYSTEMS DIVISION

Altgilbers, T. E. documentation
Bell, W. F. communication, digital
Buchsbaum, W. H. bionics
Campbell, D. P. spacecraft
Campbell, D. P. spacecraft
Davis, G. communications systems
Drewery, C. space environment
Ficchi, R. F. education
Fields, C. W. human factors
Hampel, D. logic elements
Heizer, J. T. circuits, integrated
Kurzrok, R. M. filters, electric
Kurzrok, R. M. filters, electric
Kurzrok, R. M. filters, electric
Levy, A. circuits, packaged
Parkinson, W. A. management
Pan, Dr. W. Y. energy conversion
Pan, Dr. W. Y. circuits, integrated
Pan, Dr. W. Y. circuits, integrated
Rezek, G. circuits, packaged
Shore, D. management
Stambler, L. communications systems
Tomko, E. J. communications systems

RCA VICTOR COMPANY, LTD.

Bachynski, M. P. plasma physics
Bachynski, M. P. plasma physics
Bachynski, M. P. plasma physics
Caden, P. T. space communication
Chitre, N. K. M. communications components
Gibbs, B. W. plasma physics
Gibbs, B. W. plasma physics
Graf, K. A. antennas
Hansen, J. A. S. communications components
Jassby, D. antennas
Johnston, T. W. mathematics
Johnston, T. W. plasma physics
Kasha, M. A. plasma physics
Kasha, M. A. plasma physics
Keyes, L. A. space communication
Koch, G. M. amplification
Lawrence, H. solid-state devices
O'Donovan, M. V. communications components
Osborne, F. J. F. plasma physics
Osborne, F. J. F. plasma physics
Rumin, N. properties, atomic
Rumin, N. solid-state devices
Shek, S. filters, electric
Slaven, L. filters, electric
Szirtes, T. antennas
Szirtes, T. antennas
Szirtes, T. mechanical devices

ELECTRONIC COMPONENTS AND DEVICES

Agosto, W. displays
Austin, W. M. solid-state devices
Baar, L. television receivers
Babcock, W. E. television receivers
Bailey, W. solid-state devices
Basiulis, A. energy conversion
Basiulis, A. energy conversion
Basiulis, A. energy conversion
Becke, H. W. solid-state devices
Becke, H. W. displays
Blattner, D. J. communications components
Buzzard, R. J. energy conversion
Buzzard, R. J. energy conversion
Caplan, S. properties, atomic
Carlson, F. M. amplification
Dawson, R. solid-state devices
Dean, W. M. solid-state devices
Deegan, T. E. television receivers
Ditrick, N. solid-state devices
Duclos, R. properties, surface
Engstrom, R. W. human factors
Ernst, D. M. energy conversion
Ernst, D. M. energy conversion
Feyder, F. J. radiation effects
Feyder, F. J. radiation effects
Fox, J. A. properties, chemical
Gold, R. D. amplification
Goldsmith, N. properties, surface
Gonda, T. properties, atomic
Griswold, D. M. solid-state devices
Hall, W. B. energy conversion
Hanchett, G. D. computer components
Harbaugh, W. E. energy conversion
Harbaugh, W. E. energy conversion
Hart, O. P. solid-state devices
Helvy, F. A. radiation detection
Hoover, M. V. communications components
Jacoby, B. A. circuits, integrated
Johnson, E. O. solid-state devices
Johnson, R. solid-state devices
Johnson, R. E. television equipment
Kalish, I. H. circuits, integrated
Kashork, E. television receivers
Kessler, S. W. energy conversion
Krall, H. R. radiation detection
Kressel, H. solid-state devices
Kupsky, G. displays
Kupsky, G. solid-state devices
Lamorte, M. F. displays
Lamorte, M. F. properties, atomic
Longsderff, R. W. energy conversion
Lozier, G. S. energy conversion
McKeon, E. F. amplification
Mark, J. T. vacuum
Matheson, R. M. radiation detection
Mattson, C. H. tube components
Medwin, A. H. circuits, integrated
Mendelson, R. M. communications components
Mendelson, R. M. communications components
Mitchell, M. M. solid-state devices
Morhart, R. F. management
Morton, G. A. radiation detection
Morton, G. A. radiation detection
Moscony, J. J. laboratory equipment
Murray, L. A. properties, optical
Murray, L. A. properties, surface
Olmstead, J. properties, surface
Pennucci, N. displays
Pollack, R. H. circuits, integrated
Reich, S. television receivers
Ruedy, J. E. radiation detection
Sanquini, R. L. circuits, integrated
Schiff, P. solid-state devices
Schindler, H. C. electromagnets
Schindler, M. J. tubes, electron
Schrader, E. R. electromagnets
Schrader, E. R. electromagnets
Scott, J. H. properties, optical
Scott, J. properties, surface
Shefsiek, P. K. energy conversion
Shefsiek, P. K. energy conversion
Shefsiek, P. K. energy conversion
Smith, A. L. two components
Smith, H. radiation detection
Smith, H. M. radiation detection
Sondermeyer, J. C. amplification
Sondermeyer, J. C. amplification
Stacy, I. F. radiation effects
Stacy, I. F. radiation effects
Sterzer, F. solid-state devices
Sun, C. tubes, electron
Thompson, P. A. electromagnets
Turner, R. C. energy conversion
Veloric, H. S. solid-state devices
Vonderschmitt, B. V. circuits, integrated
Walsh, T. E. electro-optics
Walsh, T. E. electro-optics
Wasserman, R. radiation detection
Wheatley, C. F. television receivers
White, J. P. solid-state devices
Wilson, R. L. solid-state devices

RCA LABORATORIES

Abeles, B. properties, atomic
Abrahams, M. S. lasers
Adler, S. J. lasers
Amick, J. A. properties, surface
Amith, A. properties, atomic
Anderson, C. H. properties, atomic
Anderson, C. H. properties, atomic
Ando, K. properties, atomic
Ando, K. plasma physics
Belar, H. communication, voice
Bosomworth, D. R. properties, optical
Caulton, M. circuits, packaged
Cheng, K. L. properties, chemical
Cheng, K. L. properties, chemical
Clorfeine, A. S. amplification
Cohen, R. W. properties, atomic
Coutts, M. D. properties, molecular
Coutts, M. D. properties, surface
Cullen, G. W. properties, electrical
Davison, E. energy conversion
Dousmanis, G. C. lasers
Dwyer, T. F. energy conversion
Fischer, G. properties, magnetic
Fischer, G. properties, surface
Fisher, A. W. properties, surface
Gahwiller, C. properties, atomic
Glicksman, M. plasma physics
Goldstein, B. properties, molecular
Goldstein, B. properties, electrical
Goodman, A. M. properties, atomic
Gorog, I. lasers
Goydish, B. L. properties, chemical
Goydish, B. L. properties, chemical
Greenaway, D. L. properties, atomic
Greenaway, D. L. properties, atomic
Gross, H. E. lasers
Hahn, A. communications components
Hammer, J. M. lasers
Hanak, J. J. properties, molecular
Hanak, J. J. properties, molecular
Hand, R. energy conversion
Harbeke, G. properties, atomic
Harrison, S. E. properties, molecular
Herzog, G. B. computer components
Hirota, R. properties, atomic
Hockings, E. F. properties, atomic
Honig, R. E. laboratory equipment
Honig, R. E. laboratory equipment
Honig, R. E. laboratory equipment
Hughes, J. J. circuits, packaged
Kaldis, E. properties, molecular
Keller, K. R. properties, molecular
Kiss, Z. J. properties, atomic
Klein, R. properties, surface
Klein, R. properties, magnetic
Klein, R. properties, atomic
Kudman, I. properties, atomic
Kudman, I. properties, atomic
Larrabee, R. D. transmission lines
Lechner, B. J. displays
Levin, E. R. properties, molecular
Liu, S. G. properties, atomic
Liu, S. G. energy conversion
Loferski, J. J. energy conversion
Lohman, R. D. circuits, integrated
Ludewig, K. H. circuits, integrated
Ludewig, K. H. properties, molecular
McEvoy, J. P. properties, surface

Patents Granted

TO RCA ENGINEERS

As Reported By RCA Domestic Patents, Princeton

RCA VICTOR HOME INSTRUMENTS

RCA LABORATORIES

(Editor's Note: Because of space limitations, a number of new patents could not be included; they will be listed in the next issue.)

COMMUNICATIONS SYSTEMS DIVISION

Arc Lamp Exhaust Flue—C. Lauxen, J. B. Long, Jr. (CSD, Cam) U.S. Pat. 3,278,790, October 11, 1966 (assigned to U.S. Gov't)

Computer System—M. Rosenblatt, D. E. Williams (CSD, Cam) U.S. Pat. 3,287,705, November 22, 1966

Information Translating Apparatus—E. D. Simshauser, R. M. Carrell (CSD, Cam) U.S. Pat. 3,286,029, November 15, 1966

Fluid Supported Apparatus—A. L. Witchey (CSD, Cam) U.S. Pat. 3,283,084, November 1, 1966

Electrostatic Web Feeding Apparatus—R. C. Hansen, M. L. Levene (CSD, Cam) U.S. Pat. 3,273,774, September 20, 1966

Character Recognition System Including Circuits for Locating Characters and Circuits for Discriminating Against Noise—S. Klein (CSD, Cam) U.S. Pat. 3,274,550, September 20, 1966

Digital Crosspoint Switch—R. C. Stiefel (CSD, N.Y.) & H. W. Townsend (Bell Labs) U.S. Pat. 3,263,030, July 26, 1966

ELECTRONIC DATA PROCESSING

Electronic Circuit Producing Pulse Sequences of Different Rates—R. A. Rodner (EDP, Fla) U.S. Pat. 3,290,606, December 6, 1966

Character Reader Utilizing Stroke and Cavity Detection for Recognition of Characters—J. M. Bailey, Jr., R. L. Adams, J. Agin (EDP, Cam) U.S. Pat. 3,290,650, December 6, 1966

Electronic Computer with Interrupt Facility—J. F. Callahan, R. D. Smith, R. H. Yen (EDP, Cam) U.S. Pat. 3,290,658, December 6, 1966

Read-Only Magnetic Memory—C. Y. Hsueh, H. P. Cichon (EDP, Cam) U.S. Pat. 3,290,-664, December 6, 1966

Information Handling Apparatus Including Time Sharing of Plural Addressable Peripheral Device Transfer Channels—B. E. Patrusky (EDP, Cam) U.S. Pat. 3,283,306, November 1, 1966

Adjustable Size Document Stacker—T. J. Misbin (EDP, Cam) U.S. Pat. 3,281,147, October 25, 1966

Multiplier Having Adder and Complementer Controlled by Multiplier Digit Comparator—R. H. Yen (EDP, Cam) U.S. Pat. 3,278,731, October 11, 1966

Exclusive-or Circuit Employing Negative Resistance Diodes—M. Cooperman (EDP, Cam) U.S. Pat. 3,278,762, October 11, 1966

Logic Circuits—M. Silverberg (EDP, Cam) U.S. Pat. 3,274,398, September 20, 1966

Trigger Circuit—A. S. Sheng (EDP, Cam) U.S. Pat. 3,274,399, September 20, 1966

Electronic Clock—M. F. Kaminsky (EDP, Cam) U.S. Pat. 3,284,715, November 8, 1966

Logic Circuits Utilizing Transistor as Level Shift Means—A. I. Pressman (EDP, Cam) U.S. Pat. 3,283,180, November 1, 1966

NATIONAL BROADCASTING COMPANY

Signal Transmission and Reception System Comprising Frequency Modulated Light Beam—J. L. Hathaway (NBC, N.Y.) U.S. Pat. 3,284,633, November 8, 1966

Meetings

JAN. 23-27, 1967: **Conference on Acoustic Noise & Its Control**, London, England, IEEE, U.K. Eire Section, et al, **Program Info.:** IEEE 345 E. 47th St. N.Y., N.Y. 10017.

JAN. 29-FEB. 3, 1967: **Winter Power Meeting**, G-P, Statler Hilton Hotel, New York. **Prog. Info.:** E. C. Day, IEEE, 345 E. 27th St., N.Y., N.Y. 10017.

FEB. 7-9, 1967: **Winter Convention on Aerospace & Electronic Systems**, G-AES, L.A. District, International Hotel, Los Angeles, Calif. **Prog. Info.:** M. R. Currie, Hughes Res. & Dev., Culver City California.

FEB. 15-17, 1967: **Int'l Solid State Circuits Conference**, G-CT, Phila. Section, Univ. of Penn. Sheraton Hotel, Philadelphia, Pa. **Prog. Info.:** J. S. Mayo, Bell Tel. Labs Room 3F332, Holmdel, New Jersey.

MARCH 1-3, 1967: **U.S. National Particle Accelerator Conference**, G-NS et al, Shoreham Hotel, Washington, D.C. **Prog. Info.:** J. A. Martin, Oak Ridge Nat'l Lab., P.O. Box X Oak Ridge, Tennessee 37830.

MARCH 20-22, 1967: **Physical Process in the Lower Atmosphere**, U. of Michigan American Meteorological Soc. **Prog. Info.:** A. X. Wiin-Nielsen, Meteorology and Oceanography Dept., U. of Michigan, 2038 East Engineering Bldg., Ann Arbor, Mich.

MARCH 20-23, 1967: **IEEE International Convention & Exhibition**, All Groups & TAB Comms., Coliseum & N.Y. Hilton Hotel, N.Y., N.Y. **Prog. Info.:** IEEE Hdqs. 345 E. 47th St., N.Y., N.Y. 10017.

APR. 5-7, 1967: **Int'l Magnetics Conference (INTERMAG)** G-Mag, Shoreham Hotel, Wash., D.C. **Prog. Info.:** R. F. Elfant, IBM, Yorktown Heights, N.Y.

APR. 11-13, 1967: **Cleveland Electronics Conference**, Cleveland Section et al, Cleveland Engrg. Center, Cleveland, Ohio. **Prog. Info.:** Mike Lapine, Cleveland Elec. Conf. Inc., 616 Hanna Bldg., Cleveland, Ohio 44115.

APR. 17-19, 1967: **Region 3 Meeting**, Region 3, Heidelberg Hotel, Jackson, Miss. **Prog. Info.:** J. E. May, 1120 Auburn Dr., Jackson, Miss.

APR. 17-19, 1967: **Thermal Balance of Spacecraft**, American Inst. of Aeronautics and Astronautics, Nat'l Bureau of Standards, Air Force. **Prog. Info.:** Y. S. Touloukian, Thermophysical Properties Research Center, Purdue U., 2595 Yeager Rd. Lafayette, Ind.

APR. 18-19, 1967: **Electronics & Instrumentation Conf. & Exhibition**, IEEE Cincinnati Sec., ISA, Carousel Inn, Cincinnati Gardens, Cincinnati, Ohio. **Prog. Info.:** IEEE Headquarters 345 E. 47th St., N.Y., N.Y. 10017.

APR. 18-20, 1967: **Spring Joint Computer Conference**, IEEE-AFIPS, Chalfonte-Haddon Hall, Atlantic City, N.J. **Prog. Info.:** M. P. Chinitz, UNIVAC, P.O. Box 500, Blue Bell, Pa.

PROFESSIONAL MEETINGS

DATES *and* DEADLINES

Be sure deadlines are met—consult your Technical Publications Administrator or your Editorial Representative for the lead time necessary to obtain RCA approvals (and government approvals, if applicable). Remember, abstracts and manuscripts must be so approved BEFORE sending them to the meeting committee.

APR. 19-20, 1967: **Electronics & Instrumentation Conference & Exhibition**, Cincinnati Section, ISA, Carousel Inn, Cincinnati Gardens, Cincinnati, Ohio. **Prog. Info.:** R. H. Englemann, Univ. of Cincinnati, Cincinnati, Ohio 45221.

APR. 19-21, 1967: **Southwestern IEEE Conf. & Exhibition (SWIEEECO)**, Region 5 Dallas Memorial Auditorium, Dallas, Texas. **Prog. Info.:** A. A. Dougal, Univ. of Texas, Engrg-Science Bldg., Austin, Texas 78712.

APR. 19-22, 1967: **Semiconductor Device Research Conf.**, IEEE Region 8 et al., Bad Nauheim, Germany. **Prog. Info.:** Prof. W. J. Kleen, 8 Munchen 8 (F.R. Germany) Blanastr. 73.

APR. 24-MAY 5, 1967: **Conference on Integrated Circuits**, Region 8, U.K. & Eire Section et al, London, England. **Prog. Info.:** IEEE Headquarters, 345 E. 47th St. N.Y., N.Y. 10017.

MAY 2-3, 1967: **Insulation Coordination Forum**, G-P, Little Rock Section, Marion Hotel, Little Rock, Arkansas. **Prog. Info.:** J. O. Noel, Illinois Power Co., 500 South 27th St. Decatur, Illinois.

MAY 3-5, 1967: **Joint Parts, Materials & Packaging Conf.** (formerly the **Electronic Components Conf.**), IEEE, G-PMP, EIA, Marriott Motor Hotel, Washington, D.C. **Prog. Info.:** C. K. Morehouse, Globe Union Inc., Box 591, Milwaukee, Wisc. 53201.

MAY 3-6, 1967: **Rare Earths**, Oak Ridge Nat'l Lab, Air Force Office of Scientific Research. **Prog. Info.:** W. C. Koehler, ORNL, Oak Ridge, Tenn.

MAY 8-10, 1967: **G-MMT Int'l Microwave Symposium**, G-MTT, Hilton Hotel & New England Life Hall, Boston, Mass. **Prog. Info.:** IEEE Headquarters, 345 E. 47th St. N.Y., N.Y. 10017.

MAY 9-11, 1967: **Packaging Industry Technical Conference**, G-IGA, Holiday Inn, New York, N.Y. **Prog. Info.:** IEEE Headquarters, 345 E. 47th St. N.Y., N.Y. 10017.

MAY 9-11, 1967: **Region 6 Conference**, Region 6, Western Skies & Holiday Inn, Albuquerque, N.M. **Prog. Info.:** O. M. Stuetzer, Sandia Corp., Albuquerque, N.M.

MAY 15-17, 1967: **IEEE Aerospace Elec. Conv.** (NAECON), IEEE Dayton Sec., G-AES, Dayton, Ohio. **Prog. Info.:** IEEE Headquarters Dayton Office, 1414 E. 3rd St., Dayton 3, Ohio.

MAY 15-17, 1967: **Power Industry Computer Application Conf. (PICA)** G-P, Pittsburgh Hilton, Pittsburgh, Pa. **Prog. Info.:** L. W. Coombe, Detroit Edison Co., 2000 Second Ave., Detroit, Mich. 48226.

MAY 16-18, 1967: **Nat'l Telemetering Conf.**, IEEE, AIAA, ISA, San Francisco, Hilton Hotel, San Francisco, Calif. **Prog. Info.:** M. A. Lowy, Gen'l Elec. Co., P.O. Box 8048, Phila., Pa.

Calls for Papers

APR. 17-19, 1967: **Region 3 Meeting**, Region 3, Heidelberg Hotel, Jackson, Miss. **Deadline:** (Papers) **2/15/67** TO: J. E. May, 1120 Auburn Dr. Jackson, Miss.

MAY 2-3, 1967: **Insulation Coordination Forum**, G-P, Little Rock Section, Marion Hotel, Little Rock, Arkansas. **Deadline Info.:** J. O. Noel, Illinois Power Co., 500 South 27th St., Decatur, Ilinois.

JUNE 5-9, 1967: **Joint Automatic Control Conference**, IEEE, AACC, Univ. of Penna., Phila., Penna. **Deadline Info.:** IEEE Headquarters, 345 E. 47th St. N.Y., N.Y. 10017.

JUNE 12-14, 1967: **IEEE Int'l Communications Conf.**, IEEE G-Com. Tech. Twin Cities Sect., Radisson Hotel, Minneapolis, Minn. **Deadline Info.:** R. J. Collins, Univ. of Minnesota, Dept. of E.E. Minneapolis, Minn. 55455.

JUNE 19-21, 1967: **San Diego Symp. for Biomedical Engrg.**, IEEE, U.S. Naval Hospital et al., San Diego, Calif. **Deadline:** (Abstract) **4/12/67**, TO: D. L. Franklin, Scripps Clinic & Res. Foundation, LaJolle, Calif.

JULY 9-14, 1967: **Summer Power Mtg.**, IEEE G-P, Portland Hilton Hotel, Portland, Oregon. **Deadline** (Papers) **4/12/67** TO: E. C. Day, IEEE, 345 E. 47th St., N.Y., N.Y. 10017.

JULY 10-14, 1967: **Nuclear & Space Radiation Effects Conference**, G-NS, Ohio State Univ., Columbus, Ohio. **Deadline Info.:** IEEE Headquarters, 345 E. 47th St., N.Y., N.Y. 10017.

JULY 18-20, 1967: **9th Electromagnetic Compatibility Symposium**, IEEE G-EMC, Shoreham Hotel, Washington, D.C. **Deadline Info.:** F. T. Mitchell, Atlantic Res. Corp., Shirley Hwy. & Edsall Rd., Alexandria, Va.

AUG. 22-25, 1967: **Western Electronic Show & Convention (WESCON)**, IEEE-WEMA, Cow Palace, San Francisco Calif. **Deadline:** (Abst.) **5/15/67** TO: WESCON, 3600 Wilshire Blvd., Los Angeles, Calif.

SEPT. 4-8, 1967: **2nd IFAC Symposium on Automatic Control in Space**, IFAC, Vienna, Austria. **Deadline** (Abstracts) **2/1/67** TO: J. A. Aseltine, TRW Sys. Space Park Drive, Houston, Texas 77058.

SEPT. 4-8, 1967: **Solid State Devices Conference**, U.K. & Erie Section et al, Univ. of Manchester & Inst. of Science & Tech., Manchester, Eng. **Deadline Info.:** L. Lawrence, Inst. of Physics & Physical Society, 47 Belgrave Sq., London, S.W. 1, England.

SEPT. 11-15, 1967: **Int'l Symp. on Info. Theory**, IEEE, G-IT, Hilton Hotel, Athens, Greece. **Deadline:** (Abstracts) **5/1/67** TO: IEEE Headquarters, 345 E. 47th St. N.Y., N.Y. 10017.

SEPT. 24-28, 1967: **Joint Power Generation Conf.**, IEEE, G-P et al., ASME, Statler Hilton Hotel, Detroit, Michigan. **Deadline:** (Abstracts) **4/1/67** TO: D. M. Sauter, Westinghouse Elec. Corp., East Pittsburgh, Pa. 15112.

SEPT. 25-27, 1967: **Int'l Elec. Conference & Exhibition of the Canadian Region**, Canadian Region, Toronto Section, Automotive Bldg. in Exhibition Park, Toronto, Ontario, Canada. **Deadline Info.:** R. G. deBuda, 1819 Yonge St., Toronto, Canada.

OCT. 9-10, 1967: **Joint Engineering Management Conf.** IEEE-ASME et al., Jack Tar Hotel, San Francisco, Calif. **Deadline:** (Abstracts) **4/1/67** TO: B. B. Winer, Westinghouse Elec. Corp., E. Pittsburgh, Penna.

OCT. 16-18, 1967: **Convention on Aerospace & Electronic Systems**, G-AES, Sheraton Park Hotel, Washington, D.C. **Deadline Info.:** E. G. Shuster, RCA, 1725 K. St. N.W., Washington, D.C. 20006.

OCT. 16-18, 1967: **Fall URSI-IEEE Meeting**, URSI-IEEE, Rackham Bldg., Univ. of Michigan, Ann Arbor, Mich. **Deadline Info.:** T. B. A. Senior, Radiation Lab., 201 Catherine St., Ann Arbor, Michigan.

OCT. 17-19, 1967: **Int'l Symposium on Antennas & Propagation**, G-AP, Rackham Bldg., Univ. of Michigan, Ann Arbor, Mich. **Deadline Info.:** T. B. A. Senior, Radiation Lab., 201 Catherine St., Ann Arbor, Michigan.

OCT. 18-20, 1967: **Electron Devices Meeting**, G-ED, Sheraton-Park Hotel, Washington, D.C. **Deadline Info.:** IEEE Headquarters, 345 E. 47th St., New York, N.Y. 10017.

OCT. 23-25, 1967: **Nat'l Electronics Conf.**, IEEE et al, McCormick Place, Chicago, Illinois. **Deadline Info.:** Nat'l Electronics Conf., 228 N. LaSalle St., Chicago, Illinois.

OCT. 1967: **Electron Devices Meeting**, G-ED, Washington, D.C. **Deadline Info.:** IEEE Headquarters, 345 E. 47th St., N.Y., N.Y. 10017.

OCT. 30-NOV. 2, 1967: **14th Nuclear Science Symposium**, G-NS, Statler Hilton Hotel, Los Angeles, Calif. **Deadline Info.:** IEEE Headquarters, 345 E. 47th St., N.Y., N.Y. 10017.

Engineering NEWS *and* HIGHLIGHTS

RCA TOP MANAGEMENT REALIGNMENT

A realignment in RCA management has been announced by **Robert W. Sarnoff**, President, RCA. The changes, to take effect January 1, 1967, involve a number of key operating and staff responsibilities which will continue to be exercised by present management personnel. In the operating area, Mr. Sarnoff announced the following changes:

W. Walter Watts, Group Executive Vice President, will assume responsibility for Defense Electronic Products, the Broadcast and Communications Products Division, and the Graphic Systems Division. Mr. Watts has previously been responsible for Consumer Products, Electronic Components and Devices, and Distributor and Commercial Relations.

Charles M. Odorizzi, Group Executive Vice President, will continue his present responsibility for RCA Communications, Inc.; the RCA Service Company, and the RCA Victor Record Division, and will assume responsibility for the RCA Magnetic Products Division. Mr. Odorizzi has previously had responsibility also for Licensing, the RCA International Division, and the Broadcast and Communications Products Division.

Delbert L. Mills, Executive Vice President, will continue his present responsibility for Consumer Products (RCA Sales Corporation, RCA Victor Home Instruments Division, RCA Victor Distributing Corp., and RCA Parts and Accessories), and will assume responsibility for Distributor and Commercial Relations. Mr. Mills has been reporting to Mr. Watts, but will now report to the President.

Three other operating executives will continue their present responsibilities, but will now report directly to the President. They are **James R. Bradburn,** Vice President and General Manager, Electronic Data Processing; **John B. Farese,** Vice President, Electronic Components and Devices, and **Charles R. Denny,** Vice President and Managing Director, RCA International Division.

Mr. Sarnoff announced the following RCA Corporate Staff appointments and changes, involving individuals reporting to the President:

Arthur L. Malcarney, appointed to the new position of Executive Vice President, Manufacturing Services and Materials. Mr. Malcarney has been a Group Executive Vice President, with responsibility for Defense Electronic Products, Electronic Data Processing, and the Graphic Systems Division.

Melvin E. Karns, continuing his responsibility as Vice President, Licensing. Mr. Karns has been reporting to Mr. Odorizzi.

Howard L. Letts, designated Executive Vice President, Finance. Mr. Letts has been Executive Vice President and Controller.

VOLKMANN GETS AUDIO AWARD

John E. Volkmann has been presented the *1966 John H. Potts Memorial Award* by the Audio Engineering Society. He is a Member, Technical Staff, of the Acoustical and Electromechanical Research Laboratory, RCA Laboratories, Princeton, N.J. Mr. Volkmann was honored for "his elegant application of acoustic principles in the development of large scale loudspeakers and sound systems".

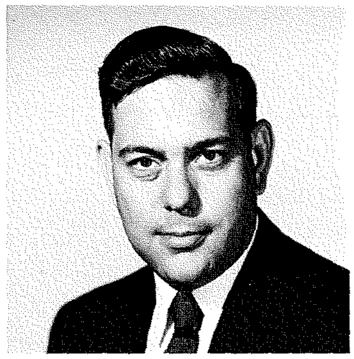

D. SHORE NAMED CHIEF DEFENSE ENGINEER

Effective December 5, 1966 **David Shore** was named Chief Defense Engineer, Defense Engineering, replacing **Dr. H. J. Watters.** Mr. Shore formerly Chief Engineer, DEP Communications Systems Division, now reports to **A. K. Weber,** Vice President, Defense Electronics Products and Graphic Systems.

David Shore received his BS in Aeronautical Engineering at the University of Michigan in 1941 and his Master's in Physics at Ohio State University in 1950. Prior to joining RCA, he was with the Air Force's Wright Air Development Center, where he became Civilian Chief of the Systems Analysis Group and was responsible for the initiation of several new aircraft and guided missile systems. Since joining RCA in 1954, he was responsible for the overall systems design of BMEWS, the Ballistic Missile Early Warning System; and has directed the development of satellites. In 1962, he founded SEER, (Systems Engineering, Evaluation and Research) with responsibility for directing company-wide efforts on major new systems. In August, 1965, Mr. Shore was appointed Chief Engineer of the Communications Systems Division in Camden and in December, 1966 was appointed Chief Defense Engineer, Defense Electronics Products, RCA, Camden, New Jersey.

DR. BACHYNSKI HONORED

Dr. M. P. Bachynski, Director, Research Labs, RCA Montreal, was named a *Fellow* of the Canadian Aeronautics and Space Institute at the annual general meeting held May 2-3, 1966 in Ottawa, Canada.

R. S. HOLMES NAMED DIVISION VICE PRESIDENT OF NEW RCA MEDICAL ELECTRONICS ACTIVITY

The appointment of **Ralph S. Holmes** as Division Vice President, Medical Electronics, has been announced by **Frank H. Erdman,** Division Vice President, RCA New Business Programs. In his new position, Mr. Holmes will report to Mr. Erdman. The appointment is a step towards implementing RCA's part of the recently announced agreement with Hoffmann-LaRoche, Inc., to collaborate in the development, production, and marketing of new and advanced medical devices.

C. K. LAW NAMED CHIEF ENGINEER OF CSD

Effective December 5, 1966 **C. K. Law** was appointed Chief Engineer, Engineering Department, of the DEP Communication Systems Division. Mr. Law now reports to **J. M. Herzberg,** Division Vice President and General Manager, CSD.

Mr. Law joined RCA in 1948 following his graduation from Purdue University with BS and MS degrees in Electrical Engineering. He worked on and supervised many of RCA's airborne communications programs for the military services, NASA (then NACA), and the FAA. Mr. Law was the program manager responsible for the development of Time Division Data Link and, later, the X-20 (Dyna-Soar) Communications and Tracking System Program. He then became Manager, Programs Management, for the Aerospace Communications and Controls Division. When the Communications Systems Division was formed, Mr. Law was appointed Manager, of Aerospace Communications Programs. He was then assigned as Manager, Defense Planning for DEP, until appointed Director, Camden Product Engineering and then in February 1966, Manager, Engineering Operations for CSD. Mr. Law is a Senior Member, IEEE.

F. J. BINGLEY RECEIVES SMPTE OUTSTANDING PAPER AWARD

F. J. Bingley, Leader, Tape Cameras, Astro-Electronics Division, Princeton, was one of three men honored at the 1966 SMPTE 100th Technical Conference for the *most outstanding papers published in the SMPTE Journal in 1965.* Mr. Bingley received an award for his paper, "A Visual Instrumentation System for a Lunar Orbiter"; a similar paper was also published in the Feb.-Mar. 1965 RCA ENGINEER.

BABCOCK WINS BEST PAPER AWARD

William E. Babcock, Manager, Special Products Development, EC&D Commercial Receiving Tube and Semiconductor Division, Somerville, N.J., has received the *"1966 Outstanding Paper Award"* from the IEEE Group on Broadcast and Television Receivers. He delivered his prize winning paper at the IEEE Chicago Spring Conference, entitled "A Developmental 15-Inch Transistorized Color Television Receiver".

... PROMOTIONS ...

to Engineering Leader & Manager

As reported by your Personnel Activity during the past two months. Location and new supervisor appear in parentheses.

Electronic Components and Devices

A. Breidegam: from Production Eng. to *Ldr, Silicon Low Power* (R. O'Brien, Mntp.)

G. V. Morris: from Mechanical Eng. to *Eng. Ldr., Equipment Projects* (L. Mineur, Mntp.)

J. S. Neilson: from Sr. Eng. to *Eng. Ldr., Design Eng.* (H. Weisberg, Mntp.)

J. C. Laberge: from Production Eng. to *Mgr. Reliability and Product Assurance, Quality Assurance Test* (K. Loofbourrow, Mntp.)

A. M. Splinter: from Eng. Ldr. to *Mgr. Photocells* (D. J. Donohue, Somerville)

R. A. Lee: from Eng. Product Devel. to *Eng. Ldr., Product Devel* (Manager, Design and App., Lancaster)

J. B. Pyle: from Eng. Product Devel. to *Eng. Ldr., Product Devel.* (Manager, Design and Applications) Lancaster

C. Haug: from Eng. Product Devel. to *Manager, Product Eng.* (A. M. Trax, Marion)

W. Carrell: from Eng. Product Devel. to *Eng. Ldr.* (R. J. Konrad, Marion)

J. M. Fanale: from Eng. Manufacturing to *Eng. Ldr., Manufacturing* (Manager, Production Eng., Lancaster)

P. D. Huston: from Eng. Product Devel. to *Eng. Ldr., Product Devel.* (Manager, Camera Tube Op. Lancaster)

E. S. Thall: from Sr. Eng., Product Devel. to *Eng. Ldr. Scranton Engr.* (Manager, Scranton Engr.)

R. C. Demmy: from Eng. Product Devel. to *Eng. Ldr., Product Devel.* (Manager, Scranton Eng.)

C. E. Doner: from Engr. Product Devel. to *Eng. Ldr., Product Devel.* (Manager, Design and Application Engr.)

D. H. Wells: from Eng. Ldr., to *Mgr. Lewiston* (G. A. Hiatt, Quality & Reliability)

H. A. Hansen: from Resident Eng. to *Eng. Ldr. Somerville* (J. W. England, Entertainment Applications)

R. B. Sullivan: from Engr., Manufacturing to *Eng. Ldr.* (J. W. Young, Manager, Findlay)

R. B. Tyler: from Manager, Process Control to *Eng. Ldr.* (R. A. Donnelly, Manager, Findlay)

RCA Service Company

V. R. Fry: from Sys. Serv. Eng. to *Ldr., Systems Ser. Eng.* (A. C. Hodges, Alexandria)

A. B. Jarvis: from Eng. to *Ldr., Eng.* (R. A. Stevens, Arlington)

C. C. Misner: from Sys. Serv. Eng. to *Ldr., Sys. Serv. Eng.* (C. W. Fisher, Springfield)

F. J. Vaughn: from Sys. Serv. Eng. to *Ldr., Sys. Serv. Eng.* (J. S. Judson, Fairbanks, Alaska)

P. D. Meadows: from Sr. Field Support Eng. to *Ldr., Field Support Eng.* (D. T. Donaldson, Cocoa, Florida)

P. G. Vise: from Sr. Field Support Eng. to *Mgr., Navigation & Data Handling Shipboard* (H. C. Jenkins, Cocoa, Florida)

J. A. Haik: from Ldr., Eng. to *Mgr., Sys. Evaluation* (P. F. Egan, College Park, Md.

B. A. Barnwell: from Eng. to *Mgr., Real-Time Computer Sys.* (C. E. Perkins, Cocoa, Florida)

J. B. Caskey: from Eng. to *Mgr., Advanced Range Instru. Ship* (L. F. Dodson, Cocoa, Florida)

H. D. Tilley: from Ldr., to *Mgr., Orbital Prog.* (K. R. Raulins, Cocoa, Florida)

C. J. Isenberger: from Eng. Facilities to *Mgr., Eng. and Cons.* (R. M. Weible, Clear, Alaska)

J. S. Thomas: from Eng. to *Mgr., Radar* (L. F. Dodson, Cocoa, Fla.)

C. N. Chilabakis: from Eng. Facilities to *Ldr., Eng. BMEWS* (V. D. Pohlhammer, Thule, Greenland)

P. B. Farwell: from Data Inst. Eng. to *Ldr., Data Instru.* (J. A. Haik, College Park, Md.)

J. J. Cain: from Eng. to *Mgr., Communications* (M. J. Van Brunt, Cocoa, Fla.)

M. C. Hume: from Data Instru. Eng. to *Ldr., Data Instru.* (R. A. Hubbard, Greenbelt, Md.)

R. Macquade: from Eng. to *Ad., Operations* (E. W. Denzler, Sparta, Wis.)

P. Napolitano: from Eng. to *Ldr., Eng.* (R. A. Hubbard, Greenbelt, Md.)

Home Instruments Engineering Division

C. E. Conn: from Mebr. Eng. Staff to *Ldr. Eng. Staff* (M. J. Obert, Indianapolis)

Missile and Surface Radar Division

D. M. Cottler: from Mgr., Product Design to *Chief Eng.* (A. Mason, SAM-D Program)

N. Lesso: from Ldr., D & D Engrs. to *Mgr., Equip. Design* (F. Tillwick, Moorestown)

H. J. Siegel: from Ldr. D & D Engrs. to *Mgr., Gen'l Engrg.* (A. Mason, Moorestown)

H. H. Anderson: from Cl. "A" Eng. to *Ldr., D & D Engrs.* (E. S. Lewis, Moorestown)

Communications Systems Division

S. Yuan: from Engrg. Scientist to *Ldr., Tech. Staff* (Dr. Guenther, Camden)

D. G. Herzog: from Engr. Design, Devel. to *Ldr. Des. & Dev. Engrs.* (D. J. Parker, Camden)

S. J. Davis: from AA Engr. to *Ldr. Sys. Proj.* (K. K. Miller, Camden)

J. J. Davaro: from A Engr. to *Ldr. Sys. Proj.* (K. K. Miller, Camden)

W. L. Carlino: from A Engr. to *Ldr. Syst. Proj.* (J. M. Osborne, Camden)

A. K. Rapp: from Sr. Proj. Mbr. to *Eng. Ldr.* (E. E. Moore, Somerville)

J. Santoro: from Ldr., Des. & Devel. to *Mgr., Minuteman Sys.* (K. K. Miller, Camden)

H. A. Brill: from Ldr., Des. & Devel. to *Adm., Tech. Proj.* (W. B. Harris, Camden)

R. E. Wolf: from Cl. "AA" Eng. to *Ldr., Des. & Devel. Eng.* (R. L. Rocamora, Gibbsboro)

A. A. Blatz: from "AA" Eng. to *Ldr. Mech. Eng.* (H. Eigner, Camden)

S. L. Buckman: from "AA" Eng. to *Ldr.* (H. Eigner, Camden)

M. L. Feistman: from A Eng. to *Ldr. Des. & Devel.* (K. K. Miller, Camden)

T. A. Franks: from Ldr. D & D Eng. to *Mgr. Emulator Micro Prog.* (J. L. Maddox, Camden)

J. A. Pierce: from Cl. "AA" Eng. to *Ldr., D & D Eng.* (B. I. Kessler)

H. W. Kaiser: from A Eng. to *Ldr. Des. & Devel.* (T. L. Genetta, Camden)

H. N. Scott: from Mgr. Tech. Serv. to *Admr. Mfg. Proj.* (A. G. Cattell, Camden)

Aerospace Systems Division

A. Amato: from Ldr. T.S. to *Mgr. Product Design* (E. B. Halton, Burlington)

M. P. Guba: from Sr. Proj. Mbr. to *Ldr. T.S.* (A. Amato, Burl.)

J. H. Groff: from Ldr. to *Proj. Eng.* (J. F. Currier, Burlington)

J. M. Laskey: from Ldr. to *Proj. Eng.* (J. F. Currier, Burlington)

G. B. Harmon: from Sr. Proj. Mbr. to *Ldr., T.S.* (E. M. Stockton, Burl.)

L. C. Drew: from Sr. Proj. Mbr. to *Ldr., T.S.* (N. L. Laschever, Burl.)

Astro-Electronics Division

R. J. Treadwell: from Eng. to *Ldr. Eng.* (W. Cable, Princeton)

J. Staniszewski: from Ldr. to *Mgr., RAE* (C. S. Constantino, Princeton)

E. A. Boyd: from Eng. to *Sr. Mbr. Tech. Staff* (R. B. Marsten, Princeton)

I. Stein: from Ldr. Eng. to *Adm., Space Power* (G. Barna, Princeton)

T. R. Wylie: from Sr. Eng. to *Ldr., Eng.* (D. Mager, Princeton)

J. Baumunk: from Ldr. Eng. to *Mgr. Data Trans.* (H. Lawrence, Princeton)

NEW HOME INSTRUMENTS ENGINEERING ORGANIZATION

Recently the Home Instruments Engineering Department has been realigned to more effectively manage the expanded development and design load in the Home Instruments Division. The organization is as follows: **K. A. Chittick**—Mgr., Engineering Administration and Services; **E. J. Evans**—Mgr., Resident Engineering, Rockville Road Plant; **R. D. Flood**—Mgr., R/V and Combination Engineering; **E. M. Hinsdale**—Acting Mgr., Advanced Systems and Development; **T. C. Jobe**—Mgr., Resident Engineering, Memphis Plant; **G. E. Kelly**—Mgr., Color Television Engineering; **R. J. Lewis**—Mgr., Black and White Television Engineering; **M. J. Obert**—Mgr., Components Engineering; **M. F. Troy**—Mgr., Equipment Development; **J. M. Wright**—Mgr., Resident Engineering, Bloomington Plant; **C. W. Hoyt**—Staff Engineer and Acting Mgr., RCA TEAM Purdue Laboratory. The above report to **Mr. Kirkwood,** the Chief Engineer.

Reporting to **E. M. Hinsdale,** Manager, Advanced Systems and Development, are: **J. Avins** — Mgr., Circuit Development, Somerville; **D. H. Fisher**—Staff Engineer; **R. N. Rhodes**—Mgr., Electronic Systems; **G. F. Rogers**—Mgr., Advanced Development.

Reporting to **M. J. Obert** are: **D. H. Cunningham**—Mgr., Electromechanical Engineering; **G. L. Hermeling**—Mgr., Tuner Engineering; **J. K. Kratz**—Mgr., Electromagnetic Engineering.

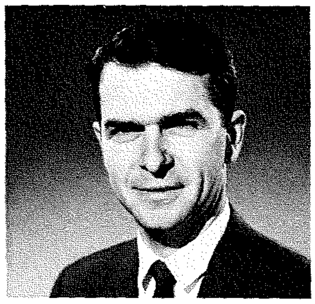

J. FRIEDMAN, NEW APPLIED RESEARCH ED REP

J. E. Friedman has been named as an additional RCA ENGINEER editorial representative for DEP Applied Research, Camden. He will work with **M. G. Pietz,** who has been Applied Research Editorial Representative for some time. Both Freedman and Pietz serve on **F. Whitmore's** DEP Editorial Board.

John E. Friedman received his BS in Engineering Physics at Lehigh University and joined the Bendix Corporation at Teterboro, N.J. in 1956. His work there included design of electrical ground support equipment for commercial and military jet aircraft, and later for missile inertial guidance platforms. While at Bendix he attended Newark College of Engineering and Fairleigh Dickinson University for further studies in communications processes. In 1960 he joined the GE Space Sciences Laboratory in Philadelphia as a scientific editor. Here he worked on basic aerospace research documents and papers in the fields of solid-state physics, IR/Optical sensors, and down-range radiation studies. Mr. Friedman has served as managing editor for the Valley Forge Association of GE Engineers and Scientists bulletin, *The Forge*, and for the *Delaware Valley Science and Engineering Newsletter* of the Engineering and Technical Societies Council in Philadelphia. He now is a publications engineer, responsible for proposals, presentations, and contract documentation, in the Technical Publications group of Applied Research, DEP.

T. W. SARNOFF RECEIVES AWARD

Thomas W. Sarnoff, Staff Executive Vice President, West Coast, NBC, received the *Humanitarian Award* for 1966 of the Broadcast Motion Picture Recording Division of the National Conference of Christians and Jews at the Third Annual Brotherhood testimonial dinner. Mr. Sarnoff has been a member of the Regional Board of the NCCJ for a number of years and this year was elected to the National Board of the Conference.

PROFESSIONAL ENGINEERS

P. M. Toscano, ASD, Burlington, PE-20714, Burl.

R. M. Fritz, MSR, Moorestown, PE-1341 E, N.J.; PE 14956, Pa.

T. A. Franks, EDP, Cherry Hill, PE-14881, N.J.

H. A. Brown, ASD, Burlington, PE-20702, Burl.

I. C. Akerblom, ASD, Burlington, PE-20810, Burl.

R. K. Gorman, ASD, Burlington, PE-20701, Burl.

M. A. Keller, SEER, Moorestown, PE-15007, New Jersey

NEW RCA TOKYO LABORATORY FACILITIES TO EXPAND RESEARCH PROGRAM THERE

Laboratories RCA, Inc., our research subsidiary in Japan (established in 1961) has begun construction on the outskirts of Tokyo for a new laboratory complex to house an expanded research program. The present basic programs in physics and chemistry will continue, but increasing emphasis also will be given to communications theory and related aspects of electronics. Outstanding work in this field is already being performed by Japanese scientists, in particular in such areas as microwave data and voice communication techniques. The new laboratory complex will double present facilities. **Dr. Maurice Glicksman,** Director of Research, Laboratories RCA, Tokyo, expects the new center to be completed by June 1967.

NEW GRAPHIC SYSTEMS LABORATORY

The Graphic Systems Applied Research Laboratory has been established at RCA Laboratories, Princeton, N.J. The new laboratory was organized to do applied research in support of the Graphic Systems Division and to insure a continuing flow of new product ideas into GSD. While it is presently concerned with printing research, its future activities will include retrieval systems, data transmission and storage, manipulation and display of graphics. **Dr. Edward W. Herold** is Manager, Graphic Systems Applied Research Laboratory, and **Dr. Kenneth H. Fischbeck** is Manager, Printing Research.

DR. SCHILLING GIVES TWO 15-WEEK COURSES IN ELECTRONICS CIRCUITS FOR SOMERVILLE ENGINEERS

Dr. Ronald B. Schilling of RCA Labs. is presenting two special courses in Electronic Circuits to ECD engineers. The first course, covering *Digital Electronics*, began on September 26, 1966, to run for 15 weeks. Some of the topics covered are RC, RL, and diode wave shaping, switching characteristics of devices, clipping and clamping networks, logic circuits, and multivibrators.

The second course, covering *Transistor Circuit Analysis*, will begin in about February 1967. Topics include basic transistor theory, transistors as circuit elements, D-C biasing and stability, low, high and broadband amplifiers, sweep circuits, oscillators, and an introduction to integrated circuits.

The courses are on Mondays from 4:45 to 6:35. They include homework, exams, and grades.—*C. W. Sall*

LANCASTER TRANSISTOR COURSE

A transistor course for engineers was organized and presented this year at the RCA Lancaster, Pa. plant. The title of the course was *Solid State Transistor Theory and Applications*. It was taught by **J. T. Gote** of the Electrical Measurements and Environmental Engineering Laboratory. The course was held for two hours per week for a sixteen week period. Two classes were held on consecutive weekdays with 75 engineers completing the 32-hour course. — *G. G. Thomas*

DEGREES GRANTED

R. P. Perry, MSR .... MSEE, University of Pa.
R. J. McGovern, ECD, Hr................ MS, Management Science 1966, Stevens Institute
H. W. Becke, ECD, Som. .... MSEE, Newark College of Engineering
R. H. Dawson, ECD, Som. .... MSEE, Polytechnic Institute of Brooklyn
Dr. R. B. Schilling, RCA Labs......... PhD, Elec. Engrg., Polytechnic Institute of Brooklyn
A. S. Waxman, RCA Labs .... PhD, Elec. Engrg., Princeton University
N. Phillips, WCD............ MS, Master of Science, University of California, Los Angeles

CONTENTS OF THE DECEMBER 1966 RCA REVIEW

(**Editor's Note:** In cooperation with the editors of the RCA REVIEW, the RCA ENGINEER will in the future announce the contents of each new issue of the RCA REVIEW. Since the RCA REVIEW is published quarterly, while the RCA ENGINEER is published bimonthly, the timing of these announcements will vary somewhat, but will be made in as early an issue of the RCA ENGINEER as possible.)

RCA REVIEW, Vol. XXVII, No. 4; December 1966

The RCA REVIEW is published quarterly in March, June, September, and December. Copies are available in all RCA libraries. Individual subscription rates are as follows:

	DOMESTIC	FOREIGN
1-year	$2.00	$2.40
2-year	3.50	4.30
3-year	4.50	5.70

For RCA employees, the above rates are discounted 20%.